School of Physics and Astronomy
Queen Mary University of London

Novel techniques for calculating inflationary observables

Shailee Varsha Imrith

Supervised by David J. Mulryne and Karim A. Malik

Submitted in partial fulfilment of the requirements for the degree of
Doctor of Philosophy

Declaration

I hereby certify that this thesis, which is approximately 43,000 words in length, has been written by me; that it is the record of the work carried out by me at the School of Physics and Astronomy, Queen Mary University of London, and that it has not been submitted in any previous application for a higher degree.

The work in this thesis has been completed in collaboration with David J. Mulryne and Arttu Rajantie and appears in the following papers:

- Non-perturbative δN formalism
  Phys. Rev. D 98, 043513 (2018)
- Calculating ζ from lattice simulations (prepared for submission to PRD)

I have made a major contribution to all the original research presented in this thesis. I have been supported by the STFC grant No. ST/M503733/1 throughout my PhD. Part of the research in this thesis utilised Queen Mary's Apocrita HPC facility, supported by QMUL Research-IT.

Shailee Varsha Imrith

Abstract

Comparing the predictions from different inflation models to observations of the Cosmic Microwave Background (CMB) and the Large-Scale Structure (LSS) is a non-trivial task. One needs to calculate the statistics of the primordial curvature perturbation, ζ, to be able to compare to observational constraints. There exist many formalisms for such calculations, each with its own benefits and drawbacks, depending on the inflation model being considered. One popular method, the δN formalism, calculates the evolution of the statistics of ζ on superhorizon scales. δN assumes that the number of e-folds as a function of the scalar fields present in the model, N, is Taylor-expandable and that the Taylor series converges sufficiently fast. Unfortunately, this assumption breaks down in some cases. As a solution, in this thesis, we first extend the standard δN formalism so that it can be applied to any arbitrary function of N, irrespective of whether the N function is Taylor-expandable or not. We test the validity of the formalism on a pre-generated N function from a realistic model and find that the method shows marked improvement over regular δN. This extension of δN, which we call 'non-perturbative δN', involves integrating the N function against a probability distribution function for the fields. When the N function is highly featured, a convenient method to perform the calculations is Monte Carlo integration. As an example, in the last part of the thesis we study massless preheating. We run our own lattice simulations and implement the non-perturbative expressions in a Monte Carlo fashion. Doing so, we calculate accurately the two- and three-point functions of ζ in this model for the first time.

Acknowledgements

I am most indebted to David Mulryne; his invaluable expertise and extremely compassionate nature makes him an excellent supervisor to work with. I also thank my amazing second supervisor, Karim Malik, for all his support and guidance throughout my PhD. I am grateful for the opportunity to collaborate with Arttu Rajantie on the work in this thesis.

There are so many people since my undergraduate years that I want to thank. In particular, my thanks go to Richard Nelson and Steve Thomas. Richard has been instrumental in my academic career, helping me with my transition from astrophysics to theoretical physics; in fact, I met David who would later become my PhD supervisor, through Richard. I would like to thank Steve Thomas for sharing his passion for astronomy and for being so generous with his time when I was learning how to use the QMUL telescope. I thank Alexander Polnarev for the amusing anecdotes and discussions after lectures.

I would like to thank Charalambos Pittordis for being such a great friend and confidant during the eight years that we've known each other; his discipline has always inspired me. I also thank Pedro Carrilho, my extremely patient and kind office neighbour who has the gift to explain very complicated things in simple ways. I thank John Ronayne for making the last three years very interesting, for all his help and expertise, good advice and great puns. My evenings and weekends as a PhD student would be very dull without the amazing company of Rebeca Carrillo, Sanson Poon, Jorge Venegas and more recently Maritza Soto. I massively appreciate Viraj Sanghai, his friendship and his banter. My thanks also go to my fellow office mates Clark Baker, Domenico Trotta, Louis Coates, Eline De Weerd, Jessie Durk, Kit Gallagher, Francesco Lovascio, Paul Hallam, Callum Boocock, John Strachan, Jack Skinner, Colin McNally, Usman Gilani and Shaoshan Zeng. Past colleagues Sophia Goldberg, Zachary Kenton, Alexander Leithes, Matthew Mutter, Nick Attree and Gavin Coleman are also dearly missed.

A big thanks to everyone in the astronomy unit, past and present, and in particular, Timothy Clifton, Chris Clarkson, Prina Patel, Alkistis Pourtsidou, Julian Adamek, Bernard Carr, Reza Tavakol, Tommi Tenkanen and Raquel Ribeiro. Thanks to Alex Owen for being so helpful with matters of the cluster.

I thank my brother, mother and family in the UK and back in Mauritius for their continuous support and encouragement. I especially miss my late father who sadly passed away when I was twelve and will not see me graduate.

This thesis is dedicated to my grandmother, Jassoda Imrith, my primary caregiver during my childhood and teenage years who, like all grandmothers, often complains that I have forgotten about her.

Contents

List of Figures

1 Introduction

"Il ne faut rien laisser au hasard."
Leave nothing to chance.

—French proverb

The currently best-fitting picture for describing the universe, known as the standard model of cosmology or the ΛCDM model, which includes the hot big bang model of the early universe, presents some serious shortcomings. The problems are namely, the *horizon problem*, the *flatness problem* and the *monopole problem*. The horizon problem refers to the question of why the universe is homogeneous and isotropic despite the fact that distant regions of space could not have been in causal contact in the past in conventional big bang cosmology. The flatness problem alludes to yet another fine-tuning problem; our universe seems to have just the right amount of matter to be flat even though this is in a sense unstable as we will see later. The monopole problem, on the other hand, is based on the prediction from Grand Unified Theories that if the early universe were very hot, a large number of very heavy, stable magnetic monopoles would have been produced. Such particles have never been observed in nature. However, unlike the horizon and the flatness problem, the existence of a monopole problem is debated (see for example, [1]). Moreover, the standard model assumes small initial over- and under-densities needed for structure formation at later times in the universe but offers no explanation for their origin.

One should note, however, that the two most serious problems, namely the horizon and flatness problems, are not *strictly* inconsistent with the standard hot big bang model. One could assume that the very early universe was extremely flat and that the universe began homogeneously over superhorizon scales, which would mean that the universe would remain homogeneous, in agreement with observations. Similarly, one could also assume initial perturbations in the density that then give rise to the structures we see in the universe today. So, these problems are just really severe limitations in the predictive power of the big bang model. The striking flatness of the universe, the unmistakable large-scale homogeneity of the universe and

the origin of the over- and under-densities cannot be predicted by the hot big bang; these have to be simply assumed in the initial conditions. It is obvious then that a theory that explains these initial conditions dynamically is very attractive.

Inflationary cosmology, an elegant theory that cures all of the above mentioned problems, was first developed in the 1980's by a number of independent authors [2–4] and is the subject of my research. Cosmic inflation is defined as a period of accelerated expansion before the hot big bang and allows regions separated by more than a horizon size today to have been in causal contact at very early times. This can lead to the observed homogeneous universe on large scales today. Inflation also drives the universe to flatness. We will return to the question of how inflation solves these problems later in the thesis. Aside from solving these problems, inflation also explains another striking observational feature: the anisotropies in the Cosmic Microwave Background. Now routinely measured by experiments like the Planck mission, the temperature fluctuations of the CMB bear testimony of the very tiny fluctuations in the primordial density of the universe whose microphysical origin is thought to come from quantum fluctuations during inflation. These fluctuations eventually form all the structures observed in the universe. In spite of its elegance, cosmic inflation is incomplete in the sense that the exact microphysics of the inflationary theory is not known. There exists a plethora of competing inflationary models and each comes with its own observational predictions. With every new experiment that provides increasingly stronger constraints on models, it becomes imperative to be able to obtain precise theoretical predictions. Analytical and numerical tools are needed to crunch the numbers for a given inflation model to allow its predictions to then be compared to observational constraints. In turn this allows us to consolidate, rule out or put constraints on the model. The aim of this thesis is to add another tool to the arsenal of tools available to inflationary cosmologists. We will see that this tool is particularly useful when the complicated dynamics during the reheating phase after inflation ends, can affect the predictions of inflation.

The thesis is structured as follows. In Chapter 1, we introduce the ΛCDM model, the problems of the standard big bang model and describe how inflation comes to the rescue. Chapter 2 provides details on the mathematical formulation of *classical* inflationary theory. In Chapter 3, we describe how quantum fluctuations during inflation become the seeds for the formation of large-scale structures. We also present detailed calculations of the power spectrum and bispectrum of the curvature perturbation in single field slow-roll inflation. Moving on to multifield inflation, we introduce the δN formalism in Chapter 4 which is a powerful tool used to calculate the non-linear evolution of the curvature perturbation on large scales. We then set the scene for our first research chapter by highlighting the limitations of the

δN formalism. Standard δN relies on the number of e-folds, N, undergone by the early universe as a function of initial conditions to be expandable as a Taylor series. In some settings, such as when reheating plays an important role, this assumption breaks down. As a solution, we consider the *Non-Perturbative δN formalism* in Chapter 5, valid even where Taylor expansion is not possible. We present our non-perturbative expressions and test their validity on a realistic example. One prominent scenario where the N function is highly featured and therefore warrants the use of the non-perturbative δN formalism is the massless preheating model where parametric resonance, a highly non-linear and out-of-equilibrium regime, naturally occurs. It makes sense therefore to take a short digression to review reheating and preheating in Chapter 6. We also discuss lattice field theory simulations, the only way to fully treat the nonlinear dynamics of reheating and in doing so, we introduce HLattice [5], a code written in fortran that simulates scalar fields and gravity in the early universe. In Chapter 7, we apply our non-perturbative δN expressions in a Monte Carlo manner to massless preheating by running our own simulations using HLattice on Queen Mary's HPC facility [6]. We finally conclude in Chapter 8. The study of the effects of non-linear dynamics during reheating on observations is complicated. This thesis is, hopefully, a step in the right direction and the method we present amounts to a unique opportunity to extract for the first time observational predictions for the curvature perturbation directly from lattice simulations.

1.1 Conventions

Throughout this thesis and unless stated otherwise, we use natural units $c = \hbar = 1$. The reduced Planck mass $M_{\rm pl} = (8\pi G_{\rm N})^{-\frac{1}{2}} = 2.4 \times 10^{18}$ GeV. The metric signature is $(-+\ +\ +)$ and Greek indices run over the four spacetime coordinates $\{0, 1, 2, 3\}$ and the lowercase Latin indices run over the spatial coordinates $\{1, 2, 3\}$. Our Fourier convention is

$$\chi_{\mathbf{k}} = \int \mathrm{d}^3\mathbf{x}\, e^{-i\mathbf{k}.\mathbf{x}} \chi(\mathbf{x}). \tag{1.1}$$

We reserve η for the slow-roll parameter and denote conformal time by τ where $\tau = \int_0^t \frac{\mathrm{dt}}{a(t)}$. Overdots represent derivatives with respect to coordinate time t and a prime denotes derivatives with respect to conformal time τ.

1.2 The ΛCDM Model

One of the fundamental assumptions of modern cosmology is the *cosmological principle* which states that the distribution of matter in the universe is homogeneous and isotropic when viewed on a large-enough scale, i.e., greater than 100 Mpc [7]. Homogeneity and isotropy can be summarized by two principles of spatial invariance. The first invariance is isomorphism under translation, namely homogeneity.

Isotropy refers to rotational invariance. The observable patch of the universe is roughly 3000 Mpc (1 Mpc = $\approx 3.26 \times 10^6$ light years). Surveys such as the 2dF galaxy redshift survey and the Sloan Digital Sky Survey suggest that the universe is homogeneous and isotropic only when coarse grained on 100 Mpc scales. The cosmological principle obviously does not hold on small distance scales as we see distinguishing features like planets, galaxies, galaxy clusters and superclusters. Further experimental evidence for homogeneity and isotropy comes from the CMB. The first successful measurement of the Cosmic Microwave Background was made in 1964 by Penzias and Wilson [8]. Their observations revealed that the CMB was characteristic of a black-body with a corresponding temperature of 2.73K. They also observed that the CMB is uniform in all directions (isotropic). Observational evidence for the homogeneity and isotropy of the universe, whether drawn from galaxy counts or the CMB [7], is invariably cited as justification for the cosmological principle.

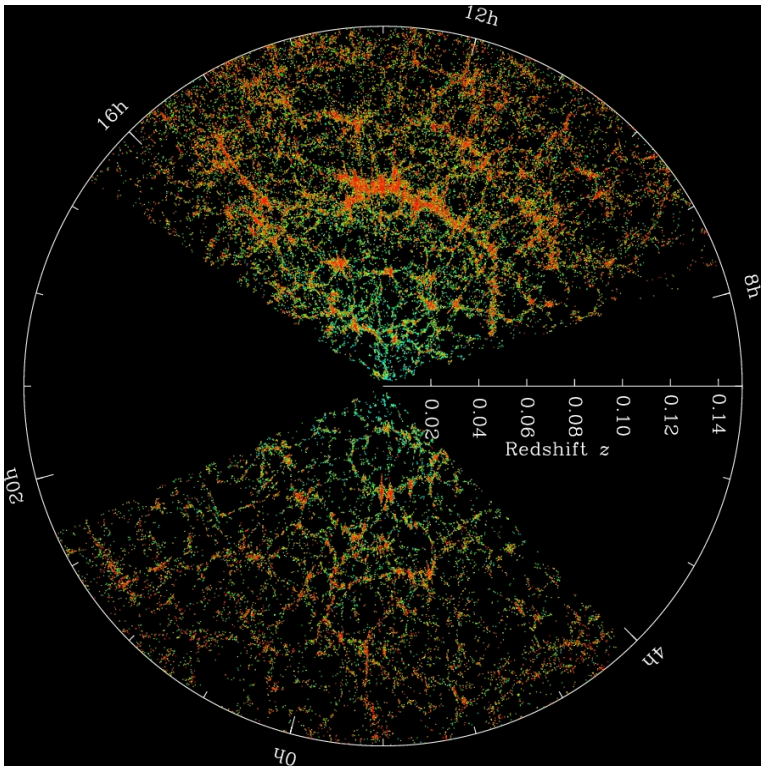

Figure 1.1: *A 2-d slice through the 3-dimensional map of the distribution of galaxies. The black regions represent regions that were not mapped due to galactic foreground. The points represent galaxies and older galaxies are shown in red. Image courtesy of the Sloan Digital Sky Survey.*

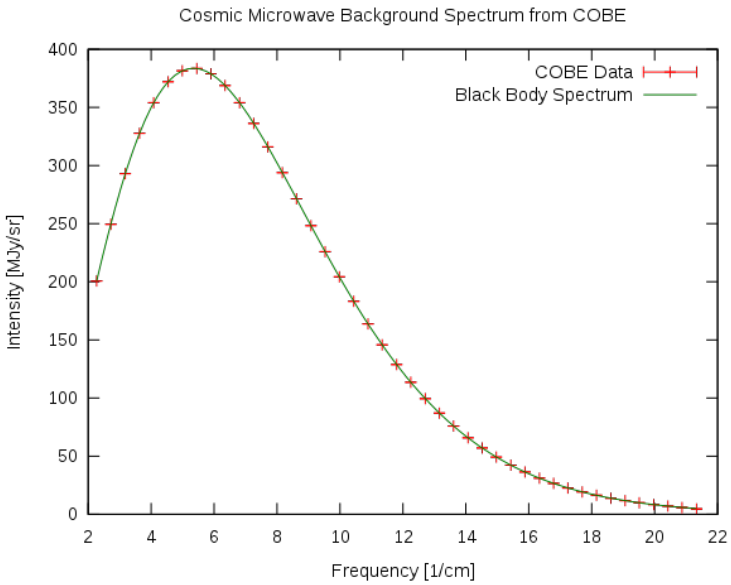

Figure 1.2: *The CMB spectrum as measured by the FIRAS instrument on COBE is the most precisely measured black body spectrum in nature. The observed data matches the theoretical blackbody curve very well. Image courtesy of NASA.*

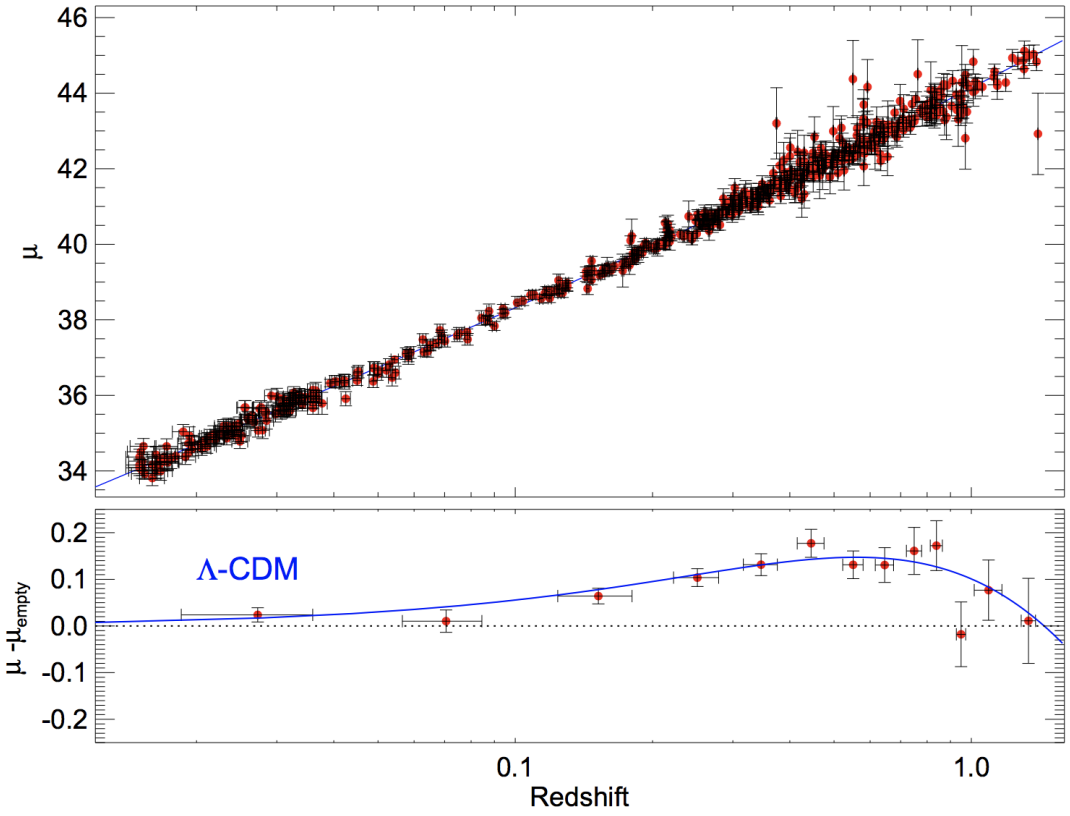

Figure 1.3: *The Hubble diagram of Type 1a supernovae correlating distance modulus (μ) vs. redshift. The distance to an empty universe model (μ_{empty}) is shown in the lower panel. The blue curve shows the expectation from the best fit ΛCDM model, i.e., 4.9% ordinary matter, 26.8% dark matter and 68.3% dark energy (cosmological constant) [9].*

Another profound discovery about the universe is the accelerating expansion of the late universe. The first compelling evidence for the late acceleration came in the late 1990's when two independent teams studying type 1a supernovae discovered that high-redshift SNe 1a were dimmer than expected [10, 11] implying the need for a cosmological constant (or more generally dark energy). This late acceleration of the universe has also been verified independently by CMB data from high multipole measurements using the South Pole Telescope (SPT) [12–14]. In terms of matter and energy, these observations imply that the universe is composed of 4.9% ordinary matter, 26.8% dark matter, which is indirectly detected by its gravitational pull on nearby matter and 68.3% dark energy, thought to be responsible for the accelerated expansion of the late universe [15]. General Relativity, the leading theory of gravity combined with the cosmological principle on large scales and the assumption that the universe is made up of a combination of standard model particles, cold dark matter and a cosmological constant gives rise to the ΛCDM model of the universe. The cosmological principle is the starting point for a set of solutions to Einstein's theory of General Relativity called *Friedmann Cosmologies* where the spacetime metric $g_{\mu\nu}$ is of the Friedmann-Lemaître-Robertson-Walker (FLRW) form.

1.2.1 The Einstein Field Equations

The ΛCDM model assumes that Einstein's General Relativity is the correct theory of gravity. This theory is well-tested on many scales [16]. The gravitational field equations can be derived by varying the Einstein-Hilbert action,

$$S_{\mathrm{EH}} = \int \left[\frac{1}{2}M_{\mathrm{pl}}^2(R - 2\Lambda) + \mathcal{L}_{\mathrm{M}}\right]\sqrt{-g}\,\mathrm{d}^4x, \tag{1.2}$$

where R is the Ricci scalar corresponding to the metric $g_{\mu\nu}$, $g = \det(g_{\mu\nu})$, Λ is the cosmological constant and where $\mathcal{L}_{\mathrm{M}}$ describes any matter fields that appear in the theory. Then using the principle of least action, one can find the Einstein field equations,

$$R_{\mu\nu} - \frac{1}{2}g_{\mu\nu}R + \Lambda g_{\mu\nu} = M_{\mathrm{pl}}^{-2}T_{\mu\nu}. \tag{1.3}$$

The spacetime curvature on the left-hand side (LHS) of the equation is coupled to the matter content of the unvierse via the energy-momentum tensor $T_{\mu\nu}$ on the right-hand side (RHS). In other words, the curvature of spacetime is directly related to the energy and momentum of whatever matter and radiation are present.

The predictions of General Relativity have been confirmed in all observations so far. Although there are many other physical theories of gravity that attempt to describe gravitation (for a thorough review, see Ref. [17]), GR is the simplest theory that is consistent with experimental data.

1.2.2 The FLRW Metric

The observation that the universe is homogeneous and isotropic on large scales implies that we can model the large scale geometry of the universe with a metric, $g_{\mu\nu}$, with homogeneous and isotropic spatial slices. This has become known as the Friedmann-Lemaître-Robertson-Walker (FLRW) metric,

$$\mathrm{d}s^2 = g_{\mu\nu}\mathrm{d}x^\mu \mathrm{d}x^\nu = -\mathrm{d}t^2 + a^2(t)\left[\frac{\mathrm{d}r^2}{1-kr^2} + r^2(\mathrm{d}\theta^2 + \sin^2\theta\,\mathrm{d}\phi^2)\right], \tag{1.4}$$

where k labels three possibilities for the spatial curvature; $k > 0$ for positive, $k = 0$ for flat and $k < 0$ for negative spatial curvatures. The scale factor $a(t)$ is a dimensionless function of coordinate time t and it increases for an expanding universe and decreases for a contracting one. $\{r, \theta, \phi\}$ are comoving spatial coordinates.

1.2.3 The Friedmann Equations

The FLRW metric analytically satisfies the Einstein field equations, Eq. (1.3), giving the Friedmann equations when the energy-momentum tensor $T_{\mu\nu}$ is similarly assumed to describe an isotropic and homogeneous perfect fluid. Perfect fluids have no viscosity and no heat flow and have an energy-momentum tensor:

$$T_{\mu\nu} = (\rho + p)u_\mu u_\nu + p g_{\mu\nu}, \tag{1.5}$$

where ρ is the energy density and p the pressure in the fluid rest frame and u^μ is the four-velocity of the fluid.

If we take $g_{\mu\nu}$ to be the FLRW metric, we can write down the elements of the Ricci tensor as well as the Ricci scalar. For example $R_{00} = -3\frac{\ddot{a}}{a}$ and $R_{11} = (\ddot{a}a + 2\dot{a}^2 + 2k)/(1 - kr^2)$. Next, we take $T_{\mu\nu}$ to be that of a perfect fluid and the fluid to be comoving with the expansion of the universe. Using the Ricci tensor and scalar on the left hand side of the Einstein field equations and the energy-momentum tensor on the right hand side in Eq. (1.3), and demanding component by component equality (because the Einstein field equations are in fact a set of equations governing each component of the curvature), we have two independent equations: the Friedmann equation (Eq. (1.6)) and the acceleration equation (Eq. (1.7)).

From these two independent equations, we can derive a third one, called the fluid equation or the continuity equation which also follows from the conservation equation $\nabla_\mu T^{\mu\nu} = 0$ which is a consequence of the Bianchi identity. Each non-interacting particles species 'A' with density ρ_A and pressure p_A obeys the fluid equation (Eq. (1.8)).

$$\left(\frac{\dot{a}}{a}\right)^2 = H^2 = \frac{\rho}{3M_{\rm pl}^2} - \frac{k}{a^2} + \frac{\Lambda}{3} \tag{1.6}$$

$$\frac{\ddot{a}}{a} = -\frac{1}{6M_{\rm pl}^2}(\rho + 3p) + \frac{\Lambda}{3} \tag{1.7}$$

$$\dot{\rho}_{\rm A} = -3\left(\frac{\dot{a}}{a}\right)(\rho_{\rm A} + p_{\rm A}) \tag{1.8}$$

$H \equiv \frac{\dot{a}}{a}$ is the Hubble parameter. The acceleration equation tells us that in the absence of Λ, the ΛCDM universe would be decelerating. As already mentioned earlier, this is against observational data. The ΛCDM model realises this late acceleration by making Λ a small positive value.

To solve the equations, one needs to specify the relationship between ρ and p, for a perfect fluid, i.e., the equation of state. Once the equation of state is specified, the above equations are all we need to describe the evolution of the universe. The equation of state parameter $\omega_{\rm A}$ is defined as $p_{\rm A} = \omega_{\rm A}\rho_{\rm A}$. The main fluids present in the ΛCDM model are baryons ($\omega_{\rm b} = 0$), radiation ($\omega_{\rm r} = \frac{1}{3}$) and Cold Dark Matter (CDM) ($\omega_{\rm CDM} = 0$) and dark energy with $\omega_\Lambda = -1$. The fluid equation gives the dynamics of these perfect fluids and when integrated, one obtains $\{\rho_{\rm b}, \rho_{\rm CDM}\} \propto a^{-3}$ and $\rho_{\rm r} \propto a^{-4}$.

1.2.4 The Cosmological Parameters

Using the Friedmann equation, the critical density of the universe is defined to be the density of a spatially flat universe and is given by $\rho_{\rm crit} = 3M_{\rm pl}^2H^2$. Dividing the Friedmann equation (Eq. (1.6)) by the critical density and re-arranging, one has

$$\Omega_{\rm tot} = \Omega_{\rm b} + \Omega_{\rm CDM} + \Omega_{\rm r} + \Omega_\Lambda = 1 - \Omega_{\rm k}, \tag{1.9}$$

where the density parameters are defined as $\Omega_{\rm A} = \frac{\rho_{\rm A}}{\rho_{\rm crit}}$, except for $\Omega_\Lambda = \frac{\Lambda}{3H^2}$ and $\Omega_{\rm k} = \frac{-k}{H^2a^2}$. The latest Planck 2018 results for these parameters are as follows [18]:

$$\Omega_{\rm b}h^2 = 0.02237 \pm 0.00015 \quad (68\%,\ \textit{Planck}\ \text{TT, TE, EE + lowE + lensing}) \tag{1.10}$$

$$\Omega_{\rm CDM}h^2 = 0.1200 \pm 0.0012 \quad (68\%,\ \textit{Planck}\ \text{TT, TE, EE + lowE + lensing}) \tag{1.11}$$

$$\Omega_\Lambda = 0.6847 \pm 0.0073 \quad (68\%,\ \textit{Planck}\ \mathrm{TT, TE, EE + lowE + lensing}) \tag{1.12}$$

where h is a dimensionless present value of the Hubble parameter defined as

$$H_0 = 100h\ \mathrm{km\ s^{-1}\ Mpc^{-1}}. \tag{1.13}$$

Presently, the best constraints on H_0 from Planck 2018 [18] are $H_0 = (67.4 \pm 0.5)\ \mathrm{km\ s^{-1}\ Mpc^{-1}}$. The present density of relativistic species is negligible compared to the other components ($\Omega_r h^2 \sim 4 \times 10^{-5}$) and so, altogether, the various components add up to give that Ω_{tot} is observationally consistent with unity and in fact,

$$\Omega_k = 0.0007 \pm 0.0019 \quad (68\%,\ \textit{Planck}\ \mathrm{TT, TE, EE + lowE + lensing + BAO}). \tag{1.14}$$

Within observational bounds, the universe is therefore flat. Although beyond the scope of our work, we note in passing that the above Planck constraints are obtained when one assumes ΛCDM cosmology. When the assumptions on the equation of state of dark energy are relaxed, it becomes hard to disentangle dark energy and curvature because degeneracies arise; see, for example, Clarkson *et al.* [19] and Witzemann *et al.* [20].

The cosmological parameters can also be determined from the large-scale structure of the universe. However, there are indications that there is a discrepancy between constraints estimated from either the CMB or the LSS. In particular, the LSS constraints imply more small scale structure than the constraints from the CMB (see, for example, Battye *et al.* [21] and Charnock *et al.* [22]).

1.2.5 Further Successes of the Hot Big Bang Model

The standard model of cosmology is spectacularly successful. It provides a reliable and vigorously tested accounting of the history of our universe from its early hot and dense state until today, about 13.8 billion years later. The discovery of the Cosmic Microwave Background radiation by Penzias and Wilson is perhaps, the most compelling observational evidence for the big bang model as it was the discovery of a predicted thermal imprint of the big bang. In addition to what we have discussed, in 1948, Alpher and Gamow[1] [26] argued that the big bang could create the observed abundances of the most common elements in the universe. Their calculations agreed with the observed helium abundance. The paper, still known as the alpha-

[1]Bethe didn't really contribute to the work; his name was added for humour.

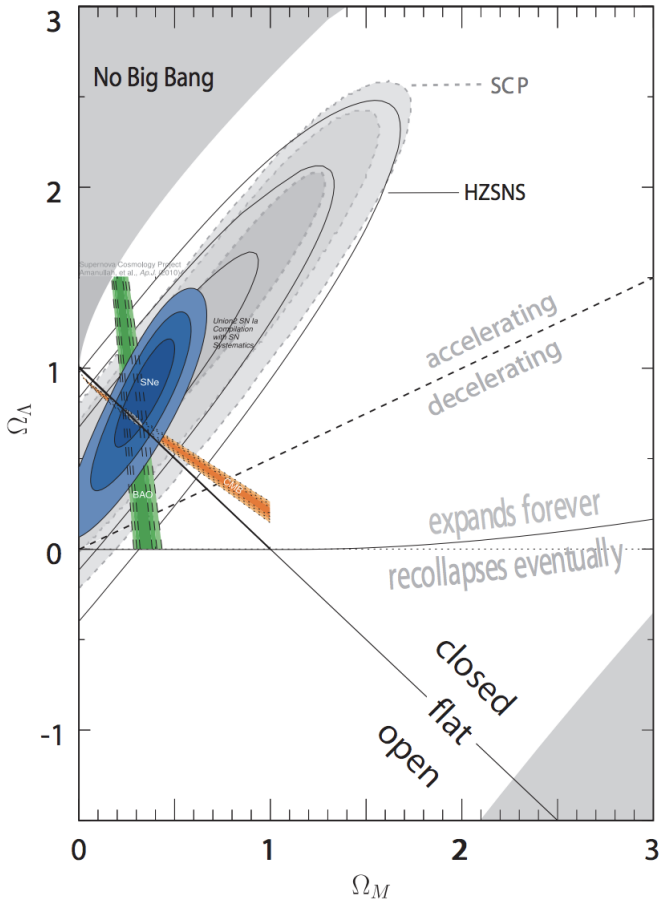

Figure 1.4: *Confidence level regions in the* $(\Omega_M, \Omega_\Lambda)$ *from CMB, BAO, SNe1a data where* $\Omega_M = \Omega_b + \Omega_{\text{CDM}}$*[10, 11, 23–25].*

beta-gamma paper, not only explained the origin of the most abundant elements in the universe, but was also the first support for the big bang model since the discovery of the Hubble's law (that distant galaxies are redshifted in proportion to their distance from us). While the original Alpher-Bethe-Gamow theory only worked for elements up to helium, subsequent improvements in the calculations showed that big bang nucleosynthesis, the production of elements heavier than the lightest isotope of hydrogen shortly after big bang, is consistent with observational constraints on all primordial elements [27].

The standard big bang model also provides a framework for understanding the formation of galaxies and other large-scale structures [28, 29]: Once the universe becomes matter dominated, primordial density inhomogeneities ($\frac{\delta\rho}{\rho} \sim 10^{-5}$) become gravitationally amplified and eventually collapse to form the structures we see today. Jeans was the first to point out that a fluid of self-gravitating particles is unstable to the growth of small inhomogeneities; this is known as Jeans instability [30, 31]. COBE confirmed the existence of these inhomogeneities in the CMB in spectacular fashion. In fact, COBE's measurements provided two key pieces of

evidence that supported the big bang theory of the universe: that the CMB has a near-perfect black-body spectrum, and that it has very small anisotropies [32].

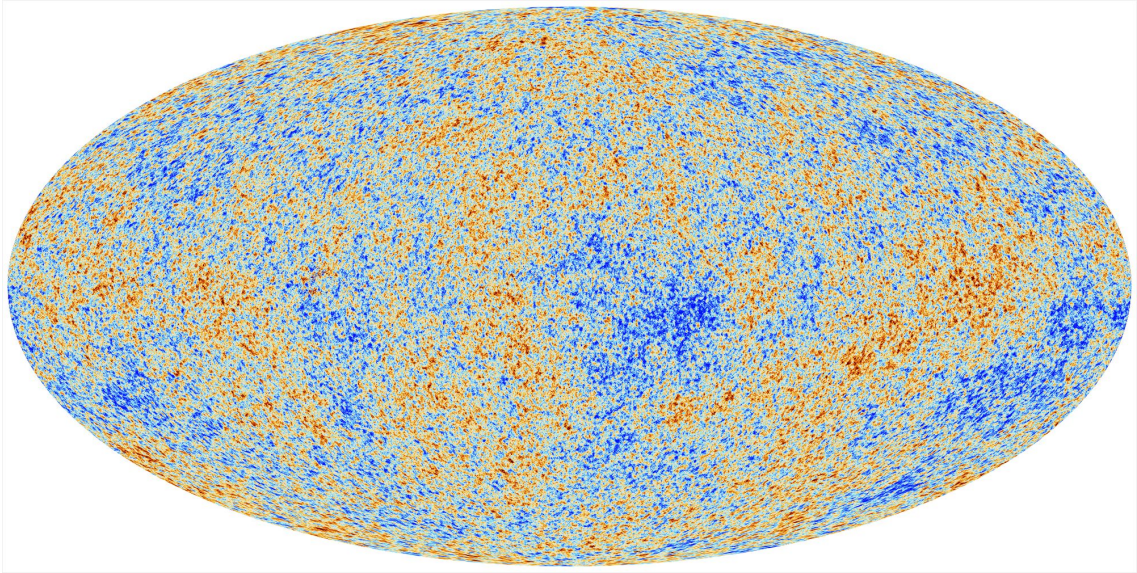

Figure 1.5: *The temperature anisotropies of the CMB as observed by Planck. The tiny temperature fluctuations correspond to regions of slightly different densities at very early times, representing the seeds of all structures in the universe today. Image credit: ESA.*

1.2.6 The Need for Inflation

Despite its numerous successes, the hot big bang model does not offer an explanation for the origin of the density perturbations that give rise to the observed large-scale structure. We will come back to this question later. Other non-trivial problems that plague the hot big bang model [7, 33, 34] are the horizon problem, the flatness problem and the monopole problem which we briefly describe below. Inflation, a period of accelerated expansion of the early universe, was introduced to solve these problems. Accelerated expansion of the FLRW universe implies $\ddot{a} > 0$ and this correlates with a shrinking comoving Hubble radius. Using Eq. (1.6) and Eq. (1.7), a shrinking comoving Hubble radius can be connected to the acceleration and pressure of the universe by

$$\frac{\mathrm{d}}{\mathrm{d}t}\left(\frac{1}{aH}\right) < 0 \Rightarrow \frac{\mathrm{d}^2 a}{\mathrm{d}t^2} > 0 \Rightarrow p < -\frac{\rho}{3}. \tag{1.15}$$

The Flatness Problem

Observations indicate that the universe is flat, i.e., it has exactly the required density of matter to be flat [35]. In other words, the universe is very close to critical density which corresponds to a density parameter $\Omega_{\mathrm{tot}} = 1$ (*cf.* Eq. (1.9) and Eq. (1.14)). This is a cosmological fine-tuning problem within the hot big bang model, i.e., the

matter and energy density of the universe appears to be fine-tuned to a very special value at early times and tiny deviations from that value would have extreme effects on observations. For the universe to be flat today, it means at earlier times, $\Omega_{\rm tot}$ must be extremely close to 1. In fact, one finds that [36, 37]

$$|\Omega_{\rm tot}(t_{\rm pl}) - 1| < 10^{-60} \tag{1.16}$$

where $t_{\rm pl} \sim 10^{-43}$ s is the Planckian time. Rewriting the Friedmann equation, Eq. (1.6) as:

$$|\Omega_{\rm tot} - 1| = \frac{|k|}{(aH)^2}, \tag{1.17}$$

we see that a decreasing Hubble radius as realised during inflation drives the universe to flatness and $\Omega_{tot} = 1$ becomes an attractor.

The Horizon Problem

The particle horizon, $D_H(t)$, is the maximum distance from which particles could have traveled to the observer since the beginning of the universe at time $t = t_i$ and is given by

$$D_H(t) = a(t)d_H(t), \qquad \text{where} \quad d_H(t) = \int_{t_i}^{t} \frac{\mathrm{d}t'}{a(t')}. \tag{1.18}$$

$d_H(t)$ is the comoving particle horizon. The photons in the CMB are last-scattered at the time of decoupling. The ratio of the comoving particle horizon at CMB decoupling, $d_H(t_{\rm dec})$, to the comoving particle horizon today, $d_H(t_0)$, is around 10^{-2} [38], implying that the causally connected regions at last scattering are much smaller than the horizon size today. In fact, the particle horizon size at the time of CMB last scattering corresponds to ~ 1 degree on the sky [7, 39] today and hence, ΛCDM implies that most parts that we observe in the CMB have never been in causal contact and have not communicated with each other before last scattering. The CMB comprises of $\sim 10^6$ causally disconnected regions [37]. Yet, we still observe an almost uniform temperature of the CMB, even for widely separated regions. The CMB is observed to be almost uniform with temperature fluctuations of characteristic size [40],

$$\frac{\delta T}{T} \approx 10^{-5}. \tag{1.19}$$

Because no signals can propagate faster than light, no causal physical processes can be responsible for such an unnaturally fine-tuned matter distribution. Inflationary theory allows for a solution to the horizon problem by suggesting that prior to inflation, a patch of the universe small enough to achieve thermalization can expand by a huge amount such that it is larger than the size of our presently observable universe. Inflation then expanded a small causally connected universe rapidly, freez-

ing in these physical properties. Hence, even if now distant areas in the sky appear causally disconnected, they were causally connected in the past.

The Monopole Problem

Grand Unified Theories (GUT) in particle physics seek to merge the weak, electromagnetic and strong forces into one and predict that at high temperatures (like the early universe), a number of heavy stable particles such as magnetic monopoles should be copiously produced [41, 42]. Such particles would be non-relativistic for almost all of the universe's history, giving them plenty of time to come to dominate over radiation. However, no such particles have been detected yet, placing stringent limits on the density of relic particles in the universe. It was suggested that the reason why we cannot find these particles is because inflation dilutes away any relic particles as their density is reduced by the rapid expansion. Also, given that we have to make sure that such particles are not produced again after inflation, it means that inflation has to happen at a temperature lower than the temperature at which monopoles can be produced.

It turns out that in order to solve the problems we've just discussed, the universe needs to expand about e^{60} times during inflation [37, 38]. Aside from solving the problems of the hot big bang, inflation has proved to be the most successful at predicting the properties of the anisotropies observed in the CMB. Actually, the interest in inflationary theory has persisted because of its ability to explain the origin of density perturbations in the early universe which are imprinted on the CMB. Microscopic quantum fluctuations get stretched by the inflationary expansion to macroscopic scales, larger than the physical horizon during inflation. As inflation continues, new quantum fluctuations get created, resulting in additional smaller-scale fluctuations superimposed on top of the large-scales ones. This goes on until inflation ends, creating a pattern of fluctuations and random regions of all sizes that have overdense and underdense energy densities. This spectrum of overdensities and underdensities result in an ever-so-slightly colder and hotter regions, in terms of temperature, of the CMB.

Finally, it is remarkable to note that inflation can explain both the (almost) isotropy of the CMB and the small level of anisotropy as well. Inflation is not just a theory that happened to restore the big bang or solve the problems known in the past, inflation made quantitative predictions about the statistics of the CMB anisotropies (or more striclty, the statistics of the curvature perturbation) and observations have confirmed it, including WMAP [43, 44], SDSS [45, 46], 2dF [47] and Planck [48].

Having given a brief overview of ΛCDM and why inflation is needed as well as a brief outline of its success, in the next chapter we begin to develop the quantitative theory of inflation.

2 Classical Dynamics of Inflation

In this chapter, we present a first-principles introduction to the classical dynamics of slow-roll inflation. We describe the necessary conditions for successful inflation compatible with observations and what those conditions mean for the potential of the inflaton field.

"Aux grands maux, les grands remèdes."
Desperate times, desperate measures.

—French proverb

2.1 The Physics of Inflation

During inflation, because of the expansion of space, it is important to keep track of physical lengths. Density perturbations are normally identified by their comoving wavenumber k. A scale is defined to be equal to the horizon when $k = aH$. Note that strictly speaking, we should be referring to the Hubble radius, but it is common practice to interchange 'horizon' and 'Hubble radius'. During inflation, $\frac{1}{aH}$ decreases; therefore a fixed comoving scale k^{-1} may begin its evolution considerably smaller than $\frac{1}{aH}$, and by the end of inflation be considerably larger. Thus, the scale crosses the horizon (horizon exit) during inflation, corresponding to $k = aH$. Causal physics cannot act on superhorizon scales, hence the perturbations 'freeze'. After the end of inflation, the comoving Hubble length starts to increase again and eventually the perturbations re-enter the horizon (horizon re-entry) [34, 49].

In § 1.2.6, we saw that negative pressure is needed for inflation to occur. Now we will consider how such a pressure is realised in nature using scalar fields. A scalar field associates a value to every point in space and has the special property that they can have negative pressure. The Higgs is the only scalar field that has been detected so far [50] in nature but scalar fields are ubiquitous in theories of high energy physics beyond the standard model [51, 52]. In the inflationary context, the inflaton field is a hypothetical scalar field that is theorised to have driven cosmic inflation in the very early universe. However, some have argued that it is possible

that no new field is necessary; a modified Higgs field could act as the inflaton (see for example, [53, 54]). This scenario however, more commonly known as Higgs inflation, requires that there is a non-minimal coupling between the Higgs field and the spacetime curvature. The inflationary action we will define below in Eq. (2.1) is minimally coupled to gravity in the sense that there is no direct coupling between the scalar field and the metric. A non-minimal coupling would mean that instead of the $\frac{1}{2}R$ term in the action, we have something like $\frac{1}{2}\xi\phi^2 R$ (see for example, [55]). Moreover, there are various possibilities for getting inflationary expansion. Many phenomenological models have been proposed with different predictions and different theoretical motivations, for example, inflation with non-canonical kinetic terms, multifield inflation, and inflation with modified gravity. In our discussion below, however, we will work with single field inflation to introduce the key ideas and calculations for the power spectrum and bispectrum. In Chapter 4, we will address the question of how to do calculations in a multiple field setting. Having discussed how the theory of inflation offers a very neat explanation for the homogeneity and flatness of our universe and for the microphysical origin of the density perturbations in the CMB, we now turn to the physical mechanism of inflation.

In Guth's seminal paper on inflation [56], now known as *Old Inflation*, where he proposed inflation to explain the non-detection of magnetic monopoles, the very early universe was trapped in a metastable state which it could only decay out of through the process of bubble nucleation via quantum tunnelling (see Fig. 2.1). The basic idea is that the infant universe undergoes a *phase transition* at high energies. Bubbles of true vacuum spontaneously form in the sea of false vacuum. However, even then, it was recognised by Guth that his model was problematic because the model did not reheat properly. Radiation could only be generated in collisions between bubble walls, but if inflation were to last long enough to solve the problems of the hot big bang, the bubbles won't be able to 'meet' as the universe is expanding too fast.

2.1.1 Slow-roll Inflation

The bubble collision problem was solved by A. Linde [58] and also by A. Albrecht and P. Steinhardt [59] independently. Their model is now known as *New Inflation* or *Slow-roll Inflation*. In this model, instead of quantum tunnelling to the true vacuum, the value of the field changes slowly and the potential energy gradually decreases in a process often described as the field 'slowly rolling down' a potential hill. We need to study the dynamics of a scalar field to see how this leads to inflation.

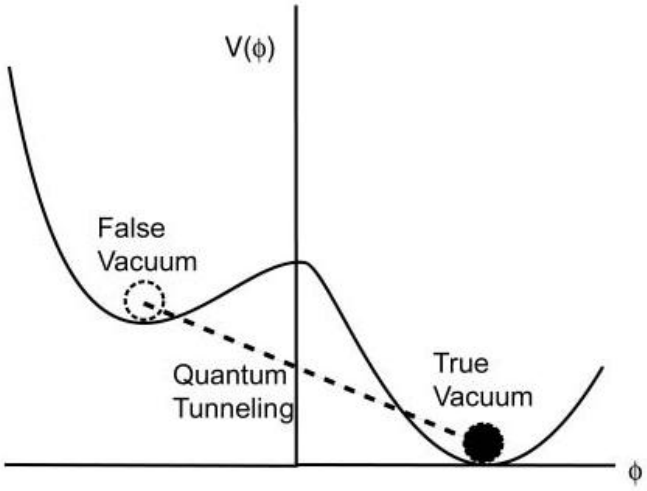

Figure 2.1: *The Old Inflation model. The Inflaton is a scalar field that is responsible for cosmic inflation in the very early universe and has a self-interacting potential, $V(\phi)$. ϕ is trapped in a false minimum and is freed from this minimum when quantum tunelling is allowed to occur. Inflation ends when ϕ tunnels through the barrier and rolls down to $V(\phi) = 0$ [57].*

Inflation with a single scalar field

The general action for a scalar field in curved spacetime is [49, 60]

$$S = \int \mathrm{d}^4x\sqrt{-g}\left(\frac{1}{2}R - \frac{1}{2}g^{\mu\nu}\partial_\mu\phi\,\partial_\nu\phi - V(\phi)\right) = S_{\,\mathrm{EH}} + S_\phi, \tag{2.1}$$

where S_{EH} is the Einstein-Hilbert action and $S_\phi = \int \mathrm{d}^4x\sqrt{-g}\left(-\frac{1}{2}g^{\mu\nu}\partial_\mu\phi\,\partial_\nu\phi - V(\phi)\right)$ is the action of a scalar field with canonical[1] kinetic term. Varying this action with respect to the metric, we get the energy-momentum tensor and we find

$$T^\phi_{\mu\nu} = \partial_\mu\phi\,\partial_\nu\phi - g_{\mu\nu}\left(\frac{1}{2}\partial^\sigma\phi\,\partial_\sigma\phi + V(\phi)\right). \tag{2.2}$$

The field equation of motion is given by varying the action with respect to the scalar field,

$$\frac{\delta S_\phi}{\delta\phi} = \frac{1}{\sqrt{-g}}\partial_\mu\left(\sqrt{-g}\partial^\mu\phi\right) + V_{,\phi} = 0, \tag{2.3}$$

where $V_{,\phi} = \frac{\partial V}{\partial\phi}$.

Now, if we take $g_{\mu\nu}$ to be the FLRW metric and take ϕ to be homogeneous, i.e., $\phi(t, \mathbf{x}) = \phi(t)$, the energy-momentum tensor takes the form of a perfect fluid, giving

$$\rho_\phi = \frac{1}{2}\dot{\phi}^2 + V(\phi) \tag{2.4}$$

[1]The action has a canonical kinetic term if: $L_\phi = X - V(\phi)$ where $X = \frac{1}{2}g^{\mu\nu}\partial_\mu\phi\,\partial_\nu\phi$. We have also set $M_{\mathrm{pl}} = 1$. The action has a non-canonical kinetic term if: $L_\phi = F(\phi, X) - V(\phi)$ where $F(\phi, X)$ is some function of the inflaton field and its derivatives. L is the *Lagrangian*.

and

$$p_\phi = \frac{1}{2}\dot{\phi}^2 - V(\phi). \tag{2.5}$$

Eq. (1.6) becomes:

$$H^2 = \frac{1}{3M_{\rm pl}^2}\left(\frac{1}{2}\dot{\phi}^2 + V(\phi)\right). \tag{2.6}$$

The equation of state is given by

$$\omega_\phi = \frac{p_\phi}{\rho_\phi} = \frac{\frac{1}{2}\dot{\phi}^2 - V(\phi)}{\frac{1}{2}\dot{\phi}^2 + V(\phi)}. \tag{2.7}$$

From Eq. (2.7), we can see that if $V(\phi)$ dominates over the kinetic energy or equivalently if $\dot{\phi}^2 \ll V(\phi)$, then $\omega_\phi < 0$, implying *negative pressure*. As we know from Eq. (1.15), $\omega_\phi < -\frac{1}{3}$ means accelerating expansion. Therefore, a scalar field can lead to inflation provided the potential is flat enough, as the scalar field would then be expected to 'roll slowly' and have negligible kinetic energy. During inflation, a grows exponentially and the potential $V(\phi)$ evolves slowly (flat potential) which means H is approximately constant.

A subtle point here is that we have set $k = 0$ since inflation drives the universe to flatness anyway. Also, $\Lambda = 0$. The dynamics of the homogeneous scalar field is determined by the Klein-Gordon equation (Eq. (2.3)),

$$\ddot{\phi} + 3H\dot{\phi} + V_{,\phi} = 0, \tag{2.8}$$

and Eq. (2.6). The term $3H\dot{\phi}$ acts as a damping term, slowing the evolution of the field.

As we will see quantitatively in § 2.1.2, to achieve slow-roll inflation this damping term must balance the driving term from the potential. The way we usually picture slow-roll inflation is shown in Fig. 2.2 where the red ball indicates the value ϕ the field takes. The inflaton 'rolls down its potential'. The kinetic energy of the field is given by $\frac{1}{2}\dot{\phi}^2$ and its potential energy is $V(\phi)$. Inflation occurs when $\dot{\phi}^2 \ll V(\phi)$, i.e., when $V(\phi)$ dominates. The CMB anisotropies are generated by quantum fluctuations in the ϕ field about 60 e-folds before the end of inflation, shown by $\phi_{\rm CMB}$ in the diagram. Inflation ends at $\phi_{\rm end}$ when $\frac{1}{2}\dot{\phi}^2$ becomes comparable to $V(\phi)$. ϕ then oscillates when it reaches the potential minimum.

If there is some coupling between the inflaton and other fields, then these oscillations will be damped and the energy will be dumped into these other fields. This

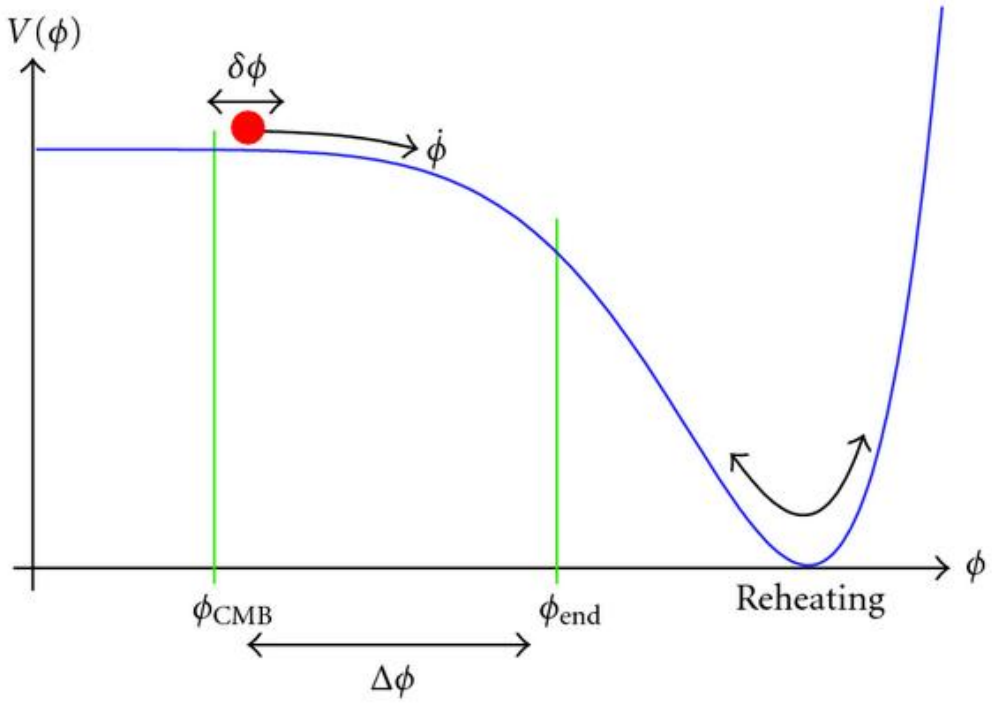

Figure 2.2: *A toy scenario for the dynamics of the scalar field during inflation. During the flat part of the potential, the universe expands exponentially [49].*

is the *reheating* epoch where the scalar field decays into particles which are either the ones that we see today or some intermediate particles which will decay later on. We will review reheating in Chapter 6.

During inflation, the quantum fluctuations in the inflaton field were stretched to macroscopic sizes. Upon leaving the horizon, no causal physics can affect the perturbations and they then re-enter the horizon at the later stages of radiation and matter domination, and thus set the initial conditions for structure formation via gravitational instability. The fluctuations seen in the CMB were generated by quantum fluctuations about 60 e-folds before the end of inflation. The number 60 comes from the fact that one needs $\sim$ 50 - 60 e-folds of inflation in order to solve the horizon problem.

2.1.2 Slow-roll Conditions

The standard approximation technique for analysing inflation is the slow-roll approximation [49, 60]. As the scalar field is slow-rolling, $\frac{1}{2}\dot{\phi}^2$ is small compared to $V(\phi)$ and Eq. (2.6) becomes:

$$H^2 \approx \frac{1}{3M_{\rm pl}^2} V(\phi). \tag{2.9}$$

For accelerated expansion to occur for a sufficient amount of time, the second time derivative of ϕ has to be small and Eq. (2.8) becomes:

$$|\ddot{\phi}| \ll |3H\dot{\phi}|, |V_{,\phi}|. \tag{2.10}$$

In the limit of zero kinetic energy, the energy-momentum tensor would be that of a cosmological constant and the expansion would be exponential (de Sitter expansion) and everlasting. For a long, finite stage of acceleration, we must require that the first slow-roll condition, $\frac{1}{2}\dot{\phi}^2 \ll V(\phi)$, holds over an extended period of time. Since the evolution of the scalar field is given by a second-order equation, the above condition could apply instantaneously but not for an extended period. If we want the first slow-roll condition to hold over an extended period, we must impose that the time-derivative of this condition also holds (see Eq. (2.10)). These two conditions can be expressed as

$$\epsilon < 1 \qquad \& \qquad |\eta| < 1 \tag{2.11}$$

where

$$\epsilon = -\frac{\dot{H}}{H^2} = -\frac{\mathrm{d}}{\mathrm{d}\mathcal{N}}(\ln H) \tag{2.12}$$

and

$$\eta = -\frac{\ddot{\phi}}{H\dot{\phi}} = \epsilon - \frac{1}{2\epsilon}\frac{\mathrm{d}\epsilon}{\mathrm{d}\mathcal{N}}. \tag{2.13}$$

ϵ and η are called the *Hubble Slow-roll parameters*. $\mathcal{N}$ is the number of e-folds of inflationary expansion, $d\mathcal{N} = d\ln a$. The slow-roll conditions may also be expressed as conditions on the shape of the inflationary potential and hence, we have the *potential slow-roll parameters*, ϵ_v and η_v,

$$\epsilon_v = \frac{M_{\mathrm{pl}}^2}{2}\left(\frac{V_{,\phi}}{V}\right)^2 \tag{2.14}$$

$$\eta_v = M_{\mathrm{pl}}^2 \frac{V_{,\phi\phi}}{V}. \tag{2.15}$$

In the slow-roll approximation, the Hubble and potential slow-roll parameters are related as

$$\epsilon \approx \epsilon_v, \qquad \eta \approx \eta_v - \epsilon_v. \tag{2.16}$$

And in the slow-roll regime,

$$\epsilon_v \ll 1 \qquad \& \qquad |\eta_v| \ll 1. \tag{2.17}$$

Violation of the slow-roll conditions results in the end of inflation. End of inflation $\iff \epsilon(\phi_{\mathrm{end}}) = 1 \iff \epsilon_v(\phi_{\mathrm{end}}) \approx 1$.

The slow-roll formulation is useful because it allows us to calculate quantities such as the number of e-folds of accelerated expansion undergone by the universe analytically,

$$\mathcal{N}(\phi) = \int_{\phi_{\rm end}}^{\phi} \frac{\mathrm{d}\phi}{\sqrt{2\epsilon}} \approx \int_{\phi_{\rm end}}^{\phi} \frac{\mathrm{d}\phi}{\sqrt{2\epsilon_v}}. \tag{2.18}$$

Moreover, we will see that the expressions for observational signatures of inflation can often be written in terms of the slow-roll parameters. The observational signatures are the statistics of perturbations produced by inflation to which we now turn our attention.

3 Quantum Fluctuations During Inflation

In this chapter, we provide the calculations for the scalar and tensor power spectra in the single field case. We then follow Maldacena's work and compute the three-point statistics in the single field case. We end the chapter by looking at some observational constraints on inflation.

"The career of a young theoretical physicist consists of treating the harmonic oscillator in ever-increasing levels of abstraction."

—Sidney Coleman

3.1 The Cosmological Perturbation Theory

In Chapter 2, we considered the classical dynamics of inflation which solves the problems of the hot big bang. The quantum theory of inflation, on the other hand, provides an explanation for the primordial temperature anisotropies observed in the CMB and the origin of the large-scale structure (LSS). Quantum fluctuations of the inflaton field (other fields can also contribute) seed the perturbations in the local density after inflation which then give rise to the inhomogeneities in the CMB and eventually lead to the LSS. It is interesting to note that inflation was not engineered to generate these primordial perturbations, rather it was found only after the initial theory that as a result of considering inflation quantum mechanically, one also finds a way to explain the origin of the perturbations.

Since during inflation, the universe is close to homogeneous, one can use cosmological perturbation theory [61–63]. We can think of this as superimposing small fluctuations on a homogeneous background [33, 49, 64]. Therefore, we can decompose all quantities $X(t, \mathbf{x})$ into a homogeneous background, $\bar{X}(t)$ that depends only on cosmic time and a spatially dependent perturbation. For example,

$$\phi(t, \mathbf{x}) = \bar{\phi}(t) + \delta\phi(t, \mathbf{x}), \tag{3.1}$$

and

$$g_{\mu\nu}(t, \mathbf{x}) = \bar{g}_{\mu\nu}(t) + \delta g_{\mu\nu}(t, \mathbf{x}) \tag{3.2}$$

where the background metric is the FLRW metric. The inhomogeneous universe contains perturbations both of the matter content and of the spacetime metric. In principle, the symmetric 4×4 tensor $\delta g_{\mu\nu}(t, \mathbf{x})$ has ten degrees of freedom which can be classified according to their behaviour under (three dimensional) spatial rotations as Scalars (S), Vectors (V) and Tensors (T) [34]. The vector modes will be neglected as they have decaying solutions. Scalar fluctuations give rise to density perturbations and tensor fluctuations lead to gravitational waves, an important prediction of inflation. What makes the SVT-decomposition so powerful is the fact that the Einstein equations for scalars, vectors and tensors do not mix at linear order and can therefore be treated separately [33, 49]. The symmetries possessed by the spatially flat homogeneous and isotropic background spacetime allow us to decompose the metric and matter perturbations into independent scalar, vector and tensor components. This simplifies the study of cosmological perturbations considerably.

Before we proceed any further, we have to address an important subtlety. One of the difficulties of cosmological perturbation theory is that there is no preferred coordinate system at the perturbed level and therefore no unique way of describing the perturbations. A coordinate system is described by the *slicing* and *threading* of spacetime [65], i.e., by foliating 4-d spacetime into spatial hypersurfaces, each with a constant time t. The metric perturbations depend on our choice of coordinates known as the 'gauge choice'. In particular, when we write down the perturbed metric, we implicitly chose a specific time slicing of the spacetime and defined specific spatial coordinates on these time slices. Making a different choice of coordinates can change the values of the perturbation variables. This leads to spurious degrees of freedom if all ten are treated independently [66]! To avoid this problem, we need to consider the complete set of perturbations, i.e., both the matter $T_{\mu\nu}$ perturbations and the metric $g_{\mu\nu}$ perturbations. The metric perturbations enter the Einstein tensor $G_{\mu\nu}$ and thus the Einstein Field Equations link the metric and matter perturbations. Also, we have to study gauge-invariant combinations of perturbations as these are independent of one another [49, 64]. Furthermore, our choice of gauge invariant variables is not unique. In fact, one is free to choose between numerous possible gauges; the choice is made for practical reasons.

Metric and Matter Perturbations

We study perturbations to the homogeneous background spacetime and the stress-energy of the universe. Note that inflation drives the universe to flatness which is why we take the flat FLRW metric to be the background metric.

Metric ($g_{\mu\nu}$) **Perturbations** [49]: The most general first-order perturbation to a spatially flat FLRW metric is [49, 67]:

$$\mathrm{d}s^2 = -(1+2\Phi)\mathrm{d}t^2 + 2a(t)B_i\mathrm{d}x^i\mathrm{d}t + a^2(t)[(1-2\Psi)\delta_{ij} + E_{ij}]\mathrm{d}x^i\mathrm{d}x^j \tag{3.3}$$

In real space, the SVT decomposition of the metric perturbations in Eq. (3.3) is

$$B_i \equiv \partial_i B - S_i, \qquad \text{where } \partial^i S_i = 0, \tag{3.4}$$

and

$$E_{ij} = 2\partial_{ij}E + \partial_i F_j + \partial_j F_i + h_{ij} \qquad \text{where } \partial^i F_i = 0, \;\; h^i_i = \partial^i h_{ij} = 0. \tag{3.5}$$

The vector perturbations S_i and F_i are not produced during inflation and we therefore ignore vector perturbations.

Matter (T^μ_ν) **Perturbations** [49]: The perturbed energy-momentum tensor[1] has the following entries:

$$T^0_0 = -(\bar{\rho} + \delta\rho) \tag{3.6}$$

$$T^0_i = (\bar{\rho} + \bar{p})av_i \tag{3.7}$$

$$T^i_0 = -(\bar{\rho} + \bar{p})(v^i - B^i)/a \tag{3.8}$$

$$T^i_j = \delta^i_j(\bar{p} + \delta p) + \Sigma^i_j \tag{3.9}$$

3.1.1 Scalars and Tensors

As previously stated, we will only work with the scalar and tensor modes as vector perturbations are not created by inflation. The scalar fluctuations are what give rise to the density fluctuations and the tensor fluctuations produce gravitational waves [33, 49]. Therefore, we can now work with the scalar perturbations and the tensor perturbations separately.

Scalar Perturbations

Scalar fluctuations change under a coordinate transformation. Therefore, in this case, we have to work with gauge-invariant variables only. Two such important gauge-invariant scalar quantities formed from combinations of matter and metric perturbations are:

[1] The energy-momentum tensor T^μ_ν consists of density ρ with perturbation $\delta\rho(t,\mathbf{x}) = \rho(t,\mathbf{x}) - \bar{\rho}(t)$, pressure p with perturbation $\delta p(t,\mathbf{x}) = p(t,\mathbf{x}) - \bar{p}(t)$, four-velocity u^μ with $g_{\mu\nu}u^\mu u_\nu = -1$ and anisotropic stress Σ^μ_ν with $\Sigma^{\mu\nu}u_\nu = \Sigma^\mu_\mu = 0$.

1) The *curvature perturbation on uniform density hypersurfaces*,

$$-\zeta = \Psi + \frac{H}{\dot{\bar{\rho}}}\delta\rho \;\approx\; \Psi + \frac{H}{\dot{\bar{\phi}}}\delta\phi \quad in\ slow-roll\ inflation. \tag{3.10}$$

Geometrically, ζ measures the spatial curvature of constant density hypersurfaces. For adiabatic initial conditions, i.e., when the entropy perturbation vanishes[2],

$$\delta p_{en} \equiv \delta p - \frac{\dot{\bar{p}}}{\dot{\bar{\rho}}}\delta\rho = 0, \tag{3.11}$$

ζ remains constant outside the horizon. In this chapter, we only study single field inflation where the condition in Eq. (3.11) is always satisfied. Therefore, in single field inflation, the perturbation $\zeta_{\mathbf{k}}$ does not evolve outside the horizon where $k \ll aH$ and $k = \frac{2\pi}{\lambda}$.

2) The *comoving curvature perturbation*,

$$\mathcal{R} = \Psi - \frac{H}{\bar{\rho}+\bar{p}}\delta q \;=\; \Psi + \frac{H}{\dot{\bar{\phi}}}\delta\phi \quad in\ slow-roll\ inflation \tag{3.12}$$

where δq is the scalar part of the 3-momentum density (see Eq. (3.7)) $T^0_i = \partial_i \delta q$ and in slow-roll inflation, $T^0_i = -\dot{\bar{\phi}}\partial_i\delta\phi$. Geometrically, $\mathcal{R}$ measures the spatial curvature of comoving (or constant ϕ) hypersurfaces. The linearised Einstein equations relate ζ and $\mathcal{R}$ by

$$-\zeta = \mathcal{R} + \frac{k^2}{(aH)^2}\frac{2\bar{\rho}}{3(\bar{p}+\bar{\rho})}\Psi_B \tag{3.13}$$

where Ψ_B is one of the Bardeen potentials [68]. Hence, ζ and $\mathcal{R}$ are equal on super-horizon scales, *i.e*, when $k \ll aH$ and during slow-roll inflation. Their amplitude is not affected by the unknown physical properties of the universe shortly after the end of inflation. Actually, we know very little about the reheating phase of the universe and it is because ζ (or $\mathcal{R}$) remains constant that we are able to obtain predictions for single field inflation. After inflation ends, the comoving horizon grows and eventually all fluctuations will re-enter the horizon. After re-entering the horizon, $\mathcal{R}$ or ζ determines the perturbations in the density, resulting in the observed CMB anisotropies and the LSS. We can choose to study the correlation function of either $\mathcal{R}$ or ζ because their correlation functions are the same at horizon crossing, *i.e*, at $k = aH$ and are conserved on superhorizon scales. The idea here is that by computing the power spectrum of $\mathcal{R}$ (or ζ) at horizon crossing, we will have a measure of the primordial scalar fluctuations. Note that in this review, we will follow the definitions and conventions as used in Ref. [49].

We define the power spectrum as follows:

[2]The definition of δp_{en} is gauge-invariant.

$$\langle \mathcal{R}_k \mathcal{R}_{k'} \rangle = (2\pi)^3 \delta^3(\mathbf{k}+\mathbf{k}') P_{\mathcal{R}}(k), \qquad \mathcal{P}_{\mathcal{R}}(k) = \frac{k^3}{2\pi^2} P_{\mathcal{R}}(k) \tag{3.14}$$

where $\langle \mathcal{R}_k \mathcal{R}_{k'} \rangle$ is the ensemble average of the fluctuations. According to the ergodic theorem [34], the ensemble average is equal to the volume average if the volume is large enough. $\mathcal{P}_{\mathcal{R}}(k)$ is the dimensionless power spectrum. The normalisation of the dimensionless power spectrum is chosen such that the variance of $\mathcal{R}$ is $\langle \mathcal{R}\mathcal{R} \rangle = \int_0^\infty \mathcal{P}_{\mathcal{R}}(k)\, \mathrm{d}\ln k$. Next, we define the scalar spectral index n_s, which measures the scale dependence of the power spectrum, as:

$$n_s - 1 = \frac{\mathrm{d}\ln \mathcal{P}_{\mathcal{R}}}{\mathrm{d}\ln k}. \tag{3.15}$$

If $n_s = 1$, it means the power spectrum does not depend on scale. We can also define the running of the spectral index by:

$$\alpha_s \equiv \frac{\mathrm{d}\, n_s}{\mathrm{d}\ln k}. \tag{3.16}$$

Sometimes, it is useful to express the power spectrum in terms of a power law in the form of:

$$\mathcal{P}_{\mathcal{R}} = A_s(k_*) \left(\frac{k}{k_*}\right)^{n_s(k_*)-1+\frac{1}{2}\alpha_s(k_*)\ln\left(\frac{k}{k_*}\right)} \tag{3.17}$$

where A_s is the amplitude of the spectrum and k_* is an arbitrary reference scale. In single-field inflation with a canonical kinetic term, the spectrum is predicted to be close to Gaussian [69, 70] and if $\mathcal{R}$ is Gaussian, then the power spectrum contains all the statistical information. Non-gaussianity can be significant in multifield inflation or in single field models with non-trivial kinetic terms and/or violation of the slow-roll conditions (see, for example [71–74]).

Tensor Perturbations

Tensor perturbations are gauge-invariant and hence we do not need to find a gauge-invariant variable in this case. We can compute the power spectrum of the amplitude of the gravitational waves, i.e., h. The gravitational waves are usually defined as the two independent components (or degrees of polarization) of the traceless transverse 3x3 tensor h_{ij}, such that the tensor metric perturbations are

$$\mathrm{d}s^2 = -\mathrm{d}t^2 + a^2(t)[\delta_{ij} + h_{ij}]\mathrm{d}x^i \mathrm{d}x^j \tag{3.18}$$

where $h_{ij,i} = h^i_i = 0$ (transverse) and $\delta^{ij} h_{ij} = 0$ (traceless). We have two possible polarisation states, i.e., $h \equiv h^+, h^\times$ and hence the power spectrum is defined as:

$$\langle h_k h_{k'} \rangle = (2\pi)^3 \delta^3(\mathbf{k}+\mathbf{k}') P_h(k), \qquad \mathcal{P}_h(k) = 2\Delta_h^2 = \frac{k^3}{\pi^2} P_h(k) \tag{3.19}$$

The tensor power spectrum is the sum of the power spectra of the two polarisation states. Similar to what we did for the scalar perturbations, we can define a tensor spectral index:

$$n_t = \frac{\mathrm{d}\ln \mathcal{P}_h}{\mathrm{d}\ln k}. \tag{3.20}$$

This means we can express the power spectrum as a power law:

$$\mathcal{P}_h = A_t(k_*)\left(\frac{k}{k_*}\right)^{n_t(k_*)} \tag{3.21}$$

where A_t is the amplitude and k_* is an arbitrary reference scale.

3.2 Computing $\mathcal{P}_\mathcal{R}(k)$ and $\mathcal{P}_h(k)$

Having defined the relationship between $\mathcal{P}_\mathcal{R}$ & $P_\mathcal{R}(k)$ and $\mathcal{P}_h$ & $P_h(k)$, it is now a question of actually computing $P_\mathcal{R}(k)$ and $P_h(k)$ [33, 49]. Computing $P_\mathcal{R}(k)$ and $P_h(k)$ from first principles is non-trivial. A summary of the computational strategy is given below, for scalar and tensor perturbations separately:

Computing $\mathcal{P}_\mathcal{R}(k)$

The metric scalar perturbations (*cf.* Eq. (3.3)) are,

$$\mathrm{d}s^2 = -(1+2\Phi)\mathrm{d}t^2 + 2a(t)B_{,i}\mathrm{d}x^i dt + a^2(t)[(1-2\Psi)\delta_{ij} + 2E_{,ij}]\mathrm{d}x^i\mathrm{d}x^j, \tag{3.22}$$

where $B_{,i} = \partial_i B$ and $E_{,ij} = \partial_{ij}E$. We choose the following gauge for the dynamical fields g_{ij} and ϕ:

$$\delta\phi = 0, \qquad g_{ij} = a^2[(1-2\mathcal{R})\delta_{ij} + h_{ij}], \qquad \partial_i h_{ij} = h^i_i = 0. \tag{3.23}$$

1) We expand the action given in Eq. (2.1) for single-field slow-roll models of inflation to second order in $\mathcal{R}$. We substitute Eq. (3.22) into Eq. (2.1) and using constraint equations, write the action in terms of $\mathcal{R}$:

$$S_{(2)} = \frac{1}{2}\int \mathrm{d}^4x\; a^3\frac{\dot\phi^2}{H^2}\left[\dot{\mathcal{R}}^2 - a^{-2}(\partial_i\mathcal{R})^2\right]. \tag{3.24}$$

2) We then define the *Mukhanov-Sasaki* variable, $\upsilon \equiv z\mathcal{R}$ where $z^2 = a^2\frac{\dot\phi^2}{H^2} = 2a^2\epsilon$ and change to conformal time, τ. Eq. (3.24) then becomes:

$$S_{(2)} = \frac{1}{2}\int \mathrm{d}\tau\mathrm{d}^3x\left[(\upsilon')^2 + (\partial_i\upsilon)^2 + \frac{z''}{z}\upsilon^2\right]. \tag{3.25}$$

3) Variation of Eq. (3.25) with respect to υ yields the *Mukhanov-Sasaki* equation for the mode functions υ_k where $\upsilon(\tau,\mathbf{x}) = \int \frac{\mathrm{d}^3k}{(2\pi)^3}\upsilon_\mathbf{k}e^{i\mathbf{kx}}$:

$$v_k'' + \left(k^2 - \frac{z''}{z}\right) v_k = 0. \tag{3.26}$$

Note that Eq. (3.26) is the equation of a simple harmonic oscillator with a time-dependent angular frequency of $k^2 - \frac{z''}{z}$.

4) We then quantize the mode functions v_k and the canonical commutation relation implies that the mode functions are normalised as follows:

$$\langle v_k, v_k \rangle = \frac{i}{\hbar}(v_k^* v_k' - v_k^{*\prime} v_k) = 1 \tag{3.27}$$

where v_k^* is the complex mode function.

5) We choose the vacuum state to be the Minkowski vacuum state for an observer in the far past, *i.e*, $\tau \to -\infty$. In this limit, Eq. (3.26) becomes:

$$v_k'' + k^2 v_k = 0 \tag{3.28}$$

Eq. (3.28) has oscillating solutions. Next, by requiring that the vacuum state is the state with minimum energy, we can impose the following initial condition:

$$\lim_{\tau \to -\infty} v_k = \frac{e^{-ik\tau}}{\sqrt{2k}}. \tag{3.29}$$

6) In the de Sitter limit, *i.e*, $\epsilon \to 0$, Eq. (3.26) reads:

$$v_k'' + \left(k^2 - \frac{2}{\tau^2}\right) v_k = 0. \tag{3.30}$$

7) To solve Eq. (3.30) above, we use our two boundary conditions, Eq. (3.27) and Eq. (3.29) which leads to the unique *Bunch-Davies mode functions*:

$$v_k = \frac{e^{-ik\tau}}{\sqrt{2k}}\left(1 - \frac{i}{k\tau}\right) \tag{3.31}$$

with superhorizon limit:

$$\lim_{k\tau \to 0} v_k = \frac{1}{i\sqrt{2}} \frac{1}{k^{\frac{3}{2}}\tau}. \tag{3.32}$$

8) From there, we compute the power spectrum P_v(k) using the superhorizon limit, Eq. (3.32). Using $\tau = \frac{1}{aH}$, we get

$$P_v(k) = \frac{1}{2k^3}(aH)^2 \tag{3.33}$$

and using

$$P_{\mathcal{R}} = \frac{1}{z^2} P_v, \tag{3.34}$$

9) we finally obtain:

$$P_\mathcal{R}(k) = \frac{1}{2k^3}\frac{H_*^4}{\dot{\phi}_*^2} \tag{3.35}$$

where $(...)_*$ means that the quantity is to be evaluated at horizon crossing, i.e., $k = aH$. Using Eq. (3.14) and the definition of ϵ in Eq. (2.12), we finally get

$$\mathcal{P}_\mathcal{R}(k) = \frac{H_*^2}{(2\pi)^2}\frac{H_*^2}{\dot{\phi}_*^2} = \frac{1}{8\pi^2}\frac{H_*^2}{M_{\rm pl}^2}\frac{1}{\epsilon_*}. \tag{3.36}$$

Computing $P_h(k)$

To compute $P_h(k)$, we first substitute Eq. (3.18), the tensor metric perturbations, into the Einstein-Hilbert action and then expand to second order:

$$S_{(2)} = \frac{M_{pl}^2}{8}\int \mathrm{d}\tau\, \mathrm{d}^3x\, a^2[(h'_{ij})^2 - (\partial_l h_{ij})^2] \tag{3.37}$$

Quantum production of tensor fluctuations during inflation follow the same logic as in the case of scalar fluctuations and the resulting form of the action turns out to be two copies of the action in Eq. (3.25), one for each polarisation mode of the gravitational waves, h_+, $h_\times$. We therefore do not need to go much into details here as the power spectrum of tensor modes can be directly inferred from our previous result,

$$\Delta_h^2(k) = \frac{4}{M_{\rm pl}^2}\left(\frac{H_*}{2\pi}\right)^2. \tag{3.38}$$

Using Eq. (3.19), we finally get

$$\mathcal{P}_h(k) = 2\Delta_h^2(k) = \frac{2}{\pi^2}\frac{H_*^2}{M_{\rm pl}^2}. \tag{3.39}$$

3.2.1 The Observable Parameters

The tensor-to-scalar ratio, r, is defined as

$$r \equiv \frac{\mathcal{P}_h}{\mathcal{P}_\mathcal{R}}. \tag{3.40}$$

Using Eq. (3.36) and Eq. (3.39), we obtain

$$r \equiv \frac{\mathcal{P}_h}{\mathcal{P}_\mathcal{R}} = 16\epsilon_*. \tag{3.41}$$

Next, from the definition of the scalar spectral index n_s in Eq. (3.15), we have

$$n_s - 1 = 2\eta_* - 4\epsilon_*. \tag{3.42}$$

We defined the tensor spectral index in Eq. (3.20)

$$n_t = -2\epsilon_*. \tag{3.43}$$

It is more convenient to express n_s, n_t and r in terms of the *potential slow-roll parameters* (ϵ_v, η_v) instead of the *Hubble slow-roll parameters* (ϵ, η). In the slow-roll approximation the Hubble and potential slow-roll parameters are related as in Eq. (2.16). It then follows that:

$$\boxed{n_s - 1 = 2\eta_v^* - 6\epsilon_v^*}, \tag{3.44}$$

$$\boxed{n_t = -2\epsilon_v^*}, \tag{3.45}$$

$$\boxed{r = 16\epsilon_v^*}. \tag{3.46}$$

We also note that single-field slow-roll models satisfy a consistency relation between r and n_t:

$$\boxed{r = -8n_t} \tag{3.47}$$

Hence, if we have the potential $V(\phi)$ for a single-field model, we can easily compute n_s, n_t and r.

3.2.2 Energy Scale of Inflation

In addition to the anisotropies in the CMB temperature, the CMB is also polarized via Thomson scattering [75] which is the elastic scattering of electromagnetic waves by a free charged particle and in the case of the CMB, mainly by electrons. CMB polarization was first detected in 2002 by DASI [76] from the South pole. The dominant contribution to CMB polarization anisotropies is from density (scalar) perturbations and these scalar perturbations only create polarization patterns of a particular type, called the E-modes. The second contribution comes from primordial gravitational wave (tensor) fluctuations from inflation which create B-mode polarization. The amplitude of the tensor fluctuations (unlike scalars) depends only on the value of the Hubble constant during inflation. Therefore, from Eq. (3.40), it follows that the amplitude of the tensor fluctuations depends on the potential of the inflaton field during inflation. We can determine the energy scale of inflation by measuring the amplitude of the primordial tensor fluctuations [49]:

$$\boxed{V^{\frac{1}{4}} \sim \left(\frac{r}{0.01}\right)^{\frac{1}{4}} 10^{16}\ GeV.} \tag{3.48}$$

$r \geqslant 0.01$ corresponds to inflation occuring at GUT scale energies [49].

3.2.3 The Lyth Bound

Using Eq. (3.36) and Eq. (3.39), we can find another interesting result by noting that the tensor-to-scalar ratio relates directly to the evolution of the inflaton as a function of the number of e-foldings, $\mathcal{N}$ [49]:

$$r = \frac{8}{M_{\rm pl}^2}\left(\frac{\mathrm{d}\phi}{\mathrm{d}\mathcal{N}}\right)^2 \tag{3.49}$$

Re-arranging, we find that we can determine the *width* of the potential or the total field evolution between the time when CMB fluctuations exited the horizon (corresponding to $\mathcal{N} = \mathcal{N}_{cmb}$) and the end of inflation ($\mathcal{N} = \mathcal{N}_{end}$):

$$\boxed{\frac{\Delta\phi}{M_{\rm pl}} = \int_{\mathcal{N}_{end}}^{\mathcal{N}_{cmb}} \mathrm{d}\mathcal{N}\sqrt{\frac{r}{8}} \iff \frac{\Delta\phi}{M_{\rm pl}} = \mathcal{O}(1) \times \left(\frac{r}{0.01}\right)^{\frac{1}{2}}.} \tag{3.50}$$

Large values of r, $r > 0.01$ imply $\Delta\phi > M_{\rm pl}$, *i.e*, *large-field inflation* (super-Planckian).

3.3 Non-Gaussianity

The 50 million pixels all-sky image from Planck is compressed to reduce all the information to $\sim 10^3$ multipole moments. This enormous compression can only be justified if the primordial perturbations were drawn from a Gaussian distribution with random phases. If the perturbations are truly Gaussian, then the power spectrum contains all the statistical information and the three-point function and all odd higher order correlation functions of ζ vanish and all even higher order correlation functions can be expressed in terms of the two-point function itself.

The primordial fluctuations are observed to be very close to Gaussian but even a small non-Gaussianity would encode a significant amount of information about the underlying theory of inflation, i.e., about the inflationary action. In fact, non-Gaussianity is an important probe of the early universe because non-Gaussianity is a direct measure of the inflaton interactions (the fields, symmetries, and couplings). Many models give predictions on the power spectrum that are consistent with observations; to truly distinguish between them, one needs to look at non-Gaussianities. Constraints on non-Gaussianity will also put constraints on alternatives to inflation [77–83].

3.3.1 Sources of Non-Gaussianity

There are several sources for a non-zero bispectrum observed in the CMB today:

- Primordial non-Gaussianity: Non-Gaussianity in the primordial curvature perturbation ζ generated by inflation. In this thesis, this is what we are interested in.
- Second-order non-Gaussianity: This arises from the non-linearities in the transfer function that relates ζ to the observed CMB temperature fluctuations at recombination.
- Secondary non-Gaussianity: This is non-Gaussianity coming from 'late' time effects after recombination. For example, gravitational lensing produced by the large-scale structure in the universe can mimic the effects of primordial non-Gaussianity [84–86].
- Foreground non-Gaussianity: The signal from the CMB is also contaminated by galactic and extra-galactic sources [87, 88].

For a complete understanding, one needs to take into consideration each of the sources of non-Gaussianity above as all of them contribute to the observed signal. Hovewer, this is beyond the scope of our work and for the rest of this thesis, we focus on only primordial non-Gaussianity.

3.4 Three and Four-Point Functions of ζ

3.4.1 The Bispectrum

The three-point function of ζ in Fourier space defines the bispectrum

$$\langle \zeta_{\mathbf{k_1}} \zeta_{\mathbf{k_2}} \zeta_{\mathbf{k_3}} \rangle = (2\pi)^3 \delta^3(\mathbf{k_1} + \mathbf{k_2} + \mathbf{k_3}) B_\zeta(k_1, k_2, k_3). \tag{3.51}$$

The delta function above that enforces momentum conservation is a consequence of the translational invariance of the background. This constrains the wavevectors $\mathbf{k_1}, \mathbf{k_2}, \mathbf{k_3}$ to form a triangle. Another thing that we notice is that B_ζ contains only the amplitudes of k's because of statistical isotropy. Physically, this means that all triangle configurations in the CMB are assumed to be drawn from the same distribution, regardless of their orientation. The size of the triangle is one degree of freedom in the sense that the bispectrum has an overall scale dependence much like the power spectrum $\mathcal{P}_\zeta(k)$. The bispectrum, however, contains a lot more information because we can also vary the shape of the triangle. If we take rotational

invariance into account, for a fixed total scale $k_t = k_1 + k_2 + k_3$, the number of independent variables is further reduced to just two, *e.g.* the two ratios k_2/k_1 and k_3/k_1. The shape of the triangle is commonly referred to three limiting cases: equilateral ($k_1 = k_2 = k_3$), squeezed ($k_3 \ll k_2 = k_1$) and folded ($k_1 = 2k_2 = 2k_3$). We show the different configurations in Fig. 3.1.

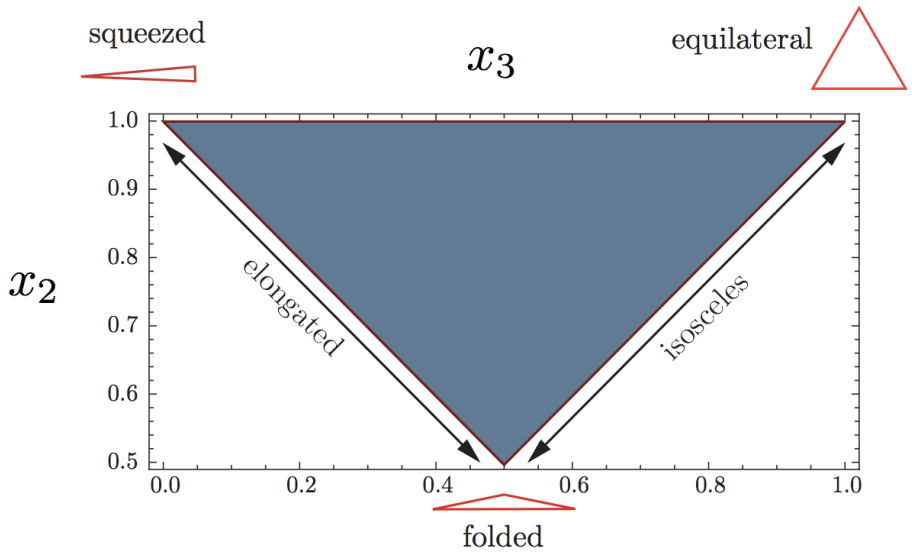

Figure 3.1: *The coordinates x_2 and x_3 are the rescaled momenta k_2/k_1 and k_3/k_1, respectively.The momenta are ordered such that $x_3 \leqslant x_2 \leqslant 1$. Figure taken from [49].*

3.4.2 Shape Functions of Non-Gaussianity

It is clear that, even if we assume statistical isotropy, there is still infinite freedom in the functional form of $B_\zeta(k_1, k_2, k_3)$ and therefore an infinite number of ways to parameterize non-Gaussianity. In this section, we will look at some common parametrizations in cosmology. Let us write the bispectrum in the following way [49, 71, 89]:

$$B_\zeta(k_1, k_2, k_3) = \frac{18}{5} f_{\mathrm{NL}} \frac{\mathcal{S}(k_1, k_2, k_3)}{(k_1 k_2 k_3)^2} \Delta_\zeta^2 \tag{3.52}$$

where f_{NL} is a constant, $\mathcal{S}$ is the shape function and $\Delta_\zeta = P_\zeta(k)k^3$ is the dimensionless power spectrum.

Local Shape

One of the first ways to parameterize the three-point correlation function was introduced by Komatsu and Spergel [90] and was done via a non-linear correction to a Gaussian perturbation ζ_{g}:

$$\zeta(\mathbf{x}) = \zeta_{\rm g}(\mathbf{x}) + \frac{3}{5} f_{\rm NL}^{\rm local} \ [\zeta_{\rm g}(\mathbf{x})^2 - \langle \zeta_{\rm g}(\mathbf{x})^2 \rangle] \tag{3.53}$$

This definition of ζ is local in real space, i.e., the non-Gaussian part of ζ is a function of only the local position $\mathbf{x}$ and has therefore been called the *local model of non-Gaussianity*. The factor 3/5 that appears in Eq. (3.53) is by convention since non-Gaussianity was first defined using the Newtonian potential, $\Phi(\mathbf{x}) = \Phi_{\rm g}(\mathbf{x}) + f_{\rm NL}^{\rm local} \ [\Phi_{\rm g}(\mathbf{x})^2 - \langle \Phi_{\rm g}(\mathbf{x})^2 \rangle]$ which is related to ζ by a factor of 3/5 in the matter-dominated era. Using Eq. (3.53) the bispectrum of local non-Gaussianity can be derived as:

$$B_\zeta(k_1, k_2, k_3) = \frac{6}{5} f_{\rm NL}^{\rm local} \times [P_\zeta(k_1)P_\zeta(k_2) + P_\zeta(k_2)P_\zeta(k_3) + P_\zeta(k_3)P_\zeta(k_1)]. \tag{3.54}$$

Comparing this to our definition in Eq. (3.52), we can read off the local shape function as

$$\mathcal{S}_{\rm local}(k_1, k_2, k_3) = \frac{1}{3}\left(\frac{k_3^2}{k_1 k_2} + 2 \text{ perms.}\right). \tag{3.55}$$

The signal for local non-Gaussianity is dominated by squeezed states, i.e., $x_3 \approx 0, x_2 \approx 1$. We show the relative signal for varying triangle configurations for the local shape in Fig. 3.2.

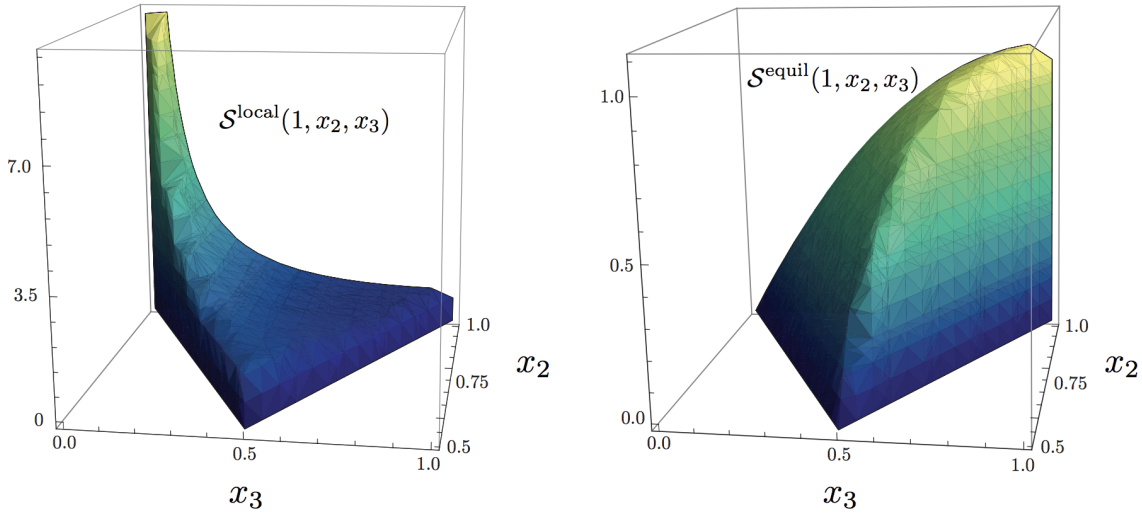

Figure 3.2: *3-D plots of the local and equilateral bispectra. Figure taken from [49].*

Equilateral Shape

The equilateral shape is given by the following shape function:

$$\mathcal{S}_{\rm equil}(k_1,k_2,k_3) = \left(\frac{k_1}{k_2} + 5 \text{ perms.}\right) - \left(\frac{k_1^2}{k_2 k_3} + 2 \text{ perms.}\right) - 2. \tag{3.56}$$

As shown in Fig. 3.2, the signal for this particular shape template peaks at the equilateral configurations, i.e., when all three modes have the same wavelengths ($k_1 = k_2 = k_3$).

Orthogonal Shape

The orthogonal shape is phenomenologically orthogonal to both the local shape and the equilateral shape and its shape function is given by [89]:

$$\mathcal{S}_{\rm ortho}(k_1,k_2,k_3) = -3.84\left(\frac{k_1^2}{k_2 k_3} + 2 \text{ perms.}\right) + 3.94\left(\frac{k_1}{k_2} + 5 \text{ perms.}\right) - 11.10. \tag{3.57}$$

The orthogonal shape peaks in the folded triangle configuration.

Physically motivated inflationary models for producing non-Gaussianity often produce signals that peak at special triangle configurations.

- Squeezed triangle: Models with multiple light fields during inflation, the curvaton scenario [91, 92], inhomogeneous reheating [93, 94] and New Ekpyrotic models [77–83].
- Equilateral triangle: Signals that peak at equilateral triangle configuration arise in models with higher-derivative interactions and non-trivial speeds of sound [95, 96].
- Folded triangle: Signals that peak in folded triangles arise in models with non-standard initial states [97].

3.4.3 The Trispectrum

Ignoring disconnected terms that arise when any two of the $\mathbf{k}$'s sum to zero, the four-point function or equivalently T_ζ is defined as

$$\langle \zeta_{\mathbf{k_1}} \zeta_{\mathbf{k_2}} \zeta_{\mathbf{k_3}} \zeta_{\mathbf{k_4}} \rangle = (2\pi)^3 \delta^3(\mathbf{k_1} + \mathbf{k_2} + \mathbf{k_3} + \mathbf{k_4}) T_\zeta(k_1,k_2,k_3,k_4) \tag{3.58}$$

Considering only local non-Gaussianity[3],

[3] This parametrization is known as the local model of non-Gaussianity with $f_{\rm NL}$ and $g_{\rm NL}$ parametrizing the first and second order deviations from Gaussianity, *cf* Eq. (3.53).

$$\zeta(\mathbf{x}) = \zeta_{\rm g}(\mathbf{x}) + \frac{3}{5} f_{\rm NL}^{\rm local} \ [\zeta_{\rm g}(\mathbf{x})^2 - \langle \zeta_{\rm g}(\mathbf{x})^2 \rangle] + \frac{9}{25} g_{\rm NL} \zeta_{\rm g}^3(\mathbf{x}), \tag{3.59}$$

then, T_ζ can be written as:

$$T_\zeta = \mathcal{T}_{\rm NL}[P_\zeta(k_3)P_\zeta(k_4)P_\zeta(k_{13}) + \ 11 \text{ perms}] + \frac{54}{25} g_{\rm NL}[P_\zeta(k_2)P_\zeta(k_3)P_\zeta(k_4) + \ 3 \text{ perms}] \tag{3.60}$$

with $k_{ij} = |\mathbf{k}_i + \mathbf{k}_j|$.
We will give observational constraints on $\mathcal{T}_{\rm NL}$ and $g_{\rm NL}$ in § 3.6.

3.5 The *in-in* Formalism

In § 3.2, we expanded the action to second order to compute the two-point statistics. In this section, we briefly outline the calculation of the three-point function by use of the *in-in* formalism[4]. This involves expanding the action up to cubic order in perturbations to obtain the third-order interacting Hamiltonian.

In standard scattering calculations, one computes transition amplitudes between an 'input' state $|in\rangle$ and an 'output' state $\langle out|$ as $\langle out| S |in\rangle$ where S is the scattering matrix. The scattering matrix describes the transition probability for a state $|in\rangle$ in the far past to become some state $\langle out|$ in the far future,

$$\langle out(+\infty)| \, |in(-\infty)\rangle \, . \tag{3.61}$$

It makes sense to impose asymptotic conditions at very early times and very late times because in Minkowski space, states are assumed to be non-interacting in the far past and the far future when the scattering particles are far from the interaction region. The aymptotic states relevant for particle physics are therefore taken to be vacuum states of the free Hamiltonian H_0. For inflationary correlations however, we are interested in the expectation values of products of operators at equal fixed times, i.e., at two "in" states. One needs to be careful when defining the time-dependence of the operators in the interacting theory. In the limit when the wavelengths are much smaller and deep inside the horizon, the interaction picture fields should have the same form as in Minkowski space. This state is the Bunch-Davies vacuum state. The *in* - *in* formalism amounts to using standard techniques of Quantum field theory (QFT) to calculate the expectation value of operators with two "in" states (see the classic papers by Maldacena [70] and Weinberg [99] and reviews by Chen [100] and Koyama [101]).

[4]The three-point function calculation can also be done using the path integral formalism, described pedagogically in [98] for the single field case.

Our task is to calculate n-point functions of the primordial curvature perturbation ζ. Let us consider expectation values of operators like $Q = \zeta_{\mathbf{k_1}}\zeta_{\mathbf{k_2}}...\zeta_{\mathbf{k_n}}$,

$$\langle Q \rangle = \langle in| \, Q(t) \, |in\rangle \tag{3.62}$$

In QFT, the expression for this quantity is

$$\langle Q(t) \rangle = \langle 0| \, \bar{T} e^{i\int_{-\infty(1-i\epsilon)}^{t} H_{\rm int}(t')dt'} \, Q(t) \, T e^{-i\int_{-\infty(1+i\epsilon)}^{t} H_{\rm int}(t'')dt''} \, |0\rangle \, , \tag{3.63}$$

where $|0\rangle$ is the free vacuum and $H_{\rm int}$ is the interacting (third-order) part of the Hamiltonian. $T(\bar{T})$ is the (anti-)time ordering symbol meaning that products of $H_{\rm int}$ in the power series expansion of the exponential are to be written from left to right in the increasing order of time arguments. To leading order, Eq. (3.63) is

$$\langle Q(t) \rangle = -i \int_{-\infty}^{t} {\rm d}t' \, \langle 0| \, [Q(t), H_{\rm int}(t')] \, |0\rangle \tag{3.64}$$

where the standard $i\epsilon$ prescription has been used to turn off the interaction in the infinite past. This equation allows us to calculate the bispectra at tree-level.

A very important theoretical calculation was derived by Maldacena [70] where he found that for single field, slow-roll models, the three-point function is given by

$$\langle \zeta_{\mathbf{k_1}}\zeta_{\mathbf{k_2}}\zeta_{\mathbf{k_3}} \rangle = (2\pi)^3\delta^3(\mathbf{k_1}+\mathbf{k_2}+\mathbf{k_3}) \frac{H_*^4}{\dot{\phi}_*^4} \frac{H_*^4}{M_{\rm pl}^4} \frac{1}{\prod_i (2k_i^3)} \mathcal{A}_* \tag{3.65}$$

where the label '*' indicates evaluation at horizon crossing time and,

$$\mathcal{A}_* = 2\frac{\ddot{\phi}_*}{H_*\dot{\phi}_*} \sum k_i^3 + \frac{\dot{\phi}_*^2}{H_*^2} \Big[\frac{1}{2} \sum k_i^3 + \frac{1}{2} \sum_{i \neq j} k_i k_j^2 + 4 \frac{\sum_{i>j} k_i^2 k_j^2}{k_1+k_2+k_3} \Big] . \tag{3.66}$$

This expression highlights an important result, later shown in more generality by Creminelli & Zaldarriaga [102] (see also Ref. [103]); there is a consistency relation involving the three-point function which is valid in any inflationary model, independent of the inflaton Lagrangian under the assumption that the inflaton is the only dynamical field [102]:

$$\lim_{k_3 \to 0} \langle \zeta_{\mathbf{k_1}}\zeta_{\mathbf{k_2}}\zeta_{\mathbf{k_3}} \rangle = (2\pi)^3\delta^3(\mathbf{k_1}+\mathbf{k_2}+\mathbf{k_3})(1-n_s)P_\zeta(k_1)P_\zeta(k_3) \tag{3.67}$$

Cheung *et al.* [104] later formalized this result. This theorem states that for single-field inflation, the squeezed limit of the three-point function is suppressed by $(1-n_s)$ and goes to zero for perfectly scale-invariant perturbations. Therefore, single-field inflation can be ruled out if there is a detection of non-Gaussianity in the squeezed limit. The relation in Eq. (3.67) is independent of the form of the potential, the

form of the kinetic term and the initial vacuum state[5]. This reduced bispectrum of $\mathcal{O}(\epsilon, \eta)$ is below current observational limits. Hence, a detection of non-Gaussianity in the squeezed limit will rule out all models of single field inflation.

3.6 Observational Constraints on Inflation

Now that we have reviewed the theoretical calculations of the correlation functions of ζ, in this section we will relate the predictions from single field inflation to the observational data. The ΛCDM model has six free parameters in total: $\Omega_{\rm b}h^2$, $\Omega_{\rm CDM}h^2$, Ω_Λ, the optical depth τ, the scalar amplitude A_s and the scalar spectral index n_s with the power law ansatz

$$\mathcal{P}_\zeta(k) = A_s\Big(\frac{k}{k_*}\Big)^{n_s-1} \tag{3.68}$$

where $k_* = 0.05\ \text{Mpc}^{-1}$ is a pivot scale. The best-fit constraints on inflation are given by Planck 2018 [48].

$$n_s = 0.9649 \pm 0.0042 \quad (68\%,\ \textit{Planck}\ \text{TT, TE, EE + lowE + lensing}) \tag{3.69}$$

$$A_s = (2.099 \pm 0.101) \times 10^{-9} \quad (68\%,\ \textit{Planck}\ \text{TT, TE, EE + lowE + lensing}) \tag{3.70}$$

The tensor-to-scalar ratio at $k_* = 0.002\ \text{Mpc}^{-1}$ is $r_{0.002} < 0.064$
$(68\%,\ \textit{Planck}\ \text{TT, TE, EE + lowE + lensing + BK14})$.

Future experiments searching for primordial tensor modes include EBEX [105], BICEP3 [106], the Atacama B-Mode Search (ABS) [107], SPIDER [108], CLASS [109], SPTpol [110], the POLARBEAR Experiment [111] and ACTPol [112].

The most accurate constraints on primordial non-Gaussianity are obtained from the Planck mission:

$$f_{\rm NL}^{\rm local} = 0.8 \pm 5.0 \tag{3.71}$$

$$f_{\rm NL}^{\rm equil} = -4 \pm 43 \tag{3.72}$$

$$f_{\rm NL}^{\rm ortho} = -26 \pm 21 \tag{3.73}$$

[5] If one wants to be pedantic, this is true assuming Bunch-Davies vacuum and that the classical solution is a dynamical attractor [104].

at 68% CL using the combination of temperature and polarisation data [113]. Planck's 2013 analysis [114] gives $\mathcal{T}_{\rm NL} < 2800$ (95 % CL). Using WMAP-5 data, Fergusson et al (2010) [115] obtain $-5.4 \times 10^5 < g_{\rm NL} < 8.6 \times 10^5$ (68 % CL). The Planck 2015 analysis [113] gives $g_{\rm NL} = (-9.0 \pm 7.7) \times 10^4$ (68 % CL).

Summary

In this chapter, we have calculated the two-point and the three-point statistics of the primoridal curvature perturbations for the single field case. For the bispectrum, we considered non-Gaussianity from quantum mechanical effects before and during horizon exit. For a single field model, ζ is conserved shortly after horizon exit and remains constant until the time of horizon re-entry. Therefore, the calculations around horizon crossing that we presented are enough to give us theoretical predictions from single field inflation. Observational data is consistent with single field inflation.

There is no reason, however, for why there cannot be more than one light field during inflation. If there are additional fields, ζ is not necessarily conserved and evolution of all isocurvature modes needs to be accounted for. Moreover, in addition to the non-Gaussianity around horizon exit, the classical non-linear evolution of ζ can generate non-Gaussianity after horizon exit. In the next chapter, we will review the δN formalism which can be used to calculate correlation functions of ζ, including non-Gaussian contributions after horizon exit.

Other techniques which we will not discuss here include numerical implementations such as PyTransport [116] and CppTransport [117] and moment transport equations [118, 119].

4 The δN Formalism

In Chapter 3, we calculated the quantum perturbations which become classical around the time of horizon crossing. In this chapter, we will develop the mathematical formalism needed to allow for the tracking of these perturbations in the following superhorizon epoch which can then be related to observationally relevant quantities: the δN formalism. The δN formalism is a powerful and widely used technique to compute the non-linear evolution of cosmological perturbations on large scales. With a review of δN, we will see how this formally allows ζ to be calculated in terms of the field perturbations at horizon exit. We will see later though (in Chaper 5) that the standard δN formalism fails in some cases and this limitation is the starting point of our research work.

"Our treatment of this science will be adequate, if it achieves the amount of precision which belongs to its subject matter. "

—Aristotle

4.1 The δN Formalism

To calculate the primordial power spectrum and primordial non-Gaussianity produced during multifield inflation, as measured by the two- and three-point function of the curvature perturbation, we need two things: firstly, an expression for the curvature perturbation ζ, here given by the Sasaki-Stewart δN formalism [120] (for a concise review of the δN formalism, see Ref. [121]) and secondly, an estimate for the scalar two- and three-point functions just after horizon exit. We will first discuss the two- and three-point functions of the scalar field perturbations in the following section. In § 4.1.2, we review the δN formalism.

4.1.1 The Flat Gauge

In § 3.1, we followed Maldacena [70] and used the comoving gauge ($\delta\phi = 0$) to calculate the scalar power spectrum for single field slow-roll inflation. The advantage

of using the comoving gauge is that for single field inflation, ζ is time-independent classically after horizon crossing [122–128]. This can also be seen in the tree-level quantum calculation of the correlations of ζ [129]: if ζ evolves after horizon crossing, this would appear in the form of divergent vertex integrals in the correlation functions [130–132]. These divergent integrals indicate that the calculations are sensitive to *infrared dynamics* (interactions continue arbitrarily into the future). Fortunately, correlation functions of ζ in single field inflationary models, calculated in the comoving gauge, do not evolve on superhorizon scales. However, in the presence of more than one field, ζ is now able to evolve in the superhorizon epoch (for example, see [118, 120, 133–142]) and the correlation functions are dependent on infrared dynamics which means that the advantage of the comoving gauge no longer applies. This motivates us to pick a different gauge for calculating correlation functions of ζ in multi-field inflationary scenarios: the spatially flat gauge.

The flat gauge is defined by $\Psi = 0$ (*cf.* Eq. (3.12)) which foliates spacetime such that the spatial hypersurfaces have a flat metric and leaves perturbations in the scalar field values,

$$\chi^I(\mathbf{x}) = \bar{\chi}^I + \delta\chi^I(\mathbf{x}) \tag{4.1}$$

where $\bar{\chi}^I$ is the background value and $\delta\chi^I(\mathbf{x})$ is the perturbation in the field. Next, the linear order scalar field perturbation field equation, in the spatially flat gauge, in a linear order perturbed FLRW spacetime for each fourier mode of comoving wavenumber k, for canonical scalar fields is

$$\delta\ddot{\chi}^I + 3H\delta\dot{\chi}^I + \left[V_{,IJ} + \left(\frac{k}{a}\right)^2\delta_{IJ} - \frac{1}{M_{\rm pl}^2 a^3}\frac{\mathrm{d}}{\mathrm{d}t}\left(\frac{a^3\dot{\bar{\chi}}^I\dot{\bar{\chi}}^J}{H}\right)\right]\delta\chi^J = 0. \tag{4.2}$$

δ_{IJ} is the Kronecker-delta. We ignore the interaction terms at leading order in the slow-roll approximation, switch to conformal time τ and re-write the above equation as

$$\delta\chi^{I\prime\prime} + 2\mathcal{H}\delta\chi^{I\prime} + \left[a^2V_{,II} + k^2\right]\delta\chi^I = 0 \tag{4.3}$$

where a prime $'$ denotes $d/d\tau$. To choose the vacuum, we note that for very high frequency modes deep inside the horizon, the field can be quantized as if it were in a Minkowski spacetime. Hence, we pick the solution that corresponds to the usual Minkowski vacuum, keeping only the positive frequencies and we have

$$\delta\chi^I \to \frac{e^{-ik\tau}}{a\sqrt{2k}}, \text{ when } \tau \to -\infty. \tag{4.4}$$

The comoving Hubble radius, $1/aH$, decreases during inflation and modes which begin inside the horizon start to exit the horizon when $k = aH$ and eventually become superhorizon, $k \ll aH$. The perturbations in canonical light fields, with potential $V_{,II} \ll H^2$, become over-damped on superhorizon scales and solving Eq. (4.3), acquire an amplitude of $H/\sqrt{2k^3}$ evaluated at the time when they freeze in at horizon exit, i.e., at $k = aH$. Therefore, the two point correlation function for the scalar field perturbations at horizon crossing is defined by

$$\langle \delta\chi^I_{\mathbf{k_1}} \delta\chi^J_{\mathbf{k_2}} \rangle = (2\pi)^3 \delta^3(\mathbf{k_1} + \mathbf{k_2}) \Sigma^{IJ}(k_1), \tag{4.5}$$

where [143, 144]:

$$\Sigma^{IJ}(k) = \frac{H_*^2}{2k^3} \delta^{IJ} \tag{4.6}$$

and the label '*' denotes evaluation at horizon crossing time. The three-point correlation function of the field perturbations at horizon crossing is given by

$$\langle \delta\chi^I_{\mathbf{k_1}} \delta\chi^J_{\mathbf{k_2}} \delta\chi^K_{\mathbf{k_3}} \rangle = (2\pi)^3 \delta^3(\mathbf{k_1} + \mathbf{k_2} + \mathbf{k_3}) \alpha^{IJK}(k_1, k_2, k_3). \tag{4.7}$$

The three-point function measures the intrinsic non-Gaussianity in the fields produced at horizon crossing. The calculation of $\alpha^{IJK}(k_1, k_2, k_3)$ mirrors that performed by Maldacena [70] and requires one to perturb the action up to third order in $\delta\chi^I$ and identify the interacting Hamiltonian. Here, we quote the results by Seery & Lidsey [72] who used the in-in formalism to calculate $\alpha^{IJK}(k_1, k_2, k_3)$ for the case of canonical scalar fields, in the equilateral limit at time t_* and found

$$\alpha^{IJK}(k_1, k_2, k_3) = \frac{4\pi^4}{k_1^3 k_2^3 k_3^3} \left(\frac{H_*}{2\pi} \right)^4 \sum_{\text{perms}} \frac{\dot{\bar{\chi}}^I_* \delta_{JK}}{4H_*} \left(-3\frac{k_2^2 k_3^2}{k_t} - \frac{k_2^2 k_3^2}{k_t^2}(k_1 + 2k_3) + \frac{1}{2}k_1^3 - k_1 k_2^2 \right) \tag{4.8}$$

where $k_t = k_1 + k_2 + k_3$ and the sum is over six (IJK) permutations while simultaneously permuting the momenta (k_1, k_2, k_3) (I is associated with k_1, J with k_2 and K with k_3). In other words, when exchanging indices I and J, for example, one should also exchange k_1 and k_2 and so on. In making this estimate, the authors have assumed that the three $\mathbf{k}$-modes have roughly the same wavenumbers, so that they cross the horizon at similar times. This means that this analytical result cannot be trusted when the crossing times are too different. We also refer the reader to the work of Kenton & Mulryne [145] who calculated the intrinsic field-space three-point function in the squeezed limit.

4.1.2 The Separate Universe Picture

The seeds of structure in the universe are supposed to originate from the quantum fluctuations of the inflaton field. As each scale leaves the horizon (horizon crossing)

during inflation, these fluctuations are promoted to classical perturbations around the time of horizon exit. The resulting inhomogeneity on cosmological scales is commonly defined by the intrinsic curvature of spatial hypersurfaces defined with respect to the matter. In multifield models, one needs to know the evolution of the curvature perturbation outside the horizon, through the end of inflation until it re-enters the horizon on each cosmologically relevant scale. One could use cosmological perturbation theory to track the superhorizon evolution of linear perturbations in the metric and matter fields in whatever gauge one chooses. Then, one can calculate the corresponding perturbation in the density and pressure and see whether ζ changes significantly. The resulting perturbation equations contain *gradient terms* that are a measure of the deviation from homogeneity. In Fourier space, the gradient terms are in powers of $\frac{k}{aH}$. $\frac{k}{aH}$ is small after horizon crossing since during inflation a is growing quasi-exponentially while H is approximately constant. This leads to a simplifying assumption where one can neglect the gradient terms and leads to a simpler alternative technique to studying the evolution of perturbations on large scales which has been employed in multifield models of inflation. This alternative approach considers the superhorizon universe as a collection of independent FLRW universes on account of the negligible gradient terms [120, 124, 125, 146–148]. In the separate universe picture, one considers the superhorizon universe to be made up of separate FLRW universes where density and pressure may take different values but are locally homogeneous. These separate universes evolve independently according to the same equations as the unperturbed background equations of motion but they have different initial conditions sourced by quantum fluctuations. By patching together these universes, one can follow the evolution of the perturbations with time. In reality this procedure only works down to a cut-off *smoothing scale* somewhat larger than the comoving horizon size. Fig 4.1 shows a schematic illustration of the separate universe picture.

Consider an unperturbed reference universe which is homogeneous and isotropic. Its line element may be written as:

$$\mathrm{d}s^2 = -\mathrm{d}t^2 + a^2(t)\delta_{ij}\mathrm{d}x^i\mathrm{d}x^j \tag{4.9}$$

where $a(t)$ is the unperturbed scale factor. As mentioned earlier, the curvature perturbation is only of interest after the universe has been smoothed on some scale $\frac{k}{a}$ bigger than the horizon H^{-1}. To define the curvature perturbation, consider fixed-t slices of spacetime to have uniform energy density and the fixed-x worldlines to be comoving. The curvature perturbation can be defined as a scalar perturbation to the spatial metric and be written as a local perturbation of the scale factor:

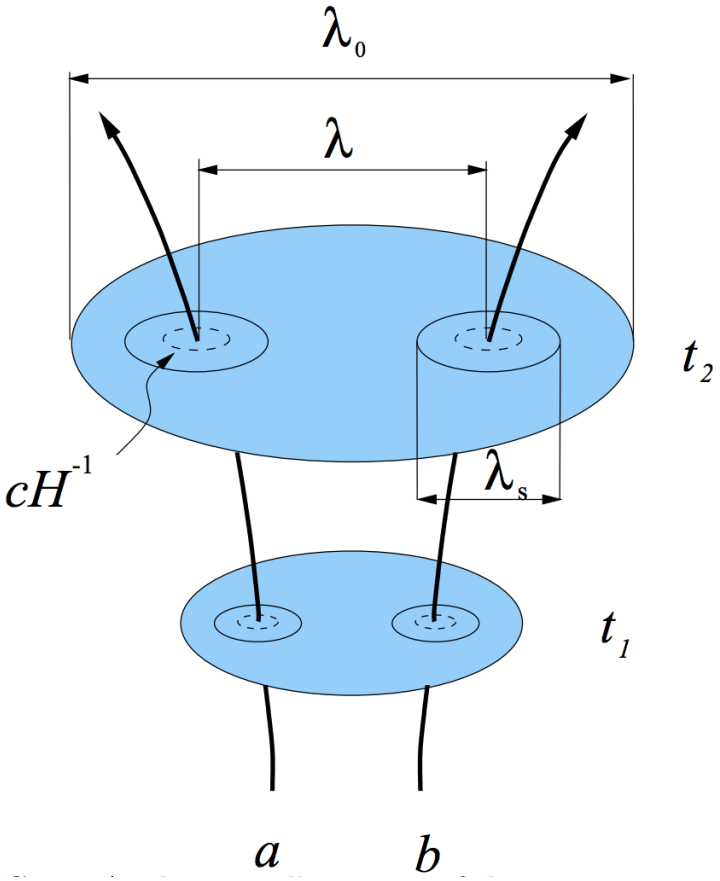

Figure 4.1: *A schematic illustration of the δN formalism: Two locally homogeneous regions (a and b) at fixed spatial coordinates, separated by a coordinate distance λ on an initial hypersurface at $t = t_1$ and subsequently on a final hypersurface at $t = t_2$. Each superhorizon sized (cH^{-1}) region is viewed as having its own FLRW region around it and that assumption is true up to some scale λ_s. The largest scale λ_0 represents the 'background' and is much bigger than even our present horizon size. Figure taken from [148].*

$$a(t)e^{\zeta(t,\mathbf{x})} = \tilde{a}(t,\mathbf{x}). \tag{4.10}$$

According to this definition, ζ is the perturbation in $\ln \tilde{a}$. One can then consider a slicing whose metric has the same form as Eq. (4.10) but without the ζ factor which we call the flat slicing. Starting from any initial flat slice at time $t = t_*$, we can then define the amount of expansion, i.e. the number of e-folds, to a final slice of uniform energy density at time t:

$$N(t,\mathbf{x}) \equiv \ln\left[\frac{\tilde{a}(t,\mathbf{x})}{a(t_*)}\right] \tag{4.11}$$

The unperturbed number of e-folds is given by:

$$\bar{N}(t) = \ln\left[\frac{a(t)}{a(t_*)}\right]. \tag{4.12}$$

Using the definition of ζ , we then have the celebrated δN formula:

$$\zeta(t, \mathbf{x}) = N(t, \mathbf{x}) - \bar{N}(t) = \delta N(t, \mathbf{x}). \tag{4.13}$$

We note that δN does not depend on the initial time t_*. It is typical to take t_* to be some time after all the relevant modes in a given correlation function have exited the horizon.

4.1.3 Standard δN: The Inflationary Prediction

The evolution of the observable universe on cosmological scales is determined by the values of one or more light scalar fields when that scale first emerges from the quantum regime a few Hubble times after horizon exit. For an inflationary model with n scalar fields, χ^I, where I runs from 1 to n we can split the field values on any initial flat slice into background and perturbed parts $\chi^I(\mathbf{x}) = \bar{\chi}^I + \delta\chi^I(\mathbf{x})$. Invoking the separate universe picture and choosing the homogeneous quantities $\bar{\chi}^I$ to correspond to the unperturbed universe, Eq. (4.13) for ζ becomes:

$$\zeta(t, \mathbf{x}) = N(\rho(t), \chi^1(\mathbf{x}), \chi^2(\mathbf{x}), \chi^3(\mathbf{x}), ...) - \bar{N}(\rho(t), \bar{\chi}^1, \bar{\chi}^2, \bar{\chi}^3, ...). \tag{4.14}$$

In this expression, the expansion N is evaluated in an unperturbed universe from an epoch when the fields have assigned values to an epoch when the energy density, $\rho(t)$, has some specified value. Using this expression, we can propagate forward the stochastic properties of ζ to a later observable time, given the properties of the initial field perturbations.

Since the observed curvature perturbation is close to Gaussian, the standard approach to applying the δN formalism is to make a Taylor expansion in the initial flat slicing field perturbations [72, 125, 149] and assuming ρ to be fixed,

$$\zeta(\mathbf{x}) \simeq \sum_I N_{,I}\delta\chi^I(\mathbf{x}) + \sum_{IJ}\frac{1}{2}N_{,IJ}(\delta\chi^I(\mathbf{x})\delta\chi^J(\mathbf{x}) - \overline{\delta\chi^I\delta\chi^J}) \tag{4.15}$$

where we use the notation $N_{,I} \equiv \frac{\partial N}{\partial\bar{\chi}^I}$ and $N_{,IJ} \equiv \frac{\partial^2 N}{\partial\bar{\chi}^I\partial\bar{\chi}^J}$ and where $\overline{\delta\chi^I\delta\chi^J} = \langle\delta\chi^I(\mathbf{x})\delta\chi^J(\mathbf{x})\rangle$. $\delta\chi^I$ express the deviations of the fields from their unperturbed values in some given region of space. From this point onward, it is quite straightforward to compute the statistics of ζ. To form the desired correlations of $\zeta(k)$, one takes the Fourier transform of Eq. (4.15) and keeps only the leading terms. One also has to specify the statistical distribution of field space perturbations on the initial flat hypersurface. The correlation functions of the field perturbations $\delta\chi^I = \chi^I - \bar{\chi}^I$ are given by Eq. (4.5) and Eq. (4.7).

The power spectrum and bispectrum of ζ is then

$$P_\zeta(k) = N_{,I} N_{,J}\, \Sigma^{IJ}(k), \tag{4.16}$$

$$B_\zeta(k_1, k_2, k_3) = N_{,I} N_{,J} N_{,K}\, \alpha^{IJK}(k_1, k_2, k_3) \; + N_{,I} N_{,J} N_{,KL}\, (\Sigma^{IK}(k_1)\Sigma^{JL}(k_2) + \text{cyclic}). \tag{4.17}$$

Taking the field perturbations to be Gaussian with an almost flat spectrum and using Eq. (4.6) such that[1]

$$\mathcal{P}_\chi = \left(\frac{H_*}{2\pi}\right)^2 \tag{4.18}$$

and that

$$\langle \zeta_{\mathbf{k_1}} \zeta_{\mathbf{k_2}} \rangle \equiv (2\pi)^3 \delta^3(\mathbf{k_1} + \mathbf{k_2}) P_\zeta(k_1), \tag{4.19}$$

we have [149]

$$\mathcal{P}_\zeta = \sum_I N_{,I}^2 \left(\frac{H_*}{2\pi}\right)^2. \tag{4.20}$$

For the bispectrum, if we assume that the intrinsic non-Gaussianity of the fields is negligible and so we ignore the first term in Eq. (4.17) which from Eq. (4.8) we see is the case for canonical fields and taking the normalization of the bispectrum as defined in Eq. (3.54), we have

$$\frac{6}{5} f_{\rm NL} = \frac{\sum_{IJ} N_{,I} N_{,J} N_{,IJ}}{[\sum_I N_{,I}^2]^2} \tag{4.21}$$

at leading order.

The standard δN gives extremely accurate results in many cases but we will see in the next chapter that there exists cases where the method breaks down. As a solution, we propose the *Non-Perturbative* δN which we will introduce in Chapter 5.

[1] Recall that the dimensionless power spectrum is defined as $\mathcal{P}_\chi = \frac{k^3}{2\pi^2} P_\chi$.

5 Non-Perturbative δN Formalism

In Chapter 4, we reviewed the standard δN formalism. In most models of inflation, the series expansion in Eq. (4.15) converges so rapidly that truncation at second order is accurate enough to calculate the three-point function of ζ. However, there are several cases where the convergence is so slow that truncating the series at first order to compute the two-point function of ζ or at second order to calculate the three-point function of ζ is not justified. This problem arises when one uses lattice simulations to probe the effects of isocurvature modes on models of reheating. For example, in the massless preheating case (see Chapter 6 and Chapter 7), the obtained $N(\chi)$ function by numerical simulations shows that ζ is quite sensitive to the value of χ. The key goal of this thesis is to calculate observational predictions for inflationary models for which standard δN formalism does not work. In this chapter, we revisit the question of how to calculate correlations of the curvature perturbation, ζ, using the δN formalism when one cannot employ a truncated Taylor expansion of N. Working in real space, we use an expansion in the cross-correlation between fields at different positions, and present simple expressions for observables such as the power spectrum and the reduced bispectrum, $f_{\rm NL}$. These take the same form as those of the usual δN expressions, but with the derivatives of N replaced by *non-perturbative δN coefficients*. We test the validity of this expression and, when compared to others in the literature, argue that our expressions are particularly well suited for use with simulations. Please note that we have repeated a few expressions from § 4.1.3 for the convenience of the reader.

"Clouds are not spheres, mountains are not cones, coastlines are not circles, and bark is not smooth, nor does lightning travel in a straight line."

—Benoît Mandelbrot

5.1 Introduction

Inflation has been extremely successful in explaining the generation of the primordial perturbations seeding the structures of our universe, but the microphysics of inflation remains unknown. The simplest model consistent with existing observational data is to assume that inflaton fluctuations are solely responsible for the observed curvature perturbations. Although such a scenario is the simplest, it is quite possible that more complicated scenarios involving additional fields, as exemplified by the curvaton model [91, 150] and the modulated reheating model [93, 94], are actually realized. To test different inflationary theories against observations, one must calculate the precise form of the correlation functions of the primordial curvature perturbation, ζ. One technique used to do this is the separate universe approximation combined with the δN formalism [120, 123, 125, 148, 149]. As we have seen in Chapter 4, in this approach, ζ is given by the perturbation in the local e-folding number

$$\zeta(\mathbf{x}) = \delta N(\mathbf{x}) = N(\vec{\chi}(\mathbf{x})) - \bar{N}\,, \tag{5.1}$$

where N is the number of e-folds between an initial flat hypersurface at some early time (such as horizon crossing) and a final uniform density hypersurface at some later time (such as the end of inflation or after reheating), and $\bar{N} = \langle N \rangle$. Throughout, angle brackets indicate an ensemble average. We consider n fields labeled, χ^I, where I runs from 1 to n, and for convenience we introduce the vector, $\vec{\chi}$, where each element represents one of the n fields.

N is calculated by assuming that locally the universe can be approximated as a Friedmann-Robertson-Walker spacetime, and hence is a function of the local field values on the initial flat hypersurface. Standard practice is to approximate δN by making a Taylor expansion in the initial field values and keeping only a small number of terms. In some cases, however, N depends very sensitively on the initial field values, and a truncated Taylor expansion is not a good approximation. Such cases include those in which a light field in addition to the inflaton influences the dynamics of non-perturbative reheating [151–154]. In this chapter we return to the issue of how to deal with such cases. As we will see, an alternative expansion is sometimes possible.

Although the primary motivation for our work is the interpretation of the results of lattice simulations, here we study the question generally. Our approach employs many of the key ideas contained in the work of Suyama and Yokoyama [155], and our results are broadly equivalent to theirs. We will now briefly review their method and highlight how our approach is different from theirs. In their work, a key step was to make a Fourier transform of the N function (treated as a function of a single

field value). They introduce the Fourier transformation of $N(\chi)$ as:

$$N(\chi) = \int \frac{\mathrm{d}\sigma}{2\pi} N_\sigma e^{i\chi\sigma}, \qquad \Longrightarrow \qquad N_\sigma = \int \mathrm{d}\chi N(\chi) e^{-i\chi\sigma}. \tag{5.2}$$

$\langle N(\chi)\rangle$ is then given by

$$\langle N(\chi)\rangle = \int \frac{\mathrm{d}\sigma}{2\pi} N_\sigma e^{-\frac{\langle\chi^2\rangle}{2}\sigma^2}, \tag{5.3}$$

where $\langle\chi^2\rangle \equiv \langle\chi^2(\mathbf{x})\rangle$. This means that once N_σ is known, one can compute $\langle N(\chi)\rangle$ by performing the one-dimensional integral above. Similarly, higher-order m-point functions of N are given by

$$\langle N(\chi(\mathbf{x_1}))...N(\chi(\mathbf{x_m}))\rangle = \int \Big(\prod_{i=1}^{m} \frac{\mathrm{d}\sigma_i}{2\pi} N_{\sigma_i} e^{-\frac{\langle\chi^2\rangle}{2}\sigma_i^2}\Big) \exp\Big(-\langle\chi^2\rangle \sum_{i<j} \sigma_i\sigma_j \xi_\chi(r_{ij})\Big) \tag{5.4}$$

where $\xi(r_{ij}) = \langle\chi(\mathbf{x_i})\chi(\mathbf{x_j})\rangle/\langle\chi^2\rangle$ and $r_{ij} = |\mathbf{x_i} - \mathbf{x_j}|$. For their method, it is required that N_σ is known to be able to calculate the m-point function by performing m-dimensional integrals.

For example, consider the analytic sine mapping, $N(\chi) = B\sin\left(\frac{\chi}{\lambda}\right)$ where B and λ are constants. N_σ in this case is given by

$$N_\sigma = B\int_{-\infty}^{\infty} \mathrm{d}\chi \sin\left(\frac{\chi}{\lambda}\right) e^{-i\chi\sigma}. \tag{5.5}$$

Noting that $\sin x = \frac{e^{ix} - e^{-ix}}{2i}$, Eq. (5.5) becomes

$$\begin{aligned} N_\sigma &= B\int_{-\infty}^{\infty} \mathrm{d}\chi \Big(\frac{e^{\frac{i\chi}{\lambda}} - e^{-\frac{i\chi}{\lambda}}}{2i}\Big) e^{-i\chi\sigma} \\ &= -\frac{iB}{2}\Big[\int_{-\infty}^{\infty} \mathrm{d}\chi\, e^{i\chi(\lambda^{-1}-\sigma)} - \int_{-\infty}^{\infty} \mathrm{d}\chi\, e^{-i\chi(\lambda^{-1}+\sigma)}\Big]. \end{aligned} \tag{5.6}$$

We then note that

$$\int_{-\infty}^{\infty} \mathrm{d}\chi\, e^{i\chi(\lambda^{-1}-\sigma)} = 2\pi\delta(\sigma - \lambda^{-1}), \quad \int_{-\infty}^{\infty} \mathrm{d}\chi\, e^{-i\chi(\lambda^{-1}+\sigma)} = 2\pi\delta(\sigma + \lambda^{-1}) \tag{5.7}$$

and Eq. (5.6) becomes

$$N_\sigma = -i\pi B\big(\delta(\sigma - \lambda^{-1}) - \delta(\sigma + \lambda^{-1})\big). \tag{5.8}$$

Using Eq. (5.3),

$$\begin{aligned}\langle N(\chi)\rangle &= \int \frac{\mathrm{d}\sigma}{2\pi}\Big[-i\pi B\big(\delta(\sigma-\lambda^{-1})-\delta(\sigma+\lambda^{-1})\big)\Big]\, e^{-\frac{\langle\chi^2\rangle}{2}\sigma^2}\\ &= -\frac{i\pi B}{2\pi}\Big[e^{-\frac{\langle\chi^2\rangle}{2}\lambda^{-2}}-e^{-\frac{\langle\chi^2\rangle}{2}\lambda^{-2}}\Big].\\ &= 0. \end{aligned} \tag{5.9}$$

For this particular example, $\langle N(\chi)\rangle = 0$. This can be directly seen from the fact that the sine mapping is an odd function. Next, moving to the two-point function using Eq. (5.4), one can write

$$\langle\zeta(\mathbf{x_1})\zeta(\mathbf{x_2})\rangle = \langle N(\chi(\mathbf{x_1})N(\chi(\mathbf{x_2})\rangle - \langle N(\chi)\rangle^2 = \langle N(\chi(\mathbf{x_1})N(\chi(\mathbf{x_2})\rangle. \tag{5.10}$$

$$\begin{aligned}\langle\zeta(\mathbf{x_1})\zeta(\mathbf{x_2})\rangle &= \int \frac{\mathrm{d}\sigma_1}{2\pi}\frac{\mathrm{d}\sigma_2}{2\pi}N_{\sigma_1}N_{\sigma_2}\, e^{-\frac{\langle\chi^2\rangle}{2}\sigma_1^2}\, e^{-\frac{\langle\chi^2\rangle}{2}\sigma_2^2}\\ &\quad\times e^{-\langle\chi^2\rangle\sigma_1\sigma_2\xi(r_{12})}. \end{aligned} \tag{5.11}$$

where $N_{\sigma_1} = -i\pi B\big(\delta(\sigma_1-\lambda^{-1})-\delta(\sigma_1+\lambda^{-1})\big)$ and $N_{\sigma_2} = -i\pi B\big(\delta(\sigma_2-\lambda^{-1})-\delta(\sigma_2+\lambda^{-1})\big)$.
Evaluating the δ functions, we then have

$$\begin{aligned}\langle\zeta(\mathbf{x_1})\zeta(\mathbf{x_2})\rangle &= -\frac{\pi^2B^2}{4\pi^2}\Big[e^{-\langle\chi^2\rangle\left(\lambda^{-2}+\lambda^{-2}\xi(r_{12})\right)}-e^{-\langle\chi^2\rangle\left(\lambda^{-2}-\lambda^{-2}\xi(r_{12})\right)}\\ &\quad -e^{-\langle\chi^2\rangle\left(\lambda^{-2}-\lambda^{-2}\xi(r_{12})\right)}+e^{-\langle\chi^2\rangle\left(\lambda^{-2}+\lambda^{-2}\xi(r_{12})\right)}\Big], \end{aligned} \tag{5.12}$$

and therefore,

$$\begin{aligned}\langle\zeta(\mathbf{x_1})\zeta(\mathbf{x_2})\rangle &= -\frac{B^2}{4}2\Big[e^{-\langle\chi^2\rangle\left(\lambda^{-2}+\lambda^{-2}\xi(r_{12})\right)}-e^{-\langle\chi^2\rangle\left(\lambda^{-2}-\lambda^{-2}\xi(r_{12})\right)}\Big]\\ &= B^2e^{-\frac{\langle\chi^2\rangle}{\lambda^2}}\Big[\frac{e^{\frac{\langle\chi^2\rangle}{\lambda^2}\xi(r_{12})}-e^{-\frac{\langle\chi^2\rangle}{\lambda^2}\xi(r_{12})}}{2}\Big]. \end{aligned} \tag{5.13}$$

Making use of the definition of $\sinh(x)$, we can finally write

$$\langle\zeta(\mathbf{x_1})\zeta(\mathbf{x_2})\rangle = B^2e^{-\frac{\langle\chi^2\rangle}{\lambda^2}}\sinh\left(\frac{\langle\chi^2\rangle}{\lambda^2}\xi(r_{12})\right). \tag{5.14}$$

We note that although this particular method is useful for analytic manipulations, it leads to expressions for the correlation functions that are less useful if an exact form for N is unknown, or, as can be the case for lattice simulations, it is not efficient even to calculate the form of the N function explicitly. The expressions we arrive at, using our 'non-perturbative' approach, are more applicable in this setting, lending themselves to a Monte Carlo approach, a point we return to later. Our methods are more closely related to the work of Bethke, Figueroa and Rajantie [156, 157] who considered the power spectrum of gravitational waves from massless preheating, though depart from both these earlier studies by considering n fields whose initial probability distribution need not be precisely Gaussian. We perform explicit calculations only for the two and three-point functions of ζ, but the method extends trivially to higher point functions. For other related work with a different approach to ours, see [158] and [159] where the authors develop and apply a non-perturbative formulation of δN by incorporating the stochastic corrections to N.

The remainder of this chapter is structured as follows: In § 5.2, we develop and describe the non-perturbative δN formalism. Our main results are presented in § 5.2.3. We then apply this formalism in § 5.3 to both analytic and non-analytic examples and make useful comparisons to regular δN formalism. Finally, we conclude in § 5.4.

5.2 Non-perturbative δN Formalism

5.2.1 Regular δN

In the standard δN approach, the field perturbations, $\delta\chi^I = \chi^I - \bar{\chi}^I$, are taken to be close to Gaussian with the power spectrum defined in Eq. (4.5). Higher order cumulants are either taken to be completely negligible, or are included in the formalism, order by order, first the three-point function on the initial hypersurface given by Eq. (4.7) and then successive higher order cumulants. To utilise Eq. (5.1), one first makes a Taylor expansion of the N function in terms of $\delta\chi^I(\mathbf{x})$, such that to second order $\zeta(\mathbf{x})$ is given by

$$\delta N(\mathbf{x}) = N_{,I}\delta\chi^I(\mathbf{x}) + \frac{1}{2}N_{,IJ}\left(\delta\chi^I(\mathbf{x})\delta\chi^J(\mathbf{x}) - \overline{\delta\chi^I\delta\chi^J}\right). \tag{5.15}$$

One then considers the Fourier transform of Eq. (5.15), and forms the desired correlation of $\zeta(k)$, typically keeping only the leading terms. Finally, applying a Wick expansion, and using Eq. (4.5) and any non-zero higher order cumulants, one produces an expression for the Fourier space correlations of ζ at the final time in terms of the correlations of the fields at the early time. For example, the two and three-point functions of ζ, defined in terms of the power spectrum P_ζ and bispectrum B_ζ

are given by

$$\begin{aligned}
\langle \zeta_{\mathbf{k_1}} \zeta_{\mathbf{k_2}} \rangle &\equiv (2\pi)^3 P_\zeta(k_1) \delta^3(\mathbf{k_1} + \mathbf{k_2}) \\
&= (2\pi)^3 N_{,I} N_{,J} \Sigma^{IJ}(k_1) \delta^3(\mathbf{k_1} + \mathbf{k_2}) \qquad (5.16) \\
\langle \zeta_{\mathbf{k_1}} \zeta_{\mathbf{k_2}} \zeta_{\mathbf{k_3}} \rangle &\equiv (2\pi)^3 B_\zeta(k_1, k_2, k_3) \delta^3(\mathbf{k_1} + \mathbf{k_2} + \mathbf{k_3}) \\
&= (2\pi)^3 \Big[N_{,I} N_{,J} N_{,K} \alpha^{IJK}(k_1, k_2, k_3) \\
&\quad + N_{,I} N_{,J} N_{,KL} \big(\Sigma^{IK}(k_1) \Sigma^{JL}(k_2) \\
&\quad + \text{cyclic} \big) \Big] \delta^3(\mathbf{k_1} + \mathbf{k_2} + \mathbf{k_3}) \,. \qquad (5.17)
\end{aligned}$$

We note that here and throughout this chapter when we discuss correlations of fields we always mean those at the initial time, and when we discuss correlations of ζ we always mean those at the final time. Finally we also note that taking $\alpha(k_1, k_2, k_3)$ to be zero (along with higher order cumulants) is a good approximation for canonical theories with the field statistics evaluated at horizon crossing, but not otherwise.

5.2.2 δN Without a Taylor Expansion

Preliminaries and notation

We will now consider how to proceed if N is not well approximated by a Taylor expansion. In this case, it proves convenient to stay in real space and calculate the correlations of ζ there, including information from all scales, and only then to Fourier transform the correlation (for each of the spatial coordinates which appear) to calculate the Fourier space correlations over observational scales or equivalently to coarse-grain the correlations over these scales. This procedure is most convenient because N is a function of the fields which are in turn a function of spatial position. One could attempt to treat $N(\vec{\chi}(\mathbf{x}))$ as a function of $\mathbf{x}$ and Fourier transform it directly, but given that it is a non-linear function of the fields, the result would not be a simple function of the Fourier coefficients of the fields, $\vec{\chi}(k)$, which are the objects we have information about.

For later convenience, therefore, let us introduce some notation for the statistics of the field space perturbations in real space as

$$\langle \delta\chi^I(\mathbf{x}_1) \delta\chi^J(\mathbf{x}_2) \rangle = \Sigma^{IJ}(r_{12}) \,, \qquad (5.18)$$

where $r_{12} = |\mathbf{x}_1 - \mathbf{x}_2|$, and

$$\langle \delta\chi^I(\mathbf{x}_1) \delta\chi^J(\mathbf{x_2}) \delta\chi^K(\mathbf{x_3}) \rangle = \alpha^{IJK}(r_{12}, r_{23}, r_{31}) \,. \qquad (5.19)$$

In an abuse of notation we use the same symbol for the correlations as for the related objects in Fourier space (defined in Eq. (4.5) and Eq. (4.7)), but it will always be clear from the context which we mean. We further define the shorthand notation

$$\langle \delta\chi^I(\mathbf{x}_1)\delta\chi^J(\mathbf{x}_1)\rangle = \Sigma^{IJ} \tag{5.20}$$

$$\langle \delta\chi^I(\mathbf{x}_1)\delta\chi^J(\mathbf{x}_1)\delta\chi^K(\mathbf{x}_1)\rangle = \alpha^{IJK}\,, \tag{5.21}$$

since when evaluated at the same spatial position the correlations are no longer functions of space.

Finally, we introduce more short hand notation such that the evaluation of a function at a given spatial position is denoted using a subscript, for example $\zeta_1 = \zeta(\mathbf{x}_1)$, $\chi^I_1 = \chi^I(\mathbf{x}_1)$ and $N_1 = N(\vec{\chi}(\mathbf{x}_1))$. This is helpful to keep our expressions to a manageable size when we are considering many spatial positions in one expression.

A non-perturbative expression

When ζ cannot be written in terms of an expansion in $\delta\chi^I(\mathbf{x})$, one cannot write the correlations of ζ in terms of a finite number of correlations of the field perturbations. Instead one must fall back on the definition of the ensemble average, and write the m-point function, $\langle\zeta(\mathbf{x}_1)...\zeta(\mathbf{x}_m)\rangle$, in terms of the full $n \times m$ joint probability distribution for the n fields evaluated at the m spatial positions. This is given as

$$\begin{aligned}\langle\zeta_1...\zeta_m\rangle &= \langle(N_1-\bar{N})...(N_m-\bar{N})\rangle \\ &= \int \mathrm{d}\vec{\chi}_1 ... \int \mathrm{d}\vec{\chi}_m (N_1-\bar{N})...(N_m-\bar{N}) \\ &\qquad \times \mathcal{P}(\vec{\chi}_1,...,\vec{\chi}_m)\,,\end{aligned} \tag{5.22}$$

where $\mathcal{P}$ is the joint probability distribution for the $m \times n$ variables χ^I_i, and we have used the subscript notation defined at the end of the previous subsection. The integral is over all the fields evaluated at the m distinct spatial positions. If N is a simple function, and if $\mathcal{P}$ can be taken to be Gaussian, which is often a very good approximation, then it is possible to evaluate Eq. (5.22) analytically. More generally it is possible to evaluate it numerically. We will see examples of both for the single field case in § (5.3).

Although not presented explicitly there, Eq. (5.22) in the single field case is the starting point for the work of Suyama and Yokoyama [155]. In that work the focus is on extracting analytic results for the moments of ζ when an analytic form for N is known. As we saw in § 5.1, they proceed by assuming that the probability distribution is exactly Gaussian, and by considering the Fourier transform of the

$N(\chi)$ function (when N is treated as function of χ). In this case general expressions for the correlations of N are known in terms of the Fourier coefficients of N and the variance of χ (these are given in Eq. (9) of Ref [155]), and they proceed to work directly with these expressions in their paper. In our work we work directly with Eq. (5.22). This more direct route still allows Eq. (5.22) to be evaluated analytically for specific forms of the $N(\chi)$ function, but also allows us to introduce additional fields, to expand the distribution, and to consider non-Gaussian initial conditions in a straightforward manner.

5.2.3 Expansions of the Probability Distribution

While it is possible to work directly with Eq. (5.22), it is rather cumbersome in practice, especially if it needs to be integrated numerically or if the probability distribution, $\mathcal{P}$, cannot be taken to be Gaussian. Moreover, if a numerical evaluation is needed the process becomes particularly involved when the correlations are converted to Fourier space, to calculate observable quantities such as the power spectrum and bispectrum on observable scales. In this case one must Fourier transform the real space correlations in each of the m spatial coordinates that appear, which requires that the integral, Eq. (5.22), is evaluated first at a sufficient number of points in real space and then transformed to Fourier space.

Two expansions

Thankfully, for many applications there is still an approximate method available even when N cannot be Taylor expanded. Rather than expanding the N function, the idea is to employ, instead, expansions of the distribution $\mathcal{P}$.

First $\mathcal{P}$ is expanded around a Gaussian distribution employing a Gauss-Hermite expansion. In the inflationary context a Gauss-Hermite expansion for the distribution of field perturbations was used by Mulryne *et al.* [140] for example, and is justified since the field perturbations produced by inflation are very close to Gaussian [70, 72, 95, 98, 160–163] (even for levels of non-Gaussianity far in excess of observational bounds).

Next, this distribution is expanded in the cross correlation between fields evaluated at different spatial positions, $\Sigma^{IJ}(r_{ij})$ with $i \neq j$, around the distribution for the field perturbations evaluated at the same spatial position, i.e, we assume that $\Sigma^{IJ}(r_{ij}) < \Sigma^{IJ}$ (recall $\Sigma^{IJ} \equiv \Sigma^{IJ}(\mathbf{0})$). This expansion has been utilised previously by Suyama and Yokoyama [155] and by Bethke *et al.* [156, 157]. It is at least partially justified if the power spectrum for the field fluctuations $\delta\chi^I(\mathbf{k}_1)$ is close to scale invariant, since then for two positions, $\mathbf{x}_1$ and $\mathbf{x}_2$, separated by a distance close to the size of the observable universe we find that $\Sigma^{IJ}(\mathbf{r}_{12})$ is roughly two orders

of magnitude smaller than Σ^{IJ}. We will always be interested either in real space correlations of ζ coarse-grained on these large observationally relevant scales, or equivalently in the Fourier space correlations for small wavenumbers. See, however, § 5.2.3 for caveats and a more detailed discussion.

An interlude on our expansions

Let us begin in the abstract, before moving to the inflationary context, and consider the distribution for a set of close to Gaussian coupled variables y_α denoted by the vector $\mathbf{y}$. This is given by the Gauss-Hermite expansion,

$$\mathcal{P}(\mathbf{y}) = \mathcal{P}_{\rm G}(\mathbf{y}) \left(1 + \frac{A^{-1}_{\alpha\epsilon} A^{-1}_{\beta\eta} A^{-1}_{\gamma\mu} \alpha_{\epsilon\eta\mu} H_{\alpha\beta\gamma}(\mathbf{z})}{6} + ...\right), \tag{5.23}$$

where the subscript G indicates a multivariate Gaussian distribution with covariance matrix $\Sigma_{\alpha\beta} \equiv \langle \delta y_\alpha \delta y_\beta \rangle = A_{\alpha\epsilon} A_{\beta\epsilon}$, and where $\alpha_{\alpha\beta\gamma} \equiv \langle \delta y_\alpha \delta y_\beta \delta y_\gamma \rangle$. $\delta y_\alpha = y_\alpha - \bar{y}_\alpha$ and $\mathbf{z}$ is the vector with elements $A^{-1}_{\alpha\beta} \delta y_\beta$. The functions in the expansion are products of Hermite polynomials defined by a generalised version of Rodrigues' formula, such that $H_{\alpha\beta\gamma} = -\partial^n / \partial z_\alpha \partial z_\beta \partial z_\gamma \exp(-\mathbf{z}^2)$. We will only need the result that $H_{\alpha\beta\gamma}(\mathbf{z}) = \delta y_\alpha \delta y_\beta \delta y_\gamma$ if $\alpha \neq \beta \neq \gamma$. A multivariate Gauss-Hermite expansion around a Gaussian distribution has been employed elsewhere in the cosmological literature for various purposes (see, for example, [118, 140, 164–170]).

Now let us consider the second expansion we will need to make. We note that if any of the elements of the covariance matrix $\Sigma_{\alpha\beta}$ are small in the sense that we can neglect terms involving their square, it is possible to make a Taylor expansion of the distribution, Eq. (5.23), in this element. For our purposes to make use of such an expansion, we will only need the following results

$$\frac{\partial \mathcal{P}_{\rm G}}{\partial \Sigma_{\alpha\beta}} = \frac{1}{2} \mathcal{P}_{\rm G} \delta y_\gamma \delta y_\delta \Sigma^{-1}_{\gamma\alpha} \Sigma^{-1}_{\delta\beta}, \tag{5.24}$$

$$\frac{\partial^2 \mathcal{P}_{\rm G}}{\partial \Sigma_{\alpha\beta} \partial \Sigma_{\gamma\delta}} \supset \frac{1}{4} \delta y_\epsilon \delta y_\eta \delta y_\mu \delta y_\nu \mathcal{P}_G \Sigma^{-1}_{\alpha\epsilon} \Sigma^{-1}_{\beta\eta} \Sigma^{-1}_{\gamma\mu} \Sigma^{-1}_{\delta\nu}. \tag{5.25}$$

In this context $A \supset B$ denotes that A contains B as well as some other terms.

Calculating correlations of ζ using the expansions

Finally, we can use these expansions in the context at hand. Here, we give the expressions we arrive at without going into details. We will explicitly show how these expressions arise in the single field case later. We assume that the distribution which appears in Eq. (5.22) for the $m \times n$ independent variables, χ^I_i, is both close to Gaussian, so that the Gauss-Hermite expansion can be employed, and moreover

that the $n \times m$ variate Gaussian which appears in this expansion can be further expanded in the cross-correlations $\Sigma^{IJ}(r_{ij})$ where $r_{ij} \neq 0$. Specialising to the two-point function and employing Eq. (5.22) with both expansions, one finds that at leading order

$$\begin{aligned} &\int \mathrm{d}\vec{\chi}_1 \mathrm{d}\vec{\chi}_2 \, \mathcal{P}(\vec{\chi}_1, \vec{\chi}_2)(N_1 - \bar{N})(N_2 - \bar{N}) \\ &\approx \Sigma^{IJ}(r_{12})\Sigma^{-1}_{IK}\Sigma^{-1}_{JM} \int \mathrm{d}\vec{\chi}_1 \mathcal{P}_{\mathrm{G}}(\vec{\chi}_1)\delta\chi_1^K(N_1 - \bar{N}) \times \int \mathrm{d}\vec{\chi}_2 \mathcal{P}_{\mathrm{G}}(\vec{\chi}_2)\delta\chi_2^M(N_2 - \bar{N}) \end{aligned} \tag{5.26}$$

where Σ^{-1}_{IJ} is the inverse of Σ^{IJ}, which for clarity we recall is the covariance matrix of field perturbations evaluated at the same point in real space. This leading term comes from the first order term in the cross-correlation Taylor expansion, which is calculated from Eq. (5.24). There is no contribution from the zeroth order term because one needs at least one $\delta\chi_i$ to accompany each N_i function so that the expectation of a given term isn't zero. Note that the Gaussian probability distribution which appears twice on the right hand side of this expression is the n dimensional distribution for fields evaluated at only a single position, and we have retained both the subscripts 1 and 2 only for clarity as to how the expression arises.

We can write Eq. (5.26) as

$$\langle \zeta_1 \zeta_2 \rangle \approx \tilde{N}_I \tilde{N}_J \Sigma^{IJ}(r_{12}), \tag{5.27}$$

where we have defined

$$\tilde{N}_I = \Sigma^{-1}_{IJ} \int \mathrm{d}\vec{\chi}_1 \, \mathcal{P}_{\mathrm{G}}(\vec{\chi}_1) N_1 \delta\chi_1^J, \tag{5.28}$$

which is analogous to the first derivative of N used in Eq. (5.15). The spatial position indicated by the subscript 1 is of course arbitrary.

Following the same procedure for the three-point function one finds that we must keep two terms at leading order, one involves the α term from the Gauss-Hermite expansion, and the second is second order in the cross-correlation expansion and arises from the term given in Eq. (5.25). These are the first terms to contribute since again we need at least one $\delta\chi_i$ to accompany each of the three N_i functions in the three-point function so that the expectation value of a given term is not zero. One finds

$$\begin{aligned} \langle \zeta_1 \zeta_2 \zeta_3 \rangle \approx \; & \tilde{N}_I \tilde{N}_J \tilde{N}_K \alpha^{IJK}(r_{12}, r_{23}, r_{31}) \\ & + \big(\tilde{N}_I \tilde{N}_J \tilde{N}_{KL} \Sigma^{IK}(r_{12}) \Sigma^{JL}(r_{23}) \\ & \quad + \text{cyclic} \big) \end{aligned} \tag{5.29}$$

where we have defined

$$\tilde{N}_{IJ} = \Sigma^{-1}_{IK}\Sigma^{-1}_{JL}\int \mathrm{d}\vec{\chi}_1\, \mathcal{P}_{\mathrm{G}}(\vec{\chi}_1)(N_1 - \bar{N})\delta\chi_1^K \delta\chi_1^L \tag{5.30}$$

analogous to the second derivative of N used in Eq. (5.15).
Later for clarity, we show in more detail how these expressions arise for the single field case; we choose to do that in the single field case so we can drop the superscripts for the fields and keep our expressions tidy.

Using these expressions, and accounting for only the second term of Eq. (5.29), the local contribution to the reduced bispectrum f_{NL}, takes the famous form

$$\frac{6}{5} f_{\mathrm{NL}} = \frac{\tilde{N}_I \tilde{N}_{IJ} \tilde{N}_J}{(\tilde{N}_K \tilde{N}_K)^2}\,. \tag{5.31}$$

It is important to note that Eqs. (5.27) and (5.29) combined with the definition of $\tilde{N}_I$ and $\tilde{N}_{IJ}$ represent a significant simplification, since the spatial dependence of the two-point function of ζ is defined entirely through that of the field fluctuations. This is an important advantage, particularly if the correlation of ζ is to be evaluated numerically, since otherwise the numerics would need to be repeated for many values of r_{12}, while in this case $\tilde{N}_I$ and $\tilde{N}_{IJ}$ need only be evaluated once. This allows us to pass immediately to Fourier space, and to write the power spectrum and bispectrum of ζ as

$$P_\zeta(k) \approx \tilde{N}_I \tilde{N}_J \Sigma^{IJ}(k) \tag{5.32}$$

$$\begin{aligned} B_\zeta(k_1, k_2, k_3) \approx\ & \tilde{N}_I \tilde{N}_J \tilde{N}_K \alpha^{IJK}(k_1, k_2, k_3) \\ & + \big(\tilde{N}_I \tilde{N}_J \tilde{N}_{KL} \Sigma^{IK}(k_1)\Sigma^{JL}(k_2) \\ & \qquad + \text{cyclic}\big). \end{aligned} \tag{5.33}$$

Further simplifications for typical applications

A further simplification occurs if we assume that the field fluctuations are uncorrelated such that Σ^{IJ} is diagonal. The simplest case is if all fields have the same variance, such that

$$\Sigma^{IJ} = \delta^{IJ} P_\chi \tag{5.34}$$

which is a good approximation at horizon crossing during inflation. More generally the covariance matrix might be diagonal but with different entries, such that

$$\Sigma^{IJ} = \delta^{IJ} P_{\chi^I} \tag{5.35}$$

where no summation is implied. This would be the case in a model with one inflaton field and a set of fields that were purely isocurvature modes during inflation. In this case one finds $\tilde{N}_I$ simplifies to

$$\tilde{N}_I = \frac{1}{P_{\chi^I}} \int \mathrm{d}\vec{\chi}_1 \mathcal{P}_{\mathrm{G}}(\vec{\chi}_1) N_1 \delta\chi_1^I \tag{5.36}$$

$$\equiv \frac{1}{P_{\chi^I}} \langle \delta\chi_1^I N_1 \rangle_{\mathrm{G}} \tag{5.37}$$

and $\tilde{N}_{IJ}$ simplifies to

$$\tilde{N}_{IJ} = \frac{1}{P_{\chi^I} P_{\chi^J}} \int \mathrm{d}\vec{\chi}_1 \mathcal{P}_{\mathrm{G}}(\vec{\chi}_1)(N_1 - \bar{N}) \delta\chi_1^I \delta\chi_1^J \tag{5.38}$$

$$\equiv \frac{1}{P_{\chi^I} P_{\chi^J}} \langle \delta\chi_1^J \delta\chi_1^I (N_1 - \bar{N}) \rangle_{\mathrm{G}} \tag{5.39}$$

because in this case, the covariance matrix is diagonal, $\mathcal{P}_{\mathrm{G}}(\vec{\chi}_1) = \prod_I \mathcal{P}_{\mathrm{UG}}(\chi_1^I)$, where subscript UG now stands for a univariate Gaussian.

Single field case: two-point and three-point functions

The expressions presented above are valid for n fields. However, we passed rather quickly over the details of the derivation. For clarity therefore, let us specialise to the single field case and calculate in more detail $\langle \zeta_1 \zeta_2 \rangle$ and $\langle \zeta_1 \zeta_2 \zeta_3 \rangle$ where we can drop the superscripts for the fields to keep things neat. The relevant m-variate Gaussian distribution function in this case is given by

$$\mathcal{P}_{\mathrm{G}}(\chi_1, \chi_2, ...\chi_m) = \frac{1}{(2\pi)^{\frac{m}{2}}} |\Sigma|^{-1/2} e^{-\frac{1}{2}\delta\chi_i \Sigma_{ij}^{-1} \delta\chi_j} \tag{5.40}$$

where $|\Sigma|$ is the determinant of the covariance matrix Σ_{ij} and the lower case Roman indices run over values $1, 2, ...m$. We want to expand in off-diagonal parts, i.e., we assume that $\frac{\Sigma_{ij}}{\Sigma_{ij}|_{i=j}}$ is small. Moreover, $\Sigma_{ij}|_{i=j} = \Sigma = \langle \delta\chi^2 \rangle$ for all i and j. In order to form the Taylor expansion of $\mathcal{P}_{\mathrm{G}}$ about the $\Sigma_{ij}|_{i\neq j} = 0$ case, let us differentiate $\mathcal{P}_{\mathrm{G}}$. We find

$$\frac{\partial \mathcal{P}_{\mathrm{G}}}{\partial \Sigma_{lm}} \supset \frac{1}{(2\pi)^{\frac{m}{2}}} |\Sigma|^{-1/2} e^{-\frac{1}{2}\delta\chi_i \Sigma_{ij}^{-1} \delta\chi_j} \Big(-\frac{1}{2} \delta\chi_p \delta\chi_q \frac{\partial \Sigma_{pq}^{-1}}{\partial \Sigma_{lm}} \Big), \tag{5.41}$$

where we have ignored the term containing the derivative of the determinant because that term does not contribute. Then using

$$\frac{\partial \Sigma_{pq}^{-1}}{\partial \Sigma_{lm}} = -\Sigma_{pl}^{-1} \Sigma_{mq}^{-1}, \tag{5.42}$$

we have

$$\frac{\partial \mathcal{P}_{\rm G}}{\partial \Sigma_{lm}} \supset \frac{1}{2}\mathcal{P}_{\rm G}\delta\chi_p\delta\chi_q\Sigma^{-1}_{pl}\Sigma^{-1}_{mq}. \tag{5.43}$$

Similarly, the second derivative gives

$$\frac{\partial^2 \mathcal{P}_{\rm G}}{\partial \Sigma_{lm}\Sigma_{no}} \supset \frac{1}{4}\mathcal{P}_{\rm G}\left(\delta\chi_p\delta\chi_q\Sigma^{-1}_{pl}\Sigma^{-1}_{mq}\right)\left(\delta\chi_k\delta\chi_f\Sigma^{-1}_{kn}\Sigma^{-1}_{of}\right) + ... \tag{5.44}$$

Therefore, the Taylor expansion of $\mathcal{P}_{\rm G}$ about $\Sigma_{ij}|_{i\neq j} = 0$ gives

$$\begin{aligned}\mathcal{P}_{\rm G} \approx\ & \mathcal{P}_{\rm G}|_\dagger + \sum_{l\neq m}\frac{1}{2}\frac{1}{\langle\delta\chi^2\rangle^2}\mathcal{P}_{\rm G}|_\dagger\delta\chi_l\delta\chi_m\Sigma_{lm} \\ & + \sum_{l\neq m}\sum_{n\neq o}\frac{1}{8}\frac{1}{\langle\delta\chi^2\rangle^4}\mathcal{P}_{\rm G}|_\dagger\delta\chi_l\delta\chi_m\delta\chi_n\delta\chi_o\Sigma_{lm}\Sigma_{no},\end{aligned} \tag{5.45}$$

where we have used $\Sigma^{-1}_{pl} = \frac{1}{\langle\delta\chi^2\rangle}\delta_{pl}$ and where '†' means that the off-diagonal parts are taken to be zero. Now that we have an expression for the Taylor-expanded $\mathcal{P}_{\rm G}$, we can substitute Eq. (5.45) into Eq. (5.22) and form correlation functions of ζ.

Let us now explicitly calculate $\langle\zeta_1\zeta_2\rangle$ using the expanded probability distribution function

$$\begin{aligned}\langle\zeta_1\zeta_2\rangle =\ & \int_{-\infty}^{\infty}{\rm d}\chi_1\int_{-\infty}^{\infty}{\rm d}\chi_2\ \Big[\mathcal{P}_{\rm G}(\chi_1,\chi_2)|_\dagger\ + \\ & \frac{1}{\langle\delta\chi^2\rangle^2}\mathcal{P}_{\rm G}(\chi_1,\chi_2)|_\dagger\ \delta\chi_1\delta\chi_2\ \Sigma_{12}\ + \\ & \frac{1}{2}\frac{1}{\langle\delta\chi^2\rangle^4}\mathcal{P}_{\rm G}(\chi_1,\chi_2)|_\dagger\ \delta\chi_1^2\delta\chi_2^2\ \Sigma_{12}^2\Big] \\ & \times(N_1-\bar{N})(N_2-\bar{N}).\end{aligned} \tag{5.46}$$

The first term that multiplies with $(N_1-\bar{N})(N_2-\bar{N})$ vanishes while the second term and the third terms give the leading and sub-leading contributions to $\langle\zeta_1\zeta_2\rangle$ respectively. Because in this case the covariance matrix is diagonal, $\mathcal{P}_{\rm G}(\chi_1,\chi_2) = \mathcal{P}_{{\rm UG}_1}\mathcal{P}_{{\rm UG}_2}$ where 'UG' stands for a univariate Gaussian. We can then write

$$\langle\zeta_1\zeta_2\rangle_{\rm leading} = \frac{\langle\delta\chi N(\chi)\rangle^2}{\langle\delta\chi^2\rangle^2}\Sigma(r_{12}). \tag{5.47}$$

The angle brackets here denote an ensemble average with χ drawn from a univariate Gaussian. Note that the $\bar{N}$ term vanishes because $\langle\delta\chi\ \bar{N}\rangle = \langle\chi\ \bar{N} - \bar{\chi}\ \bar{N}\rangle = \bar{\chi}\ \bar{N} - \bar{\chi}\ \bar{N} = 0$ and that we have now dropped the subscripts 1 and 2. Also, to make the dependence on the distance r_{12} clear, we replace Σ_{12} by $\Sigma(r_{12})$.

For the sub-leading term, we have

$$\langle\zeta_1\zeta_2\rangle_{\text{subleading}} = \frac{\langle\delta\chi^2(N(\chi)-\bar{N})\rangle^2}{2\langle\delta\chi^2\rangle^4}\Sigma(r_{12})^2 \tag{5.48}$$

Finally, we can write

$$\begin{aligned}\langle\zeta_1\zeta_2\rangle = &\frac{\langle\delta\chi N(\chi)\rangle^2}{\langle\delta\chi^2\rangle^2}\Sigma(r_{12}) \\ &+ \frac{\langle\delta\chi^2(N(\chi)-\bar{N})\rangle^2}{2\langle\delta\chi^2\rangle^4}\Sigma(r_{12})^2 + ...\end{aligned} \tag{5.49}$$

where $\bar{N} = \langle N\rangle$.

Now we will derive the three-point function, $\langle\zeta_1\zeta_2\zeta_3\rangle$, at leading order for the single field case. There is an additional term that contributes to the three-point function at leading order; it comes from allowing the field to be non-Gaussian by keeping the α term in Eq. (5.23). In this case, $\mathcal{P}_{\text{G}}$ is given by

$$\begin{aligned}\mathcal{P}_{\text{G}} \approx\ & \mathcal{P}_{\text{G}}|_\dagger + \sum_{l\neq m}\frac{1}{2}\frac{1}{\langle\delta\chi^2\rangle^2}\mathcal{P}_{\text{G}}|_\dagger\delta\chi_l\delta\chi_m\,\Sigma_{lm} \\ &+ \sum_{l\neq m}\sum_{n\neq o}\frac{1}{8}\frac{1}{\langle\delta\chi^2\rangle^4}\mathcal{P}_{\text{G}}|_\dagger\delta\chi_l\delta\chi_m\delta\chi_n\delta\chi_o\,\Sigma_{lm}\Sigma_{no} \\ &+ \sum_{p\neq q\neq r}\frac{1}{6}\frac{1}{\langle\delta\chi^2\rangle^3}\mathcal{P}_{\text{G}}|_\dagger\delta\chi_p\delta\chi_q\delta\chi_r\,\alpha_{pqr}.\end{aligned} \tag{5.50}$$

Plugging Eq. (5.50) into Eq. (5.22), for the three-point function of ζ, we see that the first two terms in Eq. (5.50) evaluate to zero because of $\bar{N}$. The two contributions at leading order are therefore

$$\begin{aligned}\langle\zeta_1\zeta_2\zeta_3\rangle = &\int_{-\infty}^{\infty}\mathrm{d}\chi_1\int_{-\infty}^{\infty}\mathrm{d}\chi_2\int_{-\infty}^{\infty}\mathrm{d}\chi_3\Big[\frac{1}{\langle\delta\chi^2\rangle^3}\mathcal{P}_{\text{G}}(\chi_1,\chi_2,\chi_3)|_\dagger\delta\chi_1\delta\chi_2\delta\chi_3\,\alpha(r_{12},r_{23},r_{31}) + \\ &\frac{1}{\langle\delta\chi^2\rangle^4}\mathcal{P}_{\text{G}}(\chi_1,\chi_2,\chi_3)|_\dagger\,\delta\chi_1\delta\chi_2\delta\chi_2\delta\chi_3\,\Sigma(r_{12})\Sigma(r_{23}) + \text{perms}\Big] \\ &\times(N_1-\bar{N})(N_2-\bar{N})(N_3-\bar{N}).\end{aligned} \tag{5.51}$$

Again, because the covariance matrix is diagonal, $\mathcal{P}_{\text{G}}(\chi_1,\chi_2,\chi_3) = \mathcal{P}_{\text{UG}_1}\mathcal{P}_{\text{UG}_2}\mathcal{P}_{\text{UG}_3}$, and finally we can write:

$$\langle\zeta_1\zeta_2\zeta_3\rangle = \frac{\langle\delta\chi N\rangle^3}{\langle\delta\chi^2\rangle^3}\alpha(r_{12},r_{23},r_{31}) + \Big(\frac{\langle\delta\chi N(\chi)\rangle^2}{\langle\delta\chi^2\rangle^2}\frac{\langle\delta\chi^2(N(\chi)-\bar{N})\rangle}{\langle\delta\chi^2\rangle^2}\Sigma(r_{12})\Sigma(r_{23}) + \text{perms}\Big), \tag{5.52}$$

where we have dropped the subscripts 1, 2 and 3.

A Monte Carlo approach

In this chapter, the examples we consider will be of cases where there is a known N function, either an analytic one, or one that has been calculated numerically. When we utilise the simplified expressions given above, we will therefore use the known N function and integrate Eqs. (5.37) and (5.39), either analytically or using numerical methods.

However, a major motivation of our work is to allow the future study of cases in which it may not be desirable to first calculate N as a function of the initial field values. We defer doing this to future work, but it is worth laying out a case for the suitability of our expressions for this purpose. It may be that the N function is highly featured, such as in the case of massless preheating [151, 152, 154, 171–173], and that first calculating the function accurately may not be the most efficient path to accurately evaluating Eq. (5.37) and Eq. (5.39). Instead one might choose to adopt a Monte Carlo approach, in which values of the initial field(s) χ^I are drawn from a Gaussian distribution, and for each draw N is evaluated numerically. $\tilde{N}_I$, for example, is then calculated by evaluating $\delta\chi^I N$ for each draw, and the values summed and divided by the number of draws. The convergence of the result can be monitored. This was the approach adopted in the gravitational wave case by Bethke *et al.* [156, 157]. In contrast to previous work [155], our expressions are ideal for this purpose. We will use our non-perturbative expressions in a Monte Carlo setting, for massless preheating, in Chapter 7.

Limitations

§ 5.2.3 represents the main results of this chapter. In § 5.3 we will see them in practice, and test their validity. First, however, let us consider what we expect to be their limitations in terms of the approximations we have employed.

The first limitation stems from the fact that we expand the probability distribution in the cross correlations between distinct spatial positions, and then integrate to calculate the correlations of ζ. This means that the resulting expansion is not guaranteed to be a good one (in the sense that it will converge), even if the expansion of the probability distribution does converge. So while $\Sigma(r_{ij}) \ll \Sigma$ is sufficient for the probability expansion to be valid, this is not sufficient for the correlations calculated from it to converge. This effectively means that we have to test the validity of our expressions on a case by case basis.

The second related issue comes from the fact that even if the series does converge, there is no guarantee that the leading term in the cross correlations is sufficient. An extreme example follows from the fact that it is possible for the "leading" term we

quote above to be zero. For the two-point function this occurs when the N function is symmetric in one of fields (about $\bar{\chi}$) – an even function in the single field case. In this case, considering Eq. (5.37) for a single field, we see that $\langle \delta\chi N(\chi) \rangle_{\rm G} = 0$. Although realistic functions of N will never be fully even or fully odd, this issue should be borne in mind.

In both cases one thing that can be done is to check that the sub-leading term is subdominant to the leading term. Although not proof of convergence this is a simple way to check that the method is working as intended. For example, in the single field case where the sourcing scalar field is Gaussian, one can compare the magnitudes of the leading and sub-leading terms in Eq. (5.49) for a given model.

An alternative approach would be to evaluate the full expression, Eq. (5.22) (specialising, for example, to the two-point function) which always remains valid, and compare with the results of the expansion method. To do so for a full range of r_{12} would of course negate the advantage of using the expansion in the first place, but one could do so for a single representative value of r_{12}. In the next section when we study simple examples numerically we will evaluate the full expression over a range of r_{12}, but we note that in more complex cases this may not be feasible.

5.3 Examples

Let us now see our expressions in practice. In this chapter we restrict ourselves to cases in which we already have an $N(\vec{\chi})$ function calculated, deferring the Monte Carlo type applications discussed in § 5.2.3 to Chapter 7.

In addition to a specific N function, for concrete applications, we must also specify the statistics of the field fluctuations $\delta\chi^I(\mathbf{x})$. In order to do so, at this point we specialise to uncoupled Gaussian perturbations, with scale invariant power spectrum, such that

$$\Sigma^{IJ}(k) = \delta^{IJ} P_\chi(k) = \delta^{IJ} \frac{P_0}{k^3}\,, \tag{5.53}$$

where P_0 is a constant. Moreover, in the examples we present we will mainly assume that only the perturbations from one field contribute significantly to ζ, and therefore we can further specialise to N being a function of just a single field.

With our convention for the Fourier Transform

$$\delta\chi(\mathbf{x}) = \frac{1}{(2\pi)^3} \int {\rm d}^3k e^{i\mathbf{k}.\mathbf{x}} \delta\chi_{\mathbf{k}}\,, \tag{5.54}$$

$\langle \delta\chi(\mathbf{x}) \delta\chi(\mathbf{x}) \rangle$ is then given by

$$\langle \delta\chi(\mathbf{x})\delta\chi(\mathbf{x})\rangle = \frac{1}{(2\pi)^6}\int \mathrm{d}^3k \int \mathrm{d}^3k' e^{i\mathbf{k}.\mathbf{x}+i\mathbf{k}'.\mathbf{x}}\langle \delta\chi_{\mathbf{k}}\delta\chi_{\mathbf{k}'}\rangle\,. \tag{5.55}$$

The equation above becomes:

$$\langle \delta\chi(\mathbf{x})\delta\chi(\mathbf{x})\rangle = \frac{1}{(2\pi)^6}\int \mathrm{d}^3k \int \mathrm{d}^3k' e^{i\mathbf{k}.\mathbf{x}+i\mathbf{k}'.\mathbf{x}}(2\pi)^3 P_\chi(k)\delta^3(\mathbf{k}+\mathbf{k}')\,, \tag{5.56}$$

where we have substituted for $\langle \delta\chi_{\mathbf{k}}\delta\chi_{\mathbf{k}'}\rangle$ using Eq. (4.5). Then, integrating the exponential term and the 3-dimensional Dirac delta function, we find:

$$\Sigma = \langle \delta\chi(\mathbf{x})\delta\chi(\mathbf{x})\rangle = \frac{1}{(2\pi)^3}\int \mathrm{d}^3k P_\chi(k). \tag{5.57}$$

Now, for the scale-invariant power spectrum $P_\chi(k) = \frac{P_0}{k^3}$ and therefore we can write:

$$\Sigma = \langle \delta\chi(\mathbf{x})\delta\chi(\mathbf{x})\rangle = \frac{1}{(2\pi)^3}\int \mathrm{d}^3k \frac{P_0}{k^3}. \tag{5.58}$$

Changing from cartesian to spherical polar coordinates gives $\int \mathrm{d}^3k \to \int \mathrm{d}k\ 4\pi k^2$ and we have

$$\Sigma = \langle \delta\chi^2(\mathbf{x})\rangle = \frac{P_0}{2\pi^2}\int \frac{\mathrm{d}k}{k}. \tag{5.59}$$

Next, introducing both the UV and IR cutoffs,

$$\Sigma = \langle \delta\chi^2(\mathbf{x})\rangle = \frac{P_0}{2\pi^2}\int_{L^{-1}}^{q_{\max}} \frac{\mathrm{d}k}{k}\,, \tag{5.60}$$

where $\sim L^{-1}$ is an IR and $q_{\max}$ a UV cutoff. In this case, the IR cutoff is just the size of the observable universe, in other words, the scale over which $\bar{\chi}$ is defined. This gives

$$\langle \delta\chi^2(\mathbf{x})\rangle = \frac{P_0}{2\pi^2}\ln(q_{\max}L)\,, \tag{5.61}$$

for the two-point function of field fluctuations evaluated at the same spatial position. Physically, the IR cutoff must be close to the size of the observable universe so that the average of $\delta\chi(\mathbf{x})$ within the observable universe is zero – to be consistent with our initial definition of $\delta\chi(\mathbf{x}) = \chi(\mathbf{x}) - \bar{\chi}$.

Next, consider the correlation of the field fluctuations at two separated positions,

$$\langle \delta\chi(\mathbf{x_1})\delta\chi(\mathbf{x_2})\rangle = \frac{1}{(2\pi)^6}\int \mathrm{d}^3k \int \mathrm{d}^3k' e^{i\mathbf{k}.\mathbf{x_1}+i\mathbf{k}'.\mathbf{x_2}}\langle \delta\chi_{\mathbf{k}}\delta\chi_{\mathbf{k}'}\rangle. \tag{5.62}$$

Substituting for $\langle \delta\chi_{\mathbf{k}}\delta\chi_{\mathbf{k}'}\rangle$, we obtain:

$$\langle \delta\chi(\mathbf{x_1})\delta\chi(\mathbf{x_2})\rangle = \frac{1}{(2\pi)^6}\int \mathrm{d}^3k \int \mathrm{d}^3k' e^{i\mathbf{k}.\mathbf{x_1}+i\mathbf{k'}.\mathbf{x_2}}(2\pi)^3 P_\chi(k)\delta^3(\mathbf{k}+\mathbf{k'}). \tag{5.63}$$

The equation above becomes

$$\langle \delta\chi(\mathbf{x_1})\delta\chi(\mathbf{x_2})\rangle = \frac{1}{(2\pi)^3}\int \mathrm{d}^3k e^{i\mathbf{k}.\mathbf{x_1}-i\mathbf{k}.\mathbf{x_2}} P_\chi(k). \tag{5.64}$$

Again, assuming that the power spectrum is scale-invariant:

$$\langle \delta\chi(\mathbf{x_1})\delta\chi(\mathbf{x_2})\rangle = \frac{1}{(2\pi)^3}\int \mathrm{d}^3k e^{i\mathbf{k}.(\mathbf{x_1}-\mathbf{x_2})} \frac{P_0}{k^3}. \tag{5.65}$$

Making use of $\mathbf{r_{12}} = \mathbf{x_1} - \mathbf{x_2}$, we get

$$\langle \delta\chi(\mathbf{x_1})\delta\chi(\mathbf{x_2})\rangle = \frac{1}{(2\pi)^3}\int \mathrm{d}^3k e^{i\mathbf{k}.\mathbf{r_{12}}} \frac{P_0}{k^3}. \tag{5.66}$$

In spherical polar coordinates,

$$\mathrm{d}^3k = k^2\ \mathrm{d}k\ \sin\theta\ \mathrm{d}\theta\ \mathrm{d}\phi, \quad \mathbf{k}.\mathbf{r_{12}} = kr_{12}\cos\theta \tag{5.67}$$

and we have

$$\langle \delta\chi(\mathbf{x_1})\delta\chi(\mathbf{x_2})\rangle = \frac{1}{(2\pi)^3}\int \mathrm{d}k\ k^2 \int_0^{2\pi} \mathrm{d}\phi \int_0^{\pi} \mathrm{d}\theta \sin\theta\ e^{ikr_{12}\cos\theta}\ \frac{P_0}{k^3}. \tag{5.68}$$

Noting that $\mathrm{d}(\cos\theta) = \sin\theta\ \mathrm{d}\theta$, we can rewrite the previous equation as

$$\langle \delta\chi(\mathbf{x_1})\delta\chi(\mathbf{x_2})\rangle = \frac{1}{(2\pi)^3}\int \mathrm{d}k\ k^2 \int_0^{2\pi} \mathrm{d}\phi \int_{+1}^{-1} \mathrm{d}(\cos\theta)\ e^{ikr_{12}\cos\theta}\ \frac{P_0}{k^3}. \tag{5.69}$$

Now, let $\cos\theta = y$. We then have:

$$\langle \delta\chi(\mathbf{x_1})\delta\chi(\mathbf{x_2})\rangle = \frac{1}{(2\pi)^3}\int \mathrm{d}k\ k^2 \int_0^{2\pi} \mathrm{d}\phi \int_{+1}^{-1} \mathrm{d}y\ e^{ikr_{12}y}\ \frac{P_0}{k^3}. \tag{5.70}$$

Evaluating $\left[\frac{e^{ikr_{12}y}}{ikr_{12}}\right]_{y=+1}^{y=-1}$ gives $-\frac{2\sin(kr_{12})}{kr_{12}}$ and we have

$$\langle \delta\chi(\mathbf{x_1})\delta\chi(\mathbf{x_2})\rangle = \frac{P_0}{2\pi^2}\int_{L^{-1}}^{q_{\max}} \frac{\mathrm{d}k}{k}\ \frac{-\sin(kr_{12})}{kr_{12}}. \tag{5.71}$$

Evaluating the above integral, one finds

$$\langle \delta\chi(\mathbf{x}_1)\delta\chi(\mathbf{x}_2)\rangle = \frac{P_0}{2\pi^2}\left(- \mathcal{C}_i\left(\frac{r_{12}}{L}\right) + \mathcal{C}_i(q_{\max} r_{12}) + \frac{\sin(\frac{r_{12}}{L})}{\frac{r_{12}}{L}} - \frac{\sin(q_{\max} r_{12})}{q_{\max} r_{12}}\right), \tag{5.72}$$

where $\mathcal{C}_i(x)$ is the cosine integral function

$$\mathcal{C}_i(x) = -\int_x^\infty \frac{\cos(t)}{t}\mathrm{d}t\,. \tag{5.73}$$

It is in this cross correlation that the expansion of § 5.2.3 was made. We also define the cross-correlation normalised to the variance as

$$\frac{\Sigma(r_{12})}{\Sigma} = \xi(r_{12}) = \frac{\langle \delta\chi(\mathbf{x}_1)\delta\chi(\mathbf{x}_2)\rangle}{\langle \delta\chi^2(\mathbf{x})\rangle}\,, \tag{5.74}$$

which we require to be small for the expansion of the probability distribution to be valid.

For a purely scale invariant spectrum and for distances much longer than the UV cutoff (i.e., $r_{12} \gg q_{\max}^{-1}$), the UV cutoff drops out and we have $\xi(r_{12}) \approx \frac{1}{N_*}\ln\left(\frac{L}{r_{12}}\right)$ [157], where $N_* \approx 60$ is the number of e-folds before the end of inflation that perturbations corresponding to the largest observable scales left the horizon. For observable scales, therefore, $\xi(r_{12}) \approx \frac{1}{60} = 0.017$. This ratio is not sufficiently small that we can have complete confidence in the expansion method, especially recalling also the limitations mentioned in § 5.2.3. We expect, however, that it will likely be sufficiently accurate in many cases.

5.3.1 Analytic Examples

The next step is to specify the $N(\chi)$ function. To begin with, for simplicity and in order to highlight some issues, we follow Ref. [155] and choose the simple analytic functions studied there.

Sine function

First we consider a sine function

$$N(\chi) = B\sin\left(\frac{\chi}{\lambda}\right) \tag{5.75}$$

We compute the two-point function of the curvature perturbation, $\langle\zeta_1\zeta_2\rangle$, for this example in several ways.

First, we directly integrate the fully non-perturbative expression for $\langle\zeta_1\zeta_2\rangle$ which arises from Eq. (5.22); this makes use of the joint probability distribution for χ_1 and χ_2 (Eq. (5.40)). Because of the simple form of the analytical function we have taken for N, the resulting integration is easily tractable analytically, and we denote the result by $\langle\zeta_1\zeta_2\rangle_{\text{Full}}$.

In § 5.2.3, we presented Eq. (5.27) as the result of our expansion method, and later presented a simplified expression for $\tilde{N}_I$ in Eq. (5.37). The second way in which we compute (an approximation to) $\langle\zeta_1\zeta_2\rangle$ is therefore to employ these formulae, leading to

$$\langle\zeta_1\zeta_2\rangle_{\text{Exp}} = \langle\delta\chi N\rangle^2 \frac{\Sigma(r_{12})}{\langle\delta\chi^2\rangle^2}\,. \tag{5.76}$$

Taking $\bar{\chi} = 0$ one finds

$$\langle\zeta_1\zeta_2\rangle_{\text{Full}} = B^2 e^{-\frac{\langle\chi^2\rangle}{\lambda^2}} \sinh\left(\frac{\langle\chi^2\rangle}{\lambda^2}\xi(r_{12})\right) \tag{5.77}$$

and to leading order

$$\langle\zeta_1\zeta_2\rangle_{\text{Exp}} = B^2 e^{-\frac{\langle\chi^2\rangle}{\lambda^2}} \frac{\langle\chi^2\rangle}{\lambda^2}\xi(r_{12}) \tag{5.78}$$

which also follows from expanding Eq. (5.77).

This example is useful, because it highlights, as was also noted in Ref. [155], the possible limitations of our expansion methods discussed in § 5.2.3. In this case, for $\langle\zeta_1\zeta_2\rangle_{\text{Exp}}$ to be a good approximation to $\langle\zeta_1\zeta_2\rangle_{\text{Full}}$, it is insufficient for only $\xi(r_{12}) \ll 1$. We have to impose a more stringent condition, namely $\xi(r_{12})\langle\chi^2\rangle = \Sigma(r_{12}) \ll \lambda^2$. One should note that this is still a significant improvement over the standard δN method of making a Taylor expansion of the N function reviewed in § 5.2.1. λ is a measure of the width of a feature in the N function, and the requirement for standard δN to work is that $\Sigma \ll \lambda^2$, while for our expansion method only that $\Sigma(r_{12}) \ll \lambda^2$ is required, which as we have seen is two orders of magnitude less stringent.

Gaussian function

For our second analytic example, we consider the $N(\chi)$ function to be an unnormalised Gaussian

$$N(\chi) = A\frac{e^{\frac{-(\chi-m_1)^2}{2\sigma_1^2}}}{\sqrt{2\pi}\sigma_1} \tag{5.79}$$

where A, m_1 and σ_1 are constants defining the amplitude, position of the peak and width of the function. In Ref. [155] the authors used a sum of normal distributions with different amplitudes and widths to represent the spiky $N(\chi)$ function that

arises in massless preheating [151, 152, 154].

Without loss of generality we can take $\bar{\chi} = 0$. Here we denote the variance of the probability distribution of the field perturbations, Σ, using $\Sigma = \sigma^2$, and doing so we find

$$\begin{aligned}\langle\zeta_1\zeta_2\rangle_{\rm Full} =& A^2\frac{e^{-\frac{m_1^2}{\sigma^2+\sigma_1^2+\Sigma(r_{12})}}}{2\pi\sqrt{(\sigma^2+\sigma_1^2)^2-\Sigma(r_{12})^2}}\\ &- A^2\frac{e^{-\frac{m_1^2}{\sigma^2+\sigma_1^2}}}{2\pi(\sigma^2+\sigma_1^2)},\end{aligned} \tag{5.80}$$

and to leading and sub-leading order, from Eq. (5.49), we have

$$\begin{aligned}\langle\zeta_1\zeta_2\rangle_{\rm Exp} =& A^2\frac{e^{-\frac{m_1^2}{\sigma^2+\sigma_1^2}}m_1^2\Sigma(r_{12})}{2\pi(\sigma^2+\sigma_1^2)^3}\\ &+A^2\frac{e^{-\frac{m_1^2}{\sigma^2+\sigma_1^2}}(-m_1^2+\sigma^2+\sigma_1^2)^2(\Sigma(r_{12}))^2}{4\pi(\sigma^2+\sigma_1^2)^5},\end{aligned} \tag{5.81}$$

which also follows from expanding Eq. (5.80).

The ratio of the sub-leading term to the leading term is

$$\text{ratio} = \frac{\Sigma(r_{12})(-m_1^2+\sigma^2+\sigma_1^2)^2}{2m_1^2(\sigma^2+\sigma_1^2)^2}\,.$$

We wish to understand when this is small, and hence when our expansion method can be trusted. Assuming $\sigma_1 \leqslant \sigma$ (the N function is of a similar width or narrower than the distribution of field perturbations), the condition required for the ratio to be small becomes $\Sigma(r_{12}) \ll m_1^2\sigma^4/(-m_1^2+\sigma^2)^2$. For fixed σ, there is then both a lower and an upper limit on m_1 in order for this condition to be satisfied. This makes sense since if m_1 is too small, which in this case means $m_1 \ll \sigma$ the N function becomes close to even. While if $m_1 \gg \sigma$ the N function is sampled only by the tail of the probability distribution, and one would not expect the expansion to be be accurate. A representative case is $m_1 \sim \mathcal{O}(\sigma)$, leading to $\Sigma(r_{12}) \ll \sigma^2$, which is the condition we assumed to make our original expansion.

The other case is where $\sigma_1 \geqslant \sigma$. In this case the distribution is now narrower than the N function, and the ratio implies we must have $\Sigma(r_{12}) \ll m_1^2\sigma_1^4/(-m_1^2+\sigma_1^2)^2$. In this case the ratio can also be satisfied as long as m_1 is not too small or too large, which in this case means neither $m_1 \ll \sigma$ nor $m_1 \gg \sigma$. In the representative case of $m_1 \sim \mathcal{O}(\sigma_1)$, the condition reduces to $\Sigma(r_{12}) \ll \sigma_1^2$, which is weak given that

$\sigma_1 > \sigma$. We would expect standard δN to work in the case ($\sigma \ll \sigma_1$), but here, as for the sinusoidal case, we have relaxed that criteria.

Lessons

It is also important to note that in all the cases above, the expansion fails because the leading contribution to the two-point function of ζ itself becomes very small. In the second example, if the N function was made up of a series of spikes (as is the case where the result of massless pre-heating is parametrised), even if the expansion failed for some members of the series, the overall value for the leading term would be dominated by members of the series for which m_1 does not fall outside the allowed range, leading to an accurate overall result. This also gives us hope that for a realistic N function, calculated, for example, from lattice simulations the expansion method we advocate will be accurate.

It seems therefore that there are two regimes in which the method has a good chance of working. One either requires that $\Sigma(r_{12})^{1/2}$ is smaller than the scale on which the N function is structured, or that $\Sigma^{1/2}$, is much larger than the scale on which the N function is structured (and so the structure is averaged over, assuming the average is not close to zero). In intermediate cases the method seems to fail. Overall, however, the message of these two analytic examples is that it is crucial to check for the validity of the approximation on a case by case basis.

5.3.2 A Non-analytic Example

Next we turn to a more realistic example. Although almost all the analysis of the curvaton scenario is based on the assumption of a perturbative curvaton decay, it is possible for the curvaton to decay through a non-perturbative process analogous to inflationary preheating [174, 175]. For our example, we consider the $N(\chi)$ function presented in Fig. 3 of Ref. [153], which was generated from a resonant curvaton decay scenario using classical lattice field theory simulations [172, 176]. The system consists of three fields: an inflaton, curvaton and a third light field, χ. The curvaton field decays into particles of χ via parametric resonance [177–179]. The authors considered only the contribution of perturbations from the χ field to ζ, and so N is a function only of this field. In order to perform the integrations necessary to study this model, we construct an interpolating function to approximate $N(\chi)$ given the data points presented in Ref. [153]. We present the data points and the interpolating function in Fig. 5.1.

In this section we will again compute the two-point function of the curvature perturbation in real space, $\langle\zeta_1\zeta_2\rangle_{\rm Full}$, from Eq. (5.22) as described above, and then using

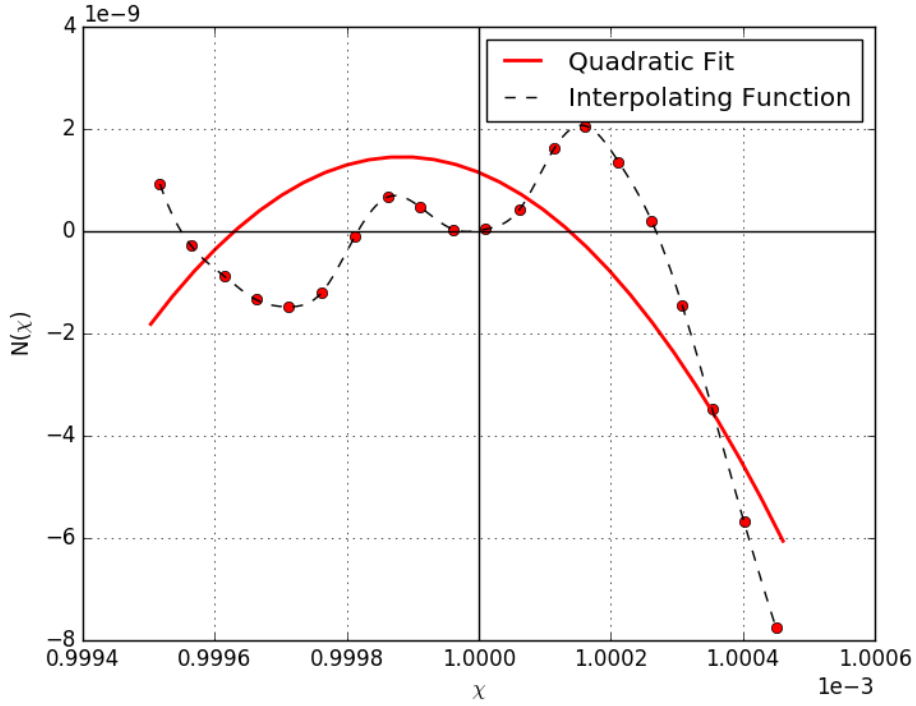

Figure 5.1: *An example of a realistic $N(\chi)$ obtained from lattice field theory simulations and centered around $\bar{\chi} = 0.001$ [153]. Red dots are the data points, the black dashed line shows the interpolating function and the solid red line represents a quadratic fit to the data points. We will use the interpolating function for our regular δN analysis.*

our expansion method (retaining only the leading term) we will calculate $\langle\zeta_1\zeta_2\rangle_{\rm Exp}$. This time both must be computed numerically, and this means we have to fix the various parameters which enter the expression presented at the start of § 5.3, in particular, the IR cutoff L^{-1} and the UV cutoff $q_{\rm max}$. We do so by assuming that perturbations which exited the horizon 60 e-folds before the end of inflation correspond to the largest observable scales today. We associate the largest observable scale today with L, and include in the calculation all shorter modes which exit the horizon until the end of inflation. Taking the scale of the shortest modes to be $r_{\rm min}$, it then follows that $L = e^{60} \times r_{\rm min} \approx 10^{26} r_{\rm min}$. The UV cutoff, defined as $q_{\rm max} = \frac{2\pi}{r_{\rm min}}$.

We will also compute the power spectrum in Fourier space, and the methods we use for this are discussed in the next subsection. Since the scales constrained by CMB anisotropy data correspond to the modes which exited during roughly 4 e-folds of inflation, when presenting our results the range of k values we will be interested in range from $\frac{2\pi}{L}$ to $e^4 \times \frac{2\pi}{L}$, i.e., from the horizon size today down to about e^4 times smaller than the horizon size.

In addition to the full and expanded expressions, we will also plot the results for the power spectrum that one attains from the regular δN method, calculating the derivatives of N locally at our choice of the value of $\bar{\chi}$. Finally using our expansion method, we will also calculate the reduced bispectrum $f_{\rm NL}$ for this model, comparing with the results which would be obtained from regular δN.

The Power Spectrum: Two Methods

We want to calculate $\langle\zeta_1\zeta_2\rangle_{\rm Full}$ to be able to determine whether our expanded method is working. Our first approach in calculating $\langle\zeta_1\zeta_2\rangle_{\rm Full}$ was using 'Method 1' because performing a one-dimensional integral is much simpler than using a three-dimensional fast Fourier transform. However, we found that the integral was sensitive to the integrand of the fitting function used, making this method unreliable for our purposes. For this reason, we were forced to go down the path of a fast Fourier transform ('Method 2'). We show how both methods work below.

1. Method 1

Our expansion method, Eq. (5.27) allows us to pass directly to Fourier space and to write the power spectrum as $P_\zeta(k)_{\rm Exp} \approx \tilde{N}_I \tilde{N}_J \Sigma^{IJ}(k)$ where $\Sigma^{IJ}(k) = \delta^{IJ}\frac{P_0}{k^3}$. However, if one wishes to work with the fully non-perturbative $\langle\zeta_1\zeta_2\rangle_{\rm Full}$, one needs to Fourier transform the real space two-point function of ζ. The route we take to

achieving this is as follows. First we define

$$\begin{aligned}\mathcal{F}\left[\,\langle\zeta_1\zeta_2\rangle_{\rm Full}\,\right] &= \langle\zeta_{\mathbf{k_1}}\zeta_{\mathbf{k_2}}\rangle_{\rm Full} \\ &= (2\pi)^3\delta^3(\mathbf{k_1}+\mathbf{k_2})P_\zeta(k_1)_{\rm Full}\,.\end{aligned} \tag{5.82}$$

Then given that the two-point function is always some function of $r_{12} = |\mathbf{r_1} - \mathbf{r_2}|$, we define $\langle\zeta_1\zeta_2\rangle_{\rm Full} = A(r_{12})$ and note

$$\mathcal{F}\left[A(r_{12})\right] = \int_{-\infty}^{\infty}\mathrm{d}^3\mathbf{r_1}\int_{-\infty}^{\infty}\mathrm{d}^3\mathbf{r_2}A(r_{12})e^{-i\mathbf{k_1}.\mathbf{r_1}}e^{-i\mathbf{k_2}.\mathbf{r_2}}\,. \tag{5.83}$$

By making a change of variables from $\mathbf{r}_1$ to $\mathbf{r}_{12}$, i.e.,

$$\mathbf{r_{12}} = \mathbf{r_1} - \mathbf{r_2} \qquad \Longrightarrow \qquad \mathbf{r_1} = \mathbf{r_{12}} + \mathbf{r_2}, \tag{5.84}$$

Eq. (5.83) can be written as

$$\mathcal{F}\left[A(r_{12})\right] = \int_{-\infty}^{\infty}\mathrm{d}^3\mathbf{r_1}\int_{-\infty}^{\infty}\mathrm{d}^3\mathbf{r_2}A(r_{12})e^{-i\mathbf{k_1}.(\mathbf{r_{12}}+\mathbf{r_2})}e^{-i\mathbf{k_2}.\mathbf{r_2}}\,. \tag{5.85}$$

Then, collecting terms, we have

$$\mathcal{F}\left[A(r_{12})\right] = \int_{-\infty}^{\infty}\mathrm{d}^3\mathbf{r_2}e^{-i\mathbf{r_2}.(\mathbf{k_1}+\mathbf{k_2})}\int_{-\infty}^{\infty}\mathrm{d}^3\mathbf{r_1}A(r_{12})e^{-i\mathbf{k_1}.\mathbf{r_{12}}}\,. \tag{5.86}$$

To pull out a delta function, we then write

$$\mathcal{F}\left[A(r_{12})\right] = (2\pi)^3\frac{1}{(2\pi)^3}\int_{-\infty}^{\infty}\mathrm{d}^3\mathbf{r_2}e^{-i\mathbf{r_2}.(\mathbf{k_1}+\mathbf{k_2})}\int_{-\infty}^{\infty}\mathrm{d}^3\mathbf{r_1}A(r_{12})e^{-i\mathbf{k_1}.\mathbf{r_{12}}}\,, \tag{5.87}$$

followed by

$$\mathcal{F}\left[A(r_{12})\right] = (2\pi)^3\delta^3(\mathbf{k_1}+\mathbf{k_2})\int_{-\infty}^{\infty}\mathrm{d}^3\mathbf{r_1}A(r_{12})e^{-i\mathbf{k_1}.\mathbf{r_{12}}}\,, \tag{5.88}$$

where we have used the Fourier transform of the Dirac delta function. Next, for the second integral, a simple shift of variables gives

$$\mathcal{F}\left[A(r_{12})\right] = (2\pi)^3\delta^3(\mathbf{k_1}+\mathbf{k_2})\int_{-\infty}^{\infty}\mathrm{d}^3\mathbf{r_{12}}A(r_{12})e^{-i\mathbf{k_1}.\mathbf{r_{12}}}\,. \tag{5.89}$$

Comparing the expression above with Eq. (5.82), we see that

$$P_\zeta(k_1)_{\rm Full} = \int_{-\infty}^{\infty}\mathrm{d}^3\mathbf{r_{12}}A(r_{12})e^{-i\mathbf{k_1}.\mathbf{r_{12}}}\,. \tag{5.90}$$

Let us now move to spherical polar coordinates such that

$$\mathrm{d}^3\mathbf{r_{12}} = r_{12}^2\,\mathrm{d}r_{12}\,\sin\theta\,\mathrm{d}\theta\,\mathrm{d}\phi \;\text{ and }\; \mathbf{k_1}.\mathbf{r_{12}} = k_1 r_{12}\cos\theta. \tag{5.91}$$

Then,

$$P_\zeta(k_1)_{\text{Full}} = \int_0^\infty \mathrm{d}r_{12}\; r_{12}^2\; A(r_{12}) \int_0^{2\pi} \mathrm{d}\phi \int_0^\pi \mathrm{d}\theta\; \sin\theta\; e^{-ik_1 r_{12}\cos\theta}. \tag{5.92}$$

Integrating w.r.t ϕ, we have

$$P_\zeta(k_1)_{\text{Full}} = \int_0^\infty \mathrm{d}r_{12}\; 2\pi\; r_{12}^2\; A(r_{12}) \int_0^\pi \mathrm{d}\theta\; \sin\theta\; e^{-ik_1 r_{12}\cos\theta}. \tag{5.93}$$

Then, noting that $\frac{\mathrm{d}}{\mathrm{d}\theta}(e^{-ik_1 r_{12}\cos\theta}) = ik_1 r_{12}\sin\theta\; e^{-ik_1 r_{12}\cos\theta}$ and using $\frac{2\sin(k_1 r_{12})}{k_1 r_{12}} = \frac{1}{ik_1 r_{12}}(e^{ik_1 r_{12}} - e^{-ik_1 r_{12}})$, we end up with

$$P_\zeta(k_1)_{\text{Full}} = 4\pi \int_0^\infty \mathrm{d}r_{12}\; r_{12}^2\; A(r_{12}) \frac{\sin(k_1 r_{12})}{k_1 r_{12}}. \tag{5.94}$$

To evaluate the power spectrum, therefore, one possibility is to first use the $N(\chi)$ function to calculate $A(r_{12})$ for a range of values of r_{12}, and then to perform this one dimensional integration. Rather than sampling $A(r_{12})$ at all positions needed by an integration algorithm, one could fit $A(r_{12})$ with an interpolating function. A problem that arises, however, is that the integral is sensitive to the value of the integrand even for $r_{12} \gg L$. A second issue is that the integrand is highly oscillatory. These issues meant we couldn't get accurate results using this strategy.

2. Method 2 (FFT)

An alternative is to evaluate instead Eq. (5.90), using a fast (discrete) Fourier transform. Although this is effectively a three dimensional integral, the speed of the algorithm involved means it is more tractable than integrating Eq. (5.94). The direct implementation of the Discrete Fourier Transform requires $\mathcal{O}(\mathcal{N}^2)$ operations where $\mathcal{N}$ is the total number of data points transformed. Using the Fast Fourier Transform, this is reduced to $\mathcal{O}(\mathcal{N}\log\mathcal{N})$.

To avoid aliasing, we make use of the Nyquist sampling theorem which means that we must sample $A(r_{12})$ with a small enough uniform intervals such that the sampling frequency is at least twice the highest frequency contained in the signal. In this case, the highest frequency that we're interested in is $e^4 \times \frac{2\pi}{L}$ and we always ensure this criteria is easily met. We must also ensure that the lowest frequency sampled is at least an order of magnitude smaller than $\frac{2\pi}{L}$.

Even when these constraints are met, the results of the Fourier transform will have a number of spurious points. In order to present a clean plot, therefore, we fit the data in log space to a polynomial. Finally we plot this fitted function. As a test that

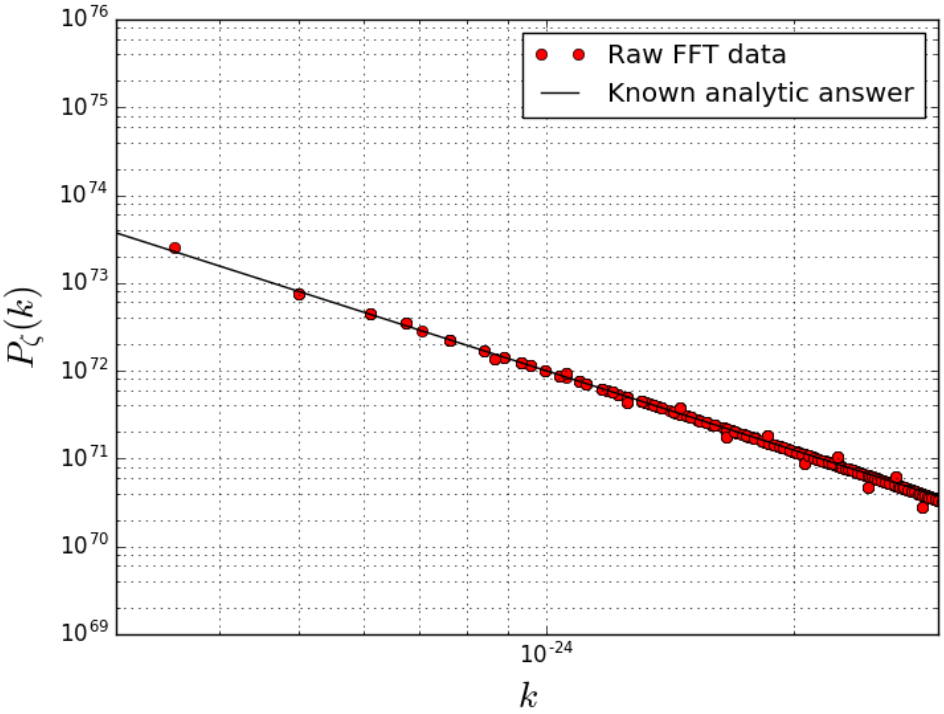

Figure 5.2: *The data points show the output of* $\mathcal{F}\left[\Sigma(r_{12})\right]$. *We know that the analytic answer of* $\mathcal{F}\left[\Sigma(r_{12})\right]$ *is* $\frac{P_0}{k^3}$ *(cf. Eq. (5.72) and Eq. (5.53)). In this plot, we show the known analytic answer in black. Here, we do not show all the points from the FFT to keep the plot clean. The spurious points on large* k *are due to aliasing and those on small* k *due to edge effects. The number of points on top of the black line far outweighs the number of spurious points.*

we are sampling the correct range and the method is working, we first applied it to a sampled version of Eq. (5.72), to ensure we recovered Eq. (5.53) with precision. We plot the results in Fig. 5.2.

Three cases

We perform our analysis for three cases and present our analysis of the two-point function and the power spectrum in Figs. 5.3-5.8. The cases we consider are

1. $\bar{\chi} = 0.001$ and $\langle \delta\chi^2 \rangle \approx 7\times10^{-15}$
2. $\bar{\chi} = 0.0009998$ and $\langle \delta\chi^2 \rangle \approx 7\times10^{-15}$
3. $\bar{\chi} = 0.001$ and $\langle \delta\chi^2 \rangle \approx 6\times10^{-14}$

For the power spectrum, we plot $P_\zeta(k)/P_{\zeta_{\rm pivot}}$ against $k/k_{\rm pivot}$. We arbitrarily choose $k_{\rm pivot} = \frac{2\pi}{L}$. We also fix $P_{\zeta_{\rm pivot}}$ to be $P_{\zeta_{\rm Full}}|_{k=k_{\rm pivot}}$ for all three ('Full', 'Expanded', 'Regular δN') methods for easy comparison; otherwise all three lines will lie on top

of each other initially as dividing by each of their corresponding pivot value of P_ζ will force them to start at the same point.

In all cases we see that the expansion method is a much better approximation to the fully non-perturbative method than regular δN, and in two of the cases does a good job at recovering the amplitude and initial scale dependence of the power spectrum. In the third case however, we can see the method is breaking down even for the largest scales.

In all three cases, we see that the 'Expanded' power spectrum either matches or is smaller that the 'Full' power spectrum on all scales while the 'Regular' power spectrum can be smaller or larger than the 'Full' answer, depending on the value of $\bar{\chi}$ and $\langle \delta\chi^2 \rangle$. For interest only, we also show the raw FFT output for the third case in Fig. 5.9.

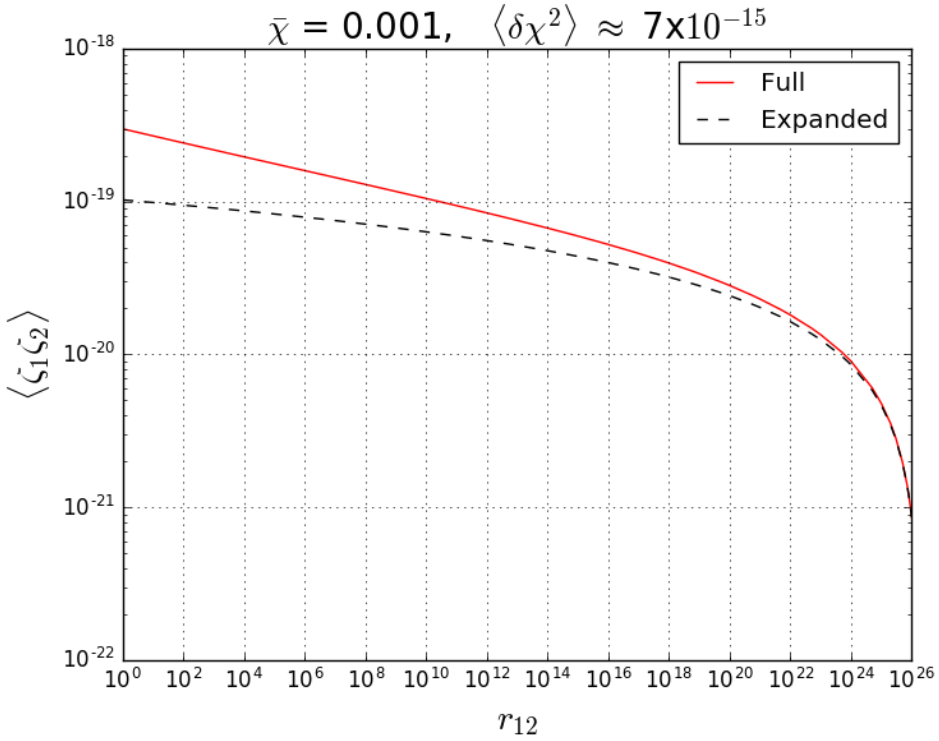

Figure 5.3: *Case 1: Correlation function of $\zeta(\chi)$ for one realization with $\bar{\chi} = 0.001$ and $\langle \delta\chi^2 \rangle \approx 7\times10^{-15}$ on a Log-Log plot. The exact correlation function ('Full') is calculated from Eq.(5.22). The approximated correlation function ('Expanded') is given by Eq.(5.27). As expected, the approximated correlation function becomes progressively worse on shorter scales.*

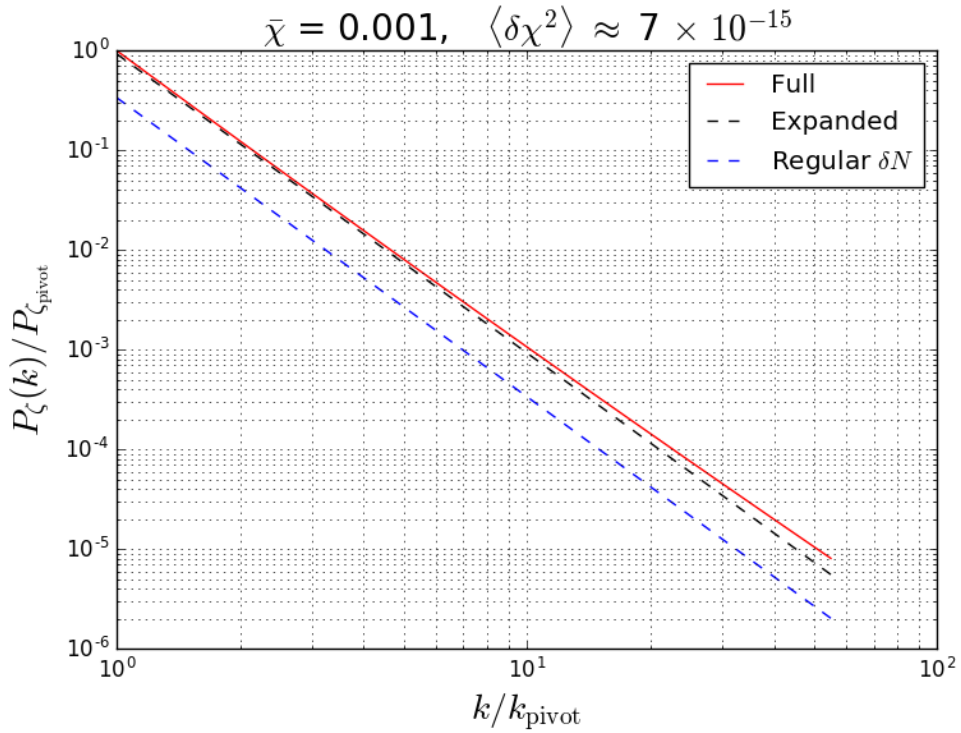

Figure 5.4: *Case 1: Log-Log plots of the power spectrum of ζ, calculated using the full, expansion and regular δN methods respectively.*

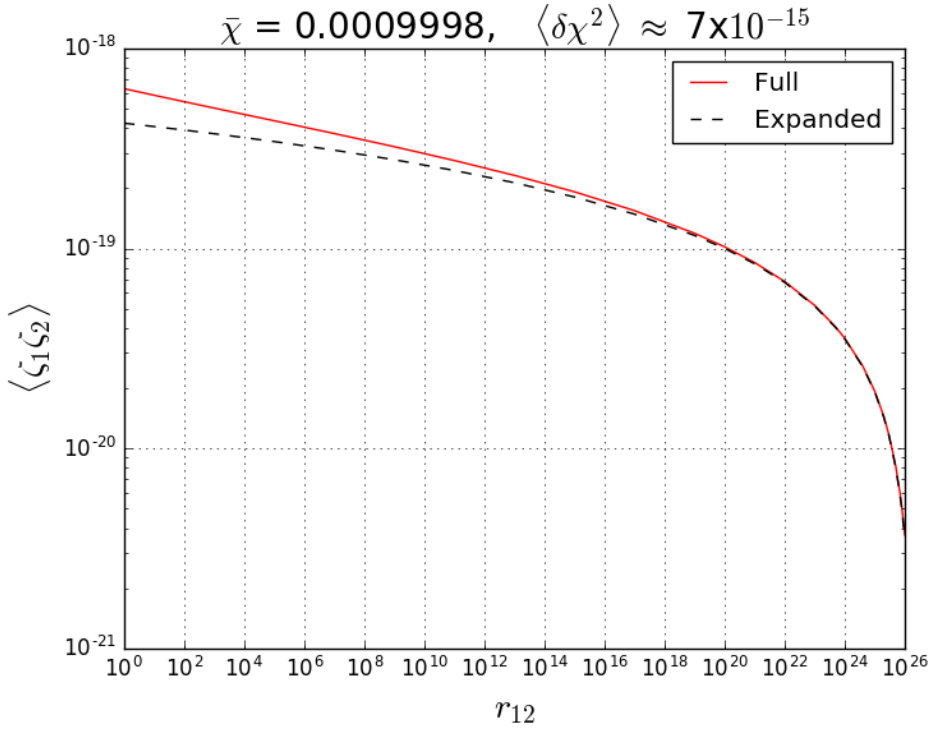

Figure 5.5: *Case 2: Here, we plot the correlation function of $\zeta(\chi)$ for one realization with $\bar{\chi} = 0.0009998$ and $\langle \delta\chi^2 \rangle \approx 7{\times}10^{-15}$ on a Log-Log plot.*

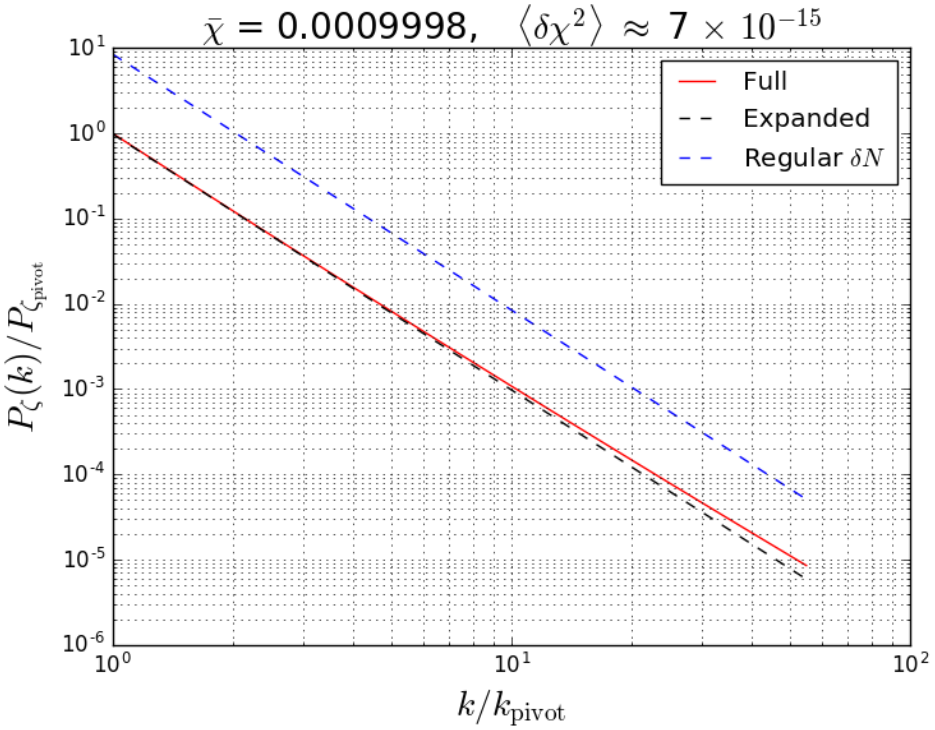

Figure 5.6: *Case 2: Log-Log plots of the power spectrum of ζ, calculated using the full, expansion and regular δN methods respectively.*

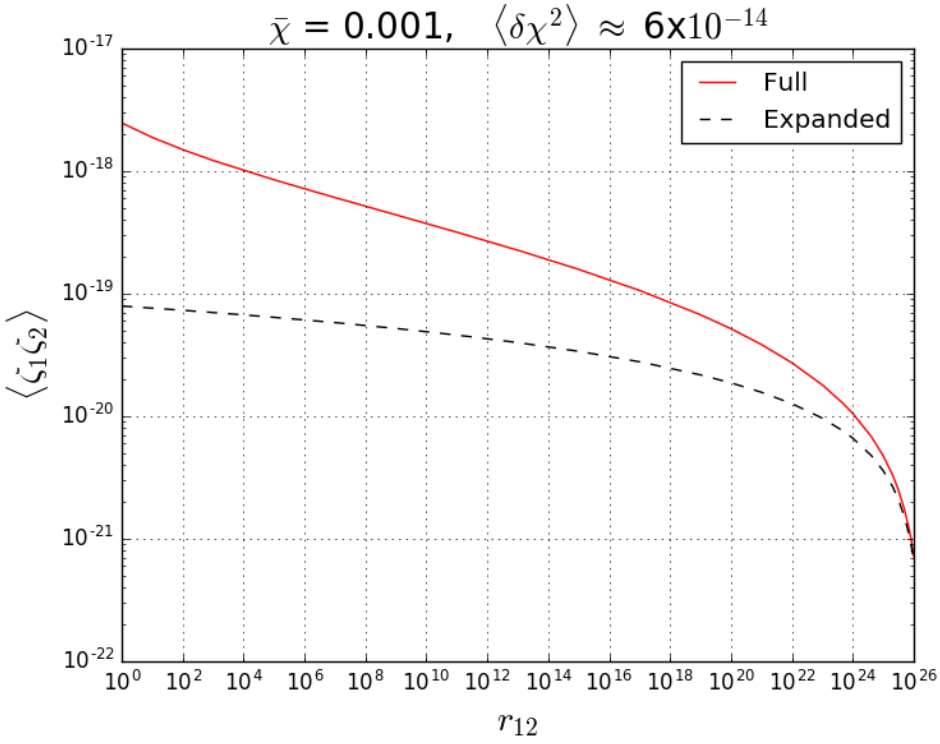

Figure 5.7: *Case 3: Here, we plot the correlation function of $\zeta(\chi)$ for one realization with $\bar{\chi} = 0.001$ and $\langle \delta\chi^2 \rangle \approx 6\times10^{-14}$. The approximated correlation function is worse in this case because the shorter tail distribution 'sees' less of the mapping.*

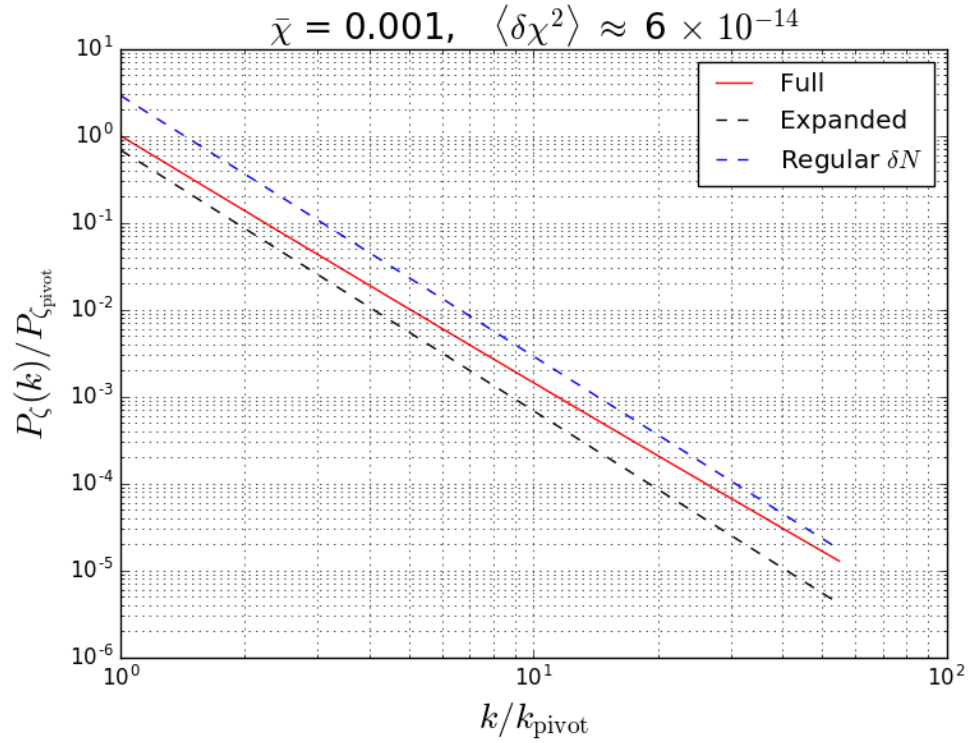

Figure 5.8: *Case 3: Log-Log plots of the power spectrum of ζ, calculated using the full, expansion and regular δN methods respectively. The effect of the shorter tail distribution is also reflected in the difference between the 'Full' and 'Expanded' power spectra.*

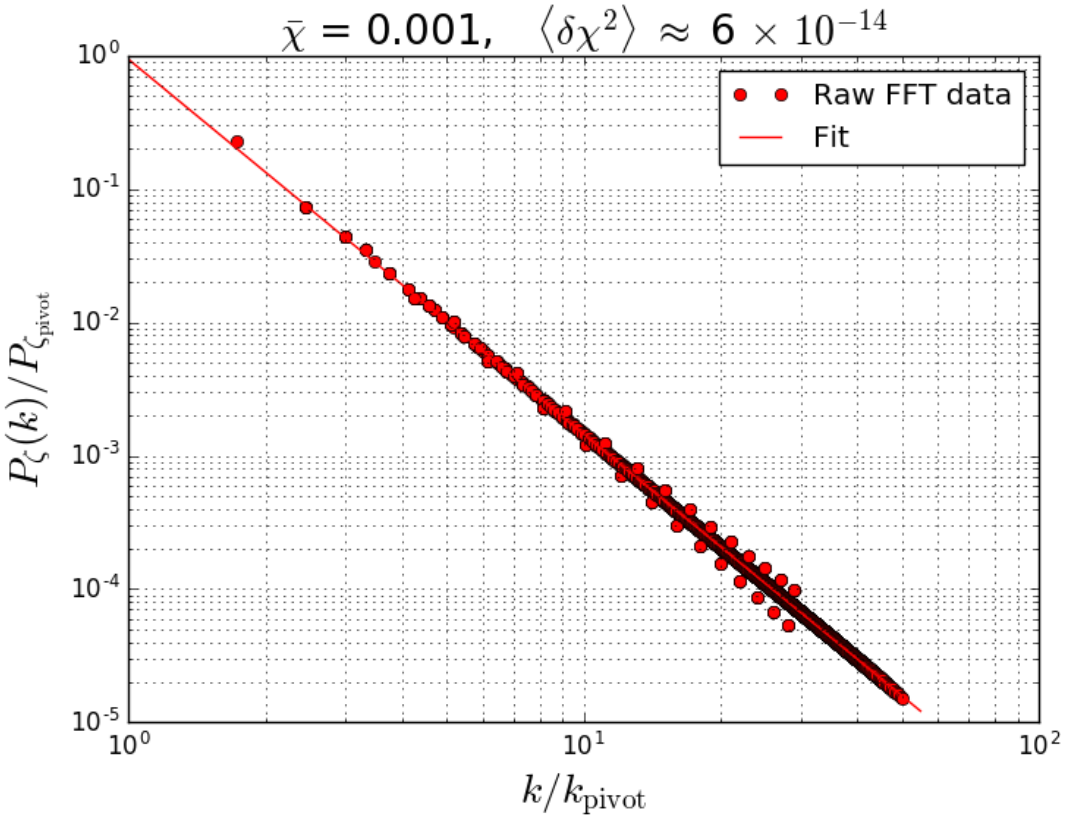

Figure 5.9: *In this figure, we show the raw FFT data points for case 3 and the same fitting polynomial to the points that was used to obtain the 'Full' answer in Fig. 5.8. Here, we choose to omit most of the spurious points from the Fourier transform for clarity.*

The Reduced Bispectrum

First, we calculate the reduced bispectrum using regular δN. For case 1, $f_{\rm NL}$ is $\mathcal{O}(10^{10})$, $f_{\rm NL}$ is negative and $\mathcal{O}(10^{7})$ for case 2 and finally, $f_{\rm NL}$ is $\mathcal{O}(10^{10})$ for case 3. Using Eq. (5.31), i.e., using the expansion method we can also calculate the reduced bispectrum in each case. We find that $f_{\rm NL}$ is enormous for all three cases: $f_{\rm NL}$ is $\mathcal{O}(10^{9})$, $\mathcal{O}(10^{8})$ and $\mathcal{O}(10^{10})$ for case 1, 2 and 3 respectively. This is to be expected since in all cases the higher order terms in the non-perturbative δN expansion are relatively large (since by eye one can see the full line deviate from the expanded line plotted using only the leading term).

However, we also find that the amplitude of the curvature perturbation for these specific examples is too small to explain the observed amplitude: $\mathcal{O}(10^{-20})$, $\mathcal{O}(10^{-19})$ and $\mathcal{O}(10^{-20})$ for case 1, 2 and 3 respectively. It is likely this can be altered by changing $\langle\delta\chi\delta\chi\rangle$. But given the $N(\chi)$ function we began with, we are limited to assuming $\langle\delta\chi\delta\chi\rangle^{1/2}$ is much smaller than the range of χ over which the N function has been calculated. Ultimately $\langle\delta\chi\delta\chi\rangle^{1/2}$ is fixed by the energy scale of inflation, but unlike in the usual approach we can't account for the effect of changing this energy scale after calculating the derivatives of N, because the non-perturbative nature of the calculation means the non-perturbation δN coefficients are affected by $\langle\delta\chi\delta\chi\rangle^{1/2}$.

In terms of the parameters we are working with, therefore, in order to agree with observation we would require that the total curvature perturbation is a mixture of the subdominant component that we have and another dominant component.

Taking the observed amplitude to be 10^{-9} [180] and taking the dominant component to be the standard adiabatic Gaussian perturbations from the inflaton ϕ, this mixture dilutes the non-Gaussianity of the total curvature perturbation. Below we give a back-of-the-envelope calculation of $f_{\rm NL,obs}$ for each of three cases where we will assume both fields (χ and ϕ) have the same variance at horizon crossing.

$f_{\rm NL,obs}$ is given by (see Eq. (5.31)):

$$f_{\rm NL,obs} = \frac{2\tilde{N}_{\phi\chi}\tilde{N}_{\phi}\tilde{N}_{\chi} + \tilde{N}_{\chi\chi}\tilde{N}_{\chi}\tilde{N}_{\chi} + \tilde{N}_{\phi\phi}\tilde{N}_{\phi}\tilde{N}_{\phi}}{(\tilde{N}_{\phi}\tilde{N}_{\phi} + \tilde{N}_{\chi}\tilde{N}_{\chi})^2} \times \frac{5}{6}. \tag{5.95}$$

However, because the inflaton perturbations are adiabatic and close to Gaussian, $f_{\rm NL,obs}$ will be dominated by:

$$f_{\rm NL,obs} \approx \frac{\tilde{N}_{\chi\chi}\tilde{N}_{\chi}\tilde{N}_{\chi}}{(\tilde{N}_{\phi}\tilde{N}_{\phi} + \tilde{N}_{\chi}\tilde{N}_{\chi})^2}. \tag{5.96}$$

For case 1, $\langle\delta\phi^2\rangle = \langle\delta\chi^2\rangle \approx 10^{-15}$ and we have computed

$$\frac{\tilde{N}_{\chi\chi}\tilde{N}_{\chi}\tilde{N}_{\chi}}{(\tilde{N}_{\chi}\tilde{N}_{\chi})^2} \sim 10^9. \tag{5.97}$$

Since the dominant contribution to the observed amplitude of the power spectrum comes from the inflaton field, we can write

$$\tilde{N}_{\phi}\tilde{N}_{\phi}\langle\delta\phi\delta\phi\rangle \sim 10^{-9} \Longrightarrow \tilde{N}_{\phi}\tilde{N}_{\phi}\ 10^{-15} \sim 10^{-9} \Longrightarrow \tilde{N}_{\phi}\tilde{N}_{\phi} \sim 10^6. \tag{5.98}$$

We have also calculated the following:

$$\tilde{N}_{\chi}\tilde{N}_{\chi}\langle\delta\chi\delta\chi\rangle \sim 10^{-20}. \tag{5.99}$$

Therefore, $\tilde{N}_{\chi}\tilde{N}_{\chi}$ is

$$\tilde{N}_{\chi}\tilde{N}_{\chi}\ 10^{-15} \sim 10^{-20} \Longrightarrow \tilde{N}_{\chi}\tilde{N}_{\chi} \sim 10^{-5} \tag{5.100}$$

Using Eq. (5.97), Eq. (5.98) and Eq. (5.100), $f_{\rm NL,obs}$ given by Eq. (5.96) is calculated to be $\mathcal{O}(10^{-13})$.

Performing similar calculations for case 2 and case 3, we have $f_{\rm NL,obs} \sim \mathcal{O}(10^{-12})$ for both case 2 and 3. For all three cases, the level of non-Gaussianity is far below the observational sensitivity [113].

5.4 Conclusion

In the regular δN formalism, the mapping between the curvature perturbation ζ and the scalar field(s) fluctuations is approximated by a Taylor expansion in the fields. This standard technique fails in some cases. Examples include the massless preheating model and the non-perturbative curvaton decay model we revisited in the examples section of this work. In this work, we discuss how to calculate correlation functions of ζ when the mapping is an arbitrary function of the scalar field(s) without making a Taylor expansion. This entails integrating the full probability distribution of the field fluctuations against copies of the N function relating e-folds to initial field values ('Non-perturbative δN formalism'). We discuss how to calculate results using a 'Full' (not approximated) implementation of this formalism, but show that this can be convoluted in practice. For observationally relevant scales the task can be made simpler using an expansion method. This leads to a set of expressions for observable quantities in terms of non-perturbative δN coefficients analogous to the usual δN coefficients ('Expanded'). We argue that the validity of the expansion method must be tested on a case by case basis and suggest ways to do this, but show that at least in the realistic example we consider it leads to a marked improvement over regular δN, and can approximate well the full result.

Our results are closely related to the work of Suyama and Yokoyama [155] and Bethke *et al.* ([156], [157]), but we diverge from their work in a number of ways. First we show how to incorporate the perturbations from n fields whose initial probability distribution need not be precisely Gaussian, and we present our expressions in an alternative way to those authors, which is more suitable for numerical analysis. The expressions are, as we discuss in § 5.2.3, particularly well suited to settings in which a Monte Carlo approach can be advantageous. We intend to employ our results in this setting in forthcoming work, directly utilising lattice simulations. It might seem odd at first that we can use the separate universe approach and information from lattice simulations, which simulate only very short scales, to infer information about perturbations on observable scales. This works, however, because the non-pertubative method works in real space initially, and at first calculates quantities such as $\langle\zeta(\mathbf{x})\zeta(\mathbf{y})\rangle$ without coarse-graining. As long as the simulations are of regions larger than the horizon during reheating, therefore, there is then no barrier to using this method together with δN to calculate $\langle\zeta(\mathbf{x})\zeta(\mathbf{y})\rangle$. This is not directly observable, since it includes information about all scales which aren't observable. After calculating it, however, we can take its Fourier transform and consider the Fourier modes over the range of observable scales (or equivalently coarse-grain the real space result on these scales) to compare with observations. The method we present, therefore, represents a unique opportunity to extract for the first time observable predictions for the curvature perturbation directly from lattice simulations.

6 Reheating

In the previous chapter, we touched on the fact that examples where standard δN fails include models of reheating and preheating and that the form of our non-perturbative expressions are suited to work with numerical lattice simulations which we will do in Chapter 7. This chapter aims to provide more context to the dynamics of reheating and to the understanding of how a highly featured N function arises from preheating. Chapter 6 starts with a discussion of the perturbative reheating process. Next, we turn our focus on the preheating stage which is characterised by exponential particle production via parametric resonance. One entire section is dedicated to a simple variant of chaotic inflation known as 'massless preheating' because it is the subject of study for our numerical simulations later on. Finally, we give an overview of lattice field theory simulations which are extremely useful for numerical analysis of preheating and which we use in Chapter 7.

"You may have to fight a battle more than once to win it."

—Margaret Thatcher

6.1 Reheating, 'The Great Thaw'

At the end of inflation, the homogeneous inflaton begins to oscillate about the minimum of its potential and the oscillations can be interpreted as a collection of scalar particles, independent from each other, oscillating coherently at the same frequency. The inflaton condensate must decay into other forms of matter and radiation since inflation leaves the universe cold and empty[1] as all the energy is in the inflaton field. Reheating is the process through which the inflaton field transfers its energy to other particles and eventually to standard model particles, thus 'reheating' the universe after inflation. These more familiar forms of matter and radiation must eventually reach thermal equilibrium at temperatures greater than 1 MeV in order to recover the working big bang nucleosynthesis scenario [38]. Reheating occurs through coupling of the inflaton field ϕ to other fields. Such couplings must at least be present

[1] One exception is warm inflation where there is particle production during inflation [181, 182].

via gravitational interactions. There are, however, many models of inflation where couplings are to the matter sector of the theory directly. Reheating was initially studied using first-order perturbation theory in Refs. [183–185] where the inflaton oscillates around its minimum, resulting in the production of particles. This so-called 'old' theory of reheating, developed soon after the first inflationary theories, was built on the concept of single body decays. Such decays can be formulated by coupling the inflaton ϕ to other scalar (χ) or fermion (ψ) fields through terms in the Lagrangian such as $g^2\sigma\phi\chi^2$ and $h\phi\bar{\psi}\psi$ (here, σ has dimensions of mass and g and h are dimensionless couplings.). For example, in [186] where reheating was dubbed 'The Great Thaw', the oscillating inflaton field produces fermion-antifermion pairs through Yukawa couplings. The elementary theory of reheating is successful in describing reheating after inflation in many models of inflation; this is why we go into details about perturbative reheating in § 6.2. However, in some cases, the first stage of reheating involves very non-linear dynamics and results in an explosive production of particles. This first stage is called *preheating* [177, 178, 187–193].

In § 6.2, we briefly discuss perturbative reheating, followed by its limitations in § 6.3.1. We then show the importance of non-perturbative effects arising from the coherent nature of the inflaton condensate. These effects include parametric resonances and tachyonic instabilities, all of which result in an exponential growth in the occupation numbers of the fields the inflaton decays to. This kind of rapid particle production is called *preheating*. The extremely rapid decay yields a distribution of products that is far from equilibrium, and only much later settles down to an equilibrium distribution. We will pay special attention to a particular model of preheating, the massless preheating model which is the subject of our main work. The review presented in § 6.2 to § 6.6 closely follows the classic paper by Kofman, Linde and Starobinsky [179] and includes material from Kofman [194], Kofman [178] and Baumann [195]. Because the authors in Ref. [179] used a slightly different definition for the reduced Planck mass, we have changed some of the expressions which follow to keep our definition of $M_{\rm pl}$ in § 1.1 consistent throughout.

6.2 The Standard Lore: Perturbative Reheating

Let us consider the archetypal chaotic inflation with potential

$$V(\phi) = \frac{1}{2}m^2\phi^2, \tag{6.1}$$

and ignore all interactions for the moment. The dynamics of the inflaton field is described by the Klein-Gordon equation (*cf.* Eq. (2.8)) coupled to the Friedmann equation:

$$\ddot{\phi} + 3H\dot{\phi} + m^2\phi = 0 \tag{6.2}$$

$$H^2 = \frac{1}{3M_{\rm pl}^2}(\frac{1}{2}\dot{\phi}^2 + \frac{1}{2}m^2\phi^2). \tag{6.3}$$

The solution to Eq. (6.2) and Eq. (6.3) during the oscillatory stage is

$$\phi(t) \approx \Phi(t)\sin(mt) \tag{6.4}$$

where

$$\Phi(t) \sim \frac{M_{\rm pl}}{mt} \sim \frac{M_{\rm pl}}{4\mathcal{N}}. \tag{6.5}$$

$\Phi(t)$ is the amplitude of oscillations and $\mathcal{N}$ is the number of oscillations since the end of inflation. During the oscillatory phase, the universe behaves in the same way as if it were dominated by non-relativistic particles of mass m since averaged over many oscillations, the scale factor grows as $a \sim t^{2/3}$ and the energy density is

$$\rho_\phi = \frac{1}{2}\dot{\phi}^2 + \frac{1}{2}m^2\phi^2 = \frac{1}{2}m^2\Phi^2 \propto a^{-3}. \tag{6.6}$$

This highlights the well-known result that the coherent oscillations of the homogeneous scalar field oscillating in a quadratic potential correspond to the matter-dominated effective equation of state of pressureless dust. We will later see in § 6.7 that for a quartic potential, the energy of the field ϕ decreases in the same way as the density of relativistic particles, i.e., $\rho_\phi \sim a^{-4}$ and the effective equation of state corresponds to the radiation dominated equation of state with $w \approx \frac{1}{3}$.

Now, let us assume that the inflaton field is coupled to another scalar field χ through the term $g^2\sigma\phi\chi^2$ in the Lagrangian where σ has dimensions of mass and g is a dimensionless coupling. Historically, reheating was first treated perturbatively where the theory was based on the concept of single-body decays. In the perturbative picture, the inflaton field is treated as a collection of scalar particles each having a finite probability of decaying. The effects generated by particle production can be included into the equation of motion for the inflaton field by adding one extra friction term $\Gamma\dot{\phi}$ to the classical equation of motion of the scalar field ϕ:

$$\ddot{\phi} + 3H\dot{\phi} + \Gamma\dot{\phi} + m^2\phi = 0. \tag{6.7}$$

The solution that then generalizes Eq. (6.4) and describes damped oscillations of the inflaton field due to particle decay as well as due to the expansion of the universe is

$$\phi(t) \approx \frac{M_{\rm pl}}{mt}\exp\big(-\frac{1}{2}\Gamma t\big)\sin(mt). \tag{6.8}$$

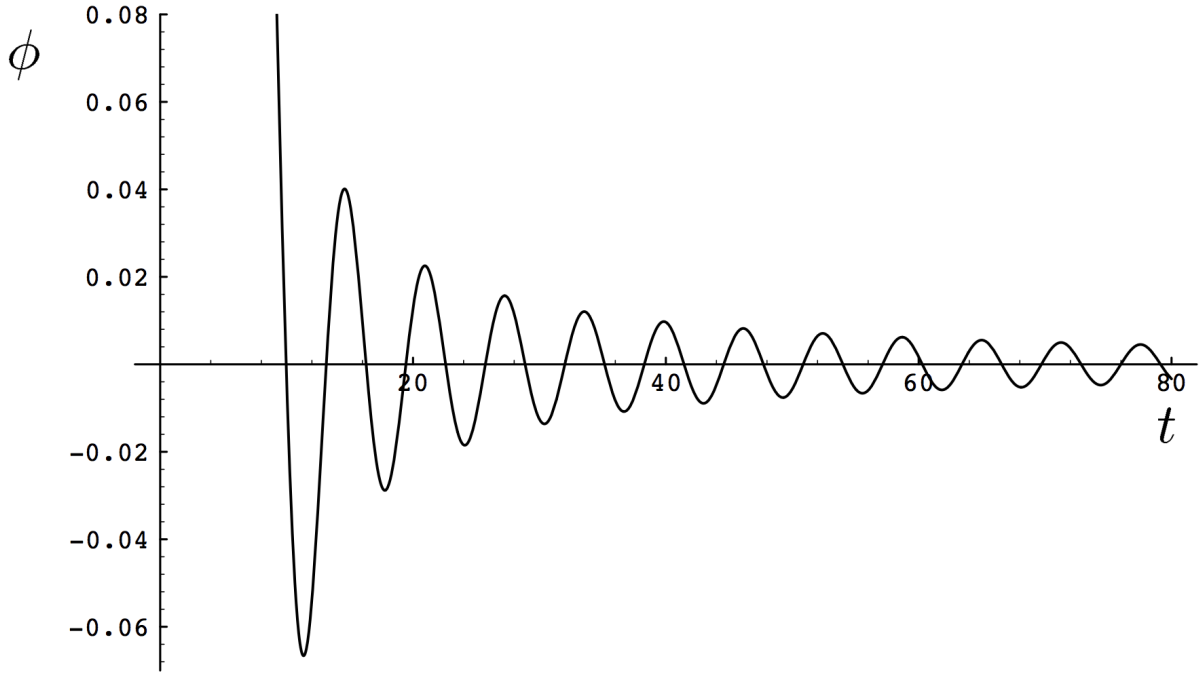

Figure 6.1: *Oscillations in the inflaton field after the end of inflation in the chaotic theory with* $V(\phi) = \frac{1}{2}m^2\phi^2$*. The value of the scalar field is given in units of* $\sqrt{8\pi}M_{\rm pl}$ *and time is measured in units of* m^{-1}*. The amplitude of the oscillations decreases over time due to the "friction term"* $3H\dot{\phi}$ *in Eq. (6.2). Figure taken from [179].*

Using standard field theory methods, we can estimate the decay rate as follows:

$$\Gamma_{\phi\to\chi\chi} = \frac{g^4\sigma^2}{8\pi m}. \tag{6.9}$$

For small coupling constants, as required for radiative corrections to not spoil the flatness of the potential during inflation, typically Γ is much smaller than the Hubble parameter at the end of inflation. At the beginning of the oscillatory phase, the inflaton field mainly loses energy due to the expansion of the universe. It is only once the Hubble expansion rate decreases to a value comparable to Γ that particle production becomes effective. The energy density of the universe at the time t_r when the rate of expansion given by the the Hubble parameter t_r^{-1} is equal to Γ is

$$\rho(t_r) = 3\Gamma^2 M_{\rm pl}^2. \tag{6.10}$$

Assuming that the decay particles interact with each other strongly enough, then thermal equilibrium quickly sets in after the decay of the inflaton condensate. By equating the energy density above to that of a thermal bath

$$\rho_{\rm rad} = \frac{\pi^2}{30}g_\star T_r^4 \tag{6.11}$$

containing $g_\star$ relativistic degrees of freedom ($g_\star \approx 100$ at the time), we obtain the

reheating temperature [194]

$$T_r \sim 0.1\sqrt{\Gamma M_{\rm pl}}. \tag{6.12}$$

It is worth noting that T_r does not depend on the initial value of ϕ but only on the underlying elementary particle theory parameters. To get a numerical estimate on the duration of reheating t_r, for the decay rate of the inflaton field and for the reheating temperature T_r, one should know the mass of the inflaton field and the coupling constants. As previously mentioned, the coupling constants cannot be too large, otherwise radiative corrections change the shape of the inflaton potential. Together with the constraints we have on the parameters of the inflaton potential (from normalisation of the CMB on large scales, $m \sim 10^{-6} M_{\rm pl}$), the largest possible decay rate in perturbation theory is $\Gamma < 10^{-20} M_{\rm pl}$. This means that perturbative reheating is slow and produces a reheating temperature which can be very low compared to the energy scale of inflation. For example, for the quadratic inflaton potential, it takes a minimum of $\sim 10^{14}$ oscillations to transfer the inflaton energy to the decay particles. Using Eq. (6.12) we can get a general estimate of the reheating temperature in perturbative reheating,

$$T_r < 10^9 \text{GeV}. \tag{6.13}$$

Such small reheating temperatures imply that GUT (Grand Unified Theory, $T_{\rm GUT} \sim 10^{16}$GeV) baryogenesis cannot work in such scenarios: such scenarios would necessitate a theory of low-temperature baryogenesis. The reheating temperature can be much higher if there is a preheating stage which we discuss next after a short discussion of the drawbacks of the elementary theory.

6.3 Parametric Resonance and Preheating

6.3.1 Limitations of Perturbative Reheating

The perturbative reheating analysis outlined in the previous section has many issues. While the heuristic equation of motion in Eq. (6.7) captures the qualitative behaviour, it does not provide a consistent description of the perturbative decay since it violates the fluctuation dissipation theorem [196]; there are always fluctuations in systems with dissipation and these fluctuations are missing from Eq. (6.7). The effects of these fluctuations on the effective mass of the inflaton condensate can significantly affect the dynamics of the system [179]. This insight, together with the insight that effective masses can be space and time dependent is at the very heart of preheating [178, 191, 197, 198]. Another problem is that for large couplings (but still small enough not to upset the flatness of the inflaton potential), perturbative methods fail.

The principal problem with perturbative reheating is that it does not take into account the coherent nature of the inflaton field. The inflaton field at the beginning of the oscillatory stage is not simply a superposition of free single inflaton states, but rather a coherently oscillating homogeneous field. This means that particle production has to be treated as a collective process in which many inflatons decay simultaneously, not independently of each other. It is justified to treat the inflaton condensate classically because of the large amplitude of the oscillation but the decay products have to be treated quantum mechanically. This is because the decay particles have vanishing occupation numbers at the end of inflation and can be assumed to start off in their vacuum because of the enormous red-shifting during the accelerated expansion. Thus it is valid to use their vacuum state as an initial condition for the resulting quantum mechanical particle production in the classical inflaton background and the improved approach lead to treating reheating as a quantum production of particles in a ϕ background [177, 199].

The perturbative analysis also ignores the significant fact that if many χ particles have been produced, the decay probability is enhanced by Bose statistics. This non-perturbative production of particles typically happens before the perturbative reheating and therefore it has been dubbed preheating. In the next section, we will account for this effect. In particular, we will show how the phenomenon of *parametric resonance* may result in explosive particle production. Despite all of these drawbacks, the perturbative elementary theory of reheating can still be applied to the late stages of reheating such as the decay of remnant inflaton particles after most of the energy has been transferred to relativistic particles. It might also still be applicable if the inflaton field decays into fermions only, with a small coupling constant $\mathrm{h}^2 \ll m/M_{\mathrm{pl}}$.

6.4 Quantum Field Theory in a Time-Dependent Background

We are still considering the chaotic inflaton potential given by Eq. (6.1). Under the influence of this potential, the homogeneous part of the inflaton executes oscillations around $\phi = 0$ which gradually decay. The majority of the inflaton energy at the end of inflation is stored in the $k = 0$ mode and since the occupation number of the inflaton $k = 0$ mode (the homogeneous part) is very large at the end of inflation it behaves essentially as a classical field. One can therefore, to first approximation, treat the inflaton field as a *classical external force* acting on the quantum field χ. As is well-known from classical mechanics a concerted choice of parameters may cause parametric oscillators to resonantly excite themselves, a feature which is known as

parametric resonance. The effective mass of χ changes very rapidly because the inflaton field is time-dependent. This then leads to the non-adiabatic excitation of the field fluctuations by parametric resonance.

Consider the *quantum* field $\hat{\chi}$ in the *classical* background $\phi(t)$,

$$\hat{\chi}(t,\mathbf{x}) = \int \frac{\mathrm{d}^3k}{(2\pi)^{3/2}}\left(\hat{a}_{\mathbf{k}}\chi_k(t)e^{-i\mathbf{k}.\mathbf{x}} + \hat{a}^{\dagger}_{\mathbf{k}}\chi^*_k(t)e^{i\mathbf{k}.\mathbf{x}}\right) \tag{6.14}$$

where $\hat{a}_{\mathbf{k}}$ and $\hat{a}^{\dagger}_{\mathbf{k}}$ are annihilation and creation Bose operators, respectively. If we assume there are no non-linearities in the χ sector of the theory, then the equation of motion for χ is linear and can be studied simply by mode by mode in Fourier space. The mode functions satisfy

$$\ddot{\chi}_k + 3H\dot{\chi}_k + \left(\frac{k^2}{a^2} + m^2_{\chi} + \mathrm{g}^2\phi^2(t)\right)\chi_k = 0. \tag{6.15}$$

Ignoring the expansion of space Eq. (6.15) becomes

$$\ddot{\chi}_k + \left(k^2 + m^2_{\chi} + \mathrm{g}^2\Phi^2\sin^2(mt)\right)\chi_k = 0. \tag{6.16}$$

Eq. (6.16) can be written in the form:

$$\ddot{\chi}_k + \omega^2_k(t)\chi_k = 0, \quad \omega^2_k(t) = k^2 + m^2_{\chi} + \mathrm{g}^2\Phi^2\sin^2(mt). \tag{6.17}$$

Defining a new dimensionless time variable $z \equiv mt$ and using $\sin^2(z) = \frac{1}{2}(1 - \cos(2z))$, this becomes the *Mathieu* equation

$$\chi''_k + (A_k - 2q\cos(2z))\chi_k = 0, \tag{6.18}$$

where

$$A_k \equiv \frac{k^2 + m^2_{\chi}}{m^2} + 2q \quad \text{and} \quad q \equiv \frac{\mathrm{g}^2\Phi^2}{4m^2}. \tag{6.19}$$

and a prime here denotes the derivative with respect to z. The occupation number n_k counts by how many quanta the respective modes χ_k are populated. We define the comoving occupation number of particles as follows:

$$n_k = \frac{\omega_k}{2}\left(\frac{|\dot{\chi}_k|^2}{\omega^2_k} + |\chi_k|^2\right) - \frac{1}{2}. \tag{6.20}$$

The growth of the mode function corresponds to particle production, like in the case of particle creation in a varying strong external gravitational field as developed by Zeldovich and Starobinsky [200]. Exponential growth of the mode functions will result in an exponential growth of the number of χ particles, with the exponent of this growth being twice the corresponding exponent of the mode functions. It is known that the Mathieu equation has instabilities for certain ranges of k; the

properties of the solutions have been classified in so-called stability/instability regions. The strength of the resonance depends on A_k and q which is described by a stability/instability chart of the Mathieu equation. Strictly speaking, A_k and q should be constant to use the Mathieu equation but as long as they are not varying too rapidly the analogy is reasonable. The solutions have exponential instabilities within certain resonance bands of widths Δk,

$$\chi_k \propto \exp(\mu_k z) \tag{6.21}$$

where μ_k are called Floquet exponents. According to Floquet theory, when A_k, q fall in an instability band, the perturbation χ_k grows exponentially with a Floquet index $\mu_k > 0$.

- $\mu_k = 0$ $|\chi_k|$ is stable.
- $\mu_k > 0$ $|\chi_k|$ grows exponentially.

Exponential instabilities correspond to exponential growth of occupation numbers (particle production)

$$n_k \propto |\chi_k|^2 \propto \exp(2\mu_k z). \tag{6.22}$$

For small q ($\lesssim 1$) the width of the instability band is small and the expansion of the universe washes out the resonance. On the other hand, for large q ($\gg 1$), broad resonance can occur for a wide range of the parameter space and momentum modes. Here, we will look at these two important regimes:

- $q \ll 1$ *Narrow resonance* at $k = m$
- $q > 1$ *Broad resonance* for $k \leqslant k_\star$.

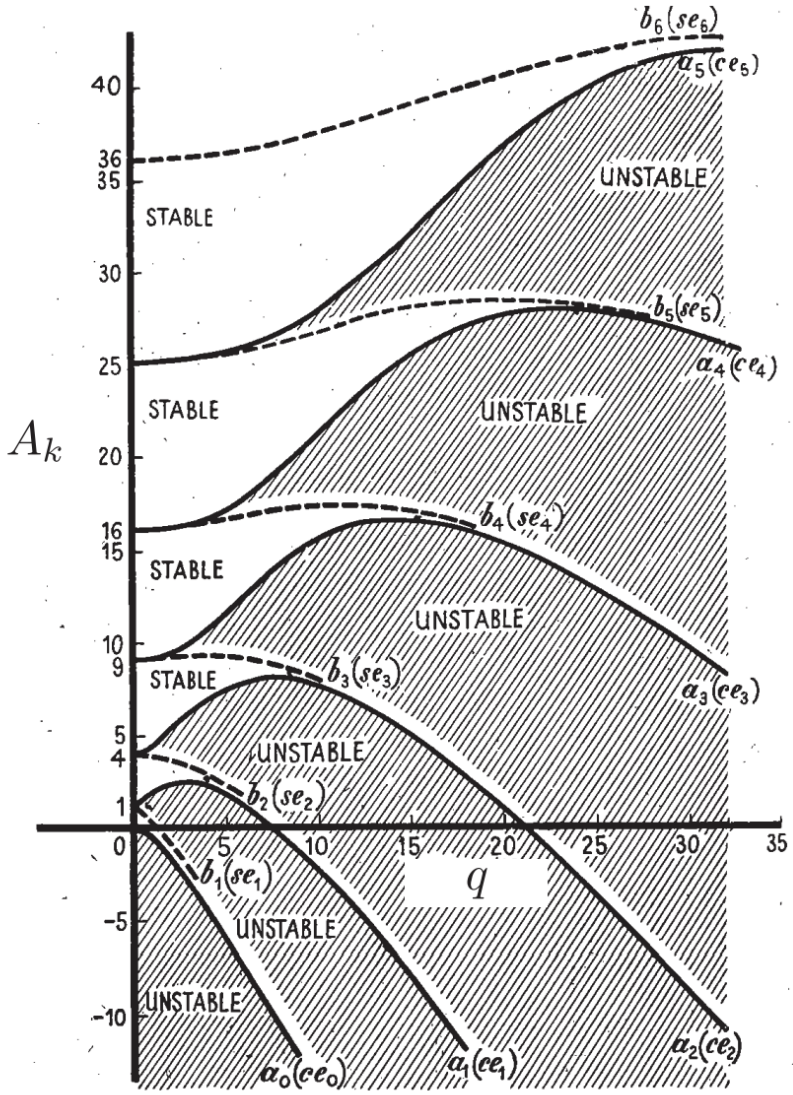

Figure 6.2: *Instability bands for the Mathieu equation [201]. The parameter q from Eq. (6.18) is plotted on the horizontal axis and A on the vertical axis. The shaded regions represent regions in parameter space where there is a parametric resonance instability.*

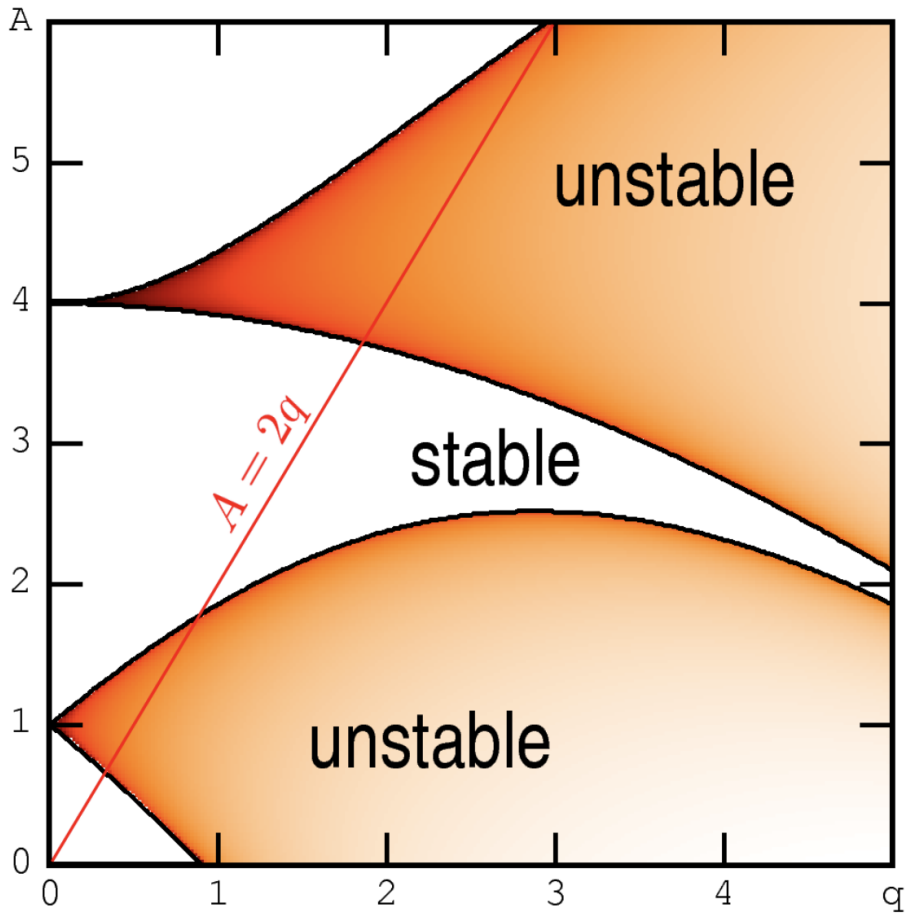

Figure 6.3: *Instability chart of the Mathieu equation taken from [202] for A, q ranging from $1-5$. Just like for Fig. 6.2, in this sketch, the instability regions ($\mu_k > 0$) are the shaded regions and the white regions are stable. The line $A = 2q$ shows the values of A_k and q for $k = 0$. For $k \neq 0$, the corresponding graphs $A_k(q)$ are found by parallelly shifting the line A_0 upwards by k^2/m^2.*

6.4.1 Narrow Resonance ($q \ll 1$)

Floquet Analysis

From the Mathieu stability/instability chart, for $q \ll 1$, resonances occur near $A_k^{(n)} \approx n^2$ and n is an integer ($n \in \mathbb{Z}$). The widths of the resonance bands is $\Delta k^{(n)} \sim mq^n$.

The structure of the instability bands is dictated by the theory of Mathieu's equation:

$$k^2 \approx m^2(n^2 - 2q \pm q^n). \tag{6.23}$$

For $q < 1$, the first band is the widest and the most important one:

$$k^2 \approx m^2(1 - 2q \pm q). \tag{6.24}$$

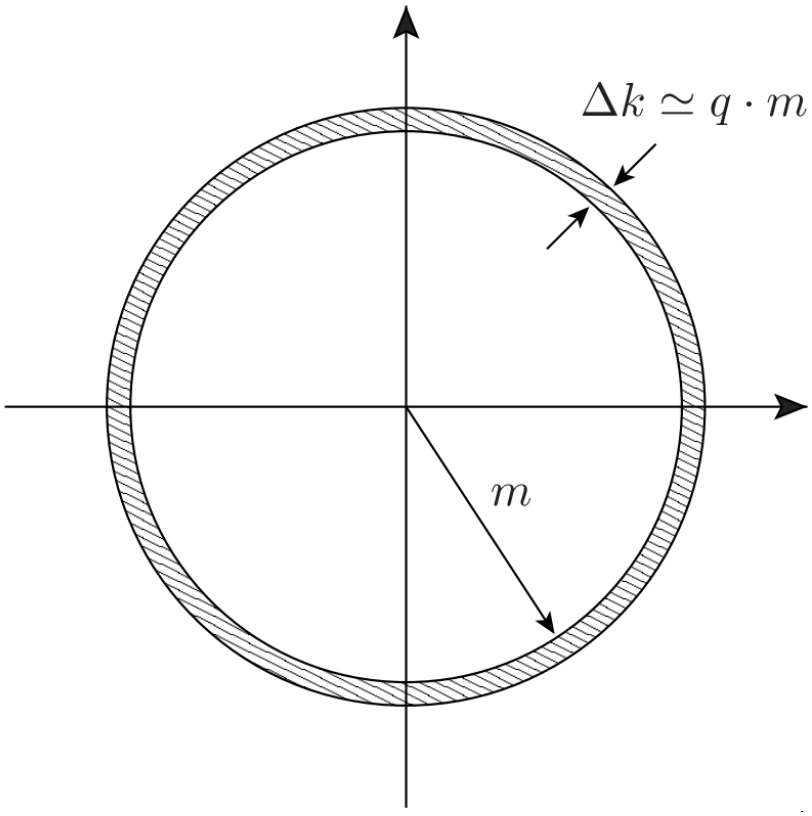

Figure 6.4: *Schematic diagram showing the resonance band in the narrow resonance case for $n = 1$. Figure taken from [195].*

It is centred around $k \approx m$, has a width mq and the instability parameter of this band is:

$$\mu_k = \sqrt{\left(\frac{q}{2}\right)^2 - \left(\frac{k}{m} - 1\right)^2}. \tag{6.25}$$

The instability parameter vanishes at the edges of the resonance band and is maximal at its centre, giving:

$$\mu_k^{\max} = \mu_{k=m} = \frac{q}{2} = \frac{g^2\Phi^2}{8m^2}. \tag{6.26}$$

The corresponding modes χ_k grow at a maximal rate of $\exp(\frac{qz}{2})$. The growth of the modes leads to the growth of the occupation numbers of the created particles n_k. n_k grows as $\exp(qz)$.

Numerical Simulations

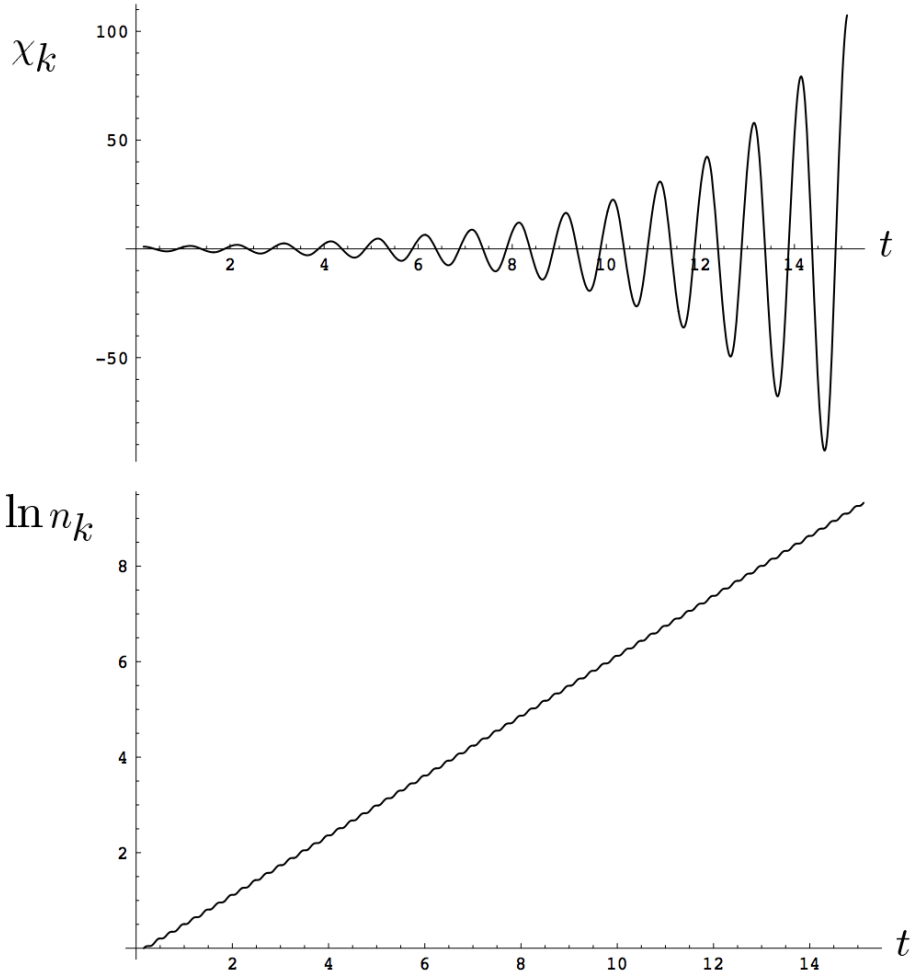

Figure 6.5: *Narrow parametric resonance for the scalar field χ in the theory $\frac{1}{2}m^2\phi^2$ in Minkowski space for $q \sim 0.1$. Time is shown in units of $m/2\pi$ which is equal to the number of oscillations of the inflaton field ϕ. For each oscillation of the inflaton field the growing modes of the χ field oscillate once. The upper figure shows the growth of the mode χ_k for the momentum k corresponding to the maximal speed of growth, $k \approx m$. The lower figure shows the logarithm of the occupation of particles n_k in this mode. The number of particles grows exponentially and $\ln n_k$ in the narrow resonance regime looks like a straight line with a constant slope. This slope divided by 4π gives the value of the parameter μ_k. In this particular case, we have $\mu_k \sim 0.05$ which matches exactly with the relation $\mu_k \sim \frac{q}{2}$ for this model. Figure taken from [179].*

Narrow Resonance in an Expanding Universe

So far, our analysis has ignored the expansion of the universe and the rescattering of the χ particles. This adds another layer of complexity to the analysis but essentially both these effects render narrow parametric resonance less effective. For instance, the expansion of the universe narrows the width of the resonance band, $\Delta k \propto \Phi(t) \propto 1/t$. The expansion of space also increases the inflaton decay rate with the friction term $3H$ and within a time $\Delta t \sim qH^{-1}$, redshifts the χ modes

out of the resonance bands. The χ boson particles may also be removed from the resonance bands as they change their momenta or decay into other particles due to secondary interactions (rescatterings). All of this means that narrow parametric resonance is quite a delicate process and to find out if it really occurs, one requires detailed numerical simulations that include all the relevant effects.

Dolgov and Kirilova [199] mention narrow parametric instability regions for the new inflationary scenario. The importance of this narrow regime for the new inflationary scenario was first recognized by Traschen and Brandenberger [177] but for many reasons, their final calculations were not quite correct. Kofman, Linde and Starobinsky [178, 179] developed a detailed theory of particle creation in the narrow resonance regime in an expanding universe for the chaotic scenario (but see also Shtanov, Traschen and Brandenberger [191] and Kaiser [203]).

Several authors have studied the narrow resonance regime without taking into account the expansion of the universe because the calculations are simpler (Yoshimura [198], Boyanovsky *et al.* [197], Boyanovsky *et al.* [204]). However, while doing so, for many parameters important features in the theory might disappear. One such example is that the effects studied by Son [205] disappear in an expanding universe.

6.4.2 Broad Resonance ($q > 1$)

The term *Broad Resonance* is used to describe parametric resonance in broad instability bands in parameter space. For $q > 1$ it can be seen from Fig. 6.2 that instabilities now occur for much broader ranges of k. In chaotic inflation the initial amplitude of the inflaton oscillations can be very large, $\Phi_0 \gtrsim M_{\rm pl}$, resulting in a broad ($q > 1$) and very efficient parametric resonance. Fig. 6.6 shows the numerical solutions for $\chi_k(t)$ and $n_k(t)$ in the broad resonance regime in Minkowski space.

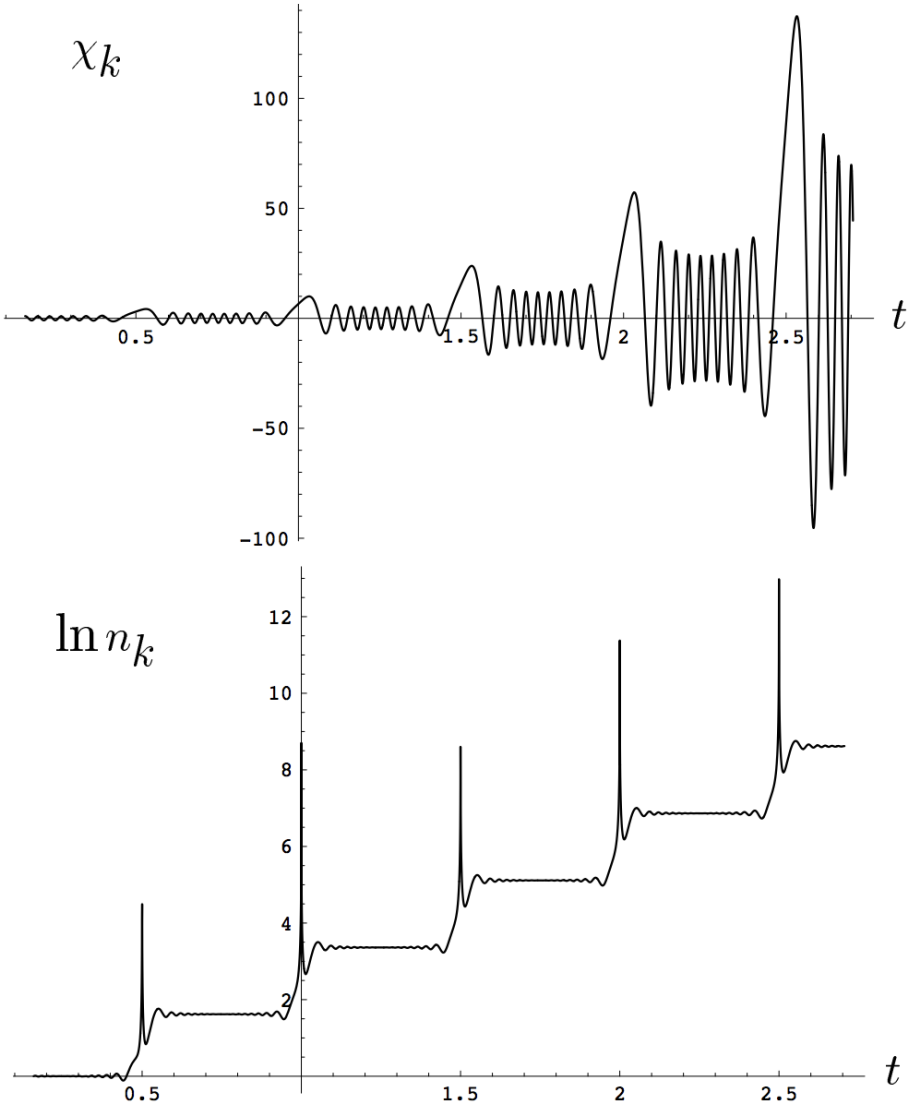

Figure 6.6: *Broad parametric resonance for the field χ for $k \approx m$ in the theory $\frac{1}{2}m^2\phi^2$ for $q \approx 200$. For each oscillation of the ϕ field, the mode of the χ field oscillates many times. The peaks in the χ_k oscillations correspond to the time when $\phi_0(t) = 0$. Figure taken from [179].*

Each peak in the χ_k oscillation corresponds to a place where $\phi(t) = 0$, i.e., particle production only occurs for very small values of $\phi(t)$. At this time the occupation number n_k is not well-defined but soon after, the occupation number stabilizes to a new, higher level and remains constant until the next jump. The structure in

Fig. 6.6 for $\ln n_k$ requires an analytic treatment. The standard condition necessary for particle production is that the adiabatic condition is violated[2], i.e., when:

$$|\dot{\omega}| > \omega^2, \qquad \text{where} \qquad \omega(t) = \sqrt{k^2 + m_\chi^2 + \mathrm{g}^2\Phi^2 \sin^2(mt)}. \tag{6.27}$$

Away from $\phi(t) = 0$, the frequency of χ changes adiabatically ($|\dot{\omega}| \ll \omega^2$) and n_k is conserved. Particle production occurs when the adiabatic condition is violated and this happens for momenta satisfying:

$$k^2 \leqslant k_\star^2 \equiv \frac{2}{3\sqrt{3}}\mathrm{g}m\Phi(t) - m_\chi^2. \tag{6.28}$$

For modes with these values of k, the adiabacity condition breaks down in each oscillation period when ϕ is close to zero. This implies that the particle number does not increase smoothly but rather in 'bursts' as was first studied in [179].

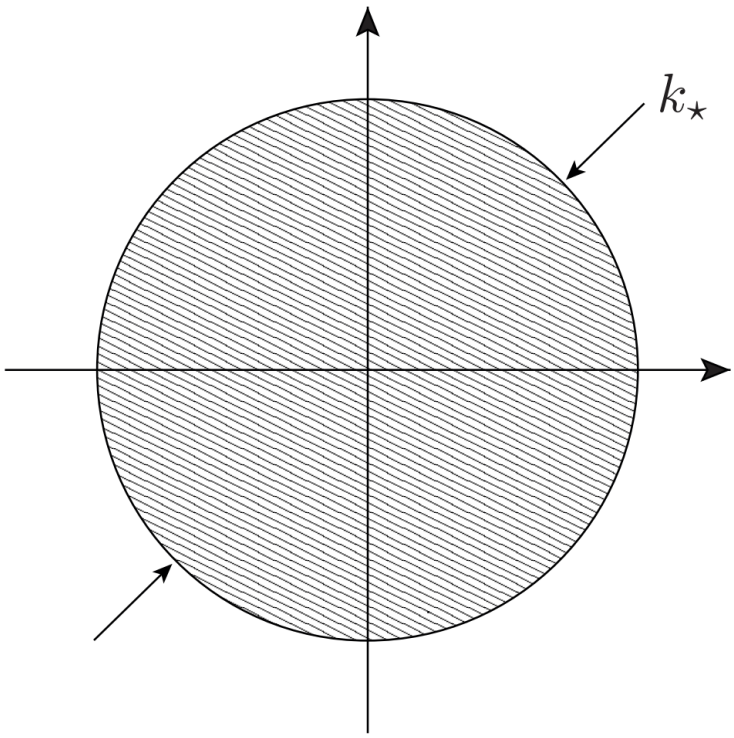

Figure 6.7: *Schematic diagram showing the range of k that are excited in broad parametric resonance. Figure taken from [195].*

[2]One should note that this condition is not necessary for the case of narrow resonance because even a small variation of $\omega(t)$ may be exponentially accumulated in the course of time. However, for broad resonance one should expect a considerable effect during each oscillation.

Broad Resonance in an Expanding Universe

In an expanding universe, the adiabacity condition is now violated for momenta satisfying [179, 195]:

$$\frac{k^2}{a^2(t)} \leqslant k_\star^2(t) \equiv \frac{2}{3\sqrt{3}} \mathrm{g} m \Phi(t) - m_\chi^2. \tag{6.29}$$

Note that the expansion of space makes broad resonance *more effective* since more k modes are redshifted into the instability band as time goes by.

Bringing back into play the expansion of the universe, the complexity of describing preheating in the broad resonance regime increases. To make things simpler, it is convenient to remove the Hubble friction term from the equation of motion by defining $X_k(t) \equiv a^{3/2}(t)\chi_k(t)$. We can then write the mode equation as:

$$\ddot{X}_k + \omega_k^2 X_k = 0, \tag{6.30}$$

where

$$\omega_k^2 \equiv \frac{k^2}{a^2} + \mathrm{g}^2\Phi^2 \sin^2(mt) + \Delta, \qquad \Delta \equiv m_\chi^2 - \frac{9}{4}H^2 - \frac{3}{2}\dot{H}. \tag{6.31}$$

Note that in the matter-dominated background that we are considering here, the last two terms on the right-hand side cancel. We will also consider here the case of light χ particles such that m_χ can be ignored. Hence, the term Δ can be neglected altogether. The equation of motion (Eq. (6.30)) represents a harmonic oscillator equation with a time-dependent frequency. Fig. 6.8 shows a simulation of broad parametric resonance in an expanding universe where $X_k(t)$ is plotted rather than $\chi_k(t)$ to illustrate the relative growth of χ to the amplitude of the oscillating field ϕ ($\Phi \propto 1/t$).

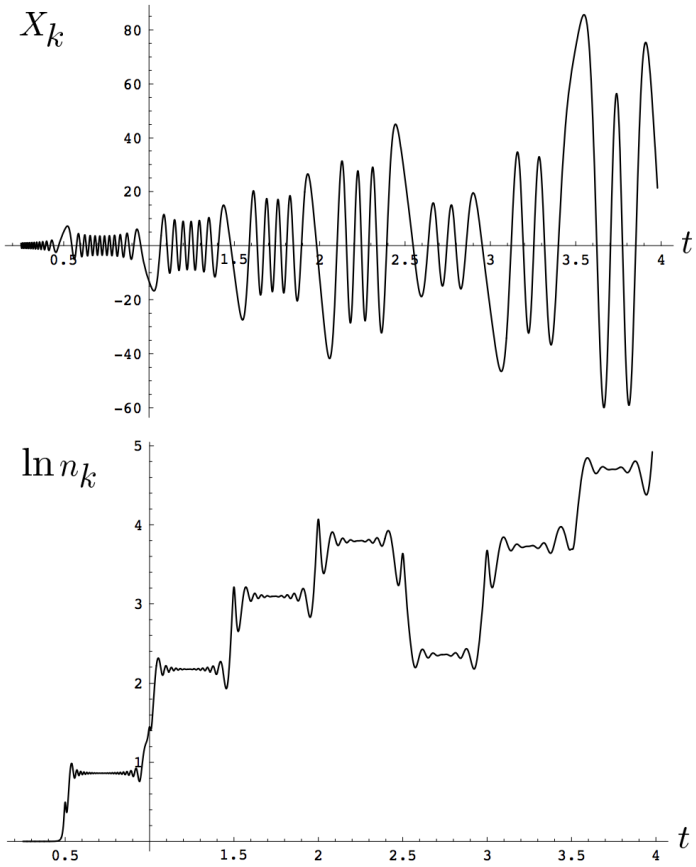

Figure 6.8: *Early stages of preheating in the theory* $\frac{1}{2}m^2\phi^2$ *in an expanding Universe with* $a \sim t^{2/3}$ *for* $g = 5 \times 10^{-4}$, $m \approx M_{\rm pl}$ *and initial* $q \sim 3 \times 10^3$. *From the behaviour of* n_k, *we see stochastic resonance. Figure is from [179].*

In the beginning we have parametric resonance very similar to the one studied in § 6.4.2. Just like before, the intervals when the field ϕ becomes small are the periods when χ particle production is most efficient. One important difference is that because of the gradual decrease in amplitude of the ϕ field, the frequency of the χ oscillations decrease in time. As a result, in the beginning within each half of a period of oscillation of the field ϕ the field χ_k oscillates many times, but then it starts oscillating more and more slowly as can be seen in Fig. 6.8. We also note that the number of particles n_k in this process typically increases but it may occasionally decrease as well. *Stochastic resonance* is a distinctive feature in an expanding universe.

To gain an understanding of this stochastic resonance effect, we analyse the behaviour of the *phases* of the functions $\chi_k(t)$ near $\phi(t) = 0$; here, broad resonance in Minkowski space and in an expanding universe is characteristically different. Indeed, Fig. 6.6 shows that for Minkowski, near all points where $\phi = 0$, the phases of χ_k are all equal. However, in an expanding universe such a regime is impossible, not just because of the redshift of the momentum k/a but mainly because the frequency of oscillations of the field χ_k decreases in time as it is proportional to Φ. The frequency of the oscillations changes significantly with each oscillation of the ϕ field. Because

for large q the phases of the field χ_k at successive moments when $\phi(t) = 0$ are practically uncorrelated with each other, at some instants the amplitude of the field χ_k decreases. Surprisingly, this stochastic effect does not destroy broad parametric resonance completely. Even though the phases of the field χ_k at the moment when $\phi(t) = 0$ in an expanding universe with $q \gg 1$ are uncorrelated and unpredictable, in 75% of all events the amplitude grows after each pass through $\phi(t) = 0$ [179]. This is confirmed by numerical simulations. Even if this was not the case and the amplitude only grew in 50% of cases, the total number of χ particles would still grow exponentially. The theory of this effect is very similar to the inflationary scenario where in most points the inflaton field rolls down but the parts of the universe where the field jumps continue to grow exponentially.

Eventually, due to the decrease in the inflaton amplitude the broad resonance becomes narrow since the parameter $q = \frac{g^2\Phi^2}{4m^2} \propto t^{-2}$. Ultimately, the resonance ceases to exist and n_k stabilizes at a constant value.

6.5 Backreaction and Rescattering

So far we have considered the parametric resonance in an expanding universe neglecting the backreaction of the amplified fluctuations of the fields ϕ and χ. The effect of the resonant amplification of $\chi_k(t)$ corresponds to the exponentially fast creation of n_χ particles. The backreaction of the exponential unstable χ field on the background dynamics slowly accumulates until it affects the process of resonance itself. Therefore preheating can be divided into two distinct stages. In the first stage the backreaction of created particles is not important. This first stage is actually quite long and for a small emough ($\lesssim 10^3$) initial value of q, preheating might end before backreaction becomes significant. In the second stage backreaction increases the frequency of oscillations of the inflaton field, which makes the process even more efficient than before. Backreaction of the χ field can have several different effects on the dynamics. In the model that we have considered, backreaction may change the value of m in the mode equation which may make the resonance narrow and eventually terminate it. Another effect is the production of ϕ particles coming from the interaction of χ particles with the oscillating field $\phi(t)$. This process is known as the scattering of χ particles on the the oscillating $\phi(t)$ field; each χ particle takes one ϕ particle away from the homogeneous oscillating field $\phi(t)$ during each interaction. Eventually when many such ϕ particles are created, this changes the effective mass of the χ field, making χ particles so heavy that they are no longer created. Given a sufficient amount of time, the scattering process can dismantle the oscillating field by decomposing it into separate ϕ particles. For a proper investigation of backreaction and rescattering, one would need to start with the general set of equations

which describe the self-consistent dynamics of the classical homogeneous inflaton field as well as the fluctuations of the fields χ and ϕ. We do not go into the details of backreaction and rescattering here; instead the reader is referred to the classic paper by Kofman, Linde and Starobinsky [179] for a proper analysis. Instead we quote the main findings of that paper. The simplest way to take into account the backreaction of the amplified quantum fluctuations χ is to use:

$$\ddot{\phi} + 3H\dot{\phi} + m^2\phi + \mathrm{g}^2\langle\chi^2\rangle\phi = 0. \tag{6.32}$$

where the vacuum expectation value for χ^2 is:

$$\langle\chi^2\rangle = \frac{1}{2\pi^2 a^3}\int_0^\infty \mathrm{d}k\; k^2|X_k(t)|^2. \tag{6.33}$$

Quantum effects contribute to the effective mass m_ϕ of the inflaton field such that: $m_\phi^2 = m^2 + \mathrm{g}^2\langle\chi^2\rangle$. It is found that the frequency of oscillations of the inflaton field does not change until the number of χ particles grows to:

$$n_k \approx \frac{2m^3}{\mathrm{g}^2}q^{1/2}. \tag{6.34}$$

Rescattering, on the other hand, increases the effective mass of χ particles making them heavy and hard to produce [179]. Despite all this analytical progress, it remains a challenge to develop a complete analytical theory of reheating. Many authors like ourselves turn to numerical simulations instead (see Chapter 7).

6.6 Remarks

Early discussions of reheating of the universe after inflation were based on the idea that the homogeneous inflaton field can be represented as a collection of the particles of the field ϕ. Each of these particles decayed independently of each other. This process can be studied by the usual perturbative approach to particle decay. Typically, it takes thousands of oscillations of the inflaton field until it decays into other particles. Later, however, it was discovered that coherent field effects such as parametric resonance can lead to the decay of the homogeneous field much faster than what would have been predicted from perturbative methods (within a few dozen oscillations). In the simplest versions of chaotic inflation, the stage of preheating is generally dominated by parametric resonance, although, as we have shown in this chapter, there are parameter ranges where this does not occur. These coherent effects produce high energy, non-thermal fluctuations that could have significant effects on the early universe. This early stage of rapid non-perturbative decay was called ‘preheating’.

While not our subject of research, for completeness, we also mention in passing that other forms of preheating have been studied in the literature. In Refs. [206, 207], it was found that another effect known as *tachyonic preheating* can lead to even faster decay than parametric resonance. This effect occurs whenever the homogeneous field rolls down a tachyonic ($V_{,\phi\phi} < 0$) region of its potential. When that occurs, a tachyonic or spinodal instability leads to exponentially rapid growth of of all long wavelengths modes with $k^2 < |V_{,\phi\phi}|$). In this case, the field decays before reaching the minimum of the potential and the reheating phase is quasi-instantaneous [206, 207]. In Refs. [206, 207], it was shown that tachyonic preheating dominates the preheating phase in hybrid models of inflation. Yet another type of preheating is *geometric preheating* (see for example, [208]) in which scalar fields are coupled to the scalar curvature R which oscillates during reheating. *Fermionic preheating* [209, 210], the resonant production of fermions, is an important issue since many problematic particles such as gravitinos are fermions and resonant production of them could have a big effect on dangerous relic abundances [209, 211].

6.7 Massless Preheating

The calculations, conclusions and figures presented in this massless preheating review section are from the paper by Greene *et al.* [173]. We will make use of some of the important findings in the next section for our latttice simulations in Chapter 7. Note that the authors of Ref. [173] used a different definition for the reduced Planck mass and therefore, the expressions that follow have been changed to keep things consistent throughout this thesis such that $M_{\rm pl}$ is still as defined in § 1.1.

6.7.1 The Conformally Invariant Case

There exists an interesting model in which the expansion of the universe can be transformed away and to which one can apply exact Floquet theory, called massless preheating [173]. By a conformal transformation, one can facilitate the investigation of preheating in this theory in an expanding universe to a much simpler theory of preheating in Minkoswki spacetime. As a result, the parametric resonance in this model does not exhibit the stochasticity we found in § 6.4.2. In this model, the universe rapidly becomes radiation dominated ($a \propto t^{1/2}$). The conformally invariant potential of this model is

$$V(\phi) = \frac{1}{4}\lambda\phi^4 + \frac{1}{2}\mathrm{g}^2\phi^2\chi^2. \tag{6.35}$$

We will see that the occurrence of resonance in the various conformally invariant models can be very different, depending on the particular values of parameters and the structure of the theory. For instance, the model $\frac{1}{4}\lambda\phi^4 + \frac{1}{2}\mathrm{g}^2\phi^2\chi^2$ with $\mathrm{g}^2 = \lambda$

or $g^2 = 3\lambda$ has only one instability band each but the structure of the bands and the characteristic exponents μ_k are completely different from each other. Only a slight change in the ratio g^2/λ is enough for the number of the instability bands to immediately become infinitely large. For this reason, it is erroneous to extrapolate the results obtained for a theory with one choice of parameters to a theory with different parameters.

6.7.2 Evolution of the Inflaton Field

Consider chaotic inflation with the potential $V(\phi) = \frac{1}{4}\lambda\phi^4$. During inflation, the leading contibution to the energy-momentum tensor is given by the inflaton scalar field ϕ. The evolution of the (flat) FLRW universe is given by the Friedmann equation:

$$H^2 = \frac{1}{3M_{pl}^2}\left(\frac{1}{2}\dot{\phi}^2 + \frac{\lambda\phi^4}{4}\right) \tag{6.36}$$

where as usual, $H = \dot{a}/a$. We also note a useful relation between $H(t)$ and $\phi(t)$ which follows from the Einstein equations:

$$\dot{H} = -\frac{\dot{\phi}^2}{2M_{\rm pl}^2}. \tag{6.37}$$

We can write the equation of motion for the classical field $\phi(t)$ as

$$\ddot{\phi} + 3H\dot{\phi} + \lambda\phi^3 = 0. \tag{6.38}$$

For large initial values of ϕ ($> M_{\rm pl}$), the friction term $3H\dot{\phi}$ in Eq. (6.38) dominates over $\ddot{\phi}$ and the potential term in Eq. (6.36) dominates over the kinetic term, giving rise to the inflationary stage. As the field ϕ decreases below $\sim M_{\rm pl}$, the 'friction' term $3H\dot{\phi}$ gradually becomes less important and inflation eventually comes to an end when $\Phi_0 \sim 2.5M_{\rm pl}$. The inflaton then rapidly oscillates around the minimum of $V(\phi)$ with a large initial amplitude of $\Phi_0 \sim 0.5M_{\rm pl}$ [173].

The shape of the potential $V(\phi)$ determines the characteristics of the classical oscillations of the homogeneous scalar field ϕ. Previously in § 6.2, we considered the quadratic potential $V(\phi) = \frac{1}{2}m^2\phi^2$. In that model, the fluctuations are harmonic, given by $\phi(t) = \Phi(t)\sin(mt)$ with the amplitude decreasing as $\Phi(t) \approx \frac{M_{\rm pl}}{mt} \propto a^{-3/2}$ and the energy density of the inflaton field decreases in the same way as the energy density of non-relativistic matter, i.e., $\propto a^{-3}$.

In the model with the potential $V(\phi) = \frac{1}{4}\lambda\phi^4$ however, the inflaton oscillations are not sinusoidal. In the limit $t \to \infty$, the amplitude Φ of the oscillations of the

field ϕ approaches the asymtotic regime

$$\Phi(t) \approx \frac{1}{\sqrt{t}}\left(\frac{3M_{\rm pl}^2}{\lambda}\right)^{1/4} \sim \frac{M_{\rm pl}}{2\mathcal{N}} \tag{6.39}$$

where $\mathcal{N}$ is the number of oscillations after the end of inflation. The energy density is $\rho_\phi = \frac{1}{2}\dot{\phi}^2 + \frac{\lambda}{4}\phi^4 \approx \frac{\lambda}{4}\Phi^4$ and using Eq. (6.39), we have $\rho_\phi \propto a^{-4}$. The energy density of the field ϕ decreases in the same way as the energy density of radiation.

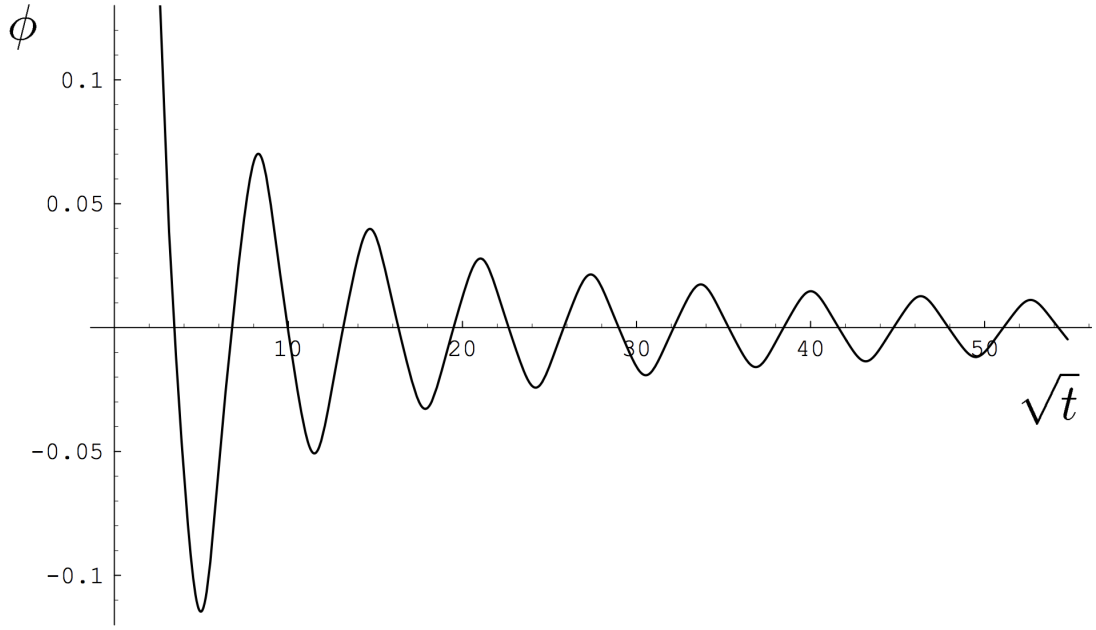

Figure 6.9: *Oscillations of the inflaton field ϕ after the end of inflation in the theory $\frac{\lambda}{4}\phi^4$. The value of the scalar is in units of $\sqrt{8\pi}M_{\rm pl}$ and time is measured in units of $(\sqrt{\lambda 8\pi}M_{\rm pl})^{-1}$. Figure taken from [173].*

To make calculations simple and in particular to find the form that the oscillations take, it is convenient to make a conformal transformation of the spacetime metric and the fields. For this we need the conformal time τ and the conformal field,

$$\varphi = a\phi. \tag{6.40}$$

Then, for the coordinates $(\tau, \mathbf{x})$ the Klein-Gordon equation becomes

$$\varphi'' + \lambda\varphi^3 - \frac{a''}{a}\varphi = 0, \tag{6.41}$$

where $'$ denotes the derivative with respect to the conformal time, $\frac{d}{d\tau}$. Writing the Friedmann equation in these new variables, we have

$$a'^2 = \frac{1}{3M_{\rm pl}^2}\left(\frac{1}{2}\left(\varphi' - \varphi\frac{a'}{a}\right)^2 + \frac{\lambda\varphi^4}{4}\right). \tag{6.42}$$

From Eq. (6.41), we can see that the equation of motion for the field φ in the new time variable τ does not look exactly as the equation for the theory $\frac{\lambda}{4}\varphi^4$ in Minkowski

space. For it to be exactly the same, we would need to add the term $\frac{\phi^2}{12}R$ in the Lagrangian. However, we can ignore this subtlety for the following reasons. Firstly, soon after the end of inflation we have $\frac{\lambda}{4}\phi^4 \gg \frac{\phi^2}{12}R$ and $\lambda\varphi^3 \gg \frac{a''}{a}\varphi$. Furthermore, it is known that, when averaged over several oscillations of the inflaton field, the energy-momentum tensor of the field ϕ in the theory $\frac{\lambda}{4}\phi^4$ is traceless ($p = \rho/3$) [212]. Therefore in this case, $R = 0$, $a(\tau) \sim \tau$ and $a'' = 0$ so that the last term in Eq. (6.41) disappears and then,

$$\varphi'' + \lambda\varphi^3 = 0. \tag{6.43}$$

Note that this equation is that of a harmonic oscillator in flat space; the expansion of the universe has been absorbed into the field and time redefinitions. Averaged over several oscillations, the Friedmann equation (Eq. (6.42)) in the regime $\phi \ll M_{\rm pl}$ is simply

$$a'^2 = \frac{1}{3M_{\rm pl}^2}\left(\frac{1}{2}\varphi'^2 + \frac{\lambda\varphi^4}{4}\right) \equiv \frac{\rho_\varphi}{3M_{\rm pl}^2}, \tag{6.44}$$

where the conformal energy density ρ_φ is given by

$$\rho_\varphi = \frac{1}{2}\varphi'^2 + \frac{\lambda}{4}\varphi^4. \tag{6.45}$$

We can express ρ_φ in terms of the amplitude of the oscillations $\tilde{\varphi}$ of the inflaton field ϕ: $\rho_\varphi = \frac{\lambda}{4}\tilde{\varphi}^4$. Then using Eq. (6.44) we can write:

$$a(\tau) = \sqrt{\frac{\lambda}{12}}\frac{\tilde{\varphi}^2}{M_{\rm pl}}\tau, \qquad t = \sqrt{\frac{\lambda}{48}}\frac{\tilde{\varphi}^2}{M_{\rm pl}}\tau^2. \tag{6.46}$$

As expected, in this regime the last term in Eq. (6.41), $\frac{a''}{a}\varphi$ vanishes. Eq. (6.43) has an oscillatory solution with a constant amplitude and can be reduced to the equation for an elliptic function. Let us define a dimensionless conformal time variable as follows:

$$x \equiv \sqrt{\lambda}\tilde{\varphi}\tau = \left(48\lambda M_{\rm pl}^2\right)^{1/4}\sqrt{t}. \tag{6.47}$$

Then, let us rescale the function $\varphi \equiv a\phi = \tilde{\varphi}f(x)$. The amplitude of the function $f(x)$ is equal to unity and $f(x)$ obeys the canonical equation for the elliptic function. The integral of Eq. 6.43, $f'^2 = \frac{1}{2}(1 - f^4)$, has the solution in terms of an elliptic cosine function

$$f(x) = cn\left(x - x_0, \frac{1}{\sqrt{2}}\right). \tag{6.48}$$

As mentioned earlier, oscillations in this theory are not sinusoidal but are given by

an elliptic function. The elliptic cosine can be written as a series,

$$f(x) = \frac{8\pi\sqrt{2}}{P} \sum_{n=1}^{\infty} \frac{e^{-\pi(n-1/2)}}{1+e^{-\pi(n-1/2)}} \cos\left(\frac{2\pi(2n-1)x}{P}\right), \tag{6.49}$$

where $P \approx 7.416$ is the period of the oscillations in units of x [173]. The amplitude of the first term in this sum is 0.9550, the amplitude of the second term is 0.04305 (much smaller) [173].

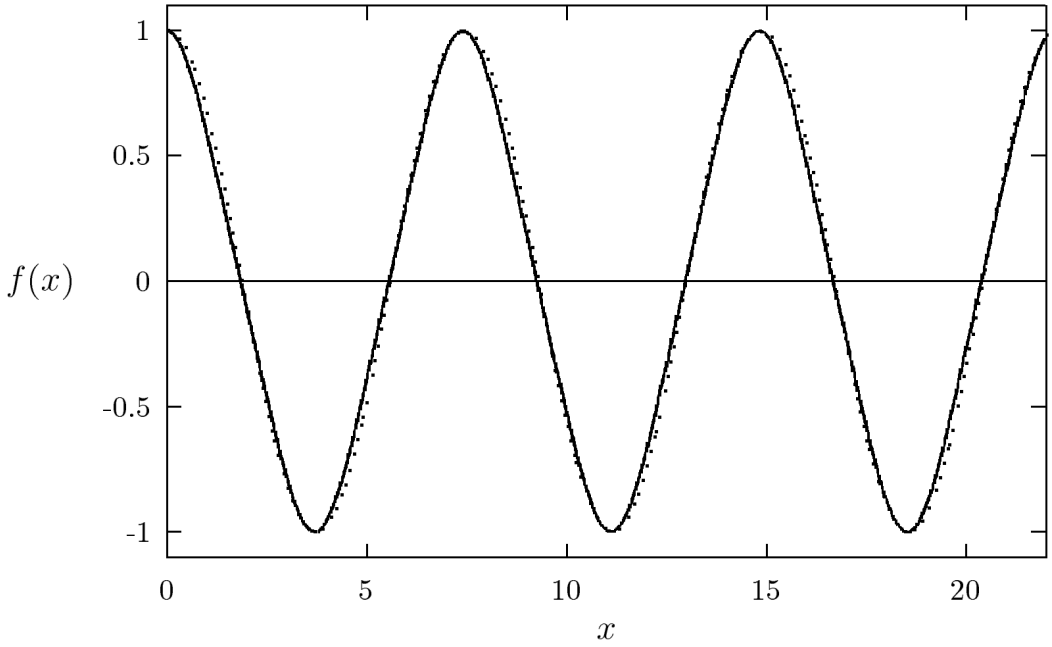

Figure 6.10: *The exact solution Eq. (6.48) for the oscillations of the inflaton field after the end of inflation in the conformally invariant theory* $\frac{1}{4}\lambda\phi^4$. *The field is shown in rescaled conformal field and time variables. The full solution is plotted as the solid curve and the dotted curve is for the leading harmonic term* $(\cos 0.8472x)$ *in the series in Eq. (6.49). Figure taken from [173].*

6.7.3 Equations for Quantum Fluctuations of the Fields ϕ and χ

In the same vein as in § 6.4, we consider the interaction between the *classical* field ϕ and the massless *quantum* scalar field $\hat{\chi}$.

$$\hat{\chi}(t,\mathbf{x}) = \int \frac{\mathrm{d}^3k}{(2\pi)^{3/2}} \left(\hat{a}_{\mathbf{k}}\chi_k(t)e^{-i\mathbf{k}.\mathbf{x}} + \hat{a}^{\dagger}_{\mathbf{k}}\chi^*_k(t)e^{i\mathbf{k}.\mathbf{x}}\right), \tag{6.50}$$

where $\hat{a}_{\mathbf{k}}$ and $\hat{a}^{\dagger}_{\mathbf{k}}$ are annihilation and creation operators. For a flat Friedmann background with scale factor $a(t)$, we have:

$$\ddot{\chi}_k + 3\frac{\dot{a}}{a}\dot{\chi}_k + \left(\frac{k^2}{a^2} + \mathrm{g}^2\phi^2\right)\chi_k = 0. \tag{6.51}$$

The self-interaction $\frac{1}{4}\lambda\phi^4$ also generates fluctuations in the field ϕ and the equation for the modes $\phi_k(t)$ is

$$\ddot{\phi}_k + 3\frac{\dot{a}}{a}\dot{\phi}_k + \left(\frac{k^2}{a^2} + 3\lambda\phi^2\right)\phi_k = 0. \tag{6.52}$$

This equation is identical to Eq. (6.51) with $\mathrm{g}^2 = 3\lambda$. Therefore the study of the fluctuations ϕ_k in the $\frac{1}{4}\lambda\phi^4$ model is a particular case of the general equation for fluctuations (Eq. (6.51)). The physical momentum $\mathbf{p} = \frac{\mathbf{k}}{a(t)}$ in Eq. (6.51) redshifts away in the same way as the background field amplitude, $\phi(t) = \frac{\varphi}{a(t)}$ and therefore, we can remove the redshifting of momenta from the evolution of χ_k. We do that by making use of the conformal transformation of the mode function $X_k(t) = a(t)\chi_k(t)$ and rewriting the mode equation for χ_k with the dimensionless conformal time variable x (see Eq. (6.47)),

$$X_k'' + \left(\kappa^2 + \frac{\mathrm{g}^2}{\lambda}cn^2\left(x, \frac{1}{\sqrt{2}}\right)\right)X_k = 0. \tag{6.53}$$

We have dropped $x_0 = 2.44$ for simplicity. Also, $\kappa^2 = \frac{k^2}{\lambda\tilde{\varphi}^2}$. We see that the equation for fluctuations does not depend on the expansion of space and is completely reduced to the similar problem in Minkowski spacetime. This feature is special to the conformally invariant theory $\frac{1}{4}\lambda\phi^4 + \frac{1}{2}\mathrm{g}^2\phi^2\chi^2$. The mode equation for φ_k is

$$\varphi_k'' + \left(\kappa^2 + 3cn^2\left(x, \frac{1}{\sqrt{2}}\right)\right)\varphi_k = 0. \tag{6.54}$$

We will use Eq. (6.53) as a master equation to investigate resonance in the conformally invariant theory. From the definition of κ, the natural unit of momenta is $\sqrt{\lambda}\tilde{\varphi}$. Eq. (6.53) describes oscillators, X_k, with a varying frequency given by

$$\omega_k^2 = \kappa^2 + \frac{\mathrm{g}^2}{\lambda}cn^2\left(x, \frac{1}{\sqrt{2}}\right). \tag{6.55}$$

This frequency varies periodically with time, x. For this particular case, the solutions X_k are exponentially unstable, i.e., $X_k(x) \propto e^{\mu_k x}$. This leads to exponentially fast creation of χ particles as the inflaton oscillates ($n_k \propto e^{2\mu_k x}$). The strength of the resonance is given by the dimensionless coupling parameter g^2/λ. This in turn means that for broad resonance to occur it is not necessary that the initial amplitude of the inflaton is large as was the case for the quadratic potential we studied in § 6.4.2. As it turns out, the strength of the resonance depends non-trivially (non-monotonically) on g^2/λ.

Mathematically speaking, the mode equations Eq. (6.53) belong to a class of *Lamé equations*. Historically, this was first discovered in [178]. In Fig. 6.11 we show the two-dimensional chart of the stability/instability bands for the Lamé equation

(Eq. (6.53)) in terms of κ^2 and g^2/λ.

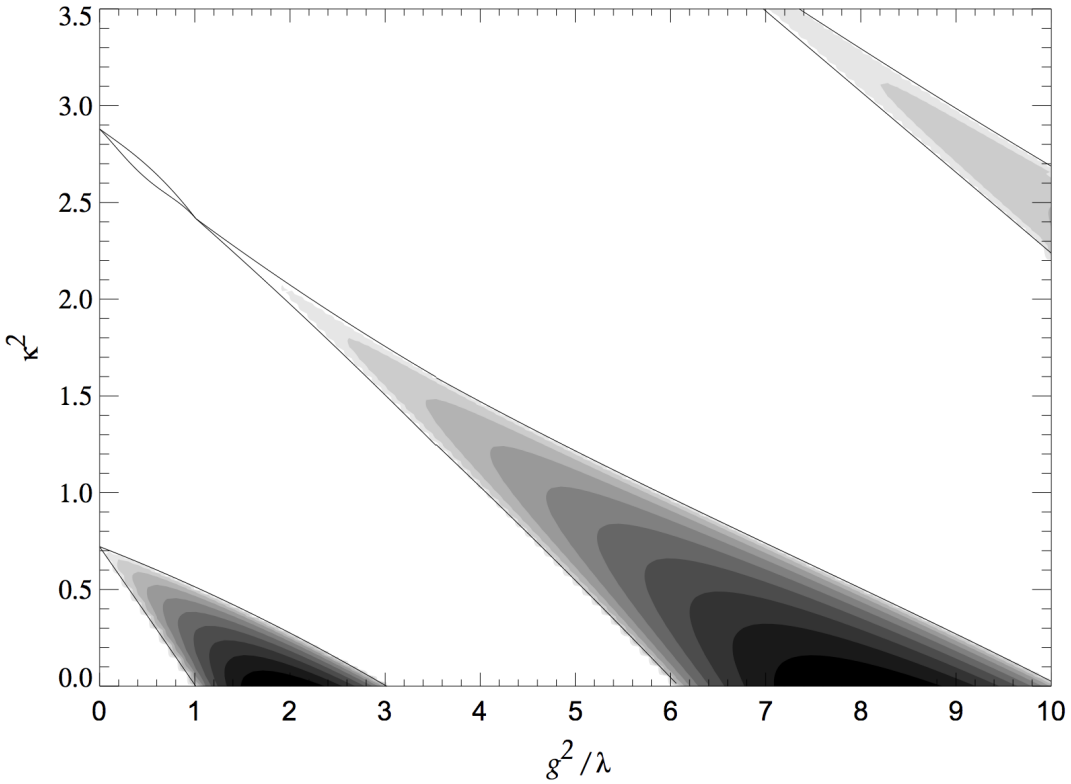

Figure 6.11: *Density plot of the Floquet chart for the Lamé equation for fluctuations $X_k(x)$ in the variables $\{\kappa^2, g^2/\lambda\}$. This was obtained from the numerical solution of Eq. (6.53). Shaded regions represent areas of instability. White regions represent the stable regions. For instability bands, a darker shade means a larger characteristic exponent μ_k. There are 10 colour steps altogether with one colour step representing an increment of $\Delta\mu_k = 0.0237$. The darkest shade represents the characteristic exponent $\mu_k = 0.237$ and the least dark shade represents $\mu_k = 0.009$. The Floquet index μ_k reaches its maxima for $g^2/\lambda = 2n^2$ at $\kappa^2 = 0$. Figure taken from [173].*

Fig. 6.12 and Fig. 6.13 show a typical resonant solution of Eq. (6.53). Here even though the plots are for $k = 1.6$ and $g^2/\lambda = 3$, the form of the solution is generic. Fig. 6.12 shows the amplification of the real part of the eigenmode $X_k(x)$ (solid curve) in an oscillating ϕ background (dotted curve). The comoving number density n_k is defined as:

$$n_k = \frac{\omega_k}{2}\left(\frac{|\dot{X}_k|^2}{\omega_k^2} + |X_k|^2\right) - \frac{1}{2}. \tag{6.56}$$

Fig. 6.13 shows the evolution of the logarithm of the comoving number density n_k (solid curve) and the evolution of the inflaton field (dotted curve). In Ref. [173], the authors attempt to find the values of the parameter g^2/λ for which there are analytic solutions to the Lamé equation in closed form. In doing so, they find that the resonance with respect to the χ particle production depends non-trivially on g^2/λ. For instance, for $\frac{g^2}{\lambda} = 1$ and $\frac{g^2}{\lambda} = 3$, the equation for the perturbations of the field χ has only one instability band. For $\frac{g^2}{\lambda} = \frac{n(n+1)}{2}$ there is only a finite number of

instability bands while there is an infinite number of instability bands for all other values of g^2/λ. Another interesting property they report is that χ particle production is least efficient for $g^2/\lambda \ll 1$ and for $g^2/\lambda = 3$. The characteristic exponent $\mu_{\max}$ for $g^2/\lambda = 2$ and $g^2/\lambda = 8$ is almost 7 times greater than the characteristic exponent $\mu_{\max}$ for $g^2/\lambda = 3$. It is for this reason that we pick $g^2/\lambda = 2$ for our lattice simulations in Chapter 7.

In such theories, the expansion of the universe does not hinder the resonance, so only backreaction of the produced particles terminates it. There are several different backreaction mechanisms which may terminate parametric resonance. For example, there is a decrease in the oscillations amplitude of the field $\varphi = a\phi$ due to the production of particles. This results in a proportional decrease in the frequency of the oscillations. The interaction of the homogeneous inflaton field with the produced particles, on the other hand, increases the frequency of the oscillations. Moreover, quantum fluctuations of the fields χ and ϕ acquire contributions to their masses. Altogether, these different effects effectively lead to a reconfiguration of the instability bands. In addition to this analytical study, computer simulations of reheating in the theory $\frac{1}{4}\lambda\phi^4$ were performed in Ref. [176] where rescattering was also included.

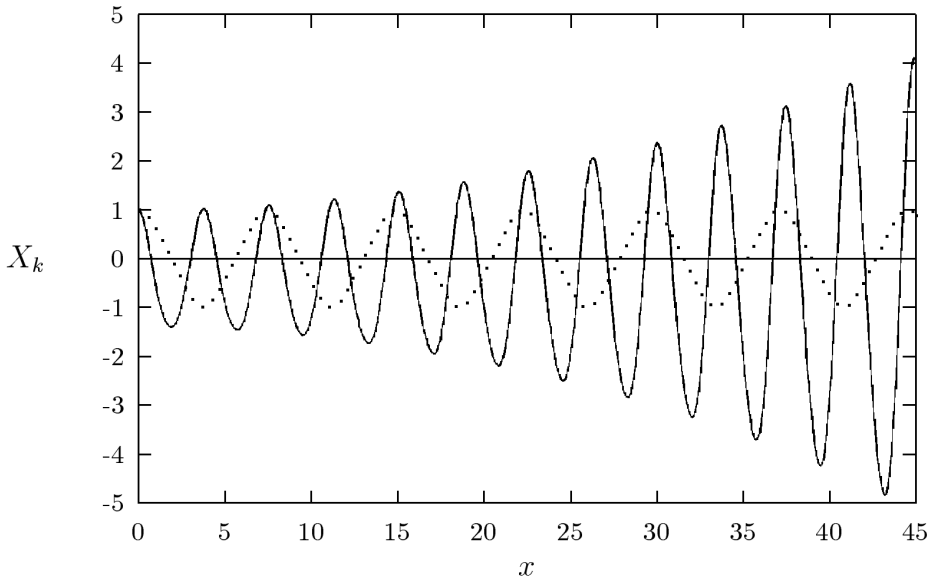

Figure 6.12: *$X_k(x)$ for $k = 1.6$ and $g^2/\lambda = 3$. Figure taken from [173].*

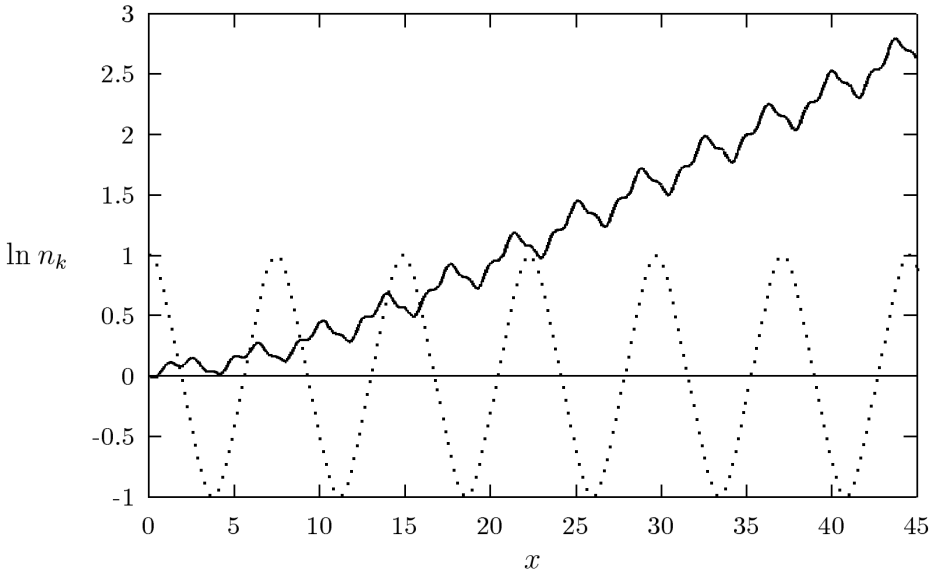

Figure 6.13: *Logarithm of comoving number density of χ particles for $k = 1.6$ and $g^2/\lambda = 3$. Figure taken from [173].*

6.8 Bird's-Eye View

It should be emphasized that preheating is but the first stage of reheating, which does not lead to a complete decay of the inflaton field in any of the models studied in this chapter. Reheating never completes at the stage of parametric resonance; eventually the resonance becomes narrow and inefficient and the final stages of the decay of the inflaton field and thermalization of its decay products can be described by the standard perturbative theory of reheating.

In § 6.3, we discussed the theory of preheating for the simple model of a massive inflaton field ϕ interacting with another scalar field χ with the quadratic potential $V(\phi) = \frac{1}{2}m^2\phi^2$ (with interaction term $g^2\phi^2\chi^2$). The theory of preheating is very complicated even in such a simple model. In the beginning particle production occurs in the regime of broad parametric resonance which gradually becomes narrow and then comes to an end. If the resonance is narrow from the very beginning or even if it is not broad enough, it remains inefficient. If we include the effects of an expanding universe we find that broad resonance is actually a stochastic process. Stochastic resonance is dramatically different from the theory of parametric resonance in Minkowski space.

In the conformally invariant theories such as the theory $\frac{1}{4}\lambda\phi^4 + \frac{1}{2}g^2\phi^2\chi^2$ (see § 6.7) with $g^2 \gg \lambda$ the resonance is broad but not stochastic because expansion of the universe does not interfere with its development. In [173], a more detailed investigation on stochastic resonance reveals that in models with $g^2 \gg \lambda$ the resonance becomes stochastic at $\Phi \lesssim \frac{g}{\sqrt{\lambda}}\frac{\pi^2 m^2}{3\lambda\sqrt{8\pi}M_{\rm pl}}$.

As we have seen, it is possible to go quite far in the investigation of preheating dynamics by developing analytical methods (for example, see [173, 179]). However, for a more complete understanding of non-perturbative effects during reheating, numerical simulations are a reliable tool. The simplest preheating model to implement for lattice simulations is massless preheating and we follow others [5, 152, 154, 156, 157, 213–215] and choose this model to study in detail in Chapter 7. In the next section, we give an overview of lattice simulations and the HLattice code that we use to run our simulations.

6.9 Lattice Field Theory Simulations

Computer simulations are a powerful and important tool for understanding the universe and for subjecting theories to rigorous testing. Numerical simulations have become in the last years one of the most effective tools to study and solve cosmological problems. The famous Millenium simulation, for example, traced more than 10 billion 'particles' to track the evolution of 20 million galaxies over the history of the Universe. Likewise, numerical simulations play a big part in the investigation of preheating and in our topic of research.

To study the early universe, one needs to describe the evolution of interacting fields in a dense and high-energy environment. The study of reheating typically involves non-perturbative interactions of fields with exponentially large occupation numbers in states far from equilibrium. In the large occupation number limit, it is possible to study preheating classically by lattice numerical simulations of the interacting classical scalar fields [172, 176, 216, 217]. In general, a lattice is defined as a discrete and regular arrangement of points. Lattice simulations are simulations on a spacetime that has been discretized onto a lattice as opposed to the continuum of spacetime. The lattice is a three-dimensional lattice where each point in the lattice corresponds to a position in space. Although it is impossible to completely remove the discrepancy between real (continuous) physics and the numerical (discrete) model, lattice simulations provide the most accurate means of studying the dynamics of preheating. The problem then becomes the discretization of the scalar field equations and solving the evolution of the system in a lattice once the initial values have been set.

There are multiple codes that have been written (some publicly available, some unreleased) to calculate the evolution of interacting scalar fields in an expanding universe. LATTICEEASY [218], for example, is a publicly availabe code which was written in C++ where the user creates a *model* file for the particular potential they are looking at. The only other file the user needs to modify is the *parameters.h* file which contains all the parameters needed for a given run of the program. LATTICEEASY has its own website and the website has documentation and a set of Mathematica notebooks for plotting all the output of the program although this can be easily done using any other standard plotting software. The parallel-programming version of LATTICEEASY is called CLUSTEREASY [219], also written in C++. CLUSTEREASY can simulate arbitrary scalar field models on distributed-memory clusters. LATTICEEASY and CLUSTEREASY can run simulations in one, two and three dimensions, with or without the expansion of the universe with customizable parameters and output. LATTICEEASY has been used to study parametric resonance [176, 179, 217, 220–224], the formation of gravitational waves, phase transitions and formation of topological defects and thermalization after reheating.

Another code for simulation preheating is DEFROST [225]. DEFROST makes use of more advanced algorithms and more careful optimization than LATTICEEASY and therefore significantly improves on the accuracy and performance achievable in simulations of preheating. Yet another publicly available code is CUDAEASY [226] which is a GPU (Graphics Processing Unit) accelerated cosmological lattice program. With CUDAEASY, simulations that used to take one day to compute can be done in hours.

For our simulations in Chapter 7 though, we will use the code HLattice, written by Zhiqi Huang in fortran 90. HLattice differs from the previous codes in three ways:

- A much higher accuracy obtained by using a modified sixth-order symplectic integrator. Other lattice codes [218, 225, 226] use the equivalent of a second-order symplectic integrator.
- Scalar, vector and tensor metric perturbations in the synchronous gauge and their feedback to the dynamics of scalar fields are all included (These are ignored in LATTICEEASY and CUDAEASY).

For our purposes, the metric feedback is negligible and therefore, our primary reason for choosing HLattice is its accuracy and the fact that it is freely available, easy to use and was used by Bond *et al.* [154] to compute $N(\chi)$ in the massless preheating case whose results we use as a check for our simulations in Chapter 7. In the rest of this section, we will briefly review HLattice to have an understanding of the essentials in lattice simulations.

6.9.1 HLattice

HLattice is a free code that simulates scalar fields in the early universe. The latest version is HLattice V2.0 which can be downloaded at `http://www.cita.utoronto.ca/~zqhuang/hlat/`. Ref. [5] provides all the relevant details on HLattice and also presents the calculation of gravity waves from preheating after inflation for $V = \frac{1}{4}\lambda\phi^4 + \frac{1}{2}g^2\phi^2\chi^2$ using HLattice. The reader is referred to the above mentioned paper for more details.

Lattice Theory and the Discrete Fourier Transform (DFT)

Let us take a look at which equations are being integrated on the lattice and what discretization scheme HLattice uses.

A grid point in the lattice is labelled with three integer numbers (i_1, i_2, i_3) and since the simulation is implemented in a cubical fundamental box, we need to apply periodic boundary condtions as follows:

$$f_{i_1+n,i_2,i_3} = f_{i_1,i_2+n,i_3} = f_{i_1,i_2,i_3+n} = f_{i_1,i_2,i_3}. \tag{6.57}$$

Here, f represents all physical quantities we are interested in (the scalar fields, the metric and their temporal/spatial derivatives). The scalar fields are evolved in configuration space and the lattice version of the equation of motion is given by:

$$\Big(\frac{\mathrm{d}^2}{\mathrm{d}t^2} - \frac{\nabla^2}{a^2} + 3H\frac{\mathrm{d}}{\mathrm{d}t}\Big)\phi_l|_{i_1,i_2,i_3} + \frac{\partial V}{\partial \phi_l}|_{i_1,i_2,i_3} = 0, \tag{6.58}$$

where ∇^2 is the discrete Laplacian operator. Eq. (6.58) is the equation being integrated on the lattice. The expansion rate $H = \dot{a}/a$ and acceleration $\ddot{a}$ are determined by the averaged Einstein equations:

$$H^2 = \frac{1}{3M_{\rm pl}^2}\langle\rho\rangle, \tag{6.59}$$

$$\frac{\ddot{a}}{a} = -\frac{1}{6M_{\rm pl}^2}\langle\rho + 3p\rangle, \tag{6.60}$$

where $\langle . \rangle$ represents the lattice average $\frac{1}{n^3}\sum_{\rm lattice}$ and n^3 is the number of grid points. To solve Eq. (6.58) numerically, we need to know what H is but rather than solving the constraint equation Eq. (6.59), it is useful to use the following evolution equation

$$\dot{H} = -H^2 - \frac{1}{6M_{\rm pl}^2}\langle\rho + 3p\rangle. \tag{6.61}$$

One can then use Eq. (6.59) as a measure of accuracy, defining the fractional energy noise as

$$|3H^2M_{\rm pl}^2/\langle\rho\rangle - 1|, \tag{6.62}$$

where $\langle\rho\rangle$ is the energy density averaged over the lattice and H is evaluated using Eq. (6.61). With the sixth-order symplectic integrator that HLattice uses, the fractional energy noise of the system is suppressed to $\lesssim 10^{-12}$. Such noises are $10^{-5} - 10^{-3}$ in other lattice codes [202, 218]. This is very important for calculating N accurately as discussed in Ref. [154].

Picking a discretization scheme amounts to defining the Laplacian operator ∇^2 in Eq. (6.58). Before HLattice, all calculations of gravitational waves from preheating ignored the metric feedback on the scalar fields. In retrospect, reasons of the common practice to ignore metric perturbations in lattice simulations of preheating are clear. Including them adds an unwelcome complexicity to the code; in this case, including the metric perturbations means the equation of motion involved first-order spatial derivatives as well and therefore meant that ∇ also needed to be defined properly and be consistent with the lattice ∇^2. The discretization scheme 'HLATTICE1' and later the improved version, 'HLATTICE2', were implemented for the

calculation of gravitational waves including the metric perturbations. We refer the reader to the HLattice paper [5] for more details on the implementation of these two discretization schemes. The third discretization option in HLattice is 'LATTICEEASY' which ignores the metric perturbations. The author [5] found that the metric feedback is indeed negligible, as previously conjectured, for the models studied in the paper which also includes the massless preheating model that we will study in Chapter 7. Since including metric perturbations is about ten times more computationally expensive and they are negligible for massless preheating anyway, for our simulations in Chapter (7), we pick the LATTICEEASY discretization option where the metric perturbations are turned off and combined with the sixth-order symplectic integrator, it is accurate enough to capture small effects as we will see in that chapter.

Other Features and Important Findings

HLattice was written in the synchronous gauge for sheer practical convenience: In the synchronous gauge, the gauge condition $g_{00} = g_{0i} = 0$ is local. In other gauges, the ten metric variables $g_{\mu\nu}$ are constrained by four global constraint equations and these equations have to be solved at every time step in order to eliminate the four gauge degrees of freedom. This is computationally expensive and hence why the author chooses to write the code in synchronous gauge.

To improve on accuracy, HLattice uses an accurate sixth-order symplectic integrator to integrate the equations of motion. A symplectic integrator is a very stable numerical integration system for Hamiltonian systems. Symplectic integrators have been used to study long-term evolution of many-body systems in astronomy and particle physics [227, 228]. HLattice is the first code to use the Hamiltonian constraint equation to accurately check the numerical accuracy in calculations of gravitational waves from preheating.

HLattice is the first code released that consistently evolves all components of metric perturbations together with scalar fields.

Outputs from HLattice

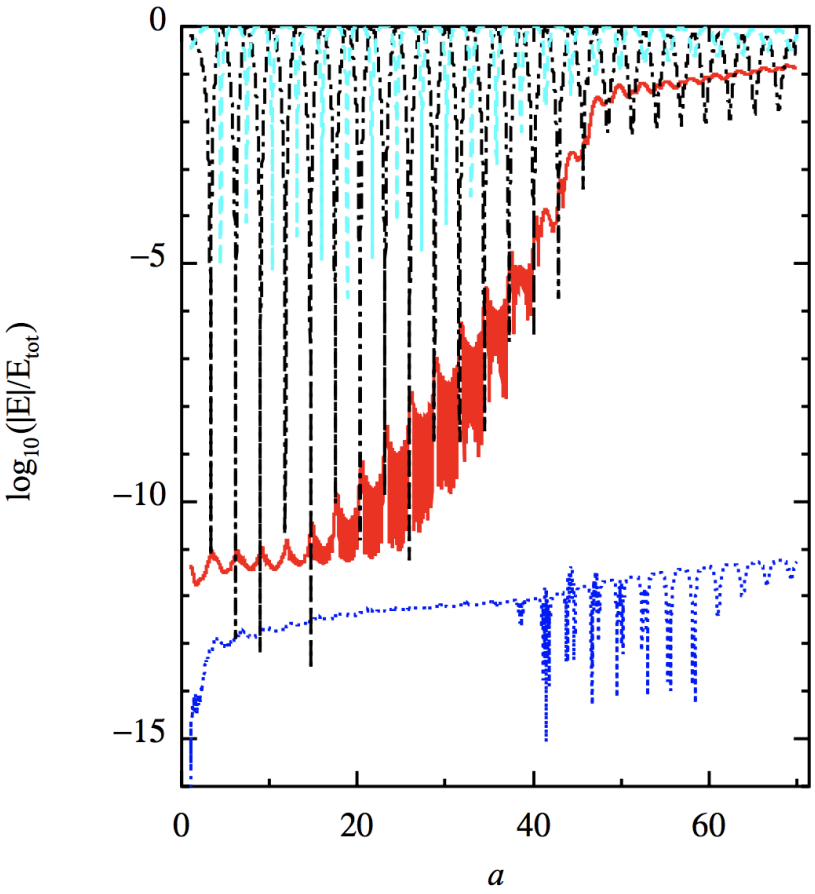

Figure 6.14: *Lattice simulation for the preheating model* $V = \frac{1}{4}\lambda\phi^4 + \frac{1}{2}g^2\phi^2\chi^2$ *using HLattice.* $\lambda = 10^{-13}$, $g^2/\lambda = 200$, *n=64, the box size* $L = 20H^{-1}$, $E_{\rm tot} = \langle\rho\rangle$ *is the mean total energy,* $E_{\rm grad}$ *is the mean gradient energy,* $E_{\rm kin}$ *is the mean kinetic energy and* $E_{\rm pot}$ *is the mean potential energy. The solid red line is* $\log_{10}(E_{\rm grad}/E_{\rm tot})$. *The dot-dashed black line is* $\log_{10}(E_{\rm pot}/E_{\rm tot})$. *The dashed cyan line is* $\log_{10}(E_{\rm kin}/E_{\rm tot})$. *The dotted blue line is* $\log_{10}|3H^2M_{\rm pl}^2/E_{\rm tot} - 1|$. *Figure is from [5].*

Fig. 6.14 shows a simulation done on an eight-core desktop PC in about half an hour using HLattice. In Chapter 7, we will show how we also use the HLattice code to implement the 'Non-Perturbative δN Formalism' in a Monte-Carlo fashion.

7 Calculating ζ from Lattice Simulations

In Chapter 5, we presented the non-perturbative δN formalism, an extension of the standard δN formalism when a truncated Taylor expansion of the N function is not valid. In that chapter, we applied our expressions to a realistic example by constructing a fitting function $N(\chi)$ and integrating copies of this function against the probability distribution to calculate $\tilde{N}_\chi$ and $\tilde{N}_{\chi\chi}$ and gave estimates for the power spectrum and reduced bispectrum. We also briefly touched on a Monte Carlo approach to non-perturbative δN formalism. One notable example where the $N(\chi)$ is not smooth and that warrants a Monte Carlo approach is preheating and in Chapter 6, we reviewed preheating and massless preheating in detail. In this chapter, we apply the non-perturbative δN formalism to massless preheating. By running our own simulations on the QMUL Apocrita cluster [6], we will see that in the case of massless preheating, the chaotic dynamics imprint regular log-spaced narrow spikes in the number of preheating e-folds $N(\chi)$. Chapter 7 is structured as follows. We begin by reviewing the work of Suyama and Yokoyama in § 7.1 where they provide a method for calculating correlators of arbitrary functions of a Gaussian field and as an application, they calculate the two-, three- and four-point functions of the primordial curvature perturbation generated in massless preheating. Their approach is to approximate each spike as a normal distribution so that $N(\chi)$ is a sum of normal distribution functions. We call their method the N_σ method because a key step in their formula was to make a fourier transform of the N function. We then present our method in § 7.2 where we make no such approximations and instead use the raw data from the lattice simulations in a Monte Carlo fashion to calculate the power spectrum and the reduced bispectrum.

"Although we often hear that data speak for themselves, their voices can be soft and sly."

—Frederick Mosteller

7.1 The N_σ Method

As we have seen in Chapter 6, during reheating particles may be produced rapidly due to non-perturbative reheating processes, often called preheatng. If particles are produced in a field that is light during inflation, this process can alter the statistics of the primordial curvature perturbation ζ over observable scales. This is because the rate of particle production is sensitive to the initial conditions of the reheating field, which are modulated over such scales. The simplest example is massless preheating [151, 152, 154, 171–173], which serves as a simple example and testing ground of methods to calculate the statistics of ζ after inflation. The chaotic nature of the motions of the inflaton field and the χ field which is coupled to the inflaton field during preheating and the termination of the growth of field perturbations by the highly non-linear dynamics make it impossible to accurately analytically derive the mapping $N(\chi)$ needed in the non-perturbative δN method presented in Chapter 5. In Fig. 7.1, the numerical results from lattice simulations for massless preheating from Ref. [154] are presented. Before moving to our work, let us first review the work of Suyama and Yokoyama [155] who also considered the problem of calculating observables in massless preheating.

The authors generate a mock $N(\chi)$ that mimics the highly featured and spiky one in Fig. 7.1 because they did not have the raw numerical data of Ref. [154] but only the numbers from Fig. 7.1. They use a public software to extract the coordinates out of the graph. In order to extract the position, height and width of each spike, they smoothed out the obtained $N(\chi)$ using a Gaussian window function with a width that is smaller than $\sqrt{\langle\chi^2\rangle}$ but large enough to eliminate the fine spikes in Fig. 7.1. The resultant smoothed graph of Fig. 7.1 in shown in Fig. 7.2. The authors then propose that although the actual form of the original $N(\chi)$ is quite complicated and disorderly, one can describe the basic behaviour of the function by the analytic approximation that $N(\chi)$ is given by the sum of normal distribution functions:

$$N(\chi) = \sum_p A_p \exp\Big(- \frac{(\chi - \chi_p)^2}{2\kappa_p^2} \Big), \tag{7.1}$$

where χ_p and κ_p are the position and width of the p-th spike, respectively. A_p is the amplitude of the p-th spike. Next, because the numerous spikes in Fig. 7.1 apparently appear to be random, the authors then decide to generate 200 realizations of the mock $N(\chi)$ where the positions χ_p, amplitudes A_p and widths κ_p are generated randomly, subject to some interval to closely match the original one. The number of spikes within a given range is fixed to be 75 for all 200 realizations. Because the procedure is probabilistic in nature, they obtain different but similar $N(\chi)$ realizations and that way, they are able to see how the results vary by each realization and

how they depend on the different choices for χ_0 and $\langle\chi^2\rangle$. One such realization is shown in Fig. 7.3.

Moving on, now that we have an analytic expression for the mock $N(\chi)$, employing Eq. (5.2)[1], one can trivially derive the analytic form of N_σ:

$$N_\sigma = \sqrt{2\pi}\sum_p A_p\kappa_p \exp\Big(-\frac{\kappa_p^2\sigma^2}{2} - i\chi_p\sigma\Big). \tag{7.2}$$

Then, using Eq. (5.3), we can also derive

$$\langle N\rangle = \sum_p A_p \frac{\epsilon_p}{\sqrt{1+\epsilon_p^2}} \exp\Big(-\frac{\eta_p^2}{2(1+\epsilon_p^2)}\Big), \tag{7.3}$$

where ϵ_p and η_p are the peak width and the peak position respectively, normalized by $\sqrt{\langle\chi^2\rangle}$ and are given by

$$\epsilon_p \equiv \frac{\kappa_p}{\sqrt{\langle\chi^2\rangle}}, \qquad \eta_p \equiv \frac{\chi_p}{\sqrt{\langle\chi^2\rangle}}. \tag{7.4}$$

$\langle\zeta_1\zeta_2\rangle = \langle N_1N_2\rangle - \langle N\rangle^2$ and

$$\begin{aligned}\langle N_1N_2\rangle \;=\; & \sum_{p_1,p_2} \frac{A_{p_1}A_{p_2}\epsilon_{p_1}\epsilon_{p_2}}{\sqrt{(1+\epsilon_{p_1}^2)(1+\epsilon_{p_2}^2)-\xi(r_{12})^2}} \\ & \times \exp\Big(-\frac{1}{2}\frac{(1+\epsilon_{p_1}^2)\eta_{p_1}^2 + (1+\epsilon_{p_2}^2)\eta_{p_2}^2 - 2\xi(r_{12})\eta_{p_1}\eta_{p_2}}{(1+\epsilon_{p_1}^2)(1+\epsilon_{p_2}^2)-\xi(r_{12})^2}\Big).\end{aligned} \tag{7.5}$$

We can obtain the same expression in Eq. (7.5) by integrating two copies of $N(\chi)$ against the joint probability function as we found in § 5.3.1 using Eq. (5.22). The authors then use the same expansion in the cross-correlation as we do, i.e., $\xi(r_{12}) \ll 1$ and calculate the amplitude of the power spectrum, $f_{\rm NL}$ and so on.

They report that typically, $f_{\rm NL} \sim \mathcal{O}(10^6)$ and that the amplitude of the power spectrum from massless preheating is about four orders of magnitude smaller than the observed amplitude. They then assume that the dominant contribution to the total curvature perturbations comes from the standard adiabatic perturbation from inflation and that this mixture dilutes the observed $f_{\rm NL}$ to $\mathcal{O}(10^{-3}) - \mathcal{O}(0.1)$. The authors were able to analytically perform the integrals for the two-point, three-point

[1]Refer to § 5.1 for a review of their method.

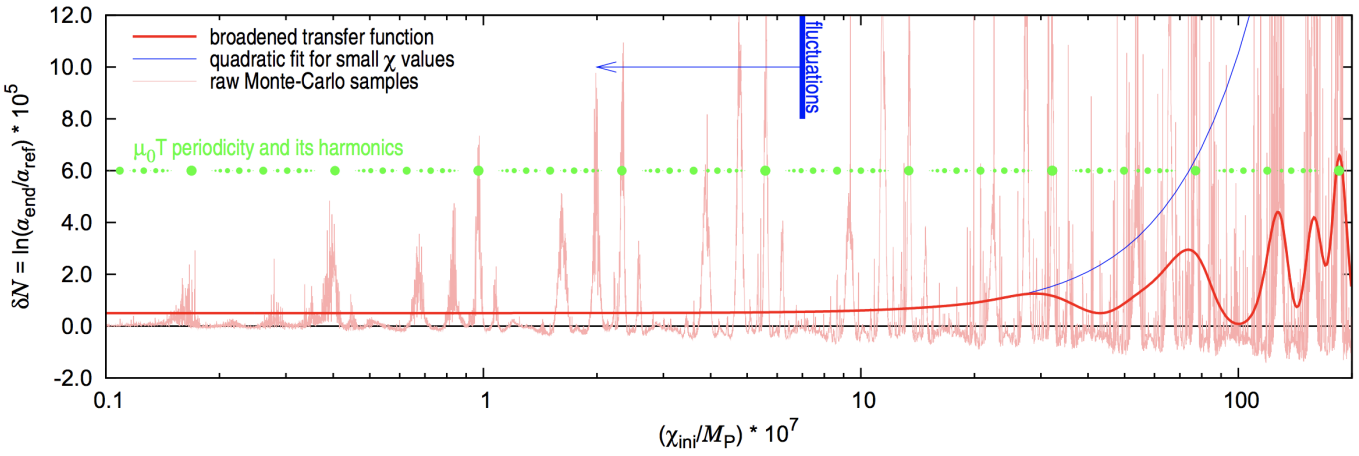

Figure 7.1: *The structure of $\delta N(\chi_i)$ on uniform Hubble hypersurfaces probed with $\sim 10^4$ lattice simulations from the end of inflation through the end of preheating for varying homogeneous χ_i initial conditions for $g^2/\lambda = 2$. Note that $M_p \equiv M_{pl} = 1/\sqrt{8\pi G_N}$. Figure taken from [154].*

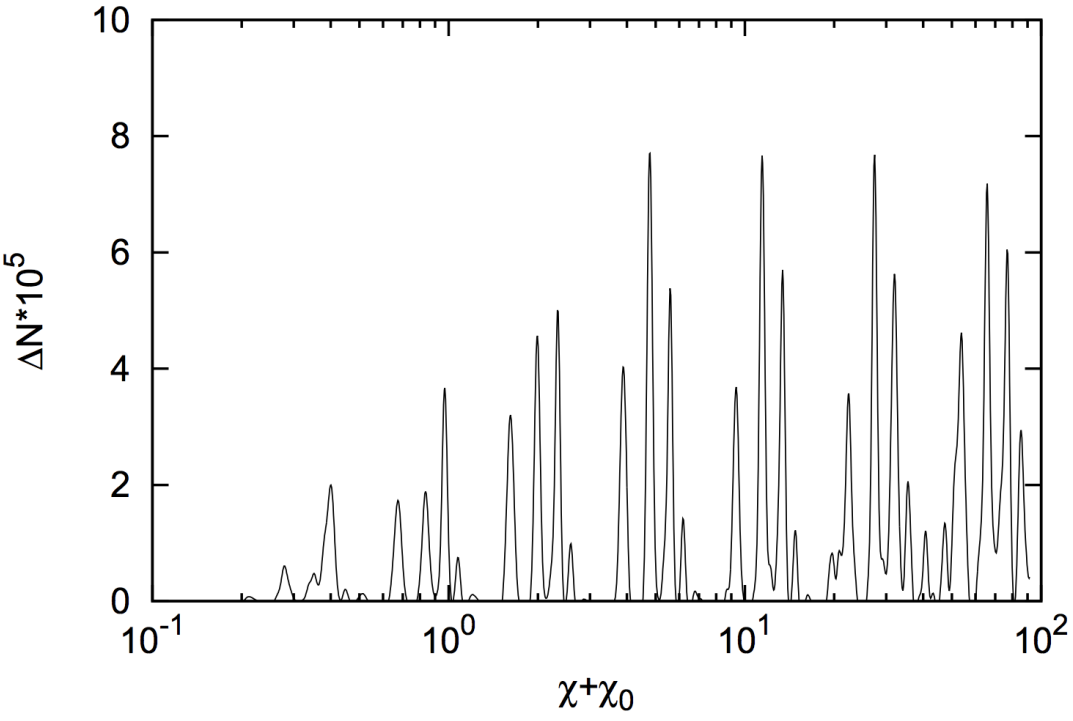

Figure 7.2: *Smoothed $N(\chi)$ of Fig. 7.1. The unit of the horizontal axis is $10^{-7} M_{pl}$. Due to the smoothing process, the height of each spike is smaller than the original one in Fig. 7.1. The width is then broadened by a bit to compensate for the loss of height. Note that, in this work, the authors choose to set $\langle\chi\rangle = 0$ and therefore their χ is different to the one used in [154] by a constant value which they denote by χ_0. Figure taken from [155].*

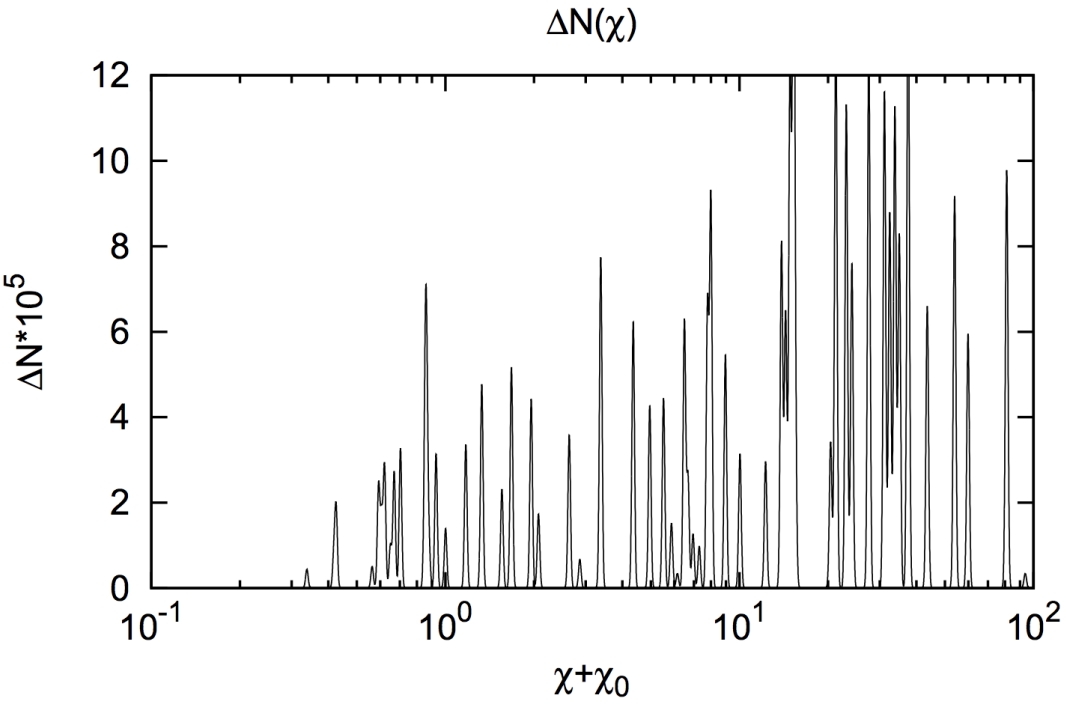

Figure 7.3: *Massless preheating: a mock $N(\chi)$ randomly generated by authors in Ref. [155]. $\chi_0 = 10$ and $\langle\chi^2\rangle = 10$ in units of $10^{-7}M_{\rm pl}$. Figure taken from [155].*

and four-point functions of ζ due to the analytic fitting formula used for the spikes.

We argue, however, that in cases where the N function is highly featured, approximating the features might not give accurate answers. Regarding our own expressions in Eq. (5.37) and Eq. (5.39), first calculating the function accurately may not even be the most efficient path to accurately evaluating $\tilde{N}_\chi$ and $\tilde{N}_{\chi\chi}$. Instead one might choose to adopt a Monte Carlo approach, in which values of the initial field(s) χ^I are drawn from a Gaussian distribution, and for each draw N is evaluated numerically. $\tilde{N}_I$, for example, is then calculated by evaluating $\delta\chi^I N$ for each draw, and the values summed and divided by the number of draws. This is the approach that we adopt in our work in the next sections.

7.2 Introduction

If more than one field is light at the end of inflation, perturbations produced by inflation evolve during the reheating phase which follows. This is both a problem and potentially an opportunity, since it makes model predictions sensitive to this complicated and poorly constrained phase of evolution. In order to compare models with observations and potentially learn about reheating, therefore, we must be able

to calculate the statistics of the curvature perturbation at the end of reheating. In this chapter we do this directly from lattice simulations for the first time.

In massless preheating, if g^2/λ is tuned to be $\sim \mathcal{O}(1)$, the non-inflaton field χ is light during inflation and accumulates quantum fluctuations substantially varying on scales much greater than the Hubble scale at the end of inflation. For $g^2/\lambda = 2$, the χ field fluctuations grow exponentially on super-horizon scales and this particular parameter choice has led to a lot of studies of whether the χ field perturbation can generate the curvature perturbation on super-horizon scales during preheating [229–235] (see [236–238] for other models of preheating). We will also set $g^2/\lambda = 2$ for our simulations.

There are two main problems for calculating ζ after massless preheating. First, as a non-perturbative process involving the excitation of the inhomogeneous modes of the fields, as we discussed in Chapter 6, it must be studied using lattice simulations. Second, since these simulations typically only capture the dynamics of a patch of the universe exponentially smaller than observable universe, and because the average evolution of such a patch can be very sensitive to initial conditions, widely used methods such as the standard δN formalism cannot be used without modification. These issues have been discussed at length in a number of publications [153, 171] and in our own earlier work on the issue [239] presented in Chapter 5, we discussed the use of a non-perturbative approach to δN. This approach allows the evolution of a given patch of the universe to be highly sensitive to initial conditions. Moreover, by working in real space there is no implicit assumption about coarse-graining at the outset. It can therefore utilise simulations of only small regions of the universe as long as they do not interact with one another (i.e. they must obey the separate universe assumption). In Chapter 5 [239] we argued that our approach to non-perturbative δN is ideally suited to use with lattice simulations, and in the current chapter we implement it to calculate the statistics of ζ after massles preheating directly from simulations.

7.3 Non-Perturbative δN Formalism

As previously seen in Chapter 4, the δN formalism [120, 125, 240–242] is a powerful technique which employs the separate universe assumption to calculate the observable statistical properties of ζ produced by scalar field models of the early universe. It assumes the number of e-folds undergone by a patch of the universe, coarse-grained on observable scales, is a function of the field's initial conditions that can be well described by the leading terms in a Taylor expansion. In Chapter 5 [239], we discussed a non-perturbative approach to calculating the statistics of ζ

that can be employed when a Taylor expansion is not a good approximation, as it is not for massless preheating. This begins with the definition of the ensemble average of any n-point correlation function in real space (Eq. (5.22)). In principle this can be evaluated directly, but as we have discussed, this is often challenging to do and we proceeded to employ an expansion which does not assume a Taylor expansion of the e-fold function, but instead a Taylor expansion in the correlation between the field's value at separated spatial positions. This leads to expressions for the correlation functions of ζ which take the same form as those of the usual δN formalism but with *non-perturbative* δN *coefficients* instead of the usual derivatives of N. We observed that in many cases our method showed noticeable improvement over standard δN, but also that the expansion can break down, and that whether this happens needs to be examined on a case by case basis.

In this chapter, we are primarily interested in the contribution to ζ from the reheating field. We will assume this field is uncorrelated to the inflaton before the start of the lattice simulations, and will therefore employ the non-perturbative expansion formalism including only one field (we will comment on the validity of this approach below). In this case the contribution to the two point function of ζ from this field, denoted χ, at leading and sub-leading order in the correlation expansion is given explicitly by (also, see Eq. (5.49):

$$\langle\zeta(\mathbf{x}_1)\zeta(\mathbf{x}_2)\rangle = \tilde{N}_\chi^2\Sigma(r_{12}) + \frac{1}{2}\tilde{N}_{\chi\chi}^2\Sigma(r_{12})^2\,, \tag{7.6}$$

where $\tilde{N}_\chi$ and $\tilde{N}_{\chi\chi}$ are our non-perturbative δN coefficients

$$\tilde{N}_\chi \;=\; \frac{\langle\delta\chi N(\chi)\rangle}{\langle\delta\chi^2\rangle}\,, \tilde{N}_{\chi\chi} = \frac{\langle\delta\chi^2(N(\chi)-\bar{N})\rangle}{\langle\delta\chi^2\rangle^2}\,. \tag{7.7}$$

In these expressions for the coefficients, the angle brackets denote an ensemble average with χ drawn from a single variate Gaussian distribution with mean value $\bar{\chi}$ and variance $\Sigma = \langle\delta\chi(\mathbf{x})\delta\chi(\mathbf{x})\rangle$. $\Sigma(r_{12})$ is the two-point function of field perturbations at separated spatial positions, $\Sigma(r_{12}) = \langle\delta\chi(\mathbf{x_1})\delta\chi(\mathbf{x_2})\rangle$. This is evaluated at the initial time before reheating, while the two point-function of ζ is evaluated at the final time after reheating.

As discussed in § 5.2.3 where we addressed the limitations of our method, we saw that the expansion method leading to Eq. (7.6) may break down and so we use the sub-leading term above as a test of the validity of the expansion, and assume that only in cases where the sub-leading term is sub-dominant by at least an order of magnitude can we trust our expansion method to calculate $\mathcal{P}_{\rm pre}$ with reasonable accuracy.

We also calculate the local non-Gaussianity which the model produces by assuming that the three-point function of field space perturbations is negligible and using the leading order expression for the three-point function of ζ in the correlation expansion

$$\langle\zeta(\mathbf{x}_1)\zeta(\mathbf{x}_2)\zeta(\mathbf{x}_3)\rangle = \tilde{N}_\chi^2\tilde{N}_{\chi\chi}\Sigma(r_{12})\Sigma(r_{23}) + \text{cyclic}\,. \tag{7.8}$$

7.4 Massless Preheating

The potential for the massless preheating model is given by Eq. (6.35) where ϕ is the inflaton field and χ the reheating field, with dimensionless coupling constants, g and λ. For small coupling ratios (g^2/λ) required to excite the first resonance band of the system, the masses of the two fields, $m_\phi = \sqrt{3\lambda}\phi$ and $m_\chi = \mathrm{g}\phi$, are comparable during inflation, and hence the χ field is light. This model is unlikely to be compatible with current observations, but still serves as a convenient testing ground for our methods. It is conformally invariant and this allows the expansion of the universe to be re-scaled away in lattice field theory simulations. During inflation, χ is approximately zero and the behaviour of the model is the same as the standard single field $\frac{\lambda}{4}\phi^4$ chaotic inflation model. We can therefore estimate the value of the ϕ field when inflation ends by assuming only ϕ drives inflation and setting the first slow-roll parameter ϵ_v to 1 (ϵ_v is defined in Eq. (2.14)). We obtain $\phi_{\rm end} \approx 2.83 M_{\rm pl}$.

7.4.1 Expressions for $\mathcal{P}_{\rm inf}$ and $\mathcal{P}_{\rm pre}$

We now begin the process of calculating the the impact of reheating on ζ using the formalism outlined above.

First let us note that we can immediately estimate the contribution to ζ from the inflaton, ϕ, under the assumption that it is uncorrelated to the reheating field. Using the formula in Eq. (2.18), we find $\phi_* \approx 21.17 M_{\rm pl}$ where '*' denotes horizon crossing time of the pivot scale of observations which we take to be 55 e-folds before the end of inflation. We can then employ the standard expression for the power spectrum of ζ (see Eq. (3.36))

$$\mathcal{P}_{\rm inf} = \frac{1}{8\pi^2}\frac{H_*^2}{M_{\rm pl}^2\epsilon_*}, \tag{7.9}$$

and use the approximation $\epsilon_* \approx \epsilon_{v_*}$, valid during slow-roll (see Eq. (2.16). On the other hand, to calculate the contribution of χ we must employ the non-perturbative δN formalism. The effective mass of the χ field is $\mathrm{g}\phi$, and we must begin the δN formalism before this field becomes heavy. We therefore set initial conditions for χ and its statistics at the time just before χ becomes massive, i.e., when $\frac{\mathrm{g}^2\phi_{\rm ini}^2}{H_{\rm ini}^2} \sim 1$. This is shortly before the end of inflation. At this point we assume again that χ can be taken to be a spectator field uncoupled to the inflaton, and therefore has a

variance (using Eq. (4.6), Eq. (5.53) and Eq. (5.61)) within our observable universe about some background value, $\bar{\chi}$, of

$$\langle \delta\chi\delta\chi \rangle|_{\rm ini} = \frac{H_{\rm ini}^2}{4\pi^2}\mathcal{N} \tag{7.10}$$

where $\mathcal{N} \approx 55$ and $H_{\rm ini}$ is the Hubble rate at this time. Assuming scale invariance of $\delta\chi$ at the initial time, one then finds the contribution to the power spectrum of ζ from preheating is

$$\mathcal{P}_{\rm pre} = \tilde{N}_\chi^2 \frac{H_{\rm ini}^2}{4\pi^2}\,. \tag{7.11}$$

The value of $\bar{\chi}$ is determined by the behaviour of the system prior to the observable number of e-folds, and for the purpose of our study we take it to be a free parameter, with the restriction that it must be much greater than the variance of χ for consistency. Evaluating $\tilde{N}_\chi$ and $\tilde{N}_{\chi\chi}$ using Eq. (7.7) requires the use of lattice simulations which we now discuss.

7.4.2 Simulations

The δN formalism requires that we record the number of e-folds that occurs between given initial conditions and some final value for the density of the universe $\rho_{\rm end}$ after reheating has occurred and the system has become adiabatic. This must be repeated for many initial conditions and the results compared with one another. In this study we will use the HLattice code [5][2], described in Chapter 6, to simulate a small patch of the universe. We therefore wish to run the code by setting initial conditions for the initial average value of the $\bar{\phi}$ and $\bar{\chi}$ fields in the patch at the initial time before the χ field becomes massive, and subsequently run the code and record the number of e-folds, $N_{\rm end}$, at the desired value of ρ, $\rho_{\rm end}$. To do so we first modify Hlattice to stop once a given value of ρ has been passed, and output values of a and ρ around this time. We then use a python script to fit $\log a$ as a function of $\log\rho$, and use this function to calculate an accurate value for $N_{\rm end}$. One issue we find, as was also reported in [154], is that since reheating is not fully complete after preheating, the equation of state $\omega = \frac{p}{\rho}$ oscillates around the radiation dominated value of 1/3 after preheating, indicating that the system is not yet fully radiation dominated and adiabatic (see Fig. 7.4). If the system were to be adiabatic, the difference in N between two different patches with different initial conditions and measured at the same successive values of ρ would become a constant (i.e., ζ would become conserved). Instead we find that this quantity is oscillating. In order to remedy this problem we follow Ref. [154] and average the result over many oscillations. In Eq. (7.7), because the averages commute, this corresponds to averaging the N that appears there over a fixed range of ρ which encompasses many oscillations once

[2]HLattice can be downloaded from *http://www.cita.utoronto.ca/ zqhuang/hlat/*.

preheating has ended. This is then taken to be our N_{end}.

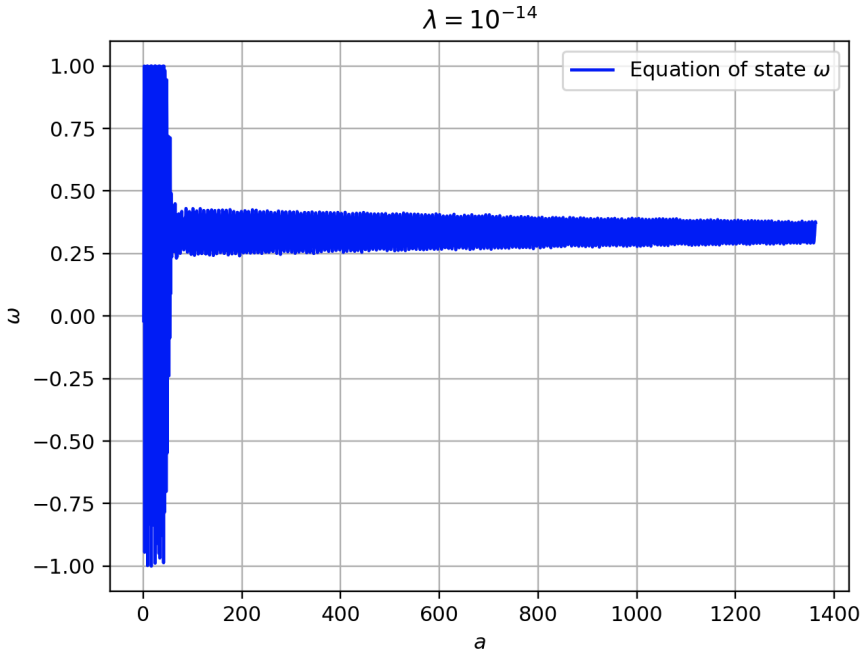

Figure 7.4: *The equation of state ω oscillates around 1/3 after preheating. The sharp transition from large amplitude oscillations to small amplitude oscillations indicates that preheating has occured. As we saw in § 6.7.2, the energy density of the inflaton field decreases in the same way as the energy density of radiation, i.e., $\omega \approx 1/3$.*

7.4.3 Simulations on the cluster

Checks

First to verify our code is working as intended we compare our results with the results of Ref. [154], where $N_{\rm end}$ is averaged in the manner described above and the difference between the answer and a fiducial for many initial conditions is plotted. Our results are given in Fig. 7.5 for $\lambda = 10^{-14}$ and $g^2/\lambda = 2$. Please note that in Fig. 7.5, $\chi_{\rm i}$ is the value of the χ field at the beginning of the lattice simulation, which corresponds to the end of inflation (not at a time just before χ becomes massive like we will consider for our purposes.). Fig. 7.5 should be compared to Fig. 7.1.

Moreover, we check that our results are insensitive to the period over which we average. Another accuracy test that we perform is to check that δN is effectively zero ($\ll 10^{-6}$) and not modulated by $\chi_{\rm i}$ for coupling ratio $\frac{g^2}{\lambda}$ outside of the resonant band, at $\frac{g^2}{\lambda} = 1$ and 3. See Fig. 7.6 for $g^2/\lambda = 1$.

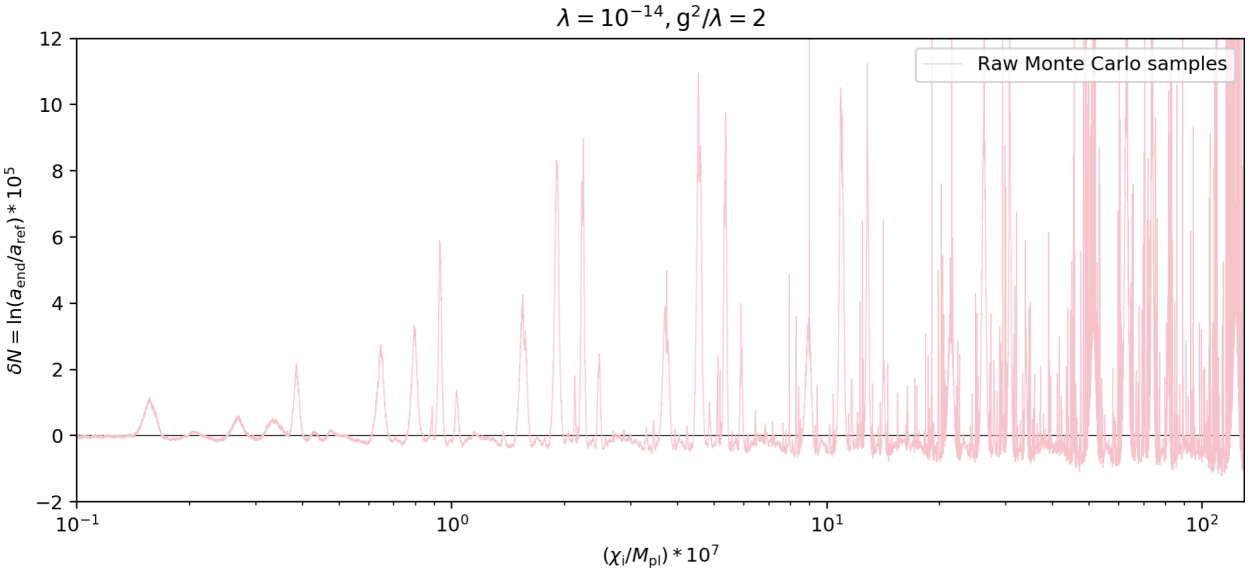

Figure 7.5: *The structure of $\delta N(\chi_i)$ on uniform density Hubble hypersurfaces evaluated with around $\sim 10^4$ lattice simulations for varying homogeneous χ_i initial conditions for $\lambda = 10^{-14}$ and $g^2/\lambda = 2$.*

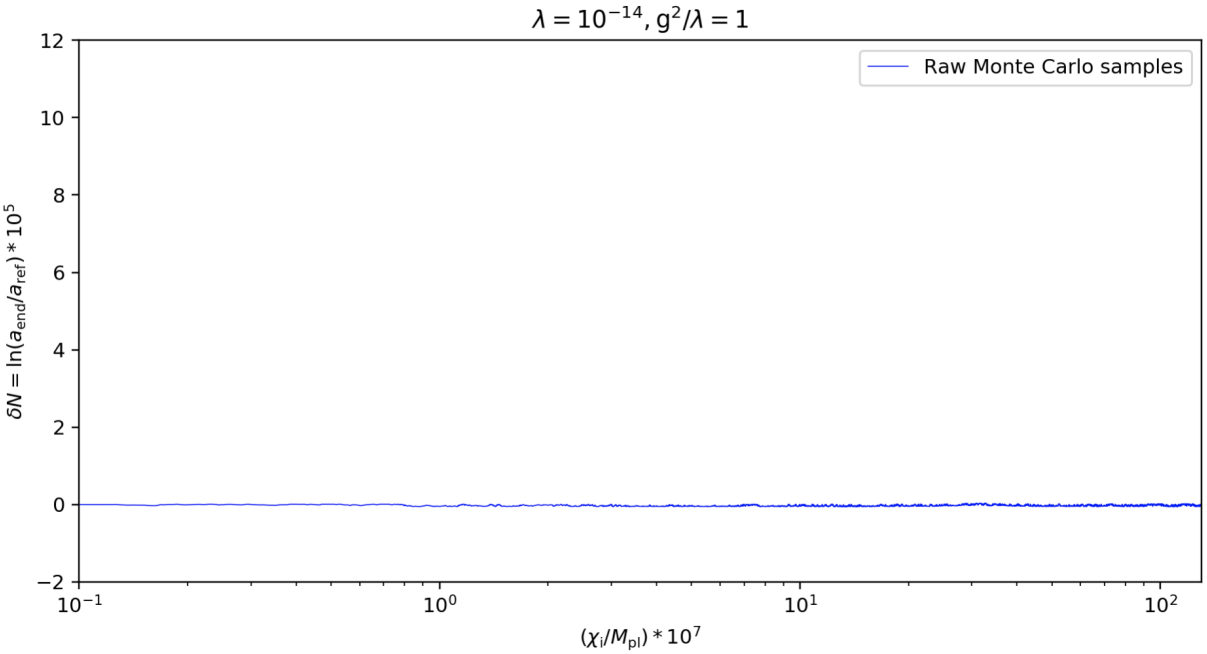

Figure 7.6: *The structure of $\delta N(\chi_i)$ on uniform density Hubble hypersurfaces evaluated with around $\sim 10^4$ lattice simulations for varying homogeneous χ_i initial conditions for $\lambda = 10^{-14}$ and $g^2/\lambda = 1$. As expected, $\delta N \ll 10^{-6}$. Similar results are obtained for $g^2/\lambda = 3$.*

Method

In contrast with previous works, to evaluate $\tilde{N}_\chi$ and $\tilde{N}_{\chi\chi}$ and calculate the power spectrum and bispectrum after reheating we work directly with lattice simulations rather than some pre-generated or approximated function $N(\chi)$. To do so we employ a Monte Carlo approach as follows. After fixing the parameters of the massless preheating potential, we calculate the energy scale and the value of ϕ at the time at which χ becomes massive. At this time the value of the χ field is drawn from a Gaussian distribution with mean value $\bar{\chi}$, and variance given by Eq. (7.10). As discussed above the mean value can be treated as a free parameter provided it is much bigger than the variance. We fix initial conditions for our use of non-perturbative δN at this time and begin our HLattice simulations. Hlattice then evolves the background scalar field equations until the end of inflation before beginning a lattice simulation. For the lattice simulation Hlattice takes the average value of the fields in the lattice patch to be given by the background scalar field values at the end of inflation, and the fields are also given an inhomogeneous (over the lattice) component which averages to zero. These inhomogeneous components represent random 'vacuum fluctuations' which are drawn from a Gaussian distribution. The initial field value is the sum of the homogeneous value and the fluctuations at that point. Finally we measure N as described above, and use this to evaluate the quantity

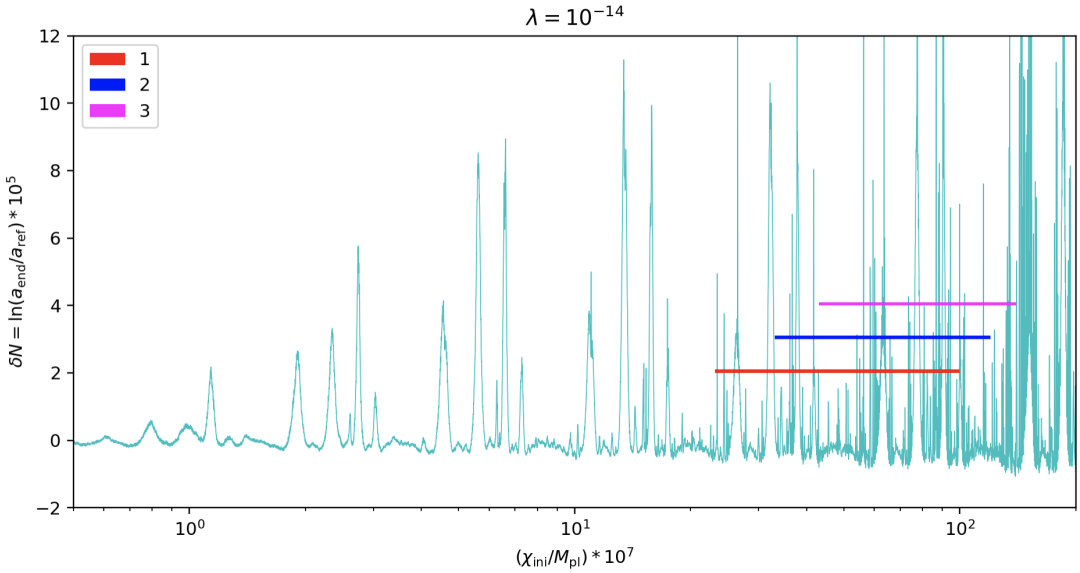

Figure 7.7: *The value of δN for $\lambda = 10^{-14}$, and for different initial field values $\chi_{\rm ini}$. The three coloured lines (red, blue and magenta) spans the range of values that $\chi_{\rm ini}$ takes, i.e., $\bar{\chi}_i \pm 3\sigma$ for each $\bar{\chi}_i$ where $i = 1, 2, 3$. Note that here, our $\chi_{\rm ini}$ is the value the field takes just before it becomes massive.*

inside the angle brackets on the right hand side of Eq. (7.7). By then repeatedly drawing a new value of χ and repeating the procedure we can calculate the averages in Eq. (7.7). The answer should converge as the number of draws increases. We find this does indeed occur with $\mathcal{O}(10^4)$ draws needed, and we use this number to generate our results. When we come to present our results we further use resampling to estimate their error. Due to the large number of runs required, we run our simulations on Queen Mary's Apocrita HPC facility [6]. For our simulations, we choose a resolution of 32^3 with comoving box size $20/H$, and choose the LATTICEEASY discretization scheme within HLattice, which is suitable because we are ignoring metric perturbations (for more details, see [5]).

7.4.4 Results

We now present some results for a number of different parameter choices, presenting both the inflationary contribution and the contribution from preheating under the assumptions made above.

Case 1 : $\lambda = 1.8 \times 10^{-13}$

We begin by taking $\lambda = 1.8 \times 10^{-13}$, with $g^2/\lambda = 2$. This value of λ leads to a contribution to the power spectrum of $\mathcal{P}_{\rm inf} = 2.10 \times 10^{-9}$ from the inflaton field, in agreement with observations. The model is still not a realistic theory of inflation because the predicted tensor-to-scalar ratio is too high to be compatible with observations [48]. There may be ways of curing this, for example by having a non-minimal coupling between the inflaton and spacetime curvature, but we will not attempt to

do that.

Recalling the discussion below Eq. (7.9) and using $H_{\rm ini}^2 \approx \lambda\, \phi_{\rm ini}^4/(12M_{\rm pl}^2)$ implies that $H_{\rm ini} = 3.22 \times 10^{-6} M_{\rm pl}$. From Eq. (7.10), we then find $\langle \delta\chi^2 \rangle = 1.44 \times 10^{-11} M_{\rm pl}^2$, which provides the square of the standard deviation of the Gaussian distribution from which we draw the initial values of χ. For the mean of the distribution, $\bar{\chi}$, we choose $\bar{\chi}_i = (i) \times 10^{-5} M_{\rm pl}$ where i runs from 2 to 9, and run 10^4 simulations for each. Since the data drawn for these values overlap, we are also able to reweight the data to calculate results for mean values in between the initial choices. Finally, by resampling the data using the so-called bootstrap approach, we can determine the approximate one sigma error on our results. The results together with uncertainties are shown in Fig. 7.8. The horizontal line shows the amplitude $\mathcal{P}_{\rm inf}$ of the perturbations generated by the inflaton field. In Fig. 7.7 for illustrative purposes we also show how the $N(\chi)$ function looks for $\lambda = 10^{-14}$. The three coloured lines superimposed on the plot are centred on three of our choices for $\bar{\chi}$, and indicate the 3σ range around this value. Fig. 7.8 indicates the results are highly sensitive to the initial $\bar{\chi}$, and this can be understood by considering Fig. 7.7 which shows that the form of the N functions sampled when drawing χ from a Gaussian distribution changes dramatically depending on the value of $\bar{\chi}$.

As we have described, the method we have outlined relies on an expansion in the probability distribution for field values at separated positions in real space. The criterion we use for the validity of the expansion requires that the leading term in Eq. (7.6) is at least an order of magnitude larger than the sub-leading one. This criterion is scale dependent and gets worse for shorter scales. Here, we consider scales which exit the horizon in the range of 55 to 51 e-folds before the end of inflation. This roughly corresponds to the range of scales observable on the CMB. We find that the expansion is valid for most of the parameter range we study, but breaks down in the regions on the plot where the magnitude of the power spectrum as calculated using the leading term drops towards zero. These regions are also accompanied by large looking error bars on our logarithmic plots. In these regions, to produce more accurate results would require the fully non-perturbative formulae for $\mathcal{P}_\zeta$, as described (and performed) in Ref. [239]. The contribution to the curvature perturbation ζ from preheating is subdominant compared with the inflaton contribution $\mathcal{P}_{\rm inf}$, and therefore not observable in the spectrum. This is similar to the results of [155], though we find that the preheating field's contribution is at least an order of magnitude larger than that calculated there – reinforcing the importance of working directly with lattice simulations. However, because the inflaton contribution is highly Gaussian, it is interesting to see whether the preheating contribution could be observed through its non-Gaussianity. To do this, we calculate the conventional

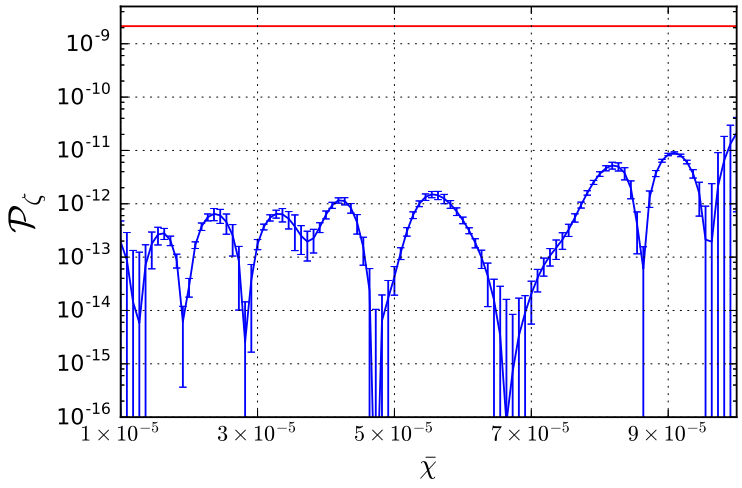

Figure 7.8: *The power spectrum of curvature perturbations produced by preheating, $\mathcal{P}_{\rm pre}$ as a function of $\bar{\chi}$ in Planck units for the case of $\lambda = 1.8\times10^{-13}$. The red line represents the inflationary contribution.*

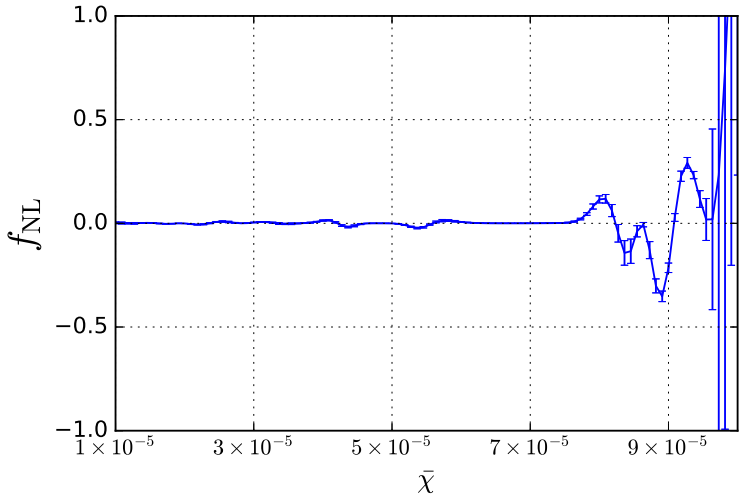

Figure 7.9: *The non-Gaussianity parameter $f_{\rm NL}$ as a function of $\bar{\chi}$ in Planck units for the case of $\lambda = 1.8\times10^{-13}$.*

non-Gaussianity parameter $f_{\rm NL}$ from the expression

$$f_{\rm NL} \approx \frac{\tilde{N}_{\chi\chi}\tilde{N}_\chi\tilde{N}_\chi H_{\rm ini}^4}{(\frac{1}{2\epsilon*}\frac{H_*^2}{M_{\rm pl}^2} + \tilde{N}_\chi\tilde{N}_\chi H_{\rm ini}^2)^2} \times \frac{5}{6}\,, \tag{7.12}$$

where we have assumed that field fluctuations before reheating are Gaussian, and the inflationary contribution to ζ is Gaussian. The results are presented in Fig. 7.9. We can see that although $f_{\rm NL}$ is generally small, it becomes of order unity for certain values of $\bar{\chi}$, making it observable. This suggests that it may also be possible to achieve an observable contribution to $f_{\rm NL}$ in more realistic models.

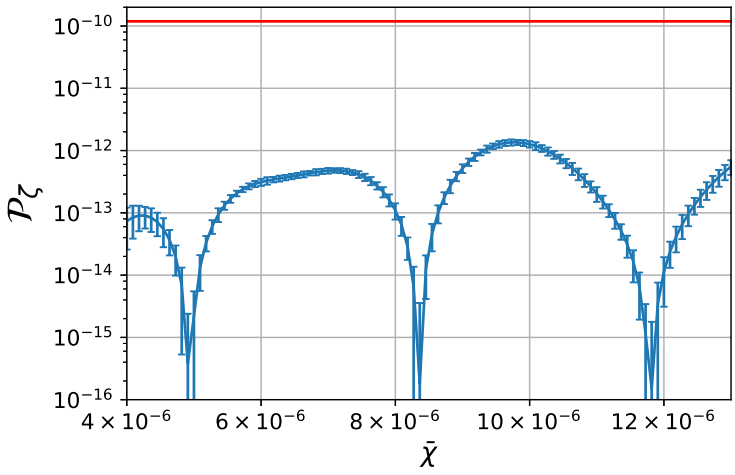

Figure 7.10: *The power spectrum of curvature perturbations produced by preheating, $\mathcal{P}_{\rm pre}$ as a function of $\bar{\chi}$ in Planck units for the case of $\lambda = 10^{-14}$. The red line represents the inflationary contribution.*

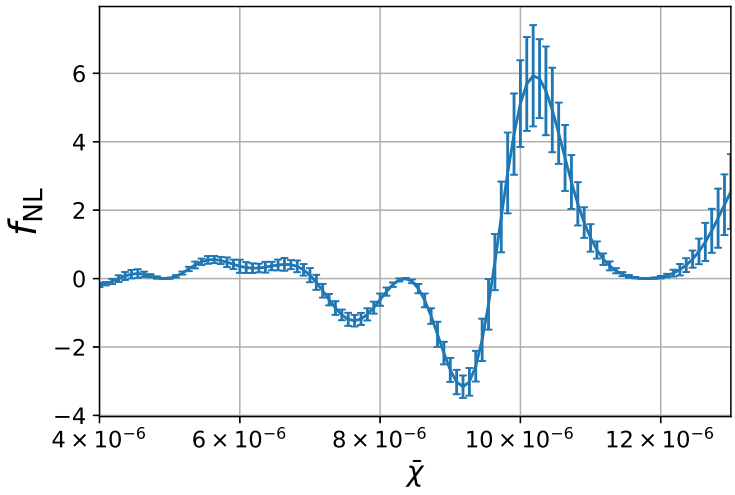

Figure 7.11: *The non-Gaussianity parameter $f_{\rm NL}$ as a function of $\bar{\chi}$ in Planck units for the case of $\lambda = 10^{-14}$.*

Case 2 : $\lambda = 10^{-14}$

As an alternative to Case 1, we also consider cases in which the inflaton contribution is below the observational value amplitude. We calculate the contribution from the preheating field to see whether it can be larger than the inflaton contribution, and whether it could account for the observed perturbation spectrum. We choose $\lambda = 10^{-14}$, again with $g^2/\lambda = 2$. This value of λ leads to an inflaton contribution to the power spectrum of $\mathcal{P}_{\rm inf} = 1.19 \times 10^{-10}$, and Hubble rate $H_{\rm ini} = 7.59 \times 10^{-7} M_{\rm pl}$. The χ field variance is $\langle \delta\chi^2 \rangle = 8.028 \times 10^{-13} M_{\rm pl}^2$. For the mean value $\bar{\chi}$, we choose $\bar{\chi}_i = (i) \times 10^{-6} M_{\rm pl}$ where i runs from 5 to 12, and proceed as in Case 1. As shown in Fig. 7.10, the preheating contribution to ζ is subdominant to that produced by the inflaton field, and therefore this case does not produce sufficient curvature perturbations to be compatible with observations. The non-Gaussianity parameter $f_{\rm NL}$ is larger than in Case 1, as shown in Fig. 7.11.

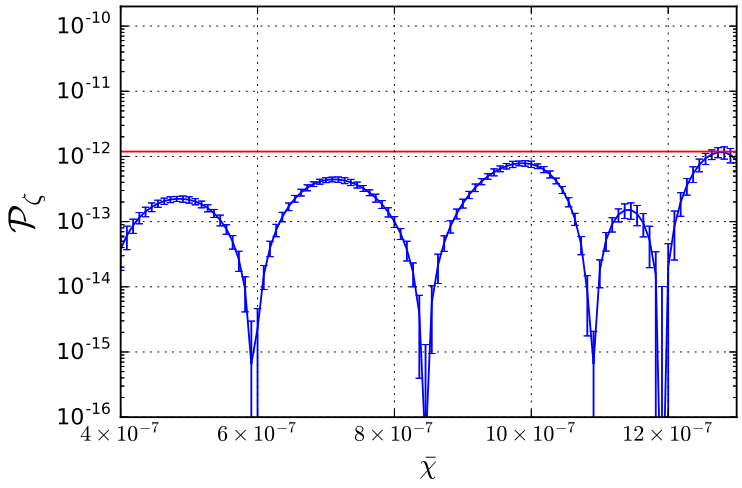

Figure 7.12: *The power spectrum of curvature perturbations produced by preheating, $\mathcal{P}_{\rm pre}$ as a function of $\bar{\chi}$ in Planck units for the case of $\lambda = 10^{-16}$. The red line represents the inflationary contribution.*

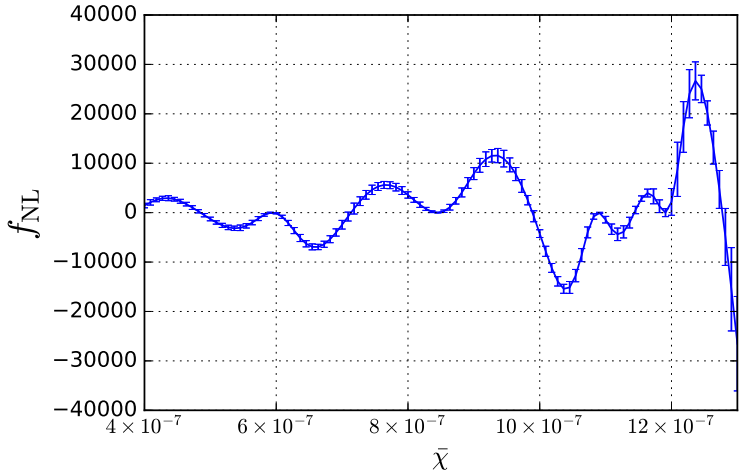

Figure 7.13: *The non-Gaussianity parameter $f_{\rm NL}$ as a function of $\bar{\chi}$ in Planck units for the case of $\lambda = 10^{-16}$.*

Case 3 : $\lambda = 10^{-16}$

For smaller values of λ, $\mathcal{P}_{\rm inf}$ is of course even smaller, and it is expected that $\mathcal{P}_{\rm pre}$ will be too. It is however interesting to explore such cases for the following reason. If the regular δN formalism was applicable one would expect both contributions to ζ to scale in proportion to the energy scale at horizon crossing, but there is no guarantee this will happen in the non-perturbative case. For $\lambda = 10^{-16}$ one finds $\mathcal{P}_{\rm inf} = 1.19 \times 10^{-12}$, $H_{\rm ini} = 7.59 \times 10^{-8} M_{\rm pl}$ and $\langle \delta\chi^2 \rangle = 8.028 \times 10^{-15} M_{\rm pl}^2$. For this case we choose representative examples $\bar{\chi}_i = (i) \times 10^{-7} M_{\rm pl}$ where i runs from 5 to 12, and our results are also presented in Fig. 7.12. Once again $\mathcal{P}_{\rm pre}$ is smaller than $\mathcal{P}_{\rm inf}$, but we see that in this case it is suppressed by a smaller factor. Again for interest we can calculate $f_{\rm NL}$, and present the results in Fig. 7.13. Once again we find that the expansion method fails in the regions where the power spectrum is most suppressed and the error bars appear largest.

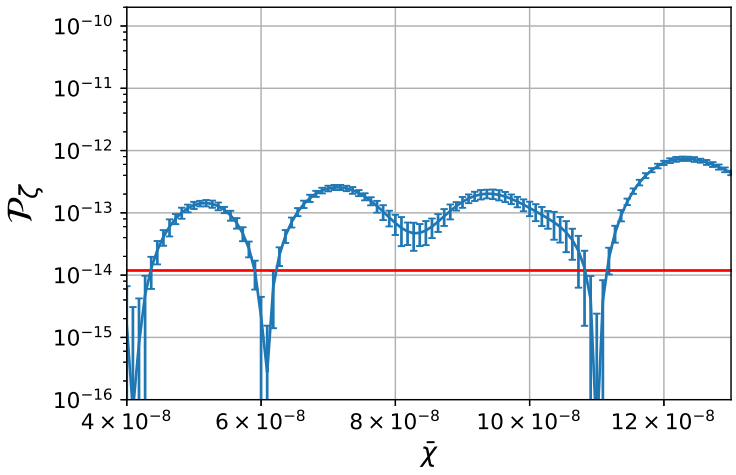

Figure 7.14: *The power spectrum of curvature perturbations produced by preheating, $\mathcal{P}_{\rm pre}$ as a function of $\bar{\chi}$ in Planck units for the case of $\lambda = 10^{-18}$. The red line represents the inflationary contribution.*

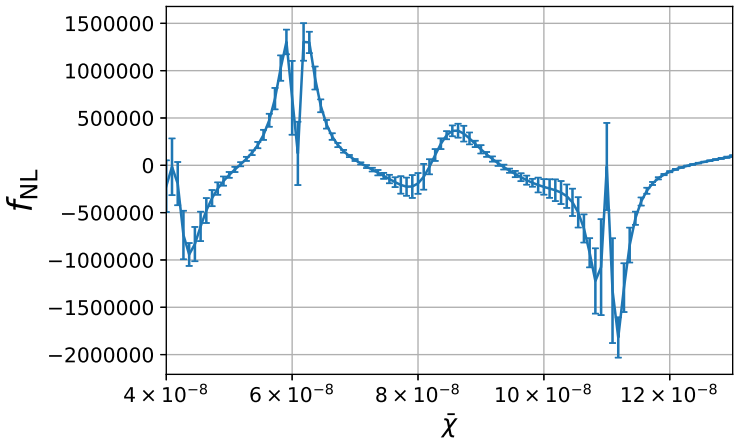

Figure 7.15: *The non-Gaussianity parameter $f_{\rm NL}$ as a function of $\bar{\chi}$ in Planck units for the case of $\lambda = 10^{-18}$.*

Case 4 : $\lambda = 10^{-18}$

Finally we consider $g^2/\lambda = 2$ and $\lambda = 10^{-18}$. In this case we have $\mathcal{P}_{\rm inf} = 1.19 \times 10^{-14}$, $H_{\rm ini} = 7.59 \times 10^{-9} M_{\rm pl}$ and $\langle \delta\chi^2 \rangle = 8.028 \times 10^{-17} M_{\rm pl}^2$. We pick $\bar{\chi}_i = (i) \times 10^{-8} M_{\rm pl}$ where i runs from 5 to 12. Results are shown in Fig. 7.14 and 7.15 for the amplitude of the power spectrum and interestingly we now find that the preheating contribution, $\mathcal{P}_{\rm pre}$, is greater than the inflationary contribution.

7.5 Discussion

It is interesting to note that in all cases the typical value of $\mathcal{P}_{\rm pre}$ is very similar. This can be understood by noting that here we have taken a range of $\bar{\chi}$ that is scaled in proportion to $1/\sqrt{\lambda}$ in each case, as is the square root of the variance of χ at the initial time. Moreover for this particular system, we find that the effect of reducing λ is to shift the pattern of spikes seen in Fig. 7.7 to lower values of χ roughly in proportion to $\sqrt{\lambda}$, but are otherwise very similar. This is a consequence of the conformal invariance of the system. Since all elements of the calculation that go into evaluating Eq. (7.6) scale in the same way, the answer is largely unchanged. This is in stark contrast with the contribution to ζ from the inflation. Nevertheless, the resulting amplitude $\mathcal{P}_{\rm pre}$ is smaller than the observed value, and therefore this mechanism cannot account for the observed curvature perturbations. In cases where the expansion method can be trusted, the spectral index of the preheating contribution is inherited directly from the spectrum of the isocurvature fluctuations at the initial time, but given the lack of compatibility with observations we don't pursue its calculation further.

The main purpose of this work was to show that through lattice simulations it is possible to calculate the power spectrum and bispectrum of the primordial curvature on observational scales when a preheating field plays a significant role. We have demonstrated this explicitly by considering the massless preheating model. We found in all the cases we looked at, that even when the homogeneous mode is within the strong resonance regime (when $g^2/\lambda \approx 2$), the contribution from the preheating field to the power spectrum is much lower than the observed value. We did find however that it could dominate over the inflaton contribution because it remains roughly constant as the energy scale is lowered, in contrast to the contribution from the inflation. This is in stark contrast to the expected behaviour for a contribution produced during inflation. We also found that it is highly sensitive to the mean value of the reheating field, and that it is roughly an order of magnitude larger than that found in earlier analytical studies. These findings indicate the importance of calculating this contribution on a case by case and model by model basis. Finally, we also experimented with reducing the ratio g^2/λ, which gradually moves the homogeneous mode out of the preheating resonance band, and as expected the contribution of the reheating field to the curvature perturbation decreased further in these cases.

For the value of λ for which the inflaton contribution to the curvature perturbation provides the observed amplitude, we found that the preheating field leads to a subdominant contribution to the power spectrum, but can provide the dominant contribution to the bispectrum for some range of initial conditions. It is worth contrasting our study with earlier ones. In contrast to early work [151–154], which we

otherwise follow closely, we do not rely on a Taylor expansion in δN, but instead compute the statistics of the curvature perturbations on large scales using an expansion in powers of the field correlator. Our methods and aims are very similar to those of [155], but that work did not work directly with simulation data, but rather the previously generated function in the work of Ref. [154]. Our study relied on an expansion of the full non-perturbative δN formalism described in Ref. [239], and we found that this was valid except in cases where the leading contribution dropped off significantly. It would be possible to do better using the fully non-perturbative method as described in that work, but this would require us to run many more simulations. Moreover we assumed that the inflaton contribution and the preheating field's contribution to ζ were uncorrelated, and we could treat the preheating field as a light Gaussian spectator right up to the point it becomes massive. In general, one can do better than these approximations either analytically or by using codes such as that described in Ref. [243]. In the present case to go beyond what we have done is not warranted, given that it would be very unlikely to change the incompatibility of the scenario with observations. Nevertheless for more realistic models, for example that of Ref. [153], one might need to turn to these methods to confront models that need to be studied with lattice simulations with observations. The present work, however, establishes the feasibility of doing this.

8 Conclusion and Summary

8.1 Context

Soon after cosmic inflation was introduced as a resolution to the problems that afflicted the hot big bang model of the universe, it was recognised that inflation can also account for the origin of the large-scale structures. The same expansion that precipitates the universe to flatness, makes our observable universe smooth and significantly alleviates the exotic-relic problem, also stretches the microscopic quantum fluctuations during inflation to macroscopic sizes, subsequently generating the small perturbations in the density at the origin of the CMB temperature fluctuations. CMB and LSS observations, therefore, creates an opportunity to put the theory of inflation to the test via the scientific method. Aside from motivational reasons, an inflationary model must be consistent with observational data to survive in the increasingly smaller parameter space owing to better experiments over time. Computing observables of an inflationary model is non-trivial and cosmologists pick the most pragmatic tool from the set of tools that is at their disposal. As we have seen in Chapter 3, the *in - in* formalism is a technique used to evaluate the statistics of the primordial curvature perturbation (the quantity that can be related to the CMB fluctuations) around the time of horizon exit. In models where ζ is not necessarily conserved, one has to also compute its non-linear evolution until the time of horizon re-entry. One such procedure is the δN formalism and we gave a short review in Chapter 4.

8.2 Research

In this thesis, we then highlighted the need for new methods by underlining the drawbacks of this technique, namely, that the assumption that we have to make for it to work might not hold in some models of inflation. Standard δN assumes that the N function is smooth and that only the first few Taylor coefficients are enough to give an accurate answer. In Chapter 5, we go around this problem by falling back to the definition of the ensemble average and instead of making an expansion in N, we make an expansion in the joint probability distribution that appears in the definition of the ensemble average. We choose to call this formalism the 'non-perturbative δN formalism'. Our main results are in § 5.2.3. The next natural step,

of course, was to juxtapose this method to the standard one. We tested it with a pre-generated $N(\chi)$ from Ref. [153] where resonant curvaton decay was studied, using a fitting function and found that the method is a noticeable improvement on the standard one. We also explored the conditions under which the method might fail. The form of our expressions makes it such that they are particularly adapted to settings where it is much more preferable to work with the raw data itself and perform calculations via repeated random sampling, i.e., using the Monte Carlo method. The massless preheating model is the ideal testing ground for our purposes since the $N(\chi)$ function obtained from lattice simulations is detailed, spiky and far from smooth. After a detailed review of reheating and preheating in Chapter 6, we ran our own lattice simulations on a cluster and used that data in combination with the non-perturbative δN in Chapter 7. By choosing to work with massless preheating, we were able to compare our results to the work of Suyama and Yokoyama who described the peaks as a sum of normal distributions and ignored the small peaks. Our results show that preheating can be the dominant contribution to the observed scalar power spectrum in the case where $\lambda = 10^{-18}$ but this contribution is not enough to explain the observed amplitude of the scalar power spectrum.

The dynamics during the reheating phase and their effects on observables are not well-understood. That lattice simulations will remain the primary tool to study these non-linear effects for at least the near future and probably even the far future is a good guess. This gives us confidence that our approach of adapting well-established techniques to the features of numerical simulations is a step in the right direction. The post-Planck mission era necessitates new ways to distinguish between competing models of inflation keeping in mind the next-generation experiments. Short of probing energy scales far exceeding the TeV scale with particle accelerators, the primordial statistics of ζ is the only way to probe physics at energy scales during or after inflation. Methods such as those developed in this thesis are therefore essential to understand the consequences of different models of inflation and reheating and to learn aboout physics at these high energy scales.

Bibliography

[1] Dvali G.R., Melfo A., and Senjanovic G., "Is There a monopole problem?," *Phys. Rev. Lett.* **75** (1995) 4559–4562, arXiv:hep-ph/9507230 [hep-ph].

[2] Guth A.H., "The Inflationary Universe: A Possible Solution to the Horizon and Flatness Problems," *Phys.Rev.* **D23** (1981) 347–356.

[3] Starobinsky A.A., "A New Type of Isotropic Cosmological Models Without Singularity," *Phys.Lett.* **B91** (1980) 99–102.

[4] Sato K., "First Order Phase Transition of a Vacuum and Expansion of the Universe," *Mon.Not.Roy.Astron.Soc.* **195** (1981) 467–479.

[5] Huang Z., "The Art of Lattice and Gravity Waves from Preheating," *Phys. Rev.* **D83** (2011) 123509, arXiv:1102.0227 [astro-ph.CO].

[6] King T., Butcher S., and Zalewski L., *Apocrita - High Performance Computing Cluster for Queen Mary University of London*, Mar., 2017. https://doi.org/10.5281/zenodo.438045.

[7] Liddle A., *An introduction to modern cosmology; 2nd ed.* Wiley, Chichester, 2003. https://cds.cern.ch/record/1010476.

[8] Penzias A. and Wilson R., "A measurement of excess antenna temperature at 4800 mc/s,".

[9] Goobar A. and Leibundgut B., "Supernova cosmology: legacy and future," *Ann. Rev. Nucl. Part. Sci.* **61** (2011) 251–279, arXiv:1102.1431 [astro-ph.CO].

[10] Supernova Search Team Collaboration, Riess A.G. *et al.*, "Observational evidence from supernovae for an accelerating universe and a cosmological constant," *Astron. J.* **116** (1998) 1009–1038, arXiv:astro-ph/9805201 [astro-ph].

[11] Supernova Cosmology Project Collaboration, Perlmutter S. *et al.*, "Measurements of Omega and Lambda from 42 high redshift supernovae," *Astrophys. J.* **517** (1999) 565–586, arXiv:astro-ph/9812133 [astro-ph].

[12] SPT Collaboration, Aylor K. *et al.*, "A Comparison of Cosmological Parameters Determined from CMB Temperature Power Spectra from the South Pole Telescope and the Planck Satellite," *Astrophys. J.* **850** (2017) no. 1, 101, arXiv:1706.10286 [astro-ph.CO].

[13] Simard G. *et al.*, "Constraints on Cosmological Parameters from the Angular Power Spectrum of a Combined 2500 deg^2 SPT-SZ and Planck Gravitational Lensing Map," *Astrophys. J.* **860** (2018) no. 2, 137, arXiv:1712.07541 [astro-ph.CO].

[14] Omori Y. *et al.*, "A 2500 deg^2 CMB Lensing Map from Combined South Pole Telescope and Planck Data," *Astrophys. J.* **849** (2017) no. 2, 124, arXiv:1705.00743 [astro-ph.CO].

[15] Planck Collaboration, Ade P.A.R. *et al.*, "Planck 2015 results. XIII. Cosmological parameters," *Astron. Astrophys.* **594** (2016) A13, arXiv:1502.01589 [astro-ph.CO].

[16] Will C., *Theory and Experiment in Gravitational Physics*. Cambridge University Press, 1993. https://books.google.co.uk/books?id=BhnUITA7sDIC.

[17] Clifton T., Ferreira P.G., Padilla A., and Skordis C., "Modified Gravity and Cosmology," *Phys. Rept.* **513** (2012) 1–189, arXiv:1106.2476 [astro-ph.CO].

[18] Planck Collaboration, Aghanim N. *et al.*, "Planck 2018 results. VI. Cosmological parameters," arXiv:1807.06209 [astro-ph.CO].

[19] Clarkson C., Cortes M., and Bassett B.A., "Dynamical Dark Energy or Simply Cosmic Curvature?," *JCAP* **0708** (2007) 011, arXiv:astro-ph/0702670 [ASTRO-PH].

[20] Witzemann A., Bull P., Clarkson C., Santos M.G., Spinelli M., and Weltman A., "Model-independent curvature determination with 21 cm intensity mapping experiments," *Mon. Not. Roy. Astron. Soc.* **477** (2018) no. 1, L122–L127, arXiv:1711.02179 [astro-ph.CO].

[21] Battye R.A., Charnock T., and Moss A., "Tension between the power spectrum of density perturbations measured on large and small scales," *Phys. Rev.* **D91** (2015) no. 10, 103508, arXiv:1409.2769 [astro-ph.CO].

[22] Charnock T., Battye R.A., and Moss A., "Planck data versus large scale structure," *Phys. Rev.* **D95** (2017) no. 12, 123535, arXiv:1703.05959 [astro-ph.CO].

[23] Amanullah R. *et al.*, "Spectra and Light Curves of Six Type Ia Supernovae at 0.511 ¡ z ¡ 1.12 and the Union2 Compilation," *Astrophys. J.* **716** (2010) 712–738, arXiv:1004.1711 [astro-ph.CO].

[24] SDSS Collaboration, Percival W.J. *et al.*, "Baryon Acoustic Oscillations in the Sloan Digital Sky Survey Data Release 7 Galaxy Sample," *Mon. Not. Roy. Astron. Soc.* **401** (2010) 2148–2168, arXiv:0907.1660 [astro-ph.CO].

[25] Komatsu E., Smith K.M., Dunkley J., Bennett C.L., Gold B., Hinshaw G., Jarosik N., Larson D., Nolta M.R., Page L., Spergel D.N., Halpern M., Hill R.S., Kogut A., Limon M., Meyer S.S., Odegard N., Tucker G.S., Weiland J.L., Wollack E., and Wright E.L., "Seven-year wilkinson microwave anisotropy probe (wmap) observations: Cosmological interpretation," *The Astrophysical Journal Supplement Series* **192** (2011) no. 2, 18. http://stacks.iop.org/0067-0049/192/i=2/a=18.

[26] Alpher R.A., Bethe H., and Gamow G., "The origin of chemical elements," *Phys. Rev.* **73** (1948) 803–804.

[27] Steigman G., "Primordial Nucleosynthesis in the Precision Cosmology Era," *Ann. Rev. Nucl. Part. Sci.* **57** (2007) 463–491, arXiv:0712.1100 [astro-ph].

[28] Bertschinger E., "Simulations of structure formation in the universe," *Ann. Rev. Astron. Astrophys.* **36** (1998) 599–654.

[29] Bertschinger E., "Cosmological perturbation theory and structure formation," in *Cosmology 2000: Proceedings, Conference, Lisbon, Portugal, 12-15 Jul 2000*, pp. 1–25. 2001. arXiv:astro-ph/0101009 [astro-ph].

[30] Peebles P.J.E., *The large-scale structure of the universe*. 1980.

[31] Efstathiou G., "Large-scale structure in the universe," *Physica Scripta* **1991** (1991) no. T36, 88. http://stacks.iop.org/1402-4896/1991/i=T36/a=009.

[32] Smoot G.F., "COBE observations and results," *AIP Conf. Proc.* **476** (1999) no. 1, 1–10, arXiv:astro-ph/9902027 [astro-ph].

[33] Lesgourgues J., *Inflationary Cosmology*. Troisième cycle de la physique en Suisse romande. vente: M.D. Reymond, Ecole polytechnique fédérale de Lausanne, Bâtiment des sciences physiques, 2006. https://books.google.co.uk/books?id=6EXtSAAACAAJ.

[34] Liddle A.R. and Lyth D.H., *Cosmological Inflation and Large-Scale Structure*. June, 2000.

[35] Planck Collaboration, Ade P.A.R. *et al.*, "Planck 2013 results. XVI. Cosmological parameters," *Astron. Astrophys.* **571** (2014) A16, arXiv:1303.5076 [astro-ph.CO].

[36] Mukhanov V., *Physical Foundations of Cosmology*. Cambridge Univ. Press, Cambridge, 2005. https://cds.cern.ch/record/991646.

[37] Peter P. and Uzan J.P., *Primordial cosmology*. Oxford Graduate Texts. Oxford Univ. Press, Oxford, 2009. https://cds.cern.ch/record/1208401.

[38] Bassett B.A., Tsujikawa S., and Wands D., "Inflation dynamics and reheating," *Rev. Mod. Phys.* **78** (2006) 537–589, arXiv:astro-ph/0507632 [astro-ph].

[39] Lyth D.H. and Liddle A.R., "The primordial density perturbation: Cosmology, inflation and the origin of structure,".

[40] Planck Collaboration, Ade P.A.R. *et al.*, "Planck 2015 results. XVI. Isotropy and statistics of the CMB," *Astron. Astrophys.* **594** (2016) A16, arXiv:1506.07135 [astro-ph.CO].

[41] 't Hooft G., "Magnetic Monopoles in Unified Gauge Theories," *Nucl. Phys.* **B79** (1974) 276–284. [,291(1974)].

[42] Polyakov A.M., "Particle Spectrum in the Quantum Field Theory," *JETP Lett.* **20** (1974) 194–195. [,300(1974)].

[43] WMAP Collaboration Collaboration, Peiris H. *et al.*, "First year Wilkinson Microwave Anisotropy Probe (WMAP) observations: Implications for inflation," *Astrophys.J.Suppl.* **148** (2003) 213, arXiv:astro-ph/0302225 [astro-ph].

[44] WMAP Collaboration Collaboration, Spergel D. *et al.*, "First year Wilkinson Microwave Anisotropy Probe (WMAP) observations: Determination of cosmological parameters," *Astrophys.J.Suppl.* **148** (2003) 175–194, arXiv:astro-ph/0302209 [astro-ph].

[45] SDSS Collaboration, Tegmark M. *et al.*, "Cosmological parameters from SDSS and WMAP," *Phys. Rev.* **D69** (2004) 103501, arXiv:astro-ph/0310723 [astro-ph].

[46] SDSS Collaboration, Tegmark M. *et al.*, "The 3-D power spectrum of galaxies from the SDSS," *Astrophys. J.* **606** (2004) 702–740, arXiv:astro-ph/0310725 [astro-ph].

[47] 2dFGRS Collaboration, Percival W.J. *et al.*, "The 2dF Galaxy Redshift Survey: The Power spectrum and the matter content of the Universe," *Mon. Not. Roy. Astron. Soc.* **327** (2001) 1297, arXiv:astro-ph/0105252 [astro-ph].

[48] Planck Collaboration, Akrami Y. *et al.*, "Planck 2018 results. X. Constraints on inflation," arXiv:1807.06211 [astro-ph.CO].

[49] Baumann D., "Inflation," in *Physics of the large and the small, TASI 09, proceedings of the Theoretical Advanced Study Institute in Elementary Particle Physics, Boulder, Colorado, USA, 1-26 June 2009*, pp. 523–686. 2011. arXiv:0907.5424 [hep-th].

[50] ATLAS Collaboration, Aad G. *et al.*, "Observation of a new particle in the search for the Standard Model Higgs boson with the ATLAS detector at the LHC," *Phys. Lett.* **B716** (2012) 1–29, arXiv:1207.7214 [hep-ex].

[51] Lyth D.H. and Riotto A., "Particle physics models of inflation and the cosmological density perturbation," *Phys.Rept.* **314** (1999) 1–146, arXiv:hep-ph/9807278 [hep-ph].

[52] Lidsey J.E., Wands D., and Copeland E.J., "Superstring cosmology," *Phys. Rept.* **337** (2000) 343–492, arXiv:hep-th/9909061 [hep-th].

[53] Bezrukov F.L. and Shaposhnikov M., "The Standard Model Higgs boson as the inflaton," *Phys. Lett.* **B659** (2008) 703–706, arXiv:0710.3755 [hep-th].

[54] Rubio J., "Higgs inflation," arXiv:1807.02376 [hep-ph].

[55] Calmet X., Kuntz I., and Moss I.G., "Non-Minimal Coupling of the Higgs Boson to Curvature in an Inflationary Universe," *Found. Phys.* **48** (2018) no. 1, 110–120, arXiv:1701.02140 [hep-ph].

[56] Guth A.H., "Inflationary universe: A possible solution to the horizon and flatness problems," *Phys. Rev. D* **23** (Jan, 1981) 347–356. https://link.aps.org/doi/10.1103/PhysRevD.23.347.

[57] Watson S., "An Exposition on inflationary cosmology," arXiv:astro-ph/0005003 [astro-ph].

[58] Linde A.D., "A New Inflationary Universe Scenario: A Possible Solution of the Horizon, Flatness, Homogeneity, Isotropy and Primordial Monopole Problems," *Phys.Lett.* **B108** (1982) 389–393.

[59] Albrecht A. and Steinhardt P.J., "Cosmology for Grand Unified Theories with Radiatively Induced Symmetry Breaking," *Phys.Rev.Lett.* **48** (1982) 1220–1223.

[60] Baumann D. and Peiris H.V., "Cosmological Inflation: Theory and Observations," *Adv. Sci. Lett.* **2** (2009) 105–120, arXiv:0810.3022 [astro-ph].

[61] Malik K.A. and Wands D., "Cosmological perturbations," *Phys. Rept.* **475** (2009) 1–51, arXiv:0809.4944 [astro-ph].

[62] Malik K.A. and Matravers D.R., "A Concise Introduction to Perturbation Theory in Cosmology," *Class.Quant.Grav.* **25** (2008) 193001, arXiv:0804.3276 [astro-ph].

[63] Mukhanov V., Feldman H., and Brandenberger R., "Theory of cosmological perturbations," *Physics Reports* **215** (1992) no. 5, 203 – 333. http://www.sciencedirect.com/science/article/pii/037015739290044Z.

[64] Lidsey J.E., Liddle A.R., Kolb E.W., Copeland E.J., Barreiro T., *et al.*, "Reconstructing the inflation potential : An overview," *Rev.Mod.Phys.* **69** (1997) 373–410, arXiv:astro-ph/9508078 [astro-ph].

[65] Misner C.W. T.K. and J. W., *Gravitation*. Jan., 1973.

[66] Malik K.A. and Matravers D.R., "Comments on gauge-invariance in cosmology," *Gen. Rel. Grav.* **45** (2013) 1989–2001, arXiv:1206.1478 [astro-ph.CO].

[67] Arnowitt R.L., Deser S., and Misner C.W., "The Dynamics of general relativity," *Gen. Rel. Grav.* **40** (2008) 1997–2027, arXiv:gr-qc/0405109 [gr-qc].

[68] Bardeen J.M., "Gauge Invariant Cosmological Perturbations," *Phys. Rev.* **D22** (1980) 1882–1905.

[69] Acquaviva V., Bartolo N., Matarrese S., and Riotto A., "Second order cosmological perturbations from inflation," *Nucl. Phys.* **B667** (2003) 119–148, arXiv:astro-ph/0209156 [astro-ph].

[70] Maldacena J.M., "Non-Gaussian features of primordial fluctuations in single field inflationary models," *JHEP* **05** (2003) 013, arXiv:astro-ph/0210603 [astro-ph].

[71] Fergusson J.R. and Shellard E.P.S., "The shape of primordial non-Gaussianity and the CMB bispectrum," *Phys. Rev.* **D80** (2009) 043510, arXiv:0812.3413 [astro-ph].

[72] Seery D. and Lidsey J.E., "Primordial non-Gaussianities from multiple-field inflation," *JCAP* **0509** (2005) .

[73] Hotchkiss S. and Sarkar S., "Non-Gaussianity from violation of slow-roll in multiple inflation," *JCAP* **1005** (2010) 024, arXiv:0910.3373 [astro-ph.CO].

[74] Noller J. and Magueijo J., "Non-Gaussianity in single field models without slow-roll," *Phys.Rev.* **D83** (2011) 103511, arXiv:1102.0275 [astro-ph.CO].

[75] Dodelson S., *Modern cosmology*. 2003.

[76] Kovac J., Leitch E.M., Pryke C., Carlstrom J.E., Halverson N.W., and Holzapfel W.L., "Detection of polarization in the cosmic microwave background using DASI," *Nature* **420** (2002) 772–787, arXiv:astro-ph/0209478 [astro-ph].

[77] Creminelli P. and Senatore L., "A Smooth bouncing cosmology with scale invariant spectrum," *JCAP* **0711** (2007) 010, arXiv:hep-th/0702165 [hep-th].

[78] Koyama K., Mizuno S., Vernizzi F., and Wands D., "Non-Gaussianities from ekpyrotic collapse with multiple fields," *JCAP* **0711** (2007) 024, arXiv:0708.4321 [hep-th].

[79] Buchbinder E.I., Khoury J., and Ovrut B.A., "Non-Gaussianities in new ekpyrotic cosmology," *Phys. Rev. Lett.* **100** (2008) 171302, arXiv:0710.5172 [hep-th].

[80] Lehners J.L. and Steinhardt P.J., "Non-Gaussian density fluctuations from entropically generated curvature perturbations in Ekpyrotic models," *Phys. Rev.* **D77** (2008) 063533, arXiv:0712.3779 [hep-th]. [Erratum: Phys. Rev.D79,129903(2009)].

[81] Lehners J.L. and Steinhardt P.J., "Intuitive understanding of non-gaussianity in ekpyrotic and cyclic models," *Phys. Rev.* **D78** (2008) 023506, arXiv:0804.1293 [hep-th]. [Erratum: Phys. Rev.D79,129902(2009)].

[82] Koyama K., Mizuno S., and Wands D., "Curvature perturbations from ekpyrotic collapse with multiple fields," *Class. Quant. Grav.* **24** (2007) 3919–3932, arXiv:0704.1152 [hep-th].

[83] Koyama K. and Wands D., "Ekpyrotic collapse with multiple fields," *JCAP* **0704** (2007) 008, arXiv:hep-th/0703040 [HEP-TH].

[84] Zaldarriaga M., "Lensing of the CMB: Non-Gaussian aspects," *Phys. Rev.* **D62** (2000) 063510, arXiv:astro-ph/9910498 [astro-ph].

[85] Lewis A. and Pratten G., "Effect of lensing non-Gaussianity on the CMB power spectra," *JCAP* **1612** (2016) no. 12, 003, arXiv:1608.01263 [astro-ph.CO].

[86] Takada M., "Lensing - induced non-Gaussian signatures in the cosmic microwave background," *Astrophys. J.* **558** (2001) 29–41, arXiv:astro-ph/0101449 [astro-ph].

[87] Jaffe A.H. *et al.*, "Determining foreground contamination in CMB observations: Diffuse galactic emission in the MAXIMA-I field," *Astrophys. J.* **615** (2004) 55–62, arXiv:astro-ph/0301077 [astro-ph].

[88] Then H., "Foreground contamination of the WMAP CMB maps from the perspective of the matched circle test," *Mon. Not. Roy. Astron. Soc.* **373** (2006) 139–145, arXiv:astro-ph/0511726 [astro-ph].

[89] Baumann D., "Lecture notes 'primordial non-gaussianity '." http://www.damtp.cam.ac.uk/user/db275/TEACHING/INFLATION/NG.pdf.

[90] Komatsu E. and Spergel D.N., "Acoustic signatures in the primary microwave background bispectrum," *Phys.Rev.* **D63** (2001) 063002, arXiv:astro-ph/0005036 [astro-ph].

[91] Linde A.D. and Mukhanov V.F., "Nongaussian isocurvature perturbations from inflation," *Phys. Rev.* **D56** (1997) R535–R539, arXiv:astro-ph/9610219 [astro-ph].

[92] Lyth D.H., Ungarelli C., and Wands D., "The Primordial density perturbation in the curvaton scenario," *Phys. Rev.* **D67** (2003) 023503, arXiv:astro-ph/0208055 [astro-ph].

[93] Dvali G., Gruzinov A., and Zaldarriaga M., "A new mechanism for generating density perturbations from inflation," *Phys.Rev.* **D69** (2004) 023505, arXiv:astro-ph/0303591 [astro-ph].

[94] Kofman L., "Probing string theory with modulated cosmological fluctuations," arXiv:astro-ph/0303614 [astro-ph].

[95] Chen X., Huang M.x., Kachru S., and Shiu G., "Observational signatures and non-Gaussianities of general single field inflation," *JCAP* **0701** (2007) 002, arXiv:hep-th/0605045 [hep-th].

[96] Silverstein E. and Tong D., "Scalar speed limits and cosmology: Acceleration from D-cceleration," *Phys.Rev.* **D70** (2004) 103505, arXiv:hep-th/0310221 [hep-th].

[97] Holman R. and Tolley A.J., "Enhanced Non-Gaussianity from Excited Initial States," *JCAP* **0805** (2008) 001, arXiv:0710.1302 [hep-th].

[98] Seery D. and Lidsey J.E., "Primordial non-Gaussianities in single field inflation," *JCAP* **0506** (2005) 003, arXiv:astro-ph/0503692 [astro-ph].

[99] Weinberg S., "Quantum contributions to cosmological correlations," *Phys. Rev.* **D72** (2005) 043514, arXiv:hep-th/0506236 [hep-th].

[100] Chen X., "Primordial Non-Gaussianities from Inflation Models," *Adv. Astron.* **2010** (2010) 638979, arXiv:1002.1416 [astro-ph.CO].

[101] Koyama K., "Non-Gaussianity of quantum fields during inflation," *Class. Quant. Grav.* **27** (2010) 124001, arXiv:1002.0600 [hep-th].

[102] Creminelli P. and Zaldarriaga M., "Single field consistency relation for the 3-point function," *JCAP* **0410** (2004) 006, arXiv:astro-ph/0407059 [astro-ph].

[103] Creminelli P., D'Amico G., Musso M., and Norena J., "The (not so) squeezed limit of the primordial 3-point function," *JCAP* **1111** (2011) 038, arXiv:1106.1462 [astro-ph.CO].

[104] Cheung C., Fitzpatrick A.L., Kaplan J., and Senatore L., "On the consistency relation of the 3-point function in single field inflation," *JCAP* **0802** (2008) 021, arXiv:0709.0295 [hep-th].

[105] Reichborn-Kjennerud B. *et al.*, "EBEX: A balloon-borne CMB polarization experiment," *Proc. SPIE Int. Soc. Opt. Eng.* **7741** (2010) 77411C, arXiv:1007.3672 [astro-ph.CO].

[106] BICEP3 Collaboration, Ahmed Z. *et al.*, "BICEP3: a 95GHz refracting telescope for degree-scale CMB polarization," *Proc. SPIE Int. Soc. Opt. Eng.* **9153** (2014) 91531N, arXiv:1407.5928 [astro-ph.IM].

[107] Essinger Hileman T. *et al.*, "The Atacama B Mode Search: CMB Polarimetry with Transition Edge Sensor Bolometers," *AIP Conf. Proc.* **1185** (2009) no. 1, 494, arXiv:1008.3915 [astro-ph.IM].

[108] Fraisse A.A. *et al.*, "SPIDER: Probing the Early Universe with a Suborbital Polarimeter," *JCAP* **1304** (2013) 047, arXiv:1106.3087 [astro-ph.CO].

[109] Eimer J.R., Bennett C.L., Chuss D.T., Marriage T.A., Wollack E.J., and Zeng L., "The Cosmology Large Angular Scale Surveyor (CLASS): 40 GHz optical design," *Proc. SPIE Int. Soc. Opt. Eng.* **8452** (2012) 845220, arXiv:1211.0041 [astro-ph.IM].

[110] Austermann J.E. *et al.*, "SPTpol: an instrument for CMB polarization measurements with the South Pole Telescope," *Proc. SPIE Int. Soc. Opt. Eng.* **8452** (2012) 84521E, arXiv:1210.4970 [astro-ph.IM].

[111] Kermish Z. *et al.*, "The POLARBEAR Experiment," *Proc. SPIE Int. Soc. Opt. Eng.* **8452** (2012) 1C, arXiv:1210.7768 [astro-ph.IM].

[112] Niemack M.D. *et al.*, "ACTPol: a polarization-sensitive receiverfor the Atacama Cosmology Telescope," *Proc. SPIE Int. Soc. Opt. Eng.* **7741** (2010) 77411S, arXiv:1006.5049 [astro-ph.IM].

[113] Planck Collaboration, Ade P.A.R. *et al.*, "Planck 2015 results. XVII. Constraints on primordial non-Gaussianity," *Astron. Astrophys.* **594** (2016) A17, arXiv:1502.01592 [astro-ph.CO].

[114] Planck Collaboration, Ade P.A.R. *et al.*, "Planck 2013 Results. XXIV. Constraints on primordial non-Gaussianity," *Astron. Astrophys.* **571** (2014) A24, arXiv:1303.5084 [astro-ph.CO].

[115] Fergusson J., Regan D., and Shellard E., "Optimal Trispectrum Estimators and WMAP Constraints," arXiv:1012.6039 [astro-ph.CO].

[116] Mulryne D.J., "PyTransport: A Python package for the calculation of inflationary correlation functions," arXiv:1609.00381 [astro-ph.CO].

[117] Seery D., "CppTransport: a platform to automate calculation of inflationary correlation functions," arXiv:1609.00380 [astro-ph.CO].

[118] Mulryne D.J., Seery D., and Wesley D., "Moment transport equations for non-Gaussianity," *JCAP* **1001** (2010) 024, arXiv:0909.2256 [astro-ph.CO].

[119] Mulryne D.J., "Transporting non-Gaussianity from sub to super-horizon scales," *JCAP* **1309** (2013) 010, arXiv:1302.3842 [astro-ph.CO].

[120] Sasaki M. and Stewart E.D., "A General analytic formula for the spectral index of the density perturbations produced during inflation," *Prog.Theor.Phys.* **95** (1996) 71–78, arXiv:astro-ph/9507001.

[121] Tanaka T., Suyama T., and Yokoyama S., "Use of delta N formalism - Difficulties in generating large local-type non-Gaussianity during inflation -," *Class. Quant. Grav.* **27** (2010) 124003, arXiv:1003.5057 [astro-ph.CO].

[122] Bardeen J.M., Steinhardt P.J., and Turner M.S., "Spontaneous creation of almost scale-free density perturbations in an inflationary universe," *Phys. Rev. D* **28** (Aug, 1983) 679–693. https://link.aps.org/doi/10.1103/PhysRevD.28.679.

[123] Lyth D.H., "Large Scale Energy Density Perturbations and Inflation," *Phys.Rev.* **D31** (1985) 1792–1798.

[124] Rigopoulos G. and Shellard E., "The separate universe approach and the evolution of nonlinear superhorizon cosmological perturbations," *Phys.Rev.* **D68** (2003) 123518, arXiv:astro-ph/0306620 [astro-ph].

[125] Lyth D.H., Malik K.A., and Sasaki M., "A General proof of the conservation of the curvature perturbation," *JCAP* **0505** (2005) 004, arXiv:astro-ph/0411220 [astro-ph].

[126] Weinberg S., "Must cosmological perturbations remain non-adiabatic after multi-field inflation?," *Phys.Rev.* **D70** (2004) 083522, arXiv:astro-ph/0405397 [astro-ph].

[127] Langlois D. and Vernizzi F., "Evolution of non-linear cosmological perturbations," *Phys.Rev.Lett.* **95** (2005) 091303, arXiv:astro-ph/0503416 [astro-ph].

[128] Langlois D. and Vernizzi F., "Conserved non-linear quantities in cosmology," *Phys.Rev.* **D72** (2005) 103501, arXiv:astro-ph/0509078 [astro-ph].

[129] Weinberg S., "A Tree Theorem for Inflation," *Phys. Rev.* **D78** (2008) 063534, arXiv:0805.3781 [hep-th].

[130] Zaldarriaga M., "Non-Gaussianities in models with a varying inflaton decay rate," *Phys.Rev.* **D69** (2004) 043508, arXiv:astro-ph/0306006 [astro-ph].

[131] Seery D., "Infrared effects in inflationary correlation functions," *Class.Quant.Grav.* **27** (2010) 124005, arXiv:1005.1649 [astro-ph.CO].

[132] Seery D., "One-loop corrections to the curvature perturbation from inflation," *JCAP* **0802** (2008) 006, arXiv:0707.3378 [astro-ph].

[133] Salopek D., Bond J., and Bardeen J.M., "Designing Density Fluctuation Spectra in Inflation," *Phys.Rev.* **D40** (1989) 1753.

[134] Polarski D. and Starobinsky A.A., "Isocurvature perturbations in multiple inflationary models," *Phys.Rev.* **D50** (1994) 6123–6129, arXiv:astro-ph/9404061 [astro-ph].

[135] García-Bellido J. and Wands D., "Metric perturbations in two field inflation," *Phys.Rev.* **D53** (1996) 5437–5445, arXiv:astro-ph/9511029 [astro-ph].

[136] Salopek D., "Characteristics of cosmic time," *Phys.Rev.* **D52** (1995) 5563–5575, arXiv:astro-ph/9506146 [astro-ph].

[137] Langlois D., "Correlated adiabatic and isocurvature perturbations from double inflation," *Phys.Rev.* **D59** (1999) 123512, arXiv:astro-ph/9906080 [astro-ph].

[138] Gordon C., Wands D., Bassett B.A., and Maartens R., "Adiabatic and entropy perturbations from inflation," *Phys.Rev.* **D63** (2001) 023506, arXiv:astro-ph/0009131 [astro-ph].

[139] Langlois D. and Vernizzi F., "A geometrical approach to nonlinear perturbations in relativistic cosmology," *Class.Quant.Grav.* **27** (2010) 124007, arXiv:1003.3270 [astro-ph.CO].

[140] Mulryne D.J., Seery D., and Wesley D., "Moment transport equations for the primordial curvature perturbation," *JCAP* **1104** (2011) 030, arXiv:1008.3159 [astro-ph.CO].

[141] Dias M. and Seery D., "Transport equations for the inflationary spectral index," *Phys.Rev.* **D85** (2012) 043519, arXiv:1111.6544 [astro-ph.CO].

[142] Seery D., Mulryne D.J., Frazer J., and Ribeiro R.H., "Inflationary perturbation theory is geometrical optics in phase space," *JCAP* **1209** (2012) 010, arXiv:1203.2635 [astro-ph.CO].

[143] Stewart E.D. and Lyth D.H., "A More accurate analytic calculation of the spectrum of cosmological perturbations produced during inflation," *Phys. Lett.* **B302** (1993) 171–175, arXiv:gr-qc/9302019 [gr-qc].

[144] Nakamura T.T. and Stewart E.D., "The Spectrum of cosmological perturbations produced by a multicomponent inflaton to second order in the slow roll approximation," *Phys. Lett.* **B381** (1996) 413–419, arXiv:astro-ph/9604103 [astro-ph].

[145] Kenton Z. and Mulryne D.J., "The squeezed limit of the bispectrum in multi-field inflation," *JCAP* **1510** (2015) no. 10, 018, arXiv:1507.08629 [astro-ph.CO].

[146] Lyth D.H. and Wands D., "Conserved cosmological perturbations," *Phys. Rev.* **D68** (2003) 103515, arXiv:astro-ph/0306498 [astro-ph].

[147] Sasaki M. and Tanaka T., "Super-horizon scale dynamics of multi-scalar inflation," *Progress of Theoretical Physics* **99** (1998) no. 5, 763–781. http://dx.doi.org/10.1143/PTP.99.763.

[148] Wands D., Malik K.A., Lyth D.H., and Liddle A.R., "A new approach to the evolution of cosmological perturbations on large scales," *Phys. Rev.* **D62** (2000) 043527, arXiv:astro-ph/0003278.

[149] Lyth D.H. and Rodríguez Y., "The inflationary prediction for primordial non-gaussianity," *Phys.Rev.Lett.* **95** (2005) 121302, arXiv:astro-ph/0504045.

[150] Lyth D.H. and Wands D., "Generating the curvature perturbation without an inflaton," *Phys.Lett.* **B524** (2002) 5–14, arXiv:hep-ph/0110002 [hep-ph].

[151] Chambers A. and Rajantie A., "Lattice calculation of non-Gaussianity from preheating," *Phys.Rev.Lett.* **100** (2008) 041302, arXiv:0710.4133 [astro-ph].

[152] Chambers A. and Rajantie A., "Non-Gaussianity from massless preheating," *JCAP* **0808** (2008) 002, arXiv:0805.4795 [astro-ph].

[153] Chambers A., Nurmi S., and Rajantie A., "Non-Gaussianity from resonant curvaton decay," *JCAP* **1001** (2010) 012, arXiv:0909.4535 [astro-ph.CO].

[154] Bond J., Frolov A.V., Huang Z., and Kofman L., "Non-Gaussian Spikes from Chaotic Billiards in Inflation Preheating," *Phys.Rev.Lett.* **103** (2009) 071301, arXiv:0903.3407 [astro-ph.CO].

[155] Suyama T. and Yokoyama S., "Statistics of general functions of a Gaussian field -application to non-Gaussianity from preheating-," *JCAP* **1306** (2013) 018, arXiv:1303.1254 [astro-ph.CO].

[156] Bethke L., Figueroa D.G., and Rajantie A., "Anisotropies in the Gravitational Wave Background from Preheating," *Phys. Rev. Lett.* **111** (2013) no. 1, 011301, arXiv:1304.2657 [astro-ph.CO].

[157] Bethke L., Figueroa D.G., and Rajantie A., "On the Anisotropy of the Gravitational Wave Background from Massless Preheating," *JCAP* **1406** (2014) 047, arXiv:1309.1148 [astro-ph.CO].

[158] Vennin V. and Starobinsky A.A., "Correlation Functions in Stochastic Inflation," *Eur. Phys. J.* **C75** (2015) 413, arXiv:1506.04732 [hep-th].

[159] Vennin V., Assadullahi H., Firouzjahi H., Noorbala M., and Wands D., "Critical Number of Fields in Stochastic Inflation," *Phys. Rev. Lett.* **118** (2017) no. 3, 031301, arXiv:1604.06017 [astro-ph.CO].

[160] Hawking S.W., "The Development of Irregularities in a Single Bubble Inflationary Universe," *Phys. Lett.* **115B** (1982) 295.

[161] Hawking S.W. and Moss I.G., "Fluctuations in the Inflationary Universe," *Nucl. Phys.* **B224** (1983) 180.

[162] Bardeen J.M., Steinhardt P.J., and Turner M.S., "Spontaneous Creation of Almost Scale - Free Density Perturbations in an Inflationary Universe," *Phys. Rev.* **D28** (1983) 679.

[163] Guth A.H. and Pi S.Y., "The Quantum Mechanics of the Scalar Field in the New Inflationary Universe," *Phys. Rev.* **D32** (1985) 1899–1920.

[164] Contaldi C.R. and Magueijo J., "Generating nonGaussian maps with a given power spectrum and bispectrum," *Phys. Rev.* **D63** (2001) 103512, arXiv:astro-ph/0101512 [astro-ph].

[165] Juszkiewicz R., Weinberg D.H., Amsterdamski P., Chodorowski M., and Bouchet F., "Weakly nonlinear Gaussian fluctuations and the Edgeworth expansion," *Astrophys. J.* **442** (1995) 39, arXiv:astro-ph/9308012 [astro-ph].

[166] Matarrese S., Verde L., and Jimenez R., "The Abundance of high-redshift objects as a probe of non-Gaussian initial conditions," *Astrophys. J.* **541** (2000) 10, arXiv:astro-ph/0001366 [astro-ph].

[167] Amendola L., "The dependence of cosmological parameters estimated from the microwave background on non-gaussianity," *Astrophys. J.* **569** (2002) 595–599, arXiv:astro-ph/0107527 [astro-ph].

[168] Amendola L., "Non Gaussian likelihood function and COBE data," *Mon. Not. Roy. Astron. Soc.* **283** (1996) 983–989.

[169] Seery D. and Hidalgo J.C., "Non-Gaussian corrections to the probability distribution of the curvature perturbation from inflation," *JCAP* **0607** (2006) 008, arXiv:astro-ph/0604579 [astro-ph].

[170] Watts P. and Coles P., "Statistical cosmology with quadratic density fields," *Mon. Not. Roy. Astron. Soc.* **338** (2003) 806, arXiv:astro-ph/0208295 [astro-ph].

[171] Kohri K., Lyth D.H., and Valenzuela-Toledo C.A., "Preheating and the non-gaussianity of the curvature perturbation," *JCAP* **1002** (2010) 023, arXiv:0904.0793 [hep-ph].

[172] Prokopec T. and Roos T.G., "Lattice study of classical inflaton decay," *Phys. Rev.* **D55** (1997) 3768–3775, arXiv:hep-ph/9610400 [hep-ph].

[173] Greene P.B., Kofman L., Linde A.D., and Starobinsky A.A., "Structure of resonance in preheating after inflation," *Phys. Rev.* **D56** (1997) 6175–6192, arXiv:hep-ph/9705347 [hep-ph].

[174] Enqvist K., Nurmi S., and Rigopoulos G.I., "Parametric Decay of the Curvaton," *JCAP* **0810** (2008) 013, arXiv:0807.0382 [astro-ph].

[175] Bastero-Gil M., Di Clemente V., and King S.F., "Preheating curvature perturbations with a coupled curvaton," *Phys. Rev.* **D70** (2004) 023501, arXiv:hep-ph/0311237 [hep-ph].

[176] Khlebnikov S.Yu. and Tkachev I.I., "Classical decay of inflaton," *Phys. Rev. Lett.* **77** (1996) 219–222, arXiv:hep-ph/9603378 [hep-ph].

[177] Traschen J.H. and Brandenberger R.H., "Particle production during out-of-equilibrium phase transitions," *Phys.Rev.* **D42** (1990) 2491–2504.

[178] Kofman L., Linde A.D., and Starobinsky A.A., "Reheating after inflation," *Phys. Rev. Lett.* **73** (1994) 3195–3198, arXiv:hep-th/9405187.

[179] Kofman L., Linde A.D., and Starobinsky A.A., "Towards the theory of reheating after inflation," *Phys. Rev.* **D56** (1997) 3258–3295, arXiv:hep-ph/9704452 [hep-ph].

[180] Planck Collaboration, Ade P.A.R. *et al.*, "Planck 2015 results. XX. Constraints on inflation," *Astron. Astrophys.* **594** (2016) A20, arXiv:1502.02114 [astro-ph.CO].

[181] Berera A., "Interpolating the stage of exponential expansion in the early universe: A Possible alternative with no reheating," *Phys. Rev.* **D55** (1997) 3346–3357, arXiv:hep-ph/9612239 [hep-ph].

[182] Berera A. and Kephart T.W., "The Ubiquitous Inflaton in String-Inspired Models," *Phys. Rev. Lett.* **83** (1999) 1084–1087, arXiv:hep-ph/9904410 [hep-ph].

[183] Abbott L.F., Farhi E., and Wise M.B., "Particle Production in the New Inflationary Cosmology," *Phys. Lett.* **117B** (1982) 29.

[184] Albrecht A., Steinhardt P.J., Turner M.S., and Wilczek F., "Reheating an Inflationary Universe," *Phys. Rev. Lett.* **48** (1982) 1437.

[185] Dolgov A.D. and Linde A.D., "Baryon Asymmetry in Inflationary Universe," *Phys. Lett.* **116B** (1982) 329.

[186] Abbott L.F., Farhi E., and Wise M.B., "Particle Production in the New Inflationary Cosmology," *Phys. Lett.* **117B** (1982) 29.

[187] Boyanovsky D., de Vega H.J., and Holman R., "Nonequilibrium evolution of scalar fields in FRW cosmologies I," *Phys. Rev.* **D49** (1994) 2769–2785, arXiv:hep-ph/9310319 [hep-ph].

[188] Boyanovsky D., de Vega H.J., Holman R., and Salgado J.F.J., "Preheating and reheating in inflationary cosmology: A Pedagogical survey," in *String theory in curved space times. Proceedings, String Gravity Meeting, Paris, France, June 6-7, 1996*, pp. 260–280. 1996. arXiv:astro-ph/9609007 [astro-ph].

[189] Fujisaki H., Kumekawa K., Yamaguchi M., and Yoshimura M., "Particle production and dissipative cosmic field," *Phys. Rev.* **D53** (1996) 6805–6812, arXiv:hep-ph/9508378 [hep-ph].

[190] Fujisaki H., Kumekawa K., Yamaguchi M., and Yoshimura M., "Particle production and gravitino abundance after inflation," *Phys. Rev.* **D54** (1996) 2494–2503, arXiv:hep-ph/9511381 [hep-ph].

[191] Shtanov Y., Traschen J.H., and Brandenberger R.H., "Universe reheating after inflation," *Phys.Rev.* **D51** (1995) 5438–5455, arXiv:hep-ph/9407247 [hep-ph].

[192] Yoshimura M., "Catastrophic particle production under periodic perturbation," *Prog. Theor. Phys.* **94** (1995) 873–898, arXiv:hep-th/9506176 [hep-th].

[193] Yoshimura M., "Baryogenesis and thermal history after inflation," *J. Korean Phys. Soc.* **29** (1996) S236, arXiv:hep-ph/9605246 [hep-ph].

[194] Kofman L.A., "The Origin of matter in the universe: Reheating after inflation," 1996. arXiv:astro-ph/9605155 [astro-ph].

[195] Baumann D., "Lecture notes 'reheating after inflation'." http://www.damtp.cam.ac.uk/user/db275/TEACHING/INFLATION/Reheating.pdf.

[196] Lozanov K., "Lectures on reheating after inflation." https://wwwmpa.mpa-garching.mpg.de/~komatsu/lecturenotes/Kaloian_Lozanov_on_Reheating.pdf.

[197] Boyanovsky D., de Vega H.J., Holman R., Lee D.S., and Singh A., "Dissipation via particle production in scalar field theories," *Phys. Rev.* **D51** (1995) 4419–4444, arXiv:hep-ph/9408214 [hep-ph].

[198] Yoshimura M., "Catastrophic particle production under periodic perturbation," *Progress of Theoretical Physics* **94** (1995) no. 5, 873–898, /oup/backfile/content_public/journal/ptp/94/5/10.1143/ptp.94.873/2/94-5-873.pdf. http://dx.doi.org/10.1143/PTP.94.873.

[199] Dolgov A.D. and Kirilova D.P., "ON PARTICLE CREATION BY A TIME DEPENDENT SCALAR FIELD," *Sov. J. Nucl. Phys.* **51** (1990) 172–177. [Yad. Fiz.51,273(1990)].

[200] Zeldovich Ya.B. and Starobinsky A.A., "Particle production and vacuum polarization in an anisotropic gravitational field," *Sov. Phys. JETP* **34** (1972) 1159–1166. [Zh. Eksp. Teor. Fiz.61,2161(1971)].

[201] McLachlan N., *Theory and Application of Mathieu Functions*. Oxford University Press, 1947.

[202] Frolov A.V., "DEFROST: A New Code for Simulating Preheating after Inflation," *JCAP* **0811** (2008) 009, arXiv:0809.4904 [hep-ph].

[203] Kaiser D.I., "Post inflation reheating in an expanding universe," *Phys. Rev.* **D53** (1996) 1776–1783, arXiv:astro-ph/9507108 [astro-ph].

[204] Boyanovsky D., D'Attanasio M., de Vega H.J., Holman R., and Lee D.S., "Reheating and thermalization: Linear versus nonlinear relaxation," *Phys. Rev.* **D52** (1995) 6805–6827, arXiv:hep-ph/9507414 [hep-ph].

[205] Son D.T., "Reheating and thermalization in a simple scalar model," *Phys. Rev.* **D54** (1996) 3745–3761, arXiv:hep-ph/9604340 [hep-ph].

[206] Felder G.N., Garcia-Bellido J., Greene P.B., Kofman L., Linde A.D., and Tkachev I., "Dynamics of symmetry breaking and tachyonic preheating," *Phys. Rev. Lett.* **87** (2001) 011601, arXiv:hep-ph/0012142 [hep-ph].

[207] Felder G.N., Kofman L., and Linde A.D., "Tachyonic instability and dynamics of spontaneous symmetry breaking," *Phys. Rev.* **D64** (2001) 123517, arXiv:hep-th/0106179 [hep-th].

[208] Bassett B.A. and Liberati S., "Geometric reheating after inflation," *Phys. Rev.* **D58** (1998) 021302, arXiv:hep-ph/9709417 [hep-ph]. [Erratum: Phys. Rev.D60,049902(1999)].

[209] Greene P.B. and Kofman L., "Preheating of fermions," *Phys. Lett.* **B448** (1999) 6–12, arXiv:hep-ph/9807339 [hep-ph].

[210] Greene P.B. and Kofman L., "On the theory of fermionic preheating," *Phys. Rev.* **D62** (2000) 123516, arXiv:hep-ph/0003018 [hep-ph].

[211] Baacke J., Heitmann K., and Patzold C., "Nonequilibrium dynamics of fermions in a spatially homogeneous scalar background field," *Phys. Rev.* **D58** (1998) 125013, arXiv:hep-ph/9806205 [hep-ph].

[212] Turner M.S., "Coherent Scalar Field Oscillations in an Expanding Universe," *Phys. Rev.* **D28** (1983) 1243.

[213] Dufaux J.F., Bergman A., Felder G.N., Kofman L., and Uzan J.P., "Theory and Numerics of Gravitational Waves from Preheating after Inflation," *Phys. Rev.* **D76** (2007) 123517, arXiv:0707.0875 [astro-ph].

[214] Garcia-Bellido J., Figueroa D.G., and Sastre A., "A Gravitational Wave Background from Reheating after Hybrid Inflation," *Phys. Rev.* **D77** (2008) 043517, arXiv:0707.0839 [hep-ph].

[215] Easther R., Giblin J.T., and Lim E.A., "Gravitational Waves From the End of Inflation: Computational Strategies," *Phys. Rev.* **D77** (2008) 103519, arXiv:0712.2991 [astro-ph].

[216] Khlebnikov S.Yu. and Tkachev I.I., "The Universe after inflation: The Wide resonance case," *Phys. Lett.* **B390** (1997) 80–86, arXiv:hep-ph/9608458 [hep-ph].

[217] Khlebnikov S.Yu. and Tkachev I.I., "Resonant decay of Bose condensates," *Phys. Rev. Lett.* **79** (1997) 1607–1610, arXiv:hep-ph/9610477 [hep-ph].

[218] Felder G.N. and Tkachev I., "LATTICEEASY: A Program for lattice simulations of scalar fields in an expanding universe," *Comput. Phys. Commun.* **178** (2008) 929–932, arXiv:hep-ph/0011159 [hep-ph].

[219] Felder G.N., "CLUSTEREASY: A program for lattice simulations of scalar fields in an expanding universe on parallel computing clusters," *Comput. Phys. Commun.* **179** (2008) 604–606, arXiv:0712.0813 [hep-ph].

[220] Khlebnikov S.Y. and Tkachev I.I., "Relic gravitational waves produced after preheating," *Phys. Rev.* **D56** (1997) 653–660, arXiv:hep-ph/9701423 [hep-ph].

[221] Kolb E.W., Riotto A., and Tkachev I.I., "GUT baryogenesis after preheating: Numerical study of the production and decay of X bosons," *Phys. Lett.* **B423** (1998) 348–354, arXiv:hep-ph/9801306 [hep-ph].

[222] Khlebnikov S., Kofman L., Linde A.D., and Tkachev I., "First order nonthermal phase transition after preheating," *Phys. Rev. Lett.* **81** (1998) 2012–2015, arXiv:hep-ph/9804425 [hep-ph].

[223] Tkachev I., Khlebnikov S., Kofman L., and Linde A.D., "Cosmic strings from preheating," *Phys. Lett.* **B440** (1998) 262–268, arXiv:hep-ph/9805209 [hep-ph].

[224] Felder G.N., Kofman L., Linde A.D., and Tkachev I., "Inflation after preheating," *JHEP* **08** (2000) 010, arXiv:hep-ph/0004024 [hep-ph].

[225] Frolov A.V., "Defrost: a new code for simulating preheating after inflation," *Journal of Cosmology and Astroparticle Physics* **2008** (2008) no. 11, 009. http://stacks.iop.org/1475-7516/2008/i=11/a=009.

[226] Sainio J., "CUDAEASY - a GPU Accelerated Cosmological Lattice Program," *Comput. Phys. Commun.* **181** (2010) 906–912, arXiv:0911.5692 [astro-ph.IM].

[227] Saha P. and Tremaine S., "Symplectic integrators for solar system dynamics," *aj* **104** (Oct., 1992) 1633–1640.

[228] Forest E., "Geometric Integration for Particle Accelerators," *J. Phys.* **A39** (2006) 5321–5378.

[229] Bassett B.A., Tamburini F., Kaiser D.I., and Maartens R., "Metric preheating and limitations of linearized gravity. 2.," *Nucl. Phys.* **B561** (1999) 188–240, arXiv:hep-ph/9901319 [hep-ph].

[230] Bassett B.A. and Viniegra F., "Massless metric preheating," *Phys. Rev.* **D62** (2000) 043507, arXiv:hep-ph/9909353 [hep-ph].

[231] Bastero-Gil M., Tristram M., Macias-Perez J.F., and Santos D., "Non-linear Preheating with Scalar Metric Perturbations," *Phys. Rev.* **D77** (2008) 023520, arXiv:0709.3510 [astro-ph].

[232] Finelli F. and Brandenberger R.H., "Parametric amplification of metric fluctuations during reheating in two field models," *Phys. Rev.* **D62** (2000) 083502, arXiv:hep-ph/0003172 [hep-ph].

[233] Nambu Y. and Araki Y., "Evolution of non-linear fluctuations in preheating after inflation," *Class. Quant. Grav.* **23** (2006) 511–526, arXiv:gr-qc/0512074 [gr-qc].

[234] Tsujikawa S. and Bassett B.A., "When can preheating affect the CMB?," *Phys. Lett.* **B536** (2002) 9–17, arXiv:astro-ph/0204031 [astro-ph].

[235] Zibin J.P., Brandenberger R.H., and Scott D., "Back reaction and the parametric resonance of cosmological fluctuations," *Phys. Rev.* **D63** (2001) 043511, arXiv:hep-ph/0007219 [hep-ph].

[236] Enqvist K., Jokinen A., Mazumdar A., Multamaki T., and Vaihkonen A., "Non-Gaussianity from instant and tachyonic preheating," *JCAP* **0503** (2005) 010, arXiv:hep-ph/0501076 [hep-ph].

[237] Enqvist K., Jokinen A., Mazumdar A., Multamki T., and Vihknen A., "Cosmological constraints on string scale and coupling arising from tachyonic instability," *Journal of High Energy Physics* **2005** (2005) no. 08, 084. http://stacks.iop.org/1126-6708/2005/i=08/a=084.

[238] Hazra D.K., Martin J., and Sriramkumar L., "The scalar bi-spectrum during preheating in single field inflationary models," *Phys. Rev.* **D86** (2012) 063523, arXiv:1206.0442 [astro-ph.CO].

[239] Imrith S.V., Mulryne D.J., and Rajantie A., "Nonperturbative δN formalism," *Phys. Rev.* **D98** (2018) no. 4, 043513, arXiv:1801.02600 [astro-ph.CO].

[240] Salopek D.S. and Bond J.R., "Nonlinear evolution of long-wavelength metric fluctuations in inflationary models," *Phys. Rev. D* **42** (Dec, 1990) 3936–3962. https://link.aps.org/doi/10.1103/PhysRevD.42.3936.

[241] Sasaki M. and Tanaka T., "Superhorizon scale dynamics of multiscalar inflation," *Prog.Theor.Phys.* **99** (1998) 763–782, arXiv:gr-qc/9801017 [gr-qc].

[242] Starobinsky A.A., "Multicomponent de Sitter (Inflationary) Stages and the Generation of Perturbations," *JETP Lett.* **42** (1985) 152–155.

[243] Dias M., Frazer J., Mulryne D.J., and Seery D., "Numerical evaluation of the bispectrum in multiple field inflationthe transport approach with code," *JCAP* **1612** (2016) no. 12, 033, arXiv:1609.00379 [astro-ph.CO].